Genetic Analysis and Cell Manipulation on Microfluidic Surfaces

Jing Zhu

Submitted in partial fulfillment of the
requirements for the degree of
Doctor of Philosophy
in the Graduate School of Arts and Sciences

COLUMBIA UNIVERSITY

2014

ABSTRACT

Genetic Analysis and Cell Manipulation on Microfluidic Surfaces

Jing Zhu

Personalized cancer medicine is a cancer care paradigm in which diagnostic and therapeutic strategies are customized for individual patients. Microsystems that are created by Micro-Electro-Mechanical Systems (MEMS) technology and integrate various diagnostic and therapeutic methods on a single chip hold great potential to enable personalized cancer medicine. Toward ultimate realization of such microsystems, this thesis focuses on developing critical functional building blocks that perform genetic variation identification (single-nucleotide polymorphism (SNP) genotyping) and specific, efficient and flexible cell manipulation on microfluidic surfaces.

For the identification of genetic variations, we first present a bead-based approach to detect single-base mutations by performing single-base extension (SBE) of SNP specific primers on solid surfaces. Successful genotyping of the SNP on exon 1 of HBB gene demonstrates the potential of the device for simple, rapid, and accurate detection of SNPs. In addition, a multi-step solution-based approach, which integrates SBE with mass-tagged dideoxynucleotides and solid-phase purification of extension products, is also presented. Rapid, accurate and simultaneous detection of 4 loci on a synthetic template demonstrates the capability of multiplex genotyping with reduced consumption of samples and reagents.

For cell manipulation, we first present a microfluidic device for cell purification with surface-immobilized aptamers, exploiting the strong temperature dependence of the affinity binding between aptamers and cells. Further, we demonstrate the feasibility of

using aptamers to specifically separate target cells from a heterogeneous solution and employing environmental changes to retrieve purified cells. Moreover, spatially specific capture and selective temperature-mediated release of cells on design-specified areas is presented, which demonstrates the ability to establish cell arrays on pre-defined regions and to collect only specifically selected cell groups for downstream analysis.

We also investigate tunable microfluidic trapping of cells by exploiting the large compliance of elastomers to create an array of cell-trapping microstructures, whose dimensions can be mechanically modulated by inducing uniform strain via the application of external force. Cell trapping under different strain modulations has been studied, and capture of a predetermined number of cells, from single cells to multiple cells, has been achieved.

In addition, to address the lack of aptamers for targets of interest, which is a major hindrance to aptamer-based cell manipulation, we present a microfluidic device for synthetically isolating cell-targeting aptamers from a randomized single-strand DNA (ssDNA) library, integrating cell culturing with affinity selection and amplification of cell-binding ssDNA. Multi-round aptamer isolation on a single chip has also been realized by using pressure-driven flow.

Finally, some perspectives on future work are presented, and strategies and notable issues are discussed for further development of MEMS/microfluidics-based devices for personalized cancer medicine.

Table of Contents

List of Figures

List of Tables

List of Abbreviations

µCE	microchip capillary electrophoresis
µTAS	Micro Total Analysis system
3-MPTS	(3-mercaptopropyl) trimethoxysilane
A	adenine
ACN	acetonitrile
ALL	acute lymphoblastic leukemia
anti-EpCAM	antiepithelial cell adhesion molecule
B&W	binding and washing
BRAF	v-raf murine sarcoma viral oncogene homolog B1
BSA	bovine serum albumin
C	cytosine
C_{18}	octadecyl carbon chain
CCD	charge-coupled device
CFD	computational fluidic dynamics
CMACS	continuous flow magnetic actuated cell separation
CTC	circulating tumor cell
CVD	chemical vapor deposition
Da	Dalton
dATP	deoxyadenosine triphosphate
DC	direct current

dCTP	deoxycytidine triphosphate
ddATP	dideoxyadenosine triphosphate
ddCTP	dideoxycytidine triphosphate
ddGTP	dideoxyguanosine triphosphate
ddNTPs	Dideoxyribonucleotide triphosphate
ddTTP	dideoxythymidine triphosphate
ddUTP	dideoxyuridine triphosphate
DEP	dielectrophoresis
dGTP	deoxyguanosine triphosphate
DI water	deionized water
DNA	deoxyribonucleic acid
dNTPs	deoxyribonucleoside 5’-triphosphate
D-PBS	Dulbecco's phosphate-buffered saline
dsDNA	double-strand DNA, double-strand oligonucleotides
dTTP	deoxythymidine triphosphate
dUTP	deoxyribouridine triphosphate
EDTA	ethylenediaminetetraacetic acid
FACS	fluorescence activated cell sorting
FAM	fluorescein amidite
FBS	fetal bovine serum
FEN	flap endonucleases
FRET	fluorescence resonance energy transfer

G	guanine
gDNA	genomic DNA
GMBS	4-maleimidobutyric acid N-hydroxysuccinimide ester
HPLC	high performance liquid chromatography
I.D.	inside diameter
JC1	5,5',6,6'-tetrachloro-1,1',3,3'-tetraethylbenzimidazolylcarbocyanine iodide
LOC	Lab on a Chip
M.W.	molecular weight
MACS	magnetic activated cell sorting
MALDI-TOF MS	matrix-assisted laser desorption/ionization time-of-flight mass spectrometry
MEMS	Micro-Electro-Mechanical System
MPSS	massively parallel signature sequencing
mRNA	messenger RNA
MS	mass spectrometry
NC	negative control
nDEP	negative DEP
NSCLC	non-small-cell lung cancer
O.D.	outside diameter
P/S	penicillin-streptomycin
Parylene	poly(p-xylyene) polymers

PCR	polymerase chain reaction
PCR-RFLP	polymerase chain reaction-restriction fragment length polymorphism
pDEP	positive DEP
PDMS	polydimethylsiloxane
PECVD	plasma-enhanced chemical vapor deposition
PI	propidium iodide
PID	proportional-integral-derivative
POC	point-of-care
PSMA	prostate-specific membrane antigen
PTK7	protein tyrosine kinase 7
qPCR	quantitative PCR, real-time PCR
qRT-PCR	real-time reverse-transcription PCR
RGD	arginine-glycine-aspartic acid
RNA	ribonucleic acid
RT-PCR	reverse transcription PCR
SBE	single-base extension
SELEX	systematic evolution of ligands by exponential enrichment
SEM	scanning electron microscope
SNP	single nucleotide polymorphisms
SPP	solid-phase purification
ssDNA	single-strand DNA, single-strand oligonucleotides

T	thymine
TCEP	tris(2-carboxyethyl)phosphine
TCR	temperature coefficient of resistance
TEAA	triethylammonium acetate buffer
U	uracil
UV	ultraviolet

Nomenclature

F_L	inertial lift force
F_D	dean drag force
d	particle diameter
ε_m	permittivity of the media
ε_p^*	complex permittivity of the particle
ε_m^*	complex permittivity of the media
E_{rms}	the room mean square of the electric field
K_d	dissociation constant
v/v	volume to volume
R	resistance
T	temperature
R_0	reference resistance
T_0	reference temperature
α	temperature coefficient of resistance
N_a	number of captured cells
N_b	maximum number of cells that can be captured due to geometric limitations
η	fraction of captured cells
τ	time constant
t	incubation duration
$\rho_{capture}$	captured cell density

c_{cell}	cell suspension concentration
m_e	mass of extended primer
m_r	mass of unextended primer
m_n	mass of corresponding ddNTP-N_3-biotin
m_b	mass loss upon phosphodiester bond formation
m_p	the mass of cleaved product
m_c	mass change upon cleavage
m/z	mass-to-charge ratio

Acknowledgements

I would like to express my sincerest thanks to my colleagues, friends and family. Without their help, support and love, completion of this thesis would not have been possible.

I would first like to thank my Ph.D. advisor, Dr. Qiao Lin. Since providing me the opportunity to join his lab at Columbia University, his never-ending support, enthusiasm and enlightening guidance has been invaluable. Throughout my graduate research career, his profound knowledge, dedicated mentoring and patience have had a tremendous impact on me, both personally and professionally.

I also want to extend my thanks to Drs. Milan Stojanovic, Renjun Pei, Jingyue Ju, James Russo, David Brenner, Sally Amundson and Ronald Warpner for their support, insight and advice on collaborative projects. Their knowledge has been a constant source of direction for my doctoral research. I would also like to thank Drs. Elon Terrell and Jung-Chi Liao for their suggestions and comments in the completion of this thesis.

Moreover, I also want to acknowledge my lab mates, members of collaborating labs, and fellow students for their help and friendship. These include a long but still incomplete list of names: ThaiHuu Nguyen, Bin Wang, Yao Zhou, John Hilton, Xian Huang, Junhui Ni, Haogang Cai, Jaeyoung Yang, Yuan Jia, Junyi Shang, Tim Olsen, Yibo Zhu, Kun Liu, Bing Song, Hao Sun, Cheng Wang, Jinho Kim, Zhixing Zhang, Stefano Ronca, Mirko Palla, Chunmei Qiu, Zengmin Li, Xiaoxu Li, Shundi Shi, Wenjin Guo, Tony Yang, Yuan Zhang, Yi Zheng, Ning Gu, Shuaimin Liu, Luozhou Li, Mihaela Barbu, Marlin Harlim, Brian Gillette, Hesam Parsa, Tassaneewan Laksanasopin, Sau Yin Chi, Yukkee Cheung,

Alan Bigelow, Guy Garty, Charles Geard, Manuela Buonanno, Andrew Harken, Stephen Marino, Brian Ponnaiya Gerhard Randers-Pehrson, and Yangping Xu.

In addition, I would like to thank my parents, Yinxuan Zhu and Ping Li, and my cousin Rui Zhu. Although they may not understand all the details of my research, their love, support and consistent encouragement have kept me going over the years.

Finally, I would like to thank my wife, Huanfen Yao, for her love, support, understanding and encouragement during the best and the worst of times. Without her selfless devotion, I could not have accomplished anything, including this thesis.

Dedicated to my parents and Huanfen

Chapter 1. Introduction

1.1. Microelectromechanical Systems and Microfluidics for Biomedical Applications

Microelectromechanical systems (MEMS) are systems that integrate small-scale electrical and mechanical components (with feature size ranging from submicrometers to hundreds of micrometers) to accomplish specific objectives. Microfluidics focuses on a special class of MEMS technology that processes or manipulates small-volume fluids (10^{-6} L to 10^{-18} L) geometrically constrained to channels with dimensions of tens to hundreds of micrometres [1], employing knowledge from the field of engineering, physics, chemistry, nanotechnology and biotechnology. Typically, a microfluidic system will integrate methods for sample and reagent introduction, fluid movement and mixing, analytical reactions, and product detection into a single device [1]. The development of microfabrication technologies for MEMS and traditional semiconductor manufacturing has, likewise, led to the rapid development of microfluidics over past 20 years. This can be seen in the diversity of functional components that have been realized onto a single chip, such as valves [2, 3], mixers [4-6] and pumps [7]. Compared with conventional platforms, microfluidics offers a number of advantages, such as very low sample and reagent consumption, high resolution and sensitivity in separations and detections, low cost, fast analysis, and small device footprint [8]. Microfluidics were first employed to the field of molecular analysis, initially for chemical sensing [9]. Now, microfluidics are widely applied to a broad range of applications such as chemical analysis [10, 11], cell biology

[12-14], genetic analysis [15-18], biosensing [19-21], and drug discovery [22, 23]. Microfluidics is the critical technology for lab-on-a-chip systems.

Lab-on-a-chip micro systems, which are also referred to as micro total analysis systems (μTAS), are chip-format devices that integrate various processes and functions, including sample preparation, reactions and detections for biological and chemical analysis (**Figure 1.1**) [24]. Such systems typically consist of subsystems that accomplish a variety of functions that involve fluidic, chemical, mechanical and electrical operations. The ultimate objective of this research is to develop integrated microsystems for personalized cancer medicine, which is a healthcare paradigm that allows physicians to tailor cancer treatment strategies for individual patients based on the exclusive patient-specific characteristics of a disease. These unique characteristics can be revealed by evidence such as identification of genetic variations, and cellular and pathological responses to pharmaceutical drug candidates [25]. As conventional methods are still time-, labor-, and resource-consuming, MEMS-based microfluidic systems, which are able to effectively and efficiently produce patient- and disease-specific information at multiple levels and thus identify the nature of cancer for each patient, become ideal platforms to realize personalized cancer medicine.

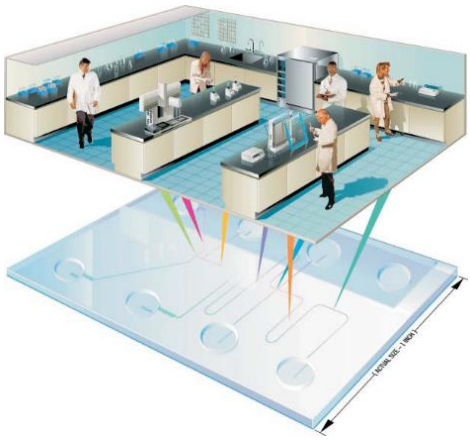

Figure 1.1: Lab-on-a-chip: Miniaturizing and integrating laboratory processes onto a single chip [24].

1.2. Personalized Cancer Medicine

Personalized cancer medicine is a cancer care paradigm in which diagnostic and therapeutic strategies are customized for individual patients. Different from traditional diagnostics and therapeutics, which rely on medical history and laboratory evaluation to determine a generic treatment scheme for patients with similar symptoms, personalized medicine utilizes patient-specific genetic, proteomic, cellular, clinical and environmental information to tailor a unique treatment approach for each individual cancer patient [25].

For example, to make an optimized medical decision toward each patient, genetic and cellular analyses are commonly employed to identify patient-specific characteristics of cancer. Advances in large-scale genomic, proteomic, and cellomic technology have led to vast improvements in the understanding and application of personalized medicine to cancer diagnosis and therapy. For example, the fine interrogation of genetic variations in DNA has revealed their impact on phenotypic differences, disease development, and drug

response, leading to a more efficient process for drug discovery [26]. However, due to the heterogeneity of the diseases at the pathological and cellular level, knowing only the genetic makeup of cancer is not sufficient to determine the outcome of a cancer treatment strategy [27]. For the same pharmaceutical drug, differences in the pathological and cellular level responses will also contribute to different therapy results. Therefore, drug candidates, chosen according to genetic information, also need to be further selected based on toxicity, side effects, and effectiveness. Since it is often not feasible to treat patients with multiple drugs, as there is potential for harmful toxicity and side effects, it is critical to use the most effective drug, which can be determined by drug screening using isolated cancer cells or tissues directly from the patient. This procedure will contribute to the optimization of treatment for an individual patient, which is the final goal of personalized cancer medicine.

1.3. Microfluidic Genetic Analysis and Cell Manipulation

Microfluidic technologies have been explored in a broad range of bioanalytical applications [28]. In particular, microfluidic genetic analysis and cell manipulation have been enabling applications such as genetic variation interrogation and cell-based drug screening, which are highly desired capabilities in personalized cancer medicine. This section provides a brief overview of related work in the literature on microfluidic approaches to genetic analysis and cell manipulation.

1.3.1. Microfluidic Genetic Analysis

The successful sequencing of the human genome [29-31] has offered opportunities to elucidate the genetic bases of evolution, biological functions and diseases [32, 33]. The

increasing demand of genome-related research requires fast, high-throughput, sensitive and reliable analytical methods, but traditional genetic analysis systems may not be able to satisfy these requirements. A fully integrated microfluidic system has the capability to integrate all the analytical steps onto a single chip at pL-nL volumes [34], and thus eliminates most of the substantial manual labor, which increases the assay speed and throughput, decreases reagent and sample consumption, and reduces the instrument size [9, 35]. Therefore, microfluidic genetic analysis systems have been developed rapidly in the last ten years, addressing bioanalytical challenges, such as DNA sequencing, SNP genotyping, gene expression analysis, and pathogen detection, thus enabling large-scale and point-of-care applications [15].

1.3.1.1. Microfluidic DNA Sequencing

Deoxyribonucleic acid (DNA), which encodes the genetic instructions used in the development and functioning of living organisms, is a long double helical polymer made from repeating deoxyribonucleotides, each containing a base, a sugar and a phosphate group [36]. In the DNA replication process, a new strand of DNA molecules is synthesized from deoxyribonucleoside 5'-trisphosphates (dNTPs), using the original strand as the template. Briefly, the 3'-hydroxyl group of the sugar in one nucleotide binds to the 5'-phosphate group of the sugar in the adjacent nucleotide by a phosphodiester bond, generating the DNA molecules with a phosphate group on the 5'-terminal of the sugar unit (5'-end) and a free hydroxyl group at the 3'-terminal of the sugar unit (3'- end). The sugars and phosphate groups support the DNA structure, and the bases carry the genetic information. There are four different bases, adenine (A), guanine (G), thymine (T) and

cytosine (C), with thymine replaced by uridine in ribonucleic acid (RNA) [37]. Since the introduction of the dideoxyribonucleotide chain terminator sequencing method (**Figure 1.2**) by Sanger, in which primer extensions terminate randomly with labeled dideoxyribonucleotide to generate different fragments to interrogate the terminating bases, DNA sequencing has revolutionized biological sciences and become one of the most powerful technologies in biology [38, 39]. To reduce the cost and increase throughput of Sanger sequencing, next-generation DNA sequencing techniques have also been evolving rapidly, such as massively parallel signature sequencing (MPSS) [40], polony sequencing [41], and DNA nanoball sequencing [42], amongst others.

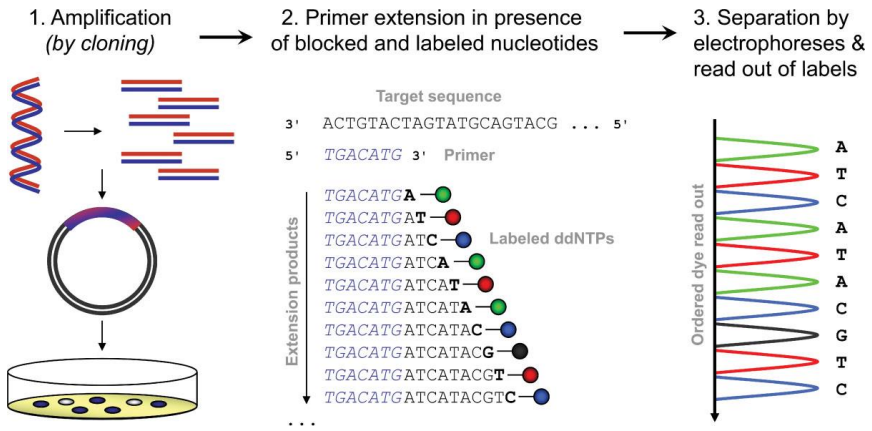

Figure 1.2: Schematic of Sanger sequencing process [43].

Driven by the ambitious goal of DNA sequencing, microfluidic devices have been developed to improve the Sanger biochemistry to provide longer reads and higher throughput, leading to significant breakthroughs. For example, microchip capillary electrophoresis (µCE) devices have realized ultrafast separation of 600 bases in 6.5 min [44] and extremely high-throughput analysis of 768 samples simultaneously [45]. A fully integrated platform has also been reported in 2006 [46], in which a nanoliter-scale device

incorporated all three Sanger sequencing steps, thermal cycling, sample purification, and capillary electrophoresis, into a 4-inch glass wafer (**Figure 1.3**). The integrated device can complete the sequencing of 1 fmole DNA template in less than 30 min with 99% accuracy.

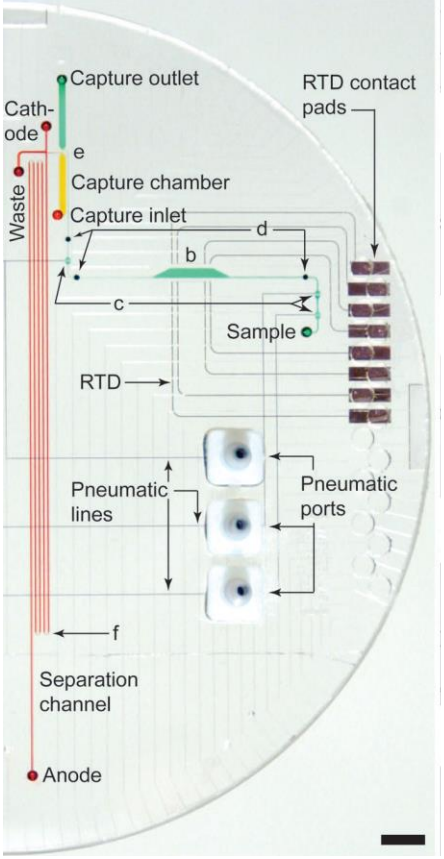

Figure 1.3: A fully integrated microfluidic device for Sanger DNA sequencing [46].

1.3.1.2. Microfluidic SNP Genotyping

Single nucleotide polymorphisms (SNPs) are genetic variations in a DNA sequence occurring when single nucleotides in the genome differ between members of a biological species. SNPs are the most abundant type of genetic variations, which includes substitutions, insertions and deletions of individual bases, and happen at specific locations in the genome. SNPs are found in more than 1% of the population [47], occur every 100 to

300 bases in the human genome, and have more than 10 million entries in public databases [48].

Although direct DNA sequencing is the most straightforward method to discover and analyze SNPs, when analyzing known SNP targets, sequencing methods are expensive, complex and usually unnecessary. Therefore, a number of alternative SNP genotyping technologies have been developed and used to analyze highly targeted SNPs, such as enzymatic cleavage, allele specific hybridization, allele specific ligation or cleavage, and allele specific primer extension [49, 50].

Enzymatic Cleavage. Polymerase chain reaction-restriction fragment length polymorphism (PCR-RFLP) is a simple and convenient laboratory technique for SNP detection [51]. It utilizes DNA sequence-specific restriction endonucleases to identify DNA polymorphisms [52]. DNA restriction enzyme can recognize PCR-amplified specific sequences and catalyze endonucleolytic cleavages, generating fragments with known lengths. The individual base variations inhibit the cleavage and thus result in DNA fragments of different lengths (**Figure 1.4A**). Thermostable flap endonucleases (FEN) are sensitive to sequence mismatches and structure-specific in DNA cleavages [53]. Invader® Assays employ FEN to cleave a three-dimensional complex formed by the hybridization of allele-specific overlapping oligonucleotides to target DNA with a polymorphic site, followed by detection of cleavage products by different methods, such fluorescence resonance energy transfer (FRET) (**Figure 1.4B**) [54]. While it is highly accurate, this method is generally time-consuming and difficult to multiplex (i.e., to detect multiple SNPs in one reaction).

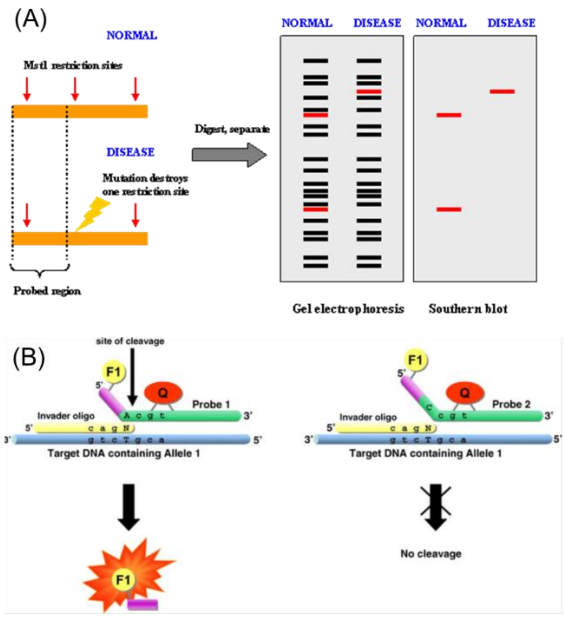

Figure 1.4: Schematic of (A) PCR-RFLP assay [37] and (B) Invasive cleavage assay [54].

Allele Specific Hybridization. Single base discrimination can be realized by utilizing thermal stability differences of perfectly matched and mismatched target-probe pairs. The effectiveness of this method mostly depends on the length, sequence and GC content of the probe, secondary structure of the target, and hybridization condition. According to this principle, a number of SNP genotyping approaches have been developed. For example, Affymetrix® Human SNP Array is based on allelic discrimination by direct hybridization of genomic DNA (gDNA) to arrays containing locus- and allele-specific oligonucleotides [50, 55]. Briefly, gDNAs are first digested and amplified, and the resulting products are then fragmented, labeled, and hybridized to the DNA array with surface-bound probes under controlled conditions. The array is finally imaged, and the genotypes can be determined according to the hybridization signal (**Figure 1.5**). However, due to insufficient accuracy caused by false positives, this method is not suitable for fine mapping of SNPs.

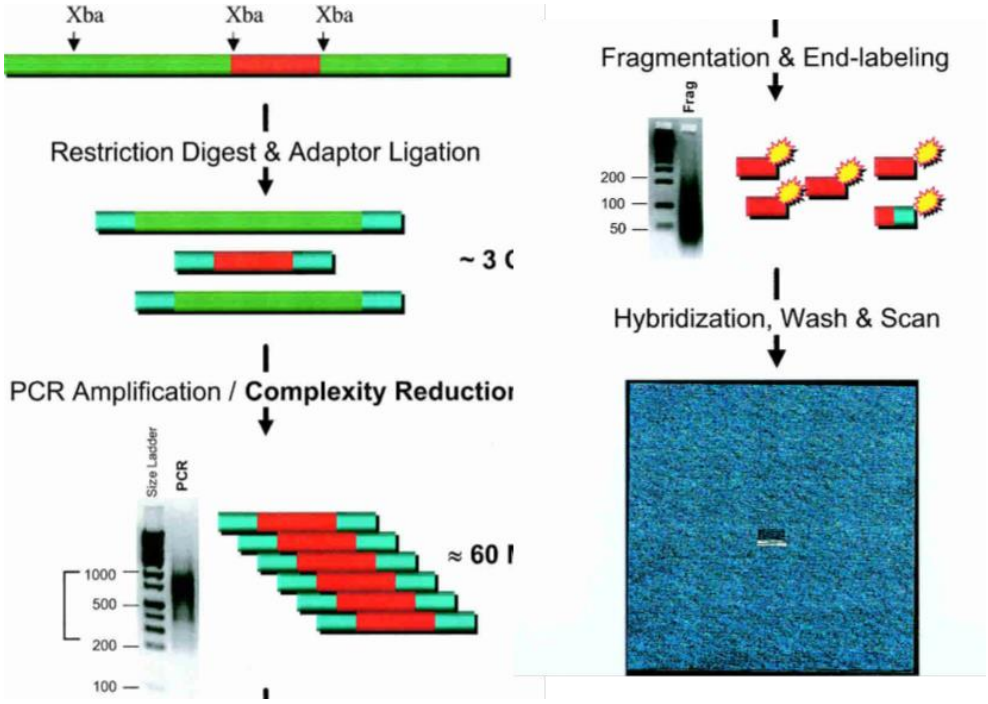

Figure 1.5: Schematic of SNP genotyping by DNA microarray hybridization [56].

Allele Specific Ligation or Cleavage. This method combines the hybridization of probes specific to the target DNA sequence and the specificity of the ligase enzyme to distinguish mismatched nucleotides. The DNA ligase will only join the two oligonucleotides together through the formation of a phosphodiester bond when they hybridize to a single-strand DNA (ssDNA) with prefect matching [57]. Usually, three oligonucleotide probes are employed, one of which binds to the template adjacent to the SNP site. The other two probes are allele specific and target the SNP site. The ligation reaction happens only if the allele specific probe perfectly matches the SNP site. The products can then be detected by various methods, such as using fluorescently and radioactively labeled probes (**Figure 1.6A**). In another example, TaqMan® Assay, two allele specific probes are labeled with different reporter dyes at 5' end and with non-

fluorescent quenchers at 3’ end. When the forward primers extend, the Taq polymerase enzyme degrades the nucleotide at the 5’ end of the perfectly matched probes, and thus releases the 5’ bound reporter dyes, exhibiting corresponding fluorescence (**Figure 1.6B**) [58]. However, the slow reaction speed and limited number of modified probes restricts its applications [49].

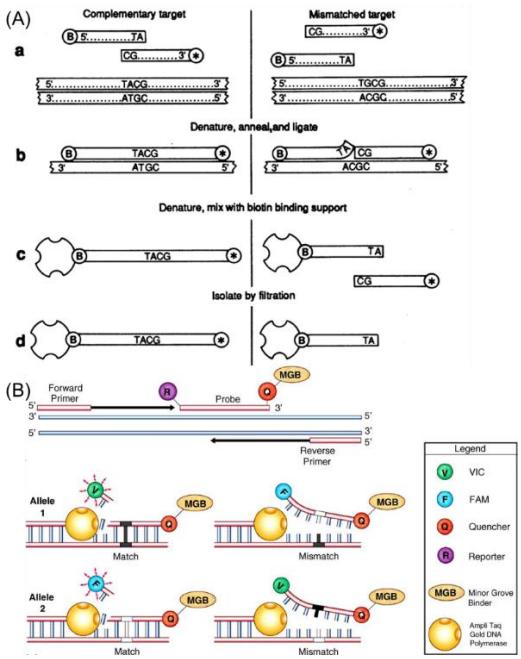

Figure 1.6: Schematic of SNP genotyping by ligation. (A) A ligation assay based on fluorescent/radioactive detection [57] ; (B) TaqMan® Assay [58].

Allele Specific Primer Extension. This method is a robust and flexible emerging method that involves allele-specific incorporation of nucleotides in primer extensions with a DNA template [49, 50]. Briefly, the primer anneals to the target DNA template with its 3’ end adjacent to the SNP site, and then extends by polymerase enzyme. The discrimination between different incorporated nucleotides can be achieved by different

methods, such as fluorescence (**Figure 1.7A**), and mass spectrometry (**Figure 1.7B**). For the fluorescence-based approach, the primers are labeled with fluorescent dyes by incorporating fluorescently tagged nucleotides, which can be used to determine the base at the SNP site, such as Illumina® Infinium Assays [59]. For the mass spectrometry-based approach, the extended primers are analyzed by mass spectrometry to identify the nucleotides incorporated according to different molecular weights, such as Sequenom® iPlex Assays [60]. While rapid, accurate and capable of multiplexing, it requires complicated design of primer and fluorescent-tagged or mass-tagged nucleotide.

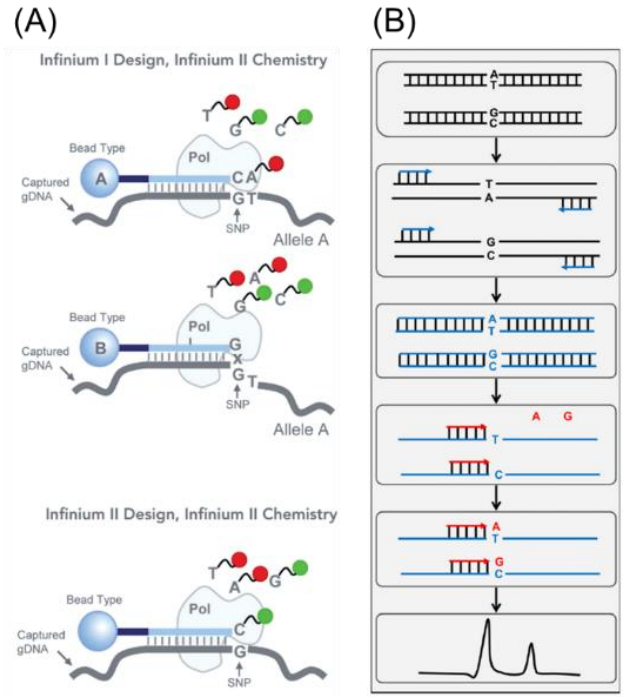

Figure 1.7: Allele specific primer extension. (A) Fluorescence based detection [59]; (B) Mass spectrometry based detection [61].

Microfluidics technology has enabled fast, low-cost and automated SNP detection with improved sensitivity, resolution, accuracy, efficiency and throughput, as well as

minimized sample consumption [62]. The SNP genotyping methods described above have been implemented in microfluidic systems, leading to significant improvements. For example, enzymatic cleavage has been integrated with µCE to determine an SNP site in a p53 suppressor gene from clinical samples in ~100s, which is 10 and 50 times faster than using traditional capillary and slab gel electrophoresis, respectively [63]. By incorporating allele specific hybridization methods, a fully integrated microfluidic device has also been reported, which is comprised of a microfluidic channel, a DNA chip platform, and a photodetector for the discrimination (**Figure 1.8**) [64], and can achieve SNP detection without DNA extraction, purification and PCR in less than 1 hour.

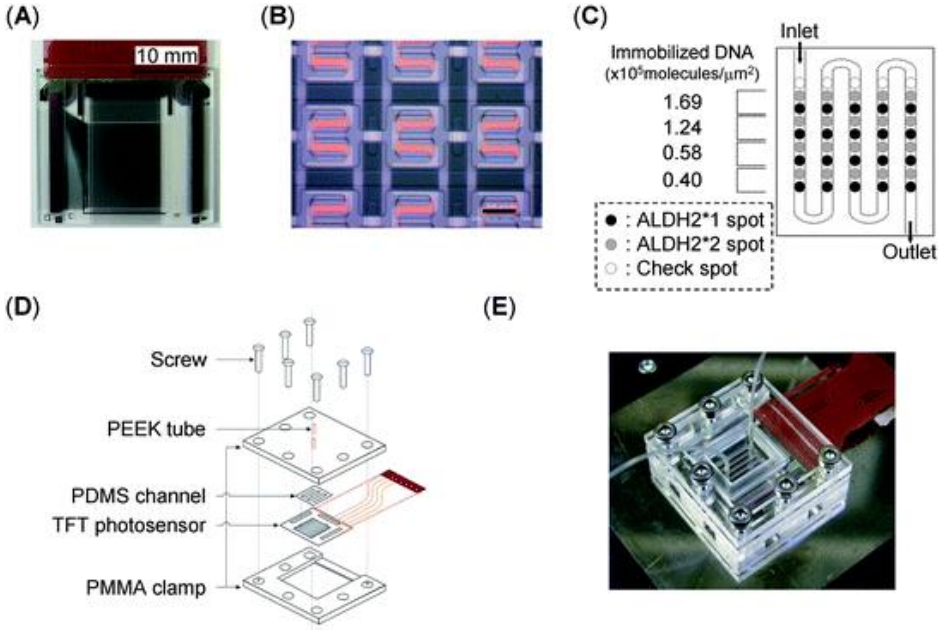

Figure 1.8: A fully integrated microfluidic device for SNP genotyping [64].

1.3.1.3. Microfluidic Gene Expression Analysis

Gene expression is the process that interprets the genetic information (genes) stored in DNA to functional gene products, such as protein, and is the most fundamental procedure

through which genotype of an organism influences the phenotype. Genes are expressed by transcribing gDNA to RNA, which may then be translated to protein. Because of the random fluctuations and complex molecular switches [65, 66], the messenger RNA (mRNA) production level may differ, even for genetically identical cells. Although we can consider RNA as a mediator between gene and protein, it is still the focus and a valuable component in the study of organism growth and development [67]. Due to instability of RNA, reverse transcription PCR (RT-PCR) of mRNA becomes an important tool for gene expression analysis, which has also been significantly improved by integrating RT-PCR and other functional units into the microfluidic platforms [15].

For example, by integrating single-cell lysis, mRNA isolation and complementary DNA (cDNA) synthesis, a multilayer PDMS microsystem has been reported [68]. In this work, the employment of on-chip microvalaves and micrpumps led to accurate fluid control, the use of a 450 pL reaction volume enhanced the reaction efficiency, and the enclosed structures reduced the risk of degradation and contamination. Expanding on this technology, an improved and fully integrated microfluidic device has been established to perform high-precision qRT-PCR analysis from 300 cells in parallel [69] (**Figure 1.9A**). Compared with previous work, a more efficient single cell capturing strategy, on-chip amplification and fluorescence-based real-time detection have been incorporated in a single microfluidic device, extensively increasing the throughput and sensitivity. In addition, the μCE device has also been integrated with single-cell capture, RT-PCR and post-PCR purification to be capable of analyzing gene expression [70] (**Figure 1.9B**). As low as 11 copies of mRNA in each reactor has been detected in this device.

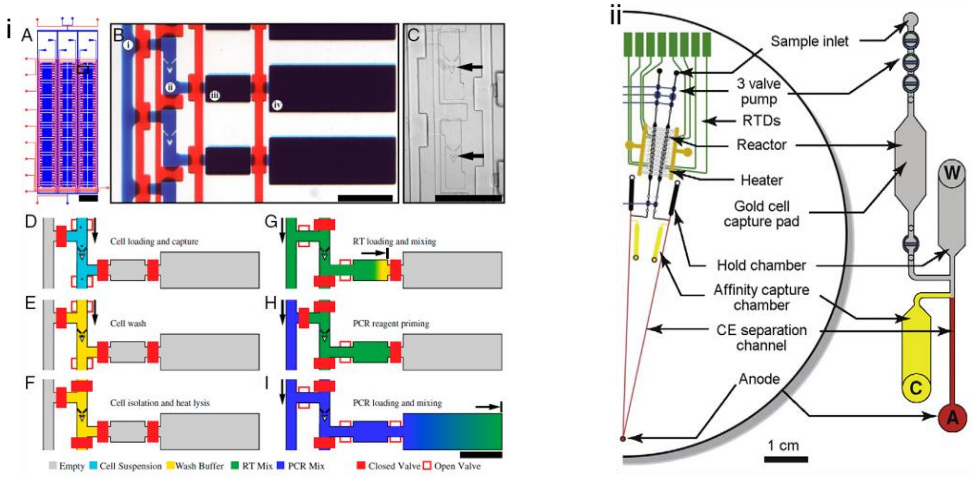

Figure 1.9: Integrated microdevice for gene expression analysis of single cells. (i) A fluorescence-based approach [69]; (ii) a μCE-based approach [70].

1.3.2. Microfluidic Cell Manipulation

Sample preparation, which plays a very important role in the quality of results, is often the most tedious step in any assay. As biological problems and analytical methods become more and more complicated, there is a rapidly growing need for systems that can reliably reproduce and prepare samples with high purity, high throughput and high recovery [71]. Recently, cell and microparticle manipulation in microfluidic systems have drawn significant attention as potential biological and chemical sample preparation platforms for their advantages of fast assay period, minimal reactant consumption and high throughput [72, 73].

In principle, microfluidic cell manipulation involves applying differential forces on target cells to guide them along prescribed paths [72]. According to the way forces are applied to cells, the separation method can be divided into 5 categories: geometry based methods, electrokinetic methods, acoustic methods, optic methods, and affinity based

methods. The details of these microfluidic cell manipulation methods will be reviewed in the sections below, with particular focus on affinity-based methods.

1.3.2.1. Geometry-Based Cell Manipulation

Geometry-based cell manipulation relies on the difference in cell size or volume to separate cells [74]. The most straightforward method is filtration. For example, an array of closely packed micropillars (**Figure 1.10A**) [75] or microsieves (**Figure 1.10B**) [76] with designed dimensions can be employed to separate cells. In such devices, solutions with different types of cells can be introduced into the main channels; small cells will be carried with the bulk fluid and pass through the intervals between pillars or the slits under the sieves, leaving larger cells entrapped in the main channels. A second geometry based cell manipulation method utilizes the nature of laminar flow in the microfluidic channel. In a micropost array with a lateral displacement, the direction of cell movement depends on the location of the cell's center. Therefore, smaller cells maintain their position in the flow, while larger cells move to the right (**Figure 1.11A**) [77]. Similarly, in another hydrodynamic approach, cells are pinched to a sidewall as they move along their center streamlines, which are linearly expanded along with the chamber expansion, and thus separated accordingly (**Figure 1.11B**) [78]. A third method exploits particle equilibration in the channel. In a spiral microchannel, the shear gradient induced Inertial Lift Force (F_L), generated in a plane Poiseuille flow, drives the suspended particles away from the microchannel center, and Dean Drag Force (F_D) moves the particles away from the channel sidewall. Both of them depend on the particle diameter (d), and the ratio of F_L and F_D on particle size ($F_L / F_D \propto d^3$) determines the position of a particle (**Figure 1.12**) [79]. A forth

method relies on physical barriers, such as microwells [80, 81] and microcups [82, 83], to restrict cells to some specific locations. The microstructures are designed according to the size of target cells, which fall down to the wells (**Figure 1.13A**) or are trapped in the cup (**Figure 1.13B**) when passing by the microstructures with carrier fluids. Although geometry-based cell manipulation does not require any chemicals or any kind of external force to drive cells, it can only be applied to cells with a particular size or volume.

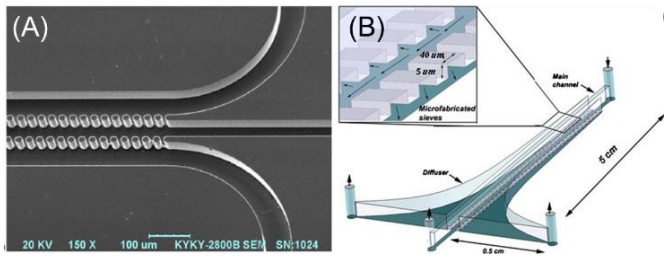

Figure 1.10: Different filtration based cell manipulation using (A) micropillar array [75] and (B) microsieves [76].

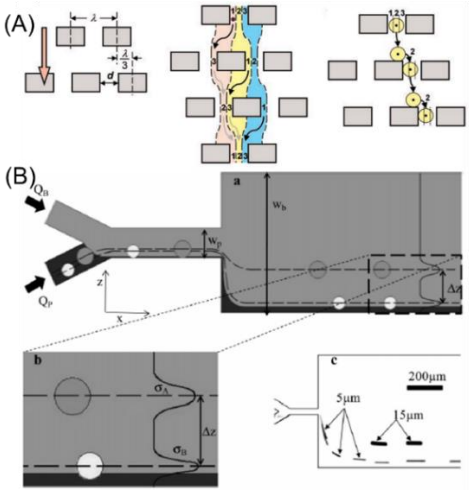

Figure 1.11: Cell manipulation according to the nature of laminar flow in a microchamber. (A) Example of using a micropost array with lateral displacement [77]. (B) Example of a pure hydrodynamic approach [78].

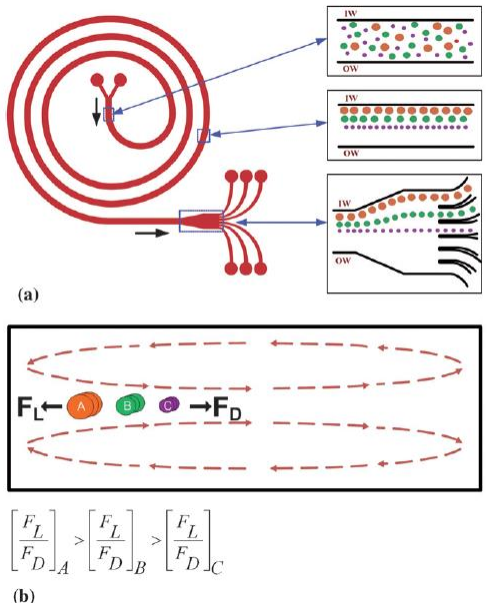

Figure 1.12: Schematic of the spiral microparticle separator based on equilibrium between Lift Force (F_L) and Drag Force (F_D) at different positions for different particle sizes [79].

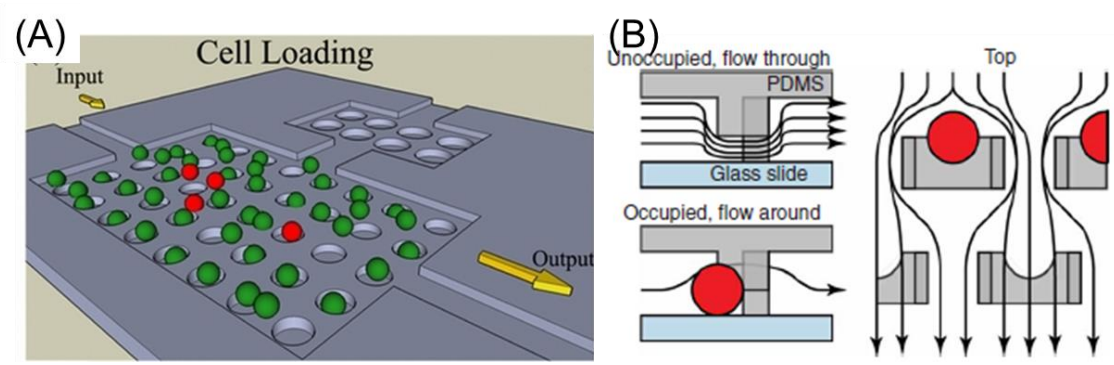

Figure 1.13: Principle of (A) microwell [81] and (B) microcup based cell trapping [83].

1.3.2.2. Electrokinetic Cell Manipulation

Electrokinetic cell manipulation depends on the phenomenon of dielectrophoresis (DEP), in which dielectric particles are polarized when placed in a non-uniform electric field [84, 85]. This polarization does not require the particle to be charged, and, overall,

the particles should be electrically neutral. The magnitude of the dielectric force generated on polarized particles depends on the electrical properties of the media and particles, the geometry of particles, and the electrical field frequency. Therefore, at a given electrical field frequency, different DEP forces will be induced on particles of different electrical properties, leading to selective manipulation of particles.

The phenomenon of DEP was first investigated by Pohl in 1951 [86]. For a homogeneous spherical particle in a conducting dielectric media, the DEP force applied onto the particle is $\vec{F}_{\mathrm{DEP}} = 2\pi\varepsilon_{\mathrm{m}} r^3 \,\mathrm{Re}[\frac{\varepsilon_{\mathrm{p}}^*(\omega) - \varepsilon_{\mathrm{m}}^*(\omega)}{\varepsilon_{\mathrm{p}}^*(\omega) + 2\varepsilon_{\mathrm{m}}^*(\omega)}] \cdot \nabla E_{\mathrm{rms}}^2$, where r is the radius of the particle, ε_{m} is the permittivity of the media, $\varepsilon_{\mathrm{p}}^*$ is the complex permittivity of the particle, $\varepsilon_{\mathrm{m}}^*$ is the complex permittivity of the media, E_{rms} is the room mean square of the electric field, and $\frac{\varepsilon_{\mathrm{p}}^*(\omega) - \varepsilon_{\mathrm{m}}^*(\omega)}{\varepsilon_{\mathrm{p}}^*(\omega) + 2\varepsilon_{\mathrm{m}}^*(\omega)}$ is Clausius-Mossotti function. When $\mathrm{Re}[\frac{\varepsilon_{\mathrm{p}}^*(\omega) - \varepsilon_{\mathrm{m}}^*(\omega)}{\varepsilon_{\mathrm{p}}^*(\omega) + 2\varepsilon_{\mathrm{m}}^*(\omega)}] > 0$, particles are attracted to the electric field intensity maxima, inducing positive DEP (p-DEP). When, $\mathrm{Re}[\frac{\varepsilon_{\mathrm{p}}^*(\omega) - \varepsilon_{\mathrm{m}}^*(\omega)}{\varepsilon_{\mathrm{p}}^*(\omega) + 2\varepsilon_{\mathrm{m}}^*(\omega)}] < 0$ particles are attracted to the electric field intensity minima, and negative DEP (n-DEP) happens [84].

Based on this principle, a variety of devices have been designed for cell manipulation. For example, platelets are the smallest cells in blood and as such, have significantly different electrical properties than other cells. Therefore, A DEP-activated cell sorter device has been reported to perform size-based fractionation of blood samples and enrichment of platelets in a continuous flow [87]. Because the DEP force on a particle has

a cubic dependence on its radius, whereas the hydrodynamic drag force under laminar flow conditions only has a linear dependence, the ratio between DEP force and drag force has a quadric dependence on cell radius. In addition, DEP force can be tuned by controlling the applied voltages, and the drag force can be modulated by altering the flow rate, so that the two forces can also be changed independently. By adjusting both flow rate and applied voltage, cells with different radii will have different deflections in the microfluidic channel, and thus can be separated (**Figure 1.14**). In another example, target cells are tagged with polystyrene beads through an antibody and antigen interaction, whereas non-target cells are not tagged [88]. After introducing an external electrical field, the dielectrophoretically labeled cells (bead bound target cells) move along the electrical field gradient. However, the non-labeled cells (non-target cells) are not affected. Therefore, the target cells are directed to the collecting channel under the combination of hydrodynamic force and dielectric force, and non-target cells are simply carried to the waste channel by the flow (**Figure 1.15**).

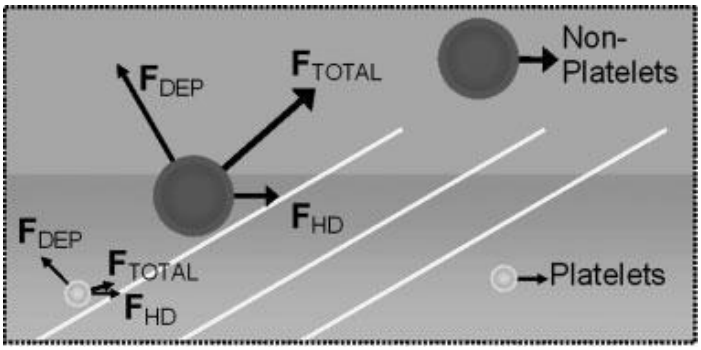

Figure 1.14: Operation principle of electrokinetic based cell manipulations according to different cell size: the larger cells experience a larger DEP force than the smaller cells causing greater deflection , and thus are separated from smaller cells [87].

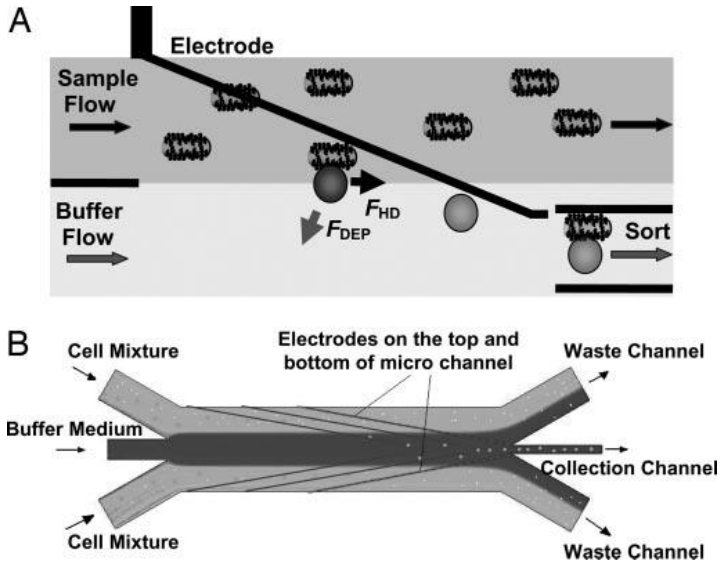

Figure 1.15: Operation principle of electrokinetic based cell manipulation according to dielectrophoretical labeling [88]: (A) cells are only deflected into the collection stream only if they are dielectrophoretically labeled. (B) Schematic of device.

1.3.2.3. Acoustic Cell Manipulation

Acoustic cell manipulation depends on the acoustic forces generated in an acoustic standing wave field [89], in which particles move toward either the pressure node or the anti-node (**Figure 1.16**), depending on the properties of particles, such as density and compressibility. According to this principle, a variety of microfluidic devices have been designed to separate cells of different size or density [89-91]. For example, a method of free flow acoustophoresis has been reported to separate micrometer-sized or smaller particles into multiple fractions in a continuous flow mode [90]. The acoustic standing wave generated by an ultrasonic transducer induces lateral displacement in the laminar flow of the microchannel, leading to a particle gradient developed across the channel

(**Figure 1.17A**). By using several outlets, particles of different size can be collected (**Figure 1.17B**).

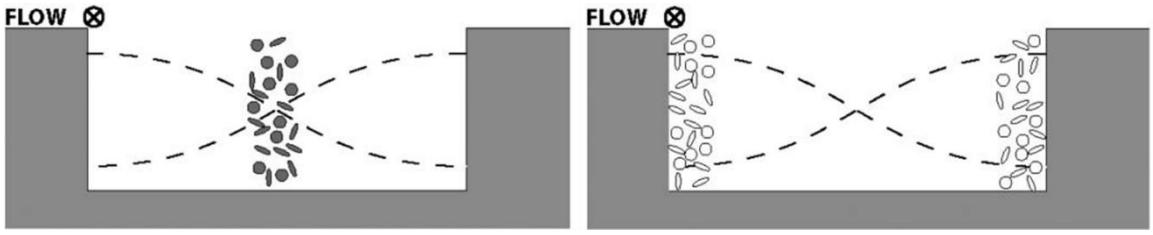

Figure 1.16: Particles positioned, by the acoustic forces, in (A) the pressure nodal plane (B) the pressure anti-nodal plane of a standing wave [89].

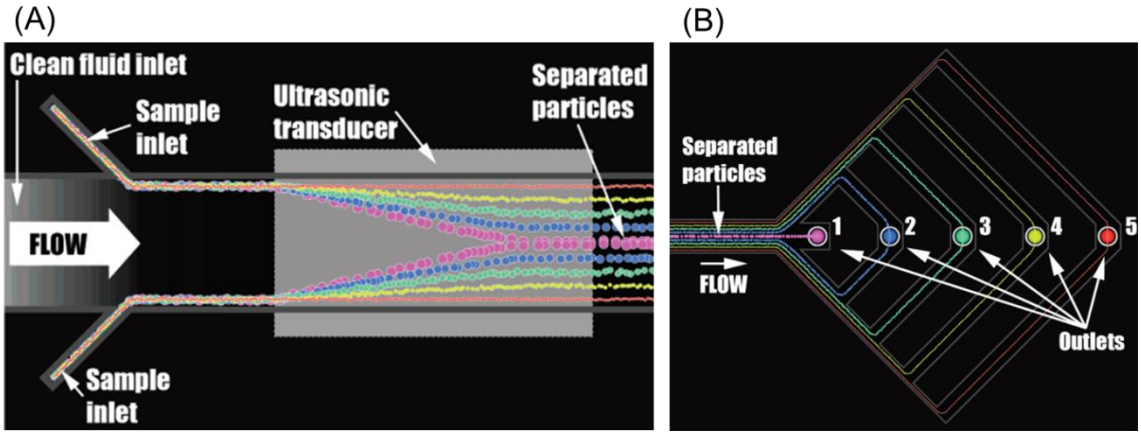

Figure 1.17: (A) Particles are moved to the center of the channel at a rate determined by their acoustic properties. (B) Fractions of separated particles are collected at five consecutive outlets. [90]

1.3.2.4. Optic Cell Manipulation

Optic cell manipulation depends on the attractive or repulsive forces generated by a highly focused laser beam. It was first used to move micrometer-sized dielectric particles in water and air [92], after which it was employed in a series of different experiments from

the cooling and trapping of neutral atoms [93] to manipulating live bacteria and viruses [94, 95]. Optical forces consist of two components: a scattering force and a gradient force [96]. The scattering force is responsible for moving microparticles along the direction of light propagation, and the gradient force is responsible for suspending microparticles. A typical experimental setup for optic cell manipulation is shown in **Figure 1.18** [96].

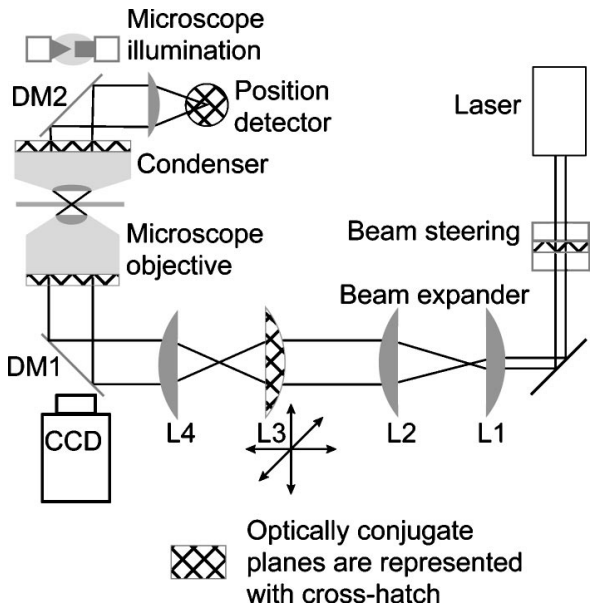

Figure 1.18: Layout of a typical cell manipulation implementation [96].

According to this principle, multiple microfluidic devices have been reported to achieve active cell manipulation [97-100]. For example, combining refractive multiple optical tweezers, microfluidics, and optical microscopy, contact-free immobilization of more than 200 yeast cells into a high-density array have been demonstrated, where the cell array can be moved to any specific region during operation (**Figure 1.19**) [97]. In another example, optical force has been used for rapid and active control of cell routing on a microfluidic chip. Cells were aligned to a narrow stream by hydrodynamic focusing, passed

through an analysis region and optical switch region, and flowed out to a waste channel. Cells identified to be target cells causes the optical switch to be activated, which deflects cell to the target output channel (**Figure 1.20**) [101].

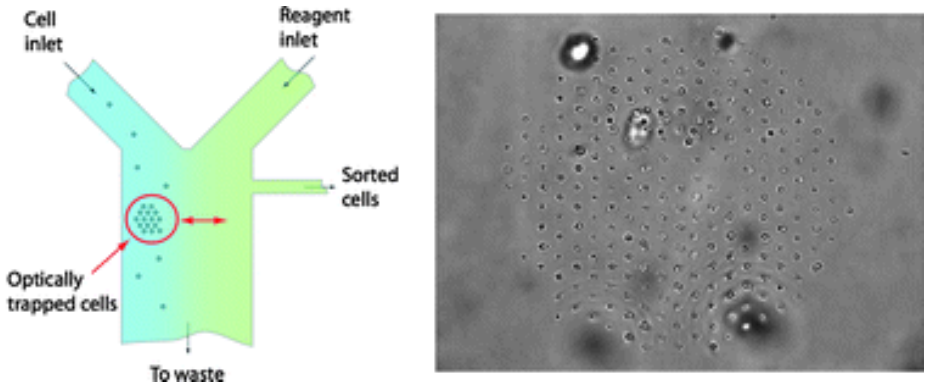

Figure 1.19: Optical cell trapping in a microfluidic device [97].

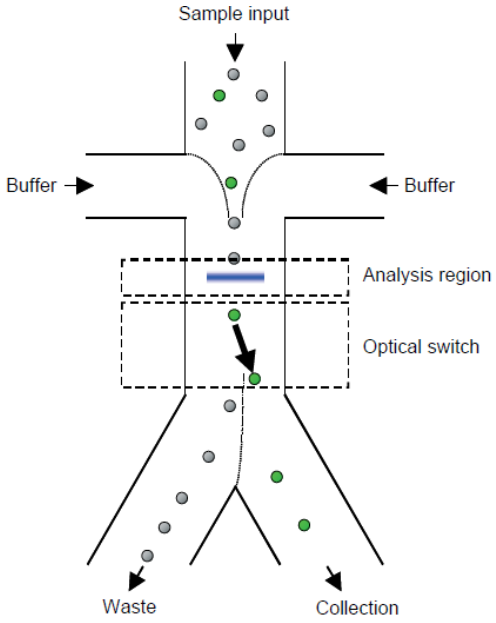

Figure 1.20: Layout of a microfluidic sorting junction and optical switch [101].

1.3.2.5. Affinity-Based Cell Manipulation

Affinity based cell manipulation is based on a highly specific interaction, such as the interaction between antigen and antibody, or receptor and ligand, and it enables target recognition. However, the application of affinity methods has some limitations. First, the interaction between probes and target cells must be much greater than the interaction between probes and non-target cells. Secondly, the immobilization of probes onto a substrate must be stable. Finally, a large effective probe area is required to enable high capture efficiency.

Antibodies are immunoglobulin found on the B cell membrane surface or in blood and other bodily fluids, and are used by the immune system to recognize and counteract foreign objects, such as bacteria and viruses. Antibodies distinguish cell types by the proteins they express. The general structures of all antibodies are very similar, and only a small region at the amino terminal end (paratope) is tremendously variable [102]. This allows the immune system to recognize an equally wide diversity of antigens [103]. The antibodies bind to unique parts of antigens, called epitopes, with a highly specific interaction [104], which allows antibodies to identify and bind only with their unique antigens in the midst of millions of different molecules that make up an organism. It enables specific cell recognition followed by manipulation.

Surface functionalization is used to immobilize cell-specific probes onto the substrate surface. Silanization is the most common method to modify various molecular functional groups to a silicon-based surface [105]. After cleaning, the surface is treated with some form of energy to generate hydroxyl groups. These reactive molecular groups can provide

a surface onto which other chemical groups can be attached. This process is usually accomplished by exposing the hydroxyl-functionalized surface to the silanization agent dissolved in a solvent (**Figure 1.21**).

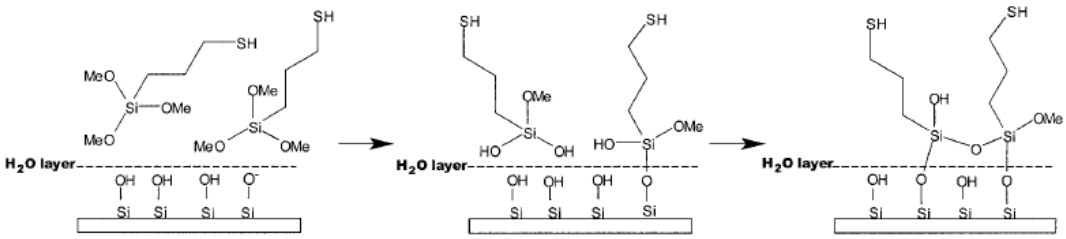

Figure 1.21: Basic process of silanization [105].

Figure 1.22 details how to immobilize a peptide, DNA, or protein on the polydimethylsiloxane (PDMS) surface, a silicon-based material, after silanization. Modification of PDMS-based microfluidic channels starts with the solution-phase oxidation reaction of PDMS surfaces (1), which is carried out by continuously passing a mixture of $H_2O/H_2O_2/HCl$ (in a volume ratio of 5:1:1) through the microchannels for 5 min. After purging the microchannels with deionized (DI) water and dry air, the hydrophilic silanol-covered PDMS surfaces (2) were obtained. The silanol-covered PDMS microchannels (2) were reacted with (3-aminopropyl) trimethoxy silane (5) to generate the amino-grafted PDMS surfaces (6). The surface-grafted amino groups were converted to the isothiocyanate groups by introducing a 0.5% (v/v) thiophosgen solution in MeCN to the microchannels (6). Again, after purging with DI water and dry air, the isothiocyanate-grafted PDMS microchannels (7) were then subjected to attachment reactions with a variety of amino-terminated biomolecules, including tripeptide RGD (arginine-glycine-aspartic acid), ssDNA and PSCA (prostate stem cell antigen) protein to produce the RGD-

grafted PDMS surfaces (8), the DNA-grafted PDMS surfaces (9), and the PSCA-grafted PDMS surfaces (10), respectively [106].

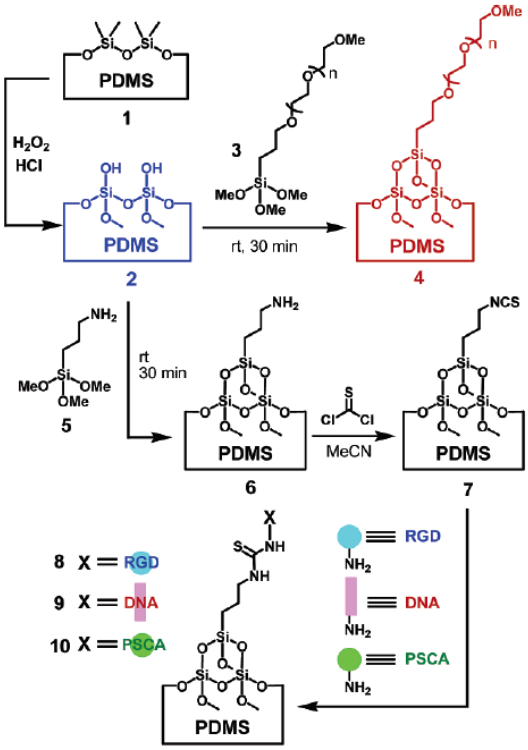

Figure 1.22: Immobilization of peptide, DNA, or protein on PDMS surface [106].

Cell capture efficiency most strongly depends on the effective area of cell-specific probe functionalized surface and the shear stress applied on cell surface [107, 108]. Biomaterial surface topography has shown to influence protein adsorption to material surface. Nanoparticles can be applied to increase the amount of probes in a certain area (**Figure 1.23**). For example, selectins are a family of cell adhesion molecules, which can be used to capture and separate CD34+ hematopoetic stem and progenitor cells and human leukemia HL60 cells from peripheral blood. Compared with direct immobilization, more

HL60 cells were captured on the selectins modified surface using nanoparticles as mediated layer (**Figure 1.24**) [107].

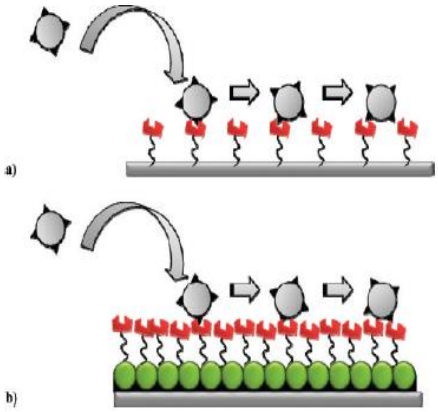

Figure 1.23: Basic principle of increasing effective area using nanoparticles [107].

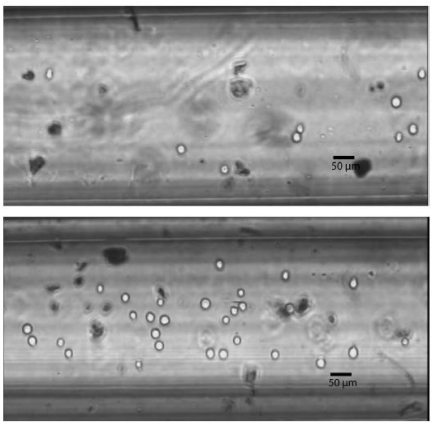

Figure 1.24: Example of nanoparticles to increase cell capture efficiency [107].

Shear stress is another important factor that affects capture efficiency. In order to optimize the required shear stress, the Hele-Shaw chamber (**Figure 1.25**) can be used to investigate dynamic cell attachment behavior at different shear stresses by creating a linear shear gradient [109]. By employing Anti-CD5 and anti-CD19 antibodies as cell capture

probes, more MOLT-3 and Raji cells were captured at lower shear stresses, respectively (**Figure 1.26**) [108].

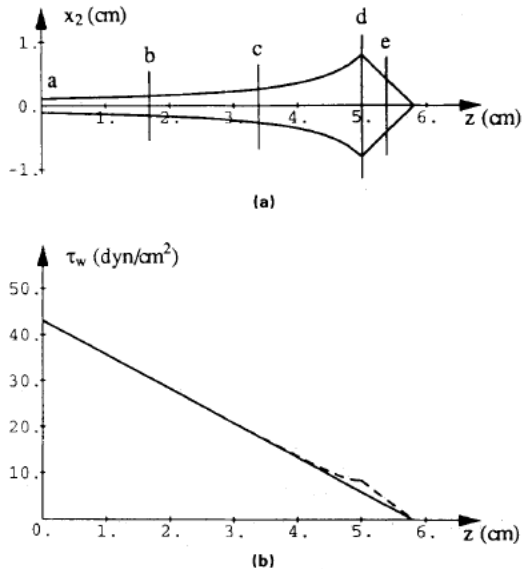

Figure 1.25: (a) Hele-Shaw chamber and (b) generated linear shear stress [109].

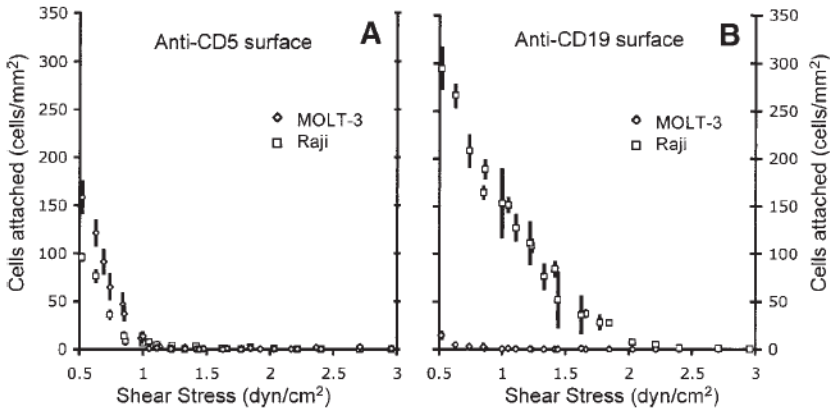

Figure 1.26: Number of cells captured under different shear stress on (a) anti-CD5 surface and (b) anti-CD19 surface [108].

According to this principle, antiepithelial cell adhesion molecule (anti-EpCAM) antibodies have been successfully immobilized onto the inner surface of a circulating tumor

cell chip (CTC-chip) containing an array of 78,000 silicon microposts with 970 mm^2 of surface area (**Figure 1.27**) [110]. This CTC-chip was able to purify spiked non-small-cell lung cancer (NSCLC) cells (NCI-H1650) in whole blood with concentration ranging from 50 to 50,000 cells/mL, and was also capable of purifying CTCs from whole blood samples donated by cancer patients, with analyzed volumes ranging from 0.9 to 5.1 mL. This work demonstrates that with proper design considerations, affinity-based methods can capture viable CTCs from whole blood sample without any preprocessing steps, and can be used in basic biological research and clinical diagnostics.

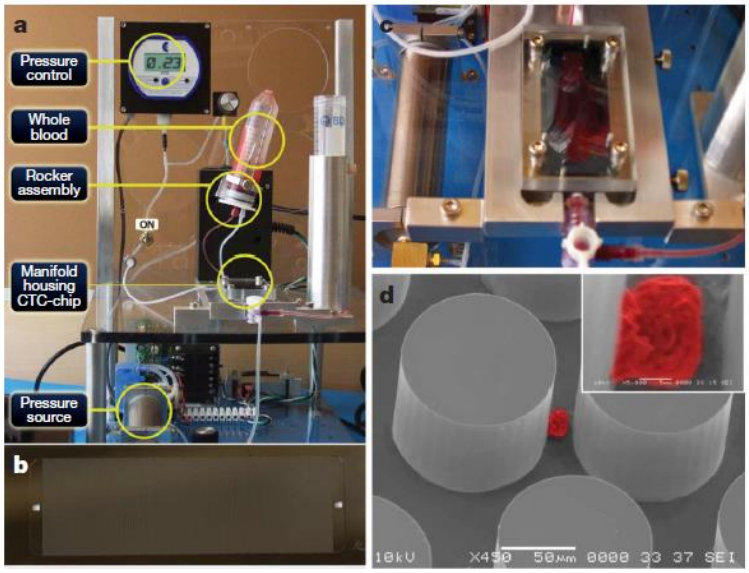

Figure 1.27: Microfluidic device for CTC isolation. a, experimental setup; b, a silicon-based CTC chip; c, whole blood sample flowing through the CTC chip; d, Scanning electron microscope (SEM) micrograph of a captured NCI-H1650 lung cancer cell [110].

Unfortunately, antibodies generally have limited stability, are expensive and time-consuming to develop [111]. Aptamers, which are oligonucleotide or peptide molecules

that bind to a specific target molecule, such as small molecules [112, 113], peptides [114], amino acids [115, 116], proteins [116], cells [117, 118], viruses [119, 120], or bacteria [121, 122], are good alternatives to antibodies. Compared with antibodies, aptamers provide a lot of advantages, such as the ability to control properties, synthetic reproducibility, biocompatibility, enhanced stability and flexible terminal modification [123], and thus are ideal specific probes for affinity-based cell manipulation, although conventional platform for developing cell-targeting aptamers are still labor-, time- and resource-intensive [124].

1.3.3. Microfluidic Aptamer Development

Aptamers are isolated from a large random sequence pool of single-stranded oligonucleotides (ssDNA or ssRNA) through an *in vitro* process known as systematic evolution of ligands by exponential enrichment (SELEX) [125-127]. A typical SELEX process for ssDNA aptamer development (**Figure 1.28**) starts from incubating a random ssDNA library of 10^{13}-10^{15} different sequences with the target. The unbound and weakly bound ssDNA is removed, leaving strongly bound ssDNA binding to the target (selection). The strongly bound ssDNA is then eluted and amplified via PCR (amplification). The amplified double strand DNA is subsequently separated into ssDNA, which is used for the next selection process. This iteration is repeated several times until the amplified ssDNA has a high binding affinity to the target.

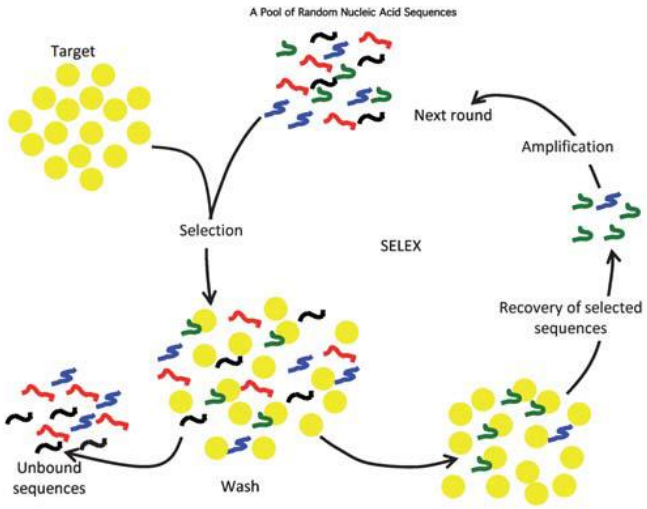

Figure 1.28: A typical SELEX process [128].

Conventional SELEX for Aptamer Development: As discussed above, a typical SELEX process includes two major steps, selection and amplification, which have been extensively explored in the field of biological research. Conventional SELEX platforms, therefore, combine different selection and amplification methods to realize the development of aptamers for a large number of target molecules.

Most current conventional SELEX processes utilize PCR to amplify the isolated sequences. Due to the designable known priming regions, PCR can rapidly and easily duplicate the separated ssDNA sequence at low cost.

The selection process commonly employs one of two separation methods: solution-based methods and solid-phase-based methods. For solution-based methods, target molecules are incubated with an ssDNA library in solution, which allows maximal binding efficiency between them. Then, the binding oligomers are separated from non-binding strands, using capillary electrophoresis [129], gel electrophoresis [130], centrifugation

[131], or electrophoretic mobility shift [132], and then used for amplification. For the solid-phase-based method, target molecules are immobilized in agarose or sepharose matrix in an affinity column [133]. The strong binding strands capture the targets, and thus remain in the column. The weak binding oligomers are removed during washing. The captured strands are then eluted by changing the environmental condition, and collected to be amplified.

These methods are labor- and time-intensive, requiring tedious pipetting steps for both selection and amplification processes, and thus cost a large amount of time and effort to successfully develop an aptamer for a single target [134]. Therefore, researchers have been investigating the integration of all necessary procedures using robotic workstations for sample and reagent dispensing [135, 136], and thus trying to eliminate human intervention during iterations. However, these automatic workstations consist of a number of expensive equipment, and require a large amount of reagents. Therefore, it is highly desired to develop a miniaturized system that can implement the whole SELEX procedure.

Microfluidic SELEX for Aptamer Development: Microfluidics, which provides better efficiency, shorter assay duration and automated reactions, has been recently investigated to address issues in conventional SELEX described above.

Hybarger and coworkers first reported a microfluidic SELEX system consisting of fused-silica microlines with surface immobilized proteins for isolation of target-binding strands, and a conventional thermal cycler for strand amplification (**Figure 1.29**) [137]. Although the system required extensive manual assembly, it proved the possibility of

performing SELEX in an integrated device and minimizing tedious manual sample transfer steps.

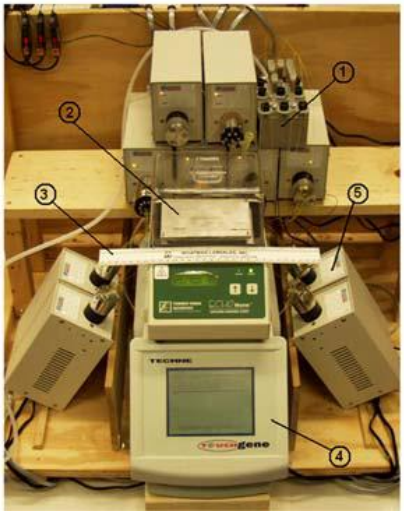

Figure 1.29: The first integrated microfluidic SELEX system prototype [137].

Since PCR in a microdevice has been well investigated since 1994 [138], researchers primarily explored the development of microfluidic device for target-binding strand selection [124, 139-141]. For example, Soh and coworkers developed a continuous flow magnetic actuated cell separation (CMACS) system to isolate weak- and un-bound oligomers (**Figure 1.30**) [139]. In their approach, targets were immobilized on magnetic beads, which were then incubated with random ssDNA library, leading to surface-bound strong binders and free weak binders. The magnetic beads were then guided to the center of the microfluidic channel through a localized magnetic field generated by surface-patterned ferromagnets. Due to the highly efficient washing provided by the continuous flow, this method could generate ssDNA aptamers with strong binding affinity in only a single round of selection.

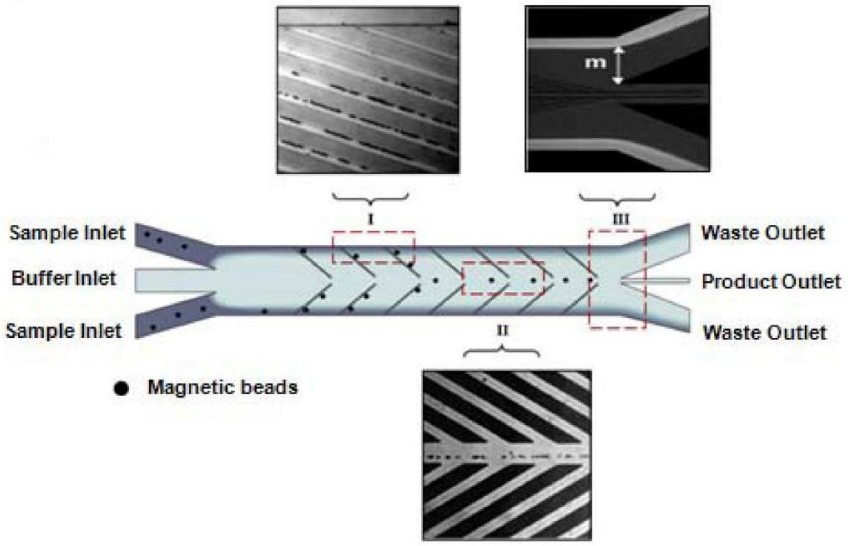

Figure 1.30: The CMACS system to isolate weak- and un-bound oligomers [139].

Recently, researchers have been working on the development of fully integrated microfluidic SELEX systems that can perform all necessary procedures without any human interference [142-146]. For example, Lee and coworkers immobilized target molecules on magnetic beads, which were retained in a single microfluidic chamber by a ferromagnet located beneath the chamber (**Figure 1.31**) [142]. The reagents, samples and products were pneumatically introduced into and sucked out of the microchamber during different stages of the SELEX process. However, the selection condition was restricted to using PCR buffer and it was unclear how to separate and collect amplified ssDNA after the amplification procedure. The use of unpurified/not well purified ssDNA significantly decreases the selection efficiency due to the competition effect, and limits the application of the microfluidic device.

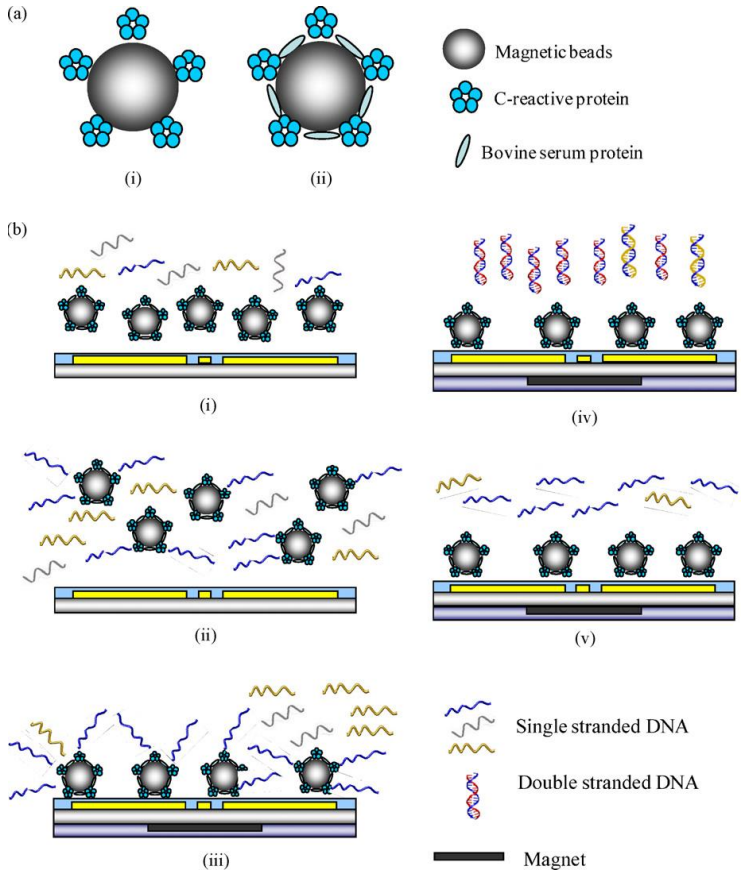

Figure 1.31: A magnetic bead based microfluidic system for integrated SELEX [142].

1.4. Objective and Significance

The completion of the Human Genome Project has enabled greater understanding of the roles of genes in human development and physiology. Applying these advances to cancer care, genetically based diagnosis can be attained by identifying genetic variations that may directly contribute to disease development of individual patients, thereby achieving one of major goals of personalized medicine [25]. On the other hand, genetic information alone may not be sufficient for personalized medicine. Diseases that are identical at the molecular level may differ at the cellular level; a drug that is effective for

one patient may not be effective for another patient with the identical genotype [27]. Thus, we envision that personalized medicine could be enabled by microsystems which combine genetic analysis and drug effect screening of cancer cells for individual patients. Such microsystems would accept whole blood samples or other body fluids from individual patients, purify and retrieve tumor cells, and then identify genetic variation and perform anti-cancer drug screening.

This thesis addresses the development of MEMS-based microfluidic devices toward personalized cancer medicine. Focusing on SNP genotyping, cell array formation, specific enrichment and nondestructive retrieval of cells using aptamers, and synthetic isolation of cell-targeting aptamers on microfluidic surfaces, these devices provide critical analytical capabilities required by genetic variation identification and cell manipulation at the individual patient level, and can hence be used as building blocks to ultimately realize fully integrated microsystems for personalized cancer diagnostics and therapeutics.

1.5. Contributions of Thesis Research

Allele-specific primer extension based SNP genotyping: Two microfluidic approaches have been developed to achieve high-throughput and multiplexed SNP genotyping. The bead-based approach uses solid-phase-based reactions in a single microchamber, in which all the reactions, including polymerase chain reaction (PCR), allele specific single base extension (SBE) and desalting, are performed. The easy design, fabrication and operation of the microfluidic device enable high-throughput detection of SNPs. Meanwhile, the solution-based approach integrates SBE, solid-phase purification (SPP), chemical cleavage and reverse-phase desalting onto a single microfluidic device.

Along with the employment of mass-tagged dideoxynucleotides, the multiplexing capability has been significantly improved. This microfluidic device is amenable to parallelization, and can be ultimately produced in array format to allow simultaneous analysis of samples from a large number of different sources, such as different patients.

Aptameric specific cell capture and temperature-mediated cell release: We employed aptamers to achieve specific cell capture on microfluidic surfaces. More importantly, the microfluidic device has been designed to investigate the temperature dependence of binding affinity between aptamers and cells, which allows for nondestructive retrieval of target cells, eliminating the use of potentially harsh chemicals. In addition, the aptamer-cell binding reaction is reversible, making the aptamer-functionalized surface regenerative and this capture and release strategy highly repeatable. The studies presented in this thesis elucidate, for the first time, the temperature dependence of aptamer-cell binding affinity in microfluidic devices for applications such as cell purification.

Mechanically tunable cell trapping: To realize controllable cell trapping, we, for the first time, exploited the large compliance of elastomers to establish a tunable cell trapping microchip. The dimensions of these microstructures can be mechanically modulated by simply inducing uniformly distributed strain via the application of an external force on the chip, so as to precisely control the number of cells captured at the single and individual cell level.

Development of cell-specific aptamers: To synthetically isolate cell-targeting aptamers from a randomized ssDNA library, we developed a microfluidic device that

integrates cell culturing with affinity selection of cell-binding ssDNA, which is then amplified by bead-based PCR. The on-chip cell culturing provides an ideal approach for cell membrane protein regeneration, as well as restraining cells in the selection chamber. The bead-based PCR significantly facilitates the ssDNA separation after the amplification process, eliminating the contamination of complementary strands. In addition, transfer between the selection and amplification chambers using pneumatic controlled pressure-driven flow realizes multi-round aptamer isolation on a single chip, as well as reducing potential damage to cells caused by electrical fields in our previous work.

1.6. Organization of Thesis

In this thesis, we focus on the development of key technologies for microfluidic cell manipulation, genetic analysis, and selection of aptamers specific to cells. Following this introduction, Chapter 2 develops a bead-based genotyping approach to detect single-base mutations associated with sickle cell anemia, in a single chamber. Chapter 3 designs, fabricates and optimizes an integrated microsystem for multiplex SNP genotyping. Compared with the bead-based approach developed in Chapter 2, this multi-step solution-based approach utilizes the mass-tagged dideoxyribonucleotides for SBE and integrates the functions of sample purification and desalting on solid-phase surfaces, and thus has an improved single-to-noise ratio and enhanced multiplexing capability. Chapter 4 investigates the temperature response of binding affinity between surface-immobilized aptamers and cells, which demonstrates the feasibility of using aptamers to specifically separate target cells from a heterogeneous solution and employing environmental changes to retrieve purified cells. Based on this technique, Chapter 5 explores the spatially specific

capture and selective temperature-mediated release of cells using the same aptamers, which provides the potential to establish cell arrays on pre-defined regions and to only collect interested cell groups for downstream analysis. Chapter 6 presents a tunable microfluidic device for physically modulated cell trapping, which enables the trapping of various numbers of cells using a unique device. Chapter 7 describes the design and some preliminary results for a hydrodynamic based SELEX platform for cell-specific aptamer development, in which multiple rounds of SELEX have been successfully performed. Conclusion and future work are presented in Chapter 8.

Chapter 2. Microfluidic Genotyping of Single-Nucleotide Polymorphisms: a Bead-Based Approach

In this chapter, a bead-based single-nucleotide polymorphism (SNP) genotyping device is presented. Polymerase chain reaction (PCR), allele specific single-base extension (SBE), and desalting on microbeads are performed in a single microchamber situated on a temperature control chip, which is coupled with matrix-assisted laser desorption/ionization time-of-flight mass spectrometry (MALDI-TOF MS) to analyze the SBE product. Experimental results from genotyping of the SNP on exon 1 of HBB gene, which causes sickle cell anemia, demonstrate the potential of the device for rapid, accurate, multiplexed and high-throughput detection of SNPs. The work presented in this chapter has resulted in a peer-reviewed conference proceeding [147] and a journal publication [148].

2.1. Introduction

Genetic mutations take many forms, ranging from chromosome anomalies to single-base substitutions [149]. Among them, SNPs, which are single nucleotide variations in the genome between different individuals, are the most common form, occurring approximately once every 1000 bases [150]. SNPs can be used as genetic markers to identify genes associated with complex disease [151, 152]. Therefore, accurate identification of SNPs is of great utility to disease diagnosis and prognosis [153-155].

Genotyping of SNPs can be based on enzymatic cleavage, allele specific hybridization, allele specific ligation or cleavage, and allele specific primer extension [49]. Enzymatic cleavage, illustrated in Invader® Assays [52, 53], utilize thermostable flap endonucleases

(FEN) and fluorescence resonance energy transfer (FRET) to recognize and detect SNP by the annealing of allele-specific overlapping oligonucleotides to the target DNA. While it is highly accurate, this method is generally time-consuming and difficult to multiplex (i.e., to detect multiple SNPs in one reaction). Allele-specific hybridization, used for example in the Affymetrix® Human SNP Array [55], is based on matched or mismatched probes annealing to the target DNA sequence adjacent to the SNP site [155]. This method allows detection of up to 2 million SNPs simultaneously, but it requires labor-intensive genomic DNA (gDNA) digestion, fractionation and amplification, and is prone to unspecific binding that leads to false positives [156]. Allele-specific ligation or cleavage combines the hybridization of probes specific to the target DNA sequence and the specificity of the ligase enzyme (e.g., SNPlex™ Assay [157]) or 5' nuclease (TaqMan® Assay [157]) to distinguish matched or mismatched nucleotides. These assays have a very high level of specificity, but their applicability is hindered by slow reaction speeds and the limited number of modified probes available [49]. Allele-specific primer extension, which involves allele-specific incorporation of nucleotides during primer extension [49, 50], is an emerging SNP genotyping method that offers flexibility and robustness. The discrimination between different incorporated nucleotides is based on either fluorescence (e.g., Illumina® Infinium Assays [158]) or mass spectrometry (e.g., Sequenom® iPlex Assays [60]). While rapid, accurate and capable of multiplexing, they require complicated design of primers and fluorescent-tagged or mass-tagged nucleotides [159, 160]. There is hence a strong need for new genotyping platforms to address these issues.

Microfluidics technology can potentially enable fast, low-cost, and automated SNP detection with improved sensitivity, resolution, accuracy, efficiency and throughput, as well as minimized sample consumption [62]. The aforementioned genotyping principles have been implemented in microfluidic systems to generate modified DNA indicative of SNPs, which is then detected by methods such as electrophoresis and bioluminescence [62, 161]. Electrophoresis, in which an applied electric field separates DNA fragments by charge-to-mass ratio, provides high accuracy with reduced buffer and sample consumption, but has limited potential in high throughput and multiplexed genotyping [63]. Alternatively, bioluminescent methods utilize fluorescent probes to provide either high sample throughput [162-165] or high accuracy [166] along with enhanced sensitivities and reduced time, sample and reactant consumption, but are limited by false positives and an inability to multiplex. Therefore, more research is needed to develop microfluidic SNP detection systems that offer improved accuracy, ability to multiplex, and increased throughput.

This chapter presents a bead-based SNP genotyping approach using solid-phase based reactions in a single microchamber on a temperature control chip. PCR, allele specific SBE and desalting on microbeads are performed in the single microchamber, and are coupled with MALDI-TOF MS to identify SBE products. The use of SBE and MALDI-TOF MS provides the possibility of accurate, fast and multiplexed detection [167-169]. The single chamber design eliminates the use of on-chip valves, resulting in greatly simplified fluid handling, and integration of PCR with SBE on-chip has the potential to improve assay efficiency. Miniaturization reduces sample and reagent consumption, and when

implemented in array format, this integrated SNP detection approach can potentially allow parallelized and high-throughput analysis of patient samples. We demonstrate this bead-based SNP genotyping approach by detecting the SNP on exon 1 of HBB gene located in chromosome 11, which alters the sixth amino acid in the beta hemoglobin to cause sickle cell anemia, a life-threatening disorder [170].

2.2. Principle and Design

2.2.1. Principle of Bead-Based SNP Genotyping

Our bead-based SNP genotyping method performs PCR, SBE, and desalting reactions on microbeads in a single microchamber. The chamber is first packed with polymer microbeads that are functionalized with reverse primers via a biotin-streptavidin link and mixed with the target template DNA and PCR reagents, followed by thermal cycling to generate double-stranded DNA (dsDNA) (**Figure 2.1A&B**), which is then purified by a buffer wash (**Figure 2.1C**). By introducing NaOH solution, template single-strand DNA (ssDNA) is chemically eluted, leaving ssDNA complementary to the template on the microbeads (**Figure 2.1D**) to be analyzed in the following steps. Subsequently, SBE reactants are introduced, and allele-specific primers anneal to the complementary strand immediately adjacent to the polymorphic site. These primers then undergo SBE, by thermally cycling the reaction mixture in the presence of dideoxyribonucleotide triphosphates (ddNTPs) and enzyme, to generate primers extended by only one base (**Figure 2.1E**) [169]. Washing with deionized water (DI water) then removes free primers, salts and any other impurities for purification of the bead-bound extended and unextended

allele-specific primers (**Figure 2.1F**). The additional nucleotide is then identified according to the difference in mass between the extended and unextended primers.

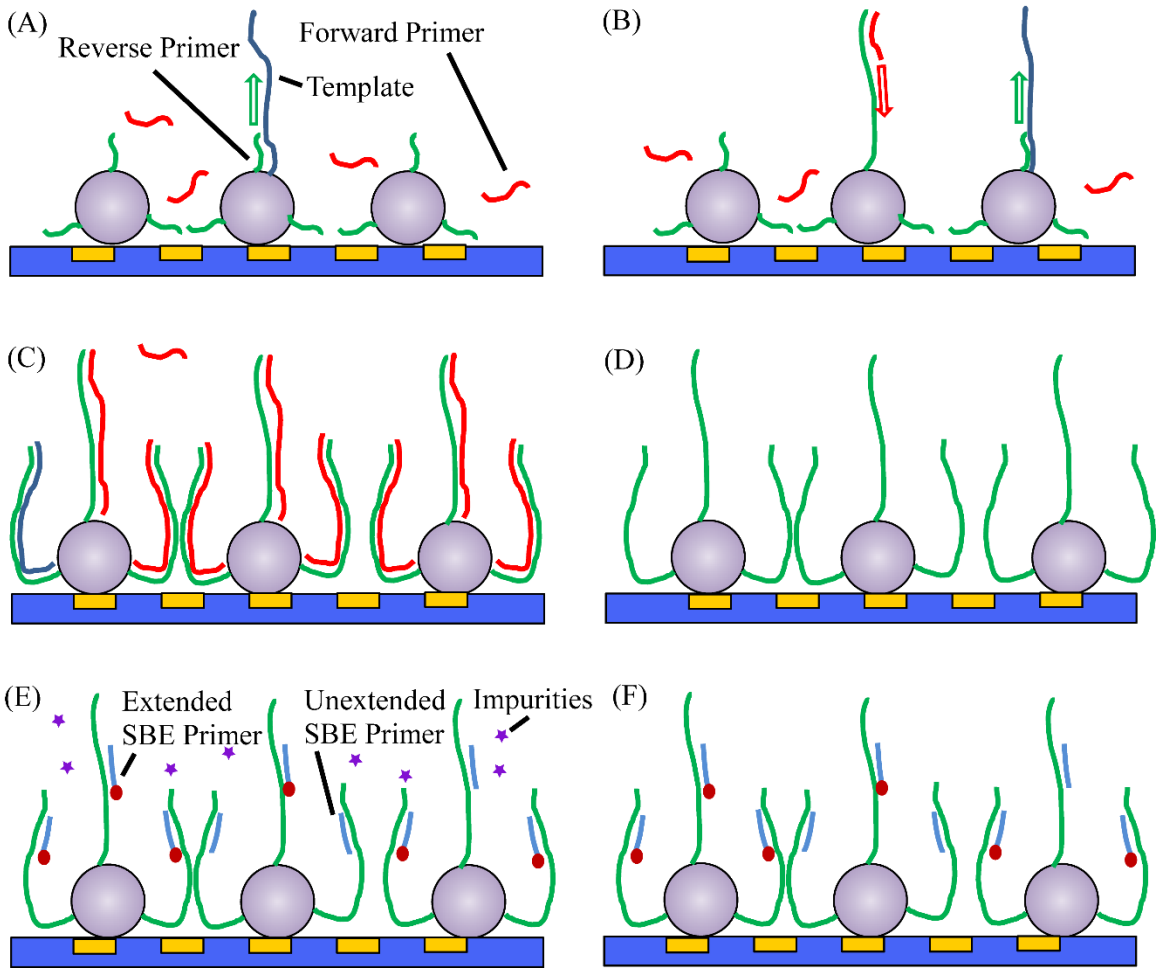

Figure 2.1: Principle of bead-based SNP detection. (A) The first cycle of PCR on bead-immobilized reverse primers generates dsDNA. (B) Additional PCR cycles generate dsDNA. (C) A buffer wash purifies bead-bound dsDNA. (D) Template ssDNA is chemically eluted from beads. (E) SBE is performed on bead-bound ssDNA complementary to the template. (F) The SBE product is purified and then desalted for subsequent MALDI-TOF MS detection.

2.2.2. Design and Fabrication

The microfluidic device used to demonstrate the bead-based SNP genotyping approach consists of a polydimethylsiloxane (PDMS) microchamber situated on a temperature control chip integrated with a micro heater and temperature sensor (**Figure 2.2A&B**). The tapered microchamber (**Figure 2.2A&B**, 150 µm in height) with an approximately 5 µL volume contains dam-like structures (**Figure 2.2A&B**, 15 µm in height), called weirs, to retain microbeads (50 - 80 µm in diameter) during wash steps. The surfaces of microchamber are coated with Parylene C to prevent evaporative loss of reactants [171]. On the temperature control chip, a resistive sensor (16.5 mm L × 50 µm W) is located beneath the center of the chamber, and a resistive serpentine-shaped heater (296 mm L × 500 µm W) surrounds the temperature sensor. Thus, the chamber is heated with its temperature near the center measured by the sensor to complete a closed-loop temperature control setup.

The temperature control chip was first fabricated using standard microfabrication techniques. Briefly, a glass slide (Fisher HealthCare, Houston, TX) was cleaned by piranha. Chrome (10 nm) and gold (100 nm) thin films were deposited by thermal evaporation and patterned by wet etching. Then, a passivation layer of 1 µm of silicon dioxide was deposited using plasma-enhanced chemical vapor deposition (PECVD). Finally, the on-chip temperature sensor and heater were equipped with contact pads (2.5 mm × 2.5 mm, also fabricated from gold), which were opened by etching the oxide layer using hydrofluoric acid and connected to measurement instruments via wire bonding (**Figure 2.2C**).

In parallel, the microfluidic chamber was fabricated from PDMS (Sylgard 184, Dow Corning Inc. Midland, MI) using soft lithography techniques. SU-8 photoresist (MicroChem Corp., Newton, MA) was spin-coated and patterned on a silicon wafer to form mold-defining microfluidic features. Next, a PDMS prepolymer solution (base and curing agent mixed in a 10:1 ratio) was cast onto the mold and cured on a hotplate at 72 °C for 1 hour (**Figure 2.2D**).

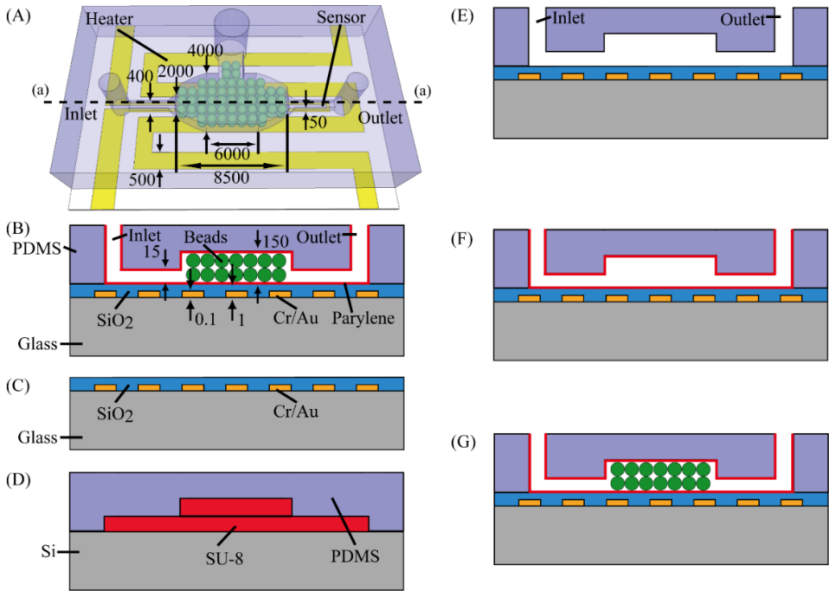

Figure 2.2: (A) Schematic of the bead-based SNP genotyping device. (B) Cross-sectional view along line a-a illustrating the layered structure of the device. (C) - (G) Fabrication process for the device: (C) Deposition, patterning and passivation of gold sensor and heater; (D) Fabrication of SU-8 mold; (E) Demolding of PDMS microchamber, and bonding between microchamber and temperature control chip; (F) Deposition of Parylene C; (G) Packing of streptavidin beads.

Subsequently, the inlet and outlet were punched on the resulting sheet bearing the microfluidic features, which was then bonded to the temperature control chip after treatment of the bonding interfaces with oxygen plasma for 15 seconds (**Figure 2.2E**).

Finally, the surface of the microchamber was coated with a thin layer of Parylene C via chemical vapor deposition (**Figure 2.2F**), prior to packing streptavidin beads (**Figure 2.2G**). An image of a fabricated device is shown in **Figure 2.3**.

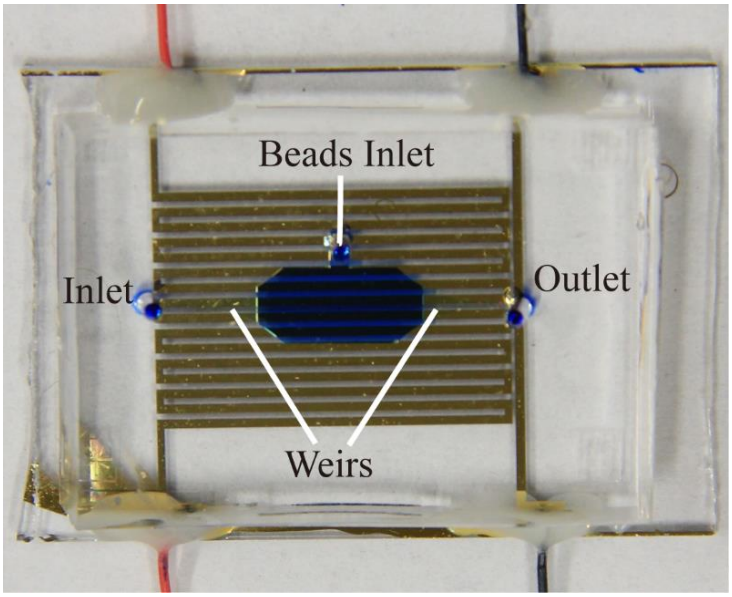

Figure 2.3: Photograph of a fabricated device.

2.3. Experimental

2.3.1. Materials

All chemicals were purchased from Sigma-Aldrich (St. Louis, MO) unless otherwise indicated. Streptavidin beads (Pierce Streptavidin Plus UltraLink Resin) were obtained from Thermo Fisher Scientific Inc. (Rockford, IL). ddNTPs were purchased from Jena Bioscience GmbH (Jena, Germany). Deoxyribonucleotide triphosphates (dNTPs) and

GoTaq Flexi DNA Polymerase were obtained from Promega Corp. (Madison, WI). Thermo Sequenase was purchased from GE Healthcare (Piscataway, NJ). Template DNA, including a mutated type (5'-CCT CAC CAC CAA CTT CAT CCA CGT TCA CCT TGC CCC ACA GGG CAG TA***A CGG CAG ACT TCT CC<u>A</u>*** CAG GAG TCA GAT GCA CCA TGG TGT CTG TTT GAG GTT GCT AGT GAA CAC AGT TGT GTC AGA AGC AAA TGT AAG CAA TAG ATG GCT CTG CCC TGA CT-3', the SNP site is underlined and SBE primer annealing site is italic) and an unmutated type (5'-CCT CAC CAC CAA CTT CAT CCA CGT TCA CCT TGC CCC ACA GGG CAG TA***A CGG CAG ACT TCT CC<u>T</u>*** CAG GAG TCA GAT GCA CCA TGG TGT CTG TTT GAG GTT GCT AGT GAA CAC AGT TGT GTC AGA AGC AAA TGT AAG CAA TAG ATG GCT CTG CCC TGA CT-3', the SNP site is underlined and SBE primer annealing site is italic) of the HBB gene, double biotin modified reverse primer (5'-double biotin-AGT CAG GGC AGA GCC ATC TA-3'), fluorescein amidite (FAM) modified forward primer (5'-FAM-CCT CAC CAC CAA CTT CAT CC-3', M.W. = 6651), and SBE primer (5'-ACG GCA GAC TTC TCC-3', M.W = 4513) were synthesized and purified by Integrated DNA Technologies (Coralville, IA).

2.3.2. Experimental Setup

Closed-loop temperature control of the microchamber was achieved using the integrated temperature sensor, heater, and the fan under the temperature control chip with a proportional-integral-derivative (PID) algorithm implemented in a LabVIEW (National Instruments Corp., TX) program on a personal computer. The resistance of the sensor was measured by a digital multimeter (34420A, Agilent Technologies Inc., CA), and the heater

and fan were connected to two DC power supplies (E3631, Agilent Technologies Inc., CA) respectively. The inlet was connected to a syringe that contained reaction buffer or washing buffer driven by a syringe pump (KD210P, KD Scientific Inc., MA). The outlet was connected to a microcentrifuge tube for collection of genotyping product to MALDI-TOF MS or experimental waste. All fluorescent images of beads were taken using an inverted epifluorescence microscope (Diaphot 300, Nikon Instruments Inc., NY) with a CCD camera (Model 190CU, Micrometrics, NH), after removing the device from the fan (**Figure 2.4**).

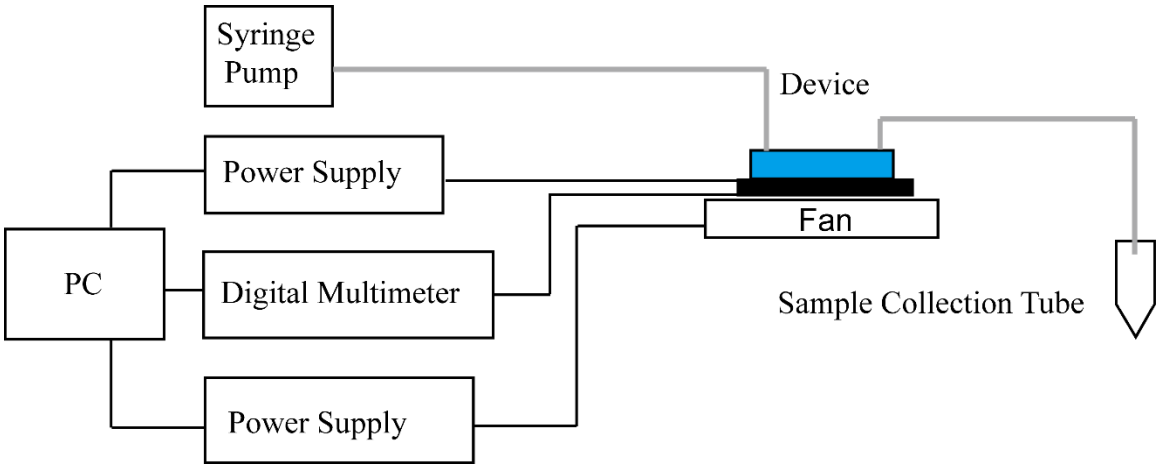

Figure 2.4: Experimental setup for bead-based SNP genotyping.

2.3.3. Experimental Procedure

Just prior to experimentation, the streptavidin beads in the microchamber were rinsed with binding and washing (B&W) buffer (5 mM Tris-HCl, 0.5 mM EDTA, 1 M NaCl, and 0.01% Tween 20, pH=7.5). The reverse primer (50 pmol) in B&W buffer was introduced and incubated with the beads for 30 min, followed by washing with B&W buffer at 10 μL/min for 10 min.

Bead-based PCR was performed for 30 thermal cycles as follows: 95 °C for 15 s, 56 °C for 30 s, and 72 °C for 30 s. A 5 μL sample of PCR reactants was introduced twice, prior to cycling and between 15th and 16th cycle, and each sample consisted of 0.08 pmol of template, 8.33 pmol of forward primer, 1× GoTaq Flexi Buffer, 0.83 units of GoTaq Flexi DNA Polymerase, 1.67 nmol of dNTP and 6.25 nmol of $MgCl_2$ (1.25 mM). The microbeads were then rinsed with 0.15 mM NaOH in B&W buffer at 5 μL/min for 10 min to elute template ssDNA, followed by a rinse of pure B&W buffer at 10 μL/min for 10 min, leaving complementary strand on the beads.

To perform SBE, the SBE primer targeting the SNP on the complementary sequence of exon 1 of the HBB gene was extended by a single base in the microchamber using ddNTPs. A 5 μL sample of SBE reactants was introduced to the microchamber twice, prior to SBE and between 5th and 6th thermal cycle, and underwent 10 thermal cycles as follows: 90 °C for 15 s, 40 °C for 30 s, and 70 °C for 30 s. Each SBE reactant consisted of 6.67 pmol of primer, 16.67 pmol of ddNTP, 1× Thermo Sequenase reaction buffer and 2.67 units of Thermo Sequenase.

The microchamber was then rinsed using B&W buffer at 5 μL/min for 10 min, followed by desalting with DI water at 5 μL/min for 20 min. Finally, the microchamber was incubated at 95 °C for 1 min, followed by a rinse with DI water at 20 μL/min and 95 °C for 3 min, to elute the hybridized primer.

2.4. Results and Discussion

This section presents and analyzes experimental results from the fabricated bead-based SNP genotyping device. We first characterize the temperature control chip. Then, bead-based PCR, chemical elution, *in-situ* desalting and thermal elution are performed using exon1 of the HBB gene to characterize each functional unit. Finally, the integrated procedure is executed on-chip to demonstrate successful SNP genotyping.

2.4.1. Temperature Control Characterization

The temperature-resistance relationship of the thin-film gold temperature sensor was calibrated following fabrication. The experimental data showed that the measured resistance (R) of the sensor exhibited a highly linear relationship with temperature (T), which can be fitted to $R = R_0 [1 + \alpha (T - T_0)]$, where R_0 is the sensor resistance at reference temperature T_0, and α is the temperature coefficient of resistance (TCR) of the sensor. The TCR was determined to be 3.06×10^{-3} °C^{-1} for a typical chip, which had a reference resistance of 83.44 Ω at a reference temperature of 21.9 °C. Time-resolved tracking of on-chip thermal cycling showed that the chamber temperatures attained specified setpoints via control of the on-chip heater and off-chip fan quickly and precisely (**Figure 2.5**). The thermal time constant of a typical temperature control chip was 126 s based on an exponential fit. The time constants of closed loop temperature control (based on an exponential fit) were 1.4s for heating from 56°C to 72°C, 1.9 s for heating from 72 °C to 95 °C and 8.7 s for cooling from 95 °C to 56 °C, which represented a significant improvement over typical time responses of conventional PCR thermal cyclers (e.g., 6s for heating from 56°C to 72°C, 8 s for heating from 72 °C to 95 °C, and 16 s for cooling from

95 °C to 56 °C for the Eppendorf Mastercycler® Personal used in our related experiments below).

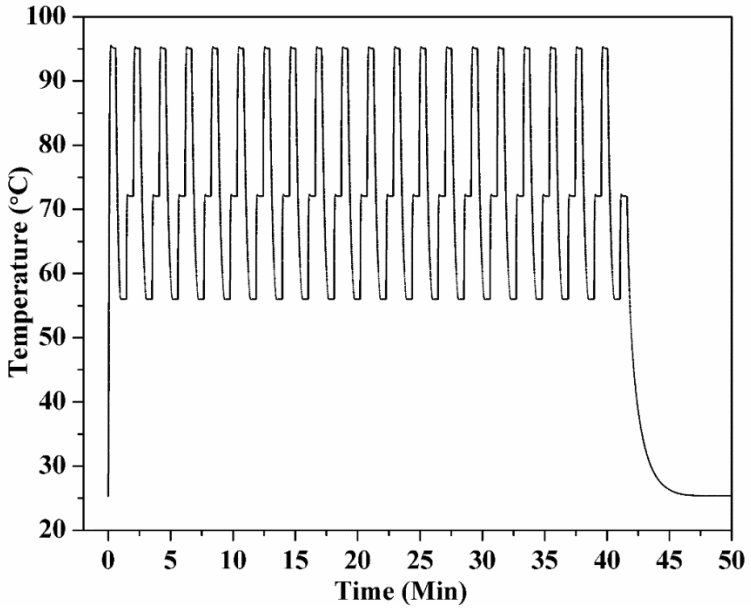

Figure 2.5: Time-resolved tracking of the chamber temperature.

2.4.2. Characterization of Bead-Based PCR and Chemical Elution

To characterize bead-based PCR, reactants were thermally cycled on-chip and fluorescent bead intensity was then measured and compared to control tests. To obtain consistent results under controlled experimental conditions, template DNA was used as the target sequence for the characterization. After B&W buffer washing, the fluorescent intensity of beads was significantly higher than those without thermal cycling, enzyme or templates, which were only 5%, 7% and 16% of the original test (**Figure 2.6A**). This indicates that the bead-based PCR process did amplify template DNA and that the fluorescently modified primer enables monitoring of this step of the SNP genotyping procedure [172].

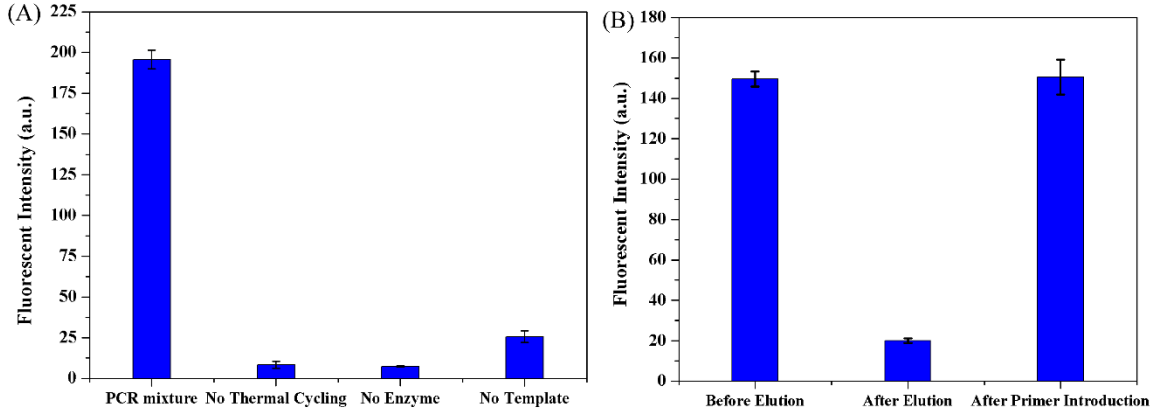

Figure 2.6: (A) Characterization of bead-based PCR: fluorescent intensity of beads with different PCR parameters, measured in arbitrary units (a.u.). (B) Verification of removal of template ssDNA by NaOH: fluorescent intensity of beads before and after rinsing with NaOH, and after introduction of FAM-modified forward primers. Error bars represent standard deviations based on four independent measurements of fluorescent microbeads.

Prior to SBE, template ssDNA generated during PCR must be removed from the bead-bound complementary strand. To test the efficiency of the chemical elution method, the template ssDNA was first amplified using fluorescently labeled forward primers and double biotinylated reverse primers in a conventional thermal cycler, and the amplification product was immobilized onto the streptavidin beads, which were packed in the microchamber afterwards. The fluorescent intensity of the beads was then measured before and after rinsing with buffer containing 0.15 mM NaOH. The fluorescent intensity of rinsed beads was 87% lower than that of pre-elution beads (**Figure 2.6B**), indicating that most template ssDNA had been removed from the bead surface. To further demonstrate that the template ssDNA had been removed from the beads, rather than the dsDNA, 5 μL of 5 μM

FAM-modified forward primers in 1× PCR buffer was introduced into the microchamber. After incubating at 56 °C for 1 min, followed by washing with B&W buffer, the fluorescent intensity of the beads was similar to that before introduction of the NaOH elution (**Figure 2.6B**), which suggested that complementary strand remained bound to the beads following the elution of template ssDNA. These results indicate a sufficiently high on-chip chemical elution efficiency using NaOH.

2.4.3. Verification of Thermal Elution and *In-Situ* Desalting

To generate a DNA solution prior to detection with MALDI-TOF MS, hybridized primers must be desalted and then thermally eluted into DI water. The effect of desalting and the efficiency of the thermal elution method were tested to ensure that DNA loss during this step would not compromise detection by MS. The fluorescently labeled forward primer in B&W buffer was first hybridized to the ssDNA on the beads and desalted with DI water. The fluorescent intensity of the beads was then measured before and after rinsing at 95 °C, and the elution product was manually pipetted to a MALDI plate and tested using MALDI-TOF MS. During desalting, the microchamber was rinsed with DI water, and the fluorescent intensity remained at 95.5% of pre-desalting intensity (**Figure 2.7A**). The chamber temperature was then elevated to elute hybridized primers. After elution, the fluorescent intensity of the beads was only 26% of pre-desalting intensity and 28% of pre-elution intensity (**Figure 2.7A**). To control for effects of temperature on fluorescent intensity, fluorescently labeled microbeads were heated in the thermal cycler for different durations. As shown in **Figure 2.7B**, it was obvious that heating for 4 min did not generate a noticeable change in fluorescent intensity, which showed that the intensity of the

fluorescent label was stable in response to elevated temperatures, and that elution of primers was indeed the reason for the decrease in fluorescent intensity. Furthermore, following MALDI-TOF MS, a distinct mass spectral peak at 6651 m/z (**Figure 2.7C**) indicated effective desalting efficiency, showing the promise of using this method to desalt and elute genotyping products. The repeated experiments have shown similar results, from all of which the mass spectral peaks can be recognized consistently. These results demonstrate effective *in-situ* desalting and efficient thermal primer elution.

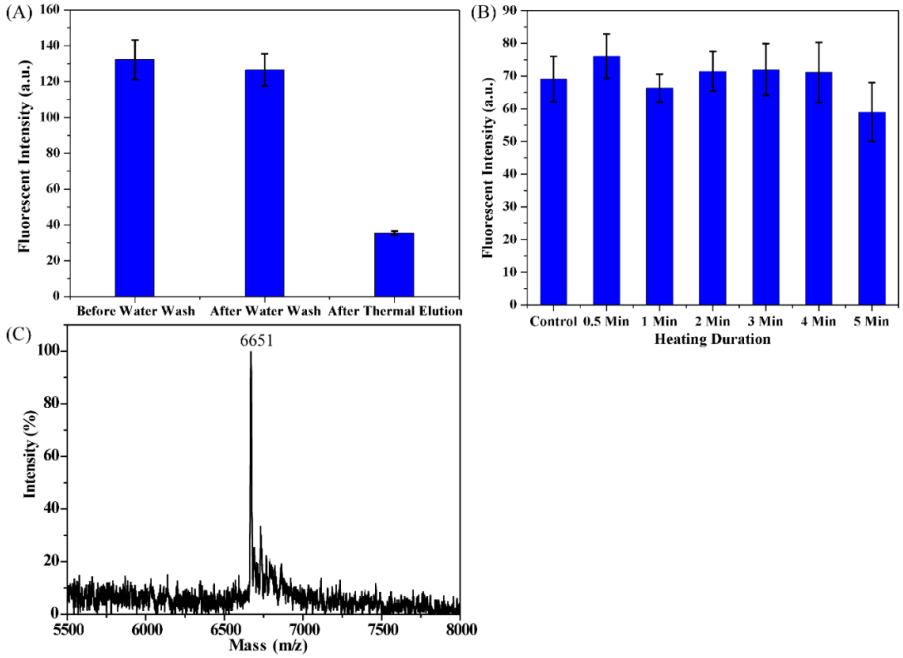

Figure 2.7: Verification of thermal elution and *in-situ* desalting. (A) Fluorescent intensity of beads before desalting, after desalting and after denaturation procedure. (B) Fluorescent intensity of FAM-labeled microbeads following heating. (C) A MALDI-TOF mass spectrum of thermally eluted FAM-modified forward primers. Error bars represent standard deviations based on four independent measurements of fluorescent microbeads.

2.4.4. Integrated SNP Detection

Having tested the individual procedures necessary for SNP detection, the procedures were integrated and the SBE products were analyzed using MALDI-TOF MS. Theoretically, the mass of extended primer can be calculated according to the equation $m_p = m_r + m_n - m_b$, where m_p is the mass of extended primer, m_r is the mass of unextended primer, m_n is the mass of corresponding ddNTP and m_b is the mass of bond formation (175 m/z). We detected SNPs on both mutated HBB gene and unmutated HBB gene. As the target nucleotides of the mutated and unmutated template DNA are adenosine and thymidine, a single dideoxyadenosine triphosphate (ddATP, M.W. = 472) and dideoxythymidine triphosphate (ddTTP, M.W. = 463) were incorporated into each primer, respectively. Thus the mass of the product for mutated and unmutated HBB gene were respectively expected to be 4810 Daltons (4513+472-175), as shown by the distinct peak at 4810 m/z in **Figure 2.8A**, and 4801 Daltons (4513+463-175), as shown by the peak at 4801 m/z in **Figure 2.8B**. The peak located at 4513 m/z in both **Figure 2.8A** and **Figure 2.8B** was induced by unextended primers, which would not compromise the identification of the nucleotide at a SNP site. Repeated experiments on genotyping of both mutated and unmutated HBB gene has shown similar mass spectra consistently, indicating successful SNP detection.

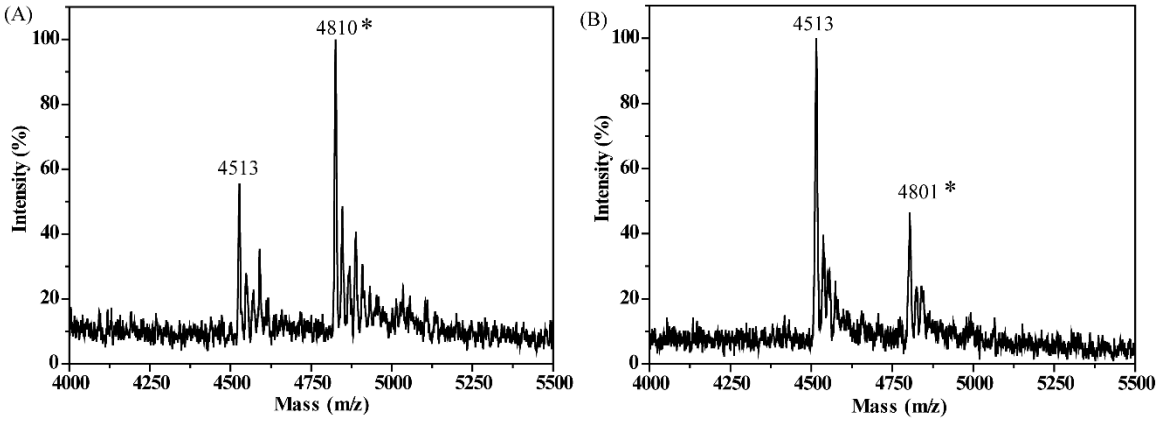

Figure 2.8: MALDI-TOF mass spectrum of SNP detection product with all operations integrated. (A) Mass spectrum of genotyping mutated HBB gene. (B) Mass spectrum of genotyping unmutated HBB gene. (*: extended SBE primer)

2.5. Conclusion

We have developed a bead-based genotyping approach by incorporating PCR, SBE and desalting using solid-phase-based reactions in a single microfluidic chamber, and coupling this method to MALDI-TOF MS. The device consists of a microchamber that is situated on a temperature control chip integrated with a temperature sensor and heater, and is equipped with weirs to retain microbeads during wash steps. The microchamber surfaces are coated with Parylene C to prevent sample loss. The integrated temperature sensor and heater allow closed-loop temperature control for thermal cycling and thermally induced primer elution. By employing such solid-phase-based reactions, our approach can significantly simplify fluid handling by avoid utilizing any on-chip valves, and hence potentially be applicable for high-throughput assays.

Our experiments have shown efficient on-chip thermal cycling using the device design, which enables effective bead-based PCR, SBE and thermal elution. In addition, successful chemical elution using NaOH has been achieved. Subsequently, the capability of the device to perform *in-situ* desalting using solid-phase-based reactions was demonstrated. Finally, genotyping of SNPs on both a mutated and an unmutated HBB gene using the presented device was performed, coupled with MALDI-TOF MS. The nucleotides at SNP sites have been successfully recognized, although a 100% nucleotide incorporation was not achieved and could be addressed by running a larger number of cycles and introducing more effective mixing during thermal cycling.

In addition to successfully detecting an individual SNP, these results also indicate the compatibility of our approach with multiplexed genotyping. For example, if multiple primers are used to perform an extension simultaneously, each primer can detect a different SNP. Because the maximum molecular weight of ddNTPs is 488 Daltons (dideoxyguanosine triphosphate, ddGTP), by ensuring that the primers are designed with a mass difference of at least 500 Daltons, the mass spectrum of each different primer and extended products will not overlap. As a result, different mass spectral peaks can be recognized in the same spectrum to detect multiple SNPs.

Further study will involve the development of device that employs a more efficient purification method and thus improve the single-to-noise ratio and enable the multiplexed SNP genotyping.

Chapter 3. Microfluidic Multiplex Genotyping of Single-Nucleotide Polymorphisms: a Multi-Step Solution-Based Approach

The bead-based single-nucleotide polymorphism (SNP) genotyping approach described in Chapter 2 demonstrated the feasibility of integrating polymerase chain reaction (PCR), allele specific single-base extension (SBE), and desalting into a single microchamber for SNP genotyping. However, due the insufficient purification method, that approach is not able to eliminate all impurities in the product and is not suitable for multiplexing.

In this chapter, a multi-step SNP genotyping microfluidic device, which performs single-base extension of SNP specific primers and solid-phase purification (SPP) of the extension products on a temperature-controlled chip, is presented. The products generated by the device are ready for immediate detection by matrix-assisted laser desorption/ionization time-of-flight mass spectrometry (MALDI-TOF MS), providing identification of the alleles at the target loci. The integrated device enables efficient and automated operation, while maintaining the high accuracy and sensitivity provided by MS. The multiplex genotyping capability was validated by performing rapid, accurate and simultaneous detection of 4 loci on a synthetic template. The work presented in this chapter has resulted in a peer-reviewed conference proceeding [173] and a journal publication [174].

3.1. Introduction

The successful sequencing of the human genome has offered opportunities for the interrogation of subtle genetic variations to elucidate the genetic bases of biological functions and diseases. SNPs are the most abundant type of genetic variations, with more than 10 million SNPs in public databases, occurring approximately once every 100 to 300 bases in the human genome [48]. SNPs provide the genetic fingerprint of an individual, which is essential for genome-wide association studies and genetic biomarker discovery. Moreover, some SNPs are often associated with a phenotypic change or may directly contribute to disease development. For example, a somatic point mutation at codon 600 of the v-raf murine sarcoma viral oncogene homolog B1 (*BRAF*) gene results in an amino acid change from valine to glutamate. This mutation activates the *BRAF* kinase and has been associated with a variety of tumor types, particularly melanomas [175, 176]. In addition, it provides a cancer therapy target and has been used in patient screening to identify responsive groups to *BRAF* kinase inhibitors, such as vemurafenib [177]. Thus, the accurate detection of SNPs is of great importance for disease prevention, diagnosis, prognosis, and prediction of drug responsiveness, and has become an indispensable tool in personalized medicine. With the increasing demand for SNP detection, there are more and more samples needed to be handled in a cost- and time-effective manner. While it is challenging, the capability to accurately process multiple different samples in parallel is becoming essential in biological applications.

A variety of biological methods have been developed for SNP genotyping, including the polymerase chain reaction-restriction fragment length polymorphism (PCR-RFLP)

[51], DNA hybridization [55], TaqMan [178], allele-specific ligation [57] and allele-specific SBE [179], using detection schemes such as fluorescence detection and mass spectrometry (MS). The introduction of micro- and nanotechnology has revolutionized biological analysis, as the miniaturization of assays facilitates integration, improves speed, efficiency and accuracy, reduces labor, and provides the potential for high-throughput and point-of-care applications. Furthermore, the use of smaller sample volumes lowers reagent consumption and energy requirements, and shortens reaction cycles [180, 181]. Integrated with micro- and nanotechnology, a variety of genotyping microdevices have been explored. For example, the allele-specific hybridization and ligation protocols with fluorescent detection have been incorporated into a microchip for the determination of influenza virus subtypes [182], and for the discrimination of single-nucleotide mismatches [183, 184]. The RFLP-based microchip combined with a capillary electrophoresis separation device has also been developed to identify SNPs in the thiopurine *S*-methyltransferase gene [185]. In addition, the TaqMan genotyping assay has been integrated into nanofluidic circuits and commercialized by Fluidigm Corporation with significant advantages over the conventional thermal cycling process [186, 187]. Nevertheless, optical detection has its intrinsic limitations, as optical signals for the use of detecting ultra-low abundance nucleotide variations tend to generate false-positive results, causing insufficient accuracy and sensitivity. Mass spectrometric detection is advantageous over optical detection in terms of sensitivity and accuracy, which are especially critical for detecting low frequency mutations, such as somatic mutations in tumors and mitochondrial mutations [188, 189]. However, the only commercially available mass spectrometric genotyping platform, the

Sequenom MassARRAY®, is not integrated into an automatic system, which requires substantial manual labor prior to mass spectrometric analysis, including traditional thermocycling, manual resin purification, and etc. The manual handling of each step would not only contribute to errors, but also limit the throughput. Moreover, its multiplexing capability is also limited, as unextended primers remain in the final sample and potentially overlap with extended primers targeting different polymorphic sites [190]. This limitation can be overcome by introducing SPP, in which only extended primers are captured for mass spectrometric analysis, eliminating interference from the excess primers [168]. Therefore, it is highly desirable to integrate SBE and SPP required for multiplex SNP genotyping in a single microfluidic device, so that samples can be processed automatically while maintaining the high accuracy and sensitivity of MS.

To achieve this goal, this chapter presents the development and testing of a multi-step SNP genotyping microfluidic device that additionally includes a two-step SPP scheme for solution-based SBE product, making multiplexing practically attainable. All required steps of the SNP genotyping reactions are integrated in the device, which is coupled to external instrumentation for MALDI-TOF MS. Experiments with uniplex and 4-plex SNP detection have demonstrated that the device is capable of accurate, rapid and automated analysis with reduced consumption of samples and reagents, and can potentially be used in high-throughput and multiplex SNP genotyping.

3.2. Principle, Device Design and Fabrication

This section describes the principle, design and fabrication of our microfluidic device. We first describe the microfluidic SBE-SPP based SNP genotyping approach, and then present the device design and fabrication.

3.2.1. Principle of Microfluidic SNP Genotyping

The principle of our microfluidic SNP genotyping assay is as follows. In the SBE reaction, a locus specific primer hybridizes to the template DNA strand with its 3' end immediately adjacent to the polymorphic site. Then, it is extended with a single dideoxyribonucleotide, bearing a biotin moiety attached via a chemically cleavable linker, complementary to the polymorphic site (**Figure 3.1A**). Next, the extended primer is extracted by streptavidin beads packed in a microchamber (**Figure 3.1B**). The captured primer extension product is then released from the solid phase via chemical cleavage using tris(2-carboxyethyl)phosphine (TCEP) (**Figure 3.1C**). Finally, the released product is desalted using octadecyl carbon chain (C_{18}) bonded silica beads in a microchannel (**Figure 3.1D**) and detected by MALDI-TOF MS (**Figure 3.1E**). The nucleotide at the SNP site is identified according to the mass difference between the resulting product and the original target primer.

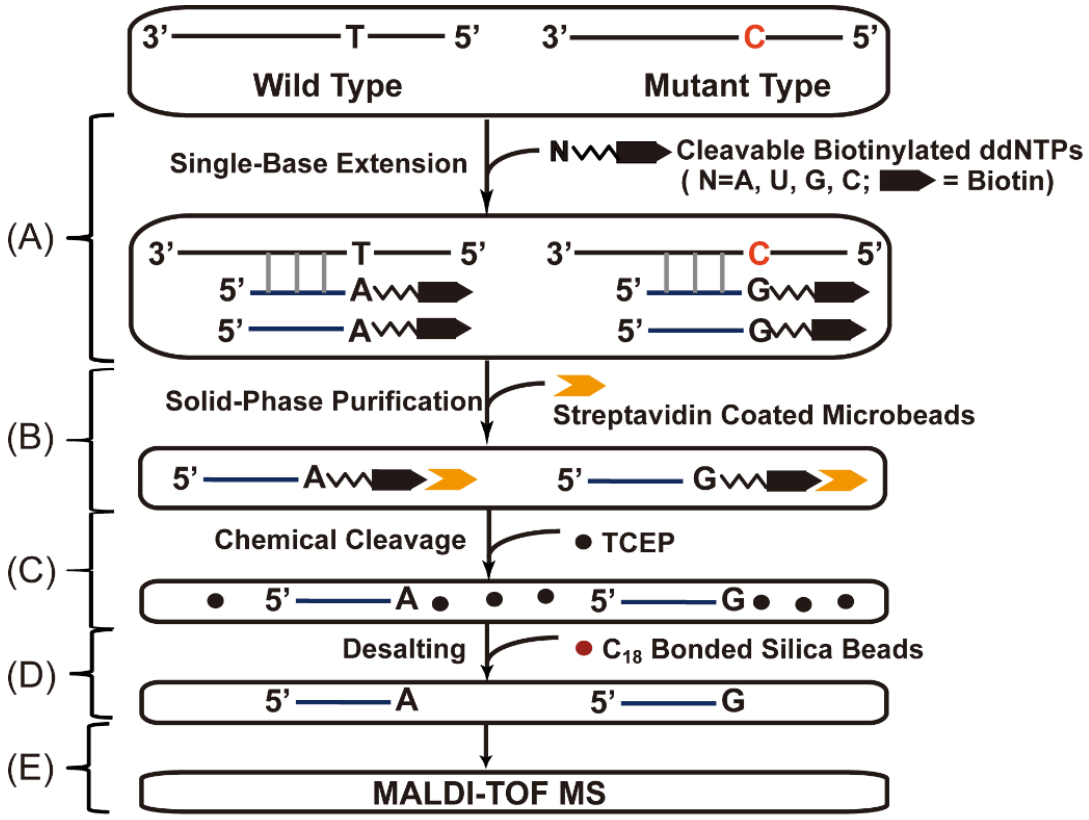

Figure 3.1: Principle of SNP genotyping by SBE-SPP. (A) SNP specific primer is extended by a single base using ddNTPs-N_3-biotin. (B) SNP specific extended primer is extracted by streptavidin coated microbeads. (C) Captured extended primer is chemically cleaved from the microbead surface. (D) The released extended primer is desalted using C_{18} bonded silica beads. (E) The desalted SNP specific primer is identified by MALDI-TOF MS.

3.2.2. Device Design and Fabrication

The SNP genotyping microfluidic device consists of two microchambers situated on a temperature controlled chip for SBE and SPP respectively, a microchannel for desalting, and four pressure-driven microvalves for fluidic control (**Figure 3.2**). The inner surfaces of the SBE microchamber (400 µm in height with an approximate 10 µL volume) are

coated with Parylene C to prevent evaporative loss of reactants [171]. The SPP microchamber (200 µm in height with an approximate 4 µL volume) contains dam-like structures called weirs (20 µm in height) at both ends to retain streptavidin coated microbeads (50 - 80 µm in diameter). The desalting microchannel (1 mm in width, 24 mm in length, and 200 µm in height with an approximate 5 µL volume) also contains weirs (20 µm in height) to retain C_{18} bonded silica beads (45 - 60 µm in diameter). The microchamber and microchannel are fully packed with streptavidin beads and C_{18} bonded silica microspheres, respectively. The weirs have a semi-circular profile and can be completely sealed by underlying elastomeric microvalves actuated by the oil-filled channels underneath (20 µm in height), driven by nitrogen gas. Two groups of temperature control units are integrated on the chip, each containing a serpentine-shaped thin-film temperature sensor (linewidth: 25 µm) and a heater (linewidth: 300 µm) beneath the center of the SBE or SPP microchambers. Therefore, the chamber temperatures can be precisely controlled in separate closed loops using the corresponding integrated temperature sensors and heaters.

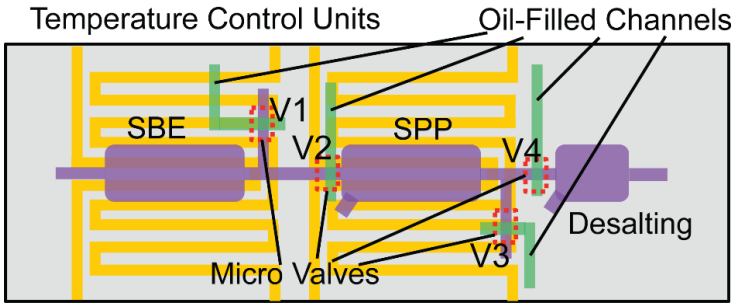

Figure 3.2: Planar schematic of the microfluidic SBE-SPP device for SNP genotyping.

The microfluidic genotyping device is fabricated using standard MEMS technology. The temperature control chip was fabricated using standard microfabrication techniques. Briefly, gold (150 nm) and chrome (5 nm) thin films were thermally evaporated onto the glass substrate, and patterned by photolithography and wet etching, resulting in resistive temperature sensors and resistive heaters (**Figure 3.3A**). Then, 1 μm of silicon dioxide was deposited using plasma-enhanced chemical vapor deposition (PECVD) to passivate the sensors and heaters (**Figure 3.3B**). The contact regions for electrical connections were opened by etching the oxide layer away with hydrofluoric acid.

The polydimethylsiloxane (PDMS) (Sylgard 184, Dow Corning Inc., Midland, MI) sheet bearing microfluidic features was fabricated using soft lithography techniques. A layer of AZ-4620 positive photoresist (20 μm, Clariant Corp., Somerville, NJ) was spin-coated on a silicon wafer (Silicon Quest International, Inc., San Jose, CA), exposed to ultraviolet light through a photomask, developed, and baked to form the weirs as well as the flow channels which have a semi-circular cross section that can be sealed completely (**Figure 3.3C**). Then, layers of SU-8 photoresist (MicroChem Corp., Newton, MA) were patterned to finalize the mold with microfluidic features. Next, a PDMS prepolymer solution (base and curing agent mixed in a 10:1 ratio) was cast onto the mold and cured on a hotplate at 72 °C for 1 h (**Figure 3.3D**). The resulting PDMS sheet was peeled off from the mold, and fluidic inlets and outlets were established via punching holes (**Figure 3.3E**).

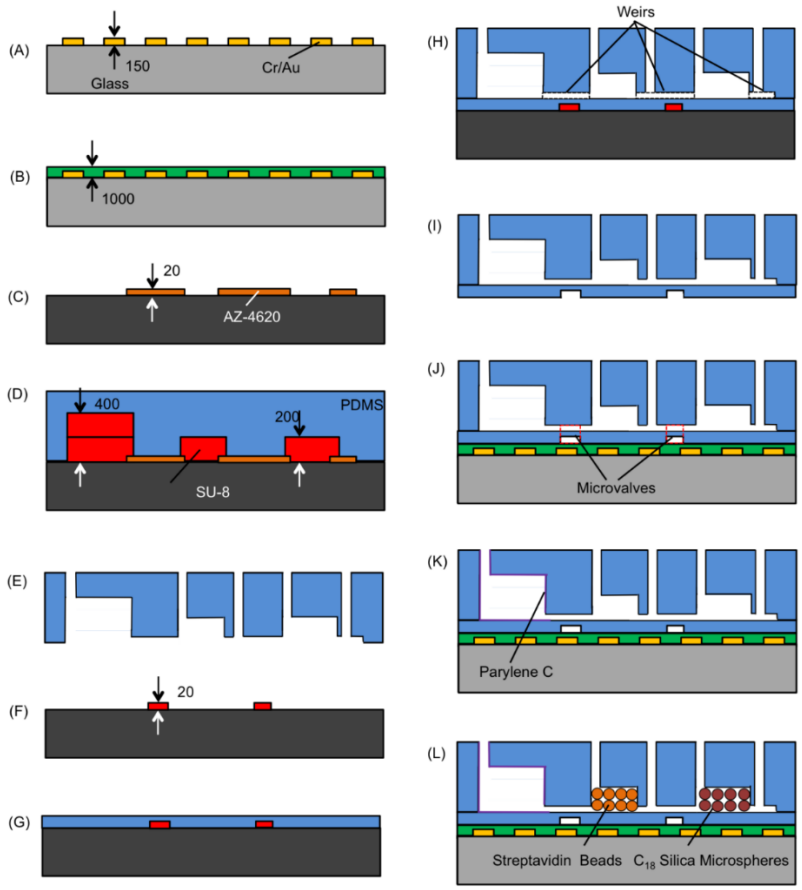

Figure 3.3: (A) Deposition and patterning of gold sensors and heaters. (B) Passivation of gold sensors and heaters. (C) Fabrication of fluidic channel mold for on-chip valves using positive photoresist AZ-4620. (D) Finalization of mold for microfluidic chambers and channels using SU-8. (E) Demolding of PDMS microfluidic channels. (F) Fabrication of SU-8 mold for oil-filled channels. (G) PDMS spin-coating. (H) Bonding of PDMS microfluidic channel to PDMS-coated mold for oil-filled channels. (I) Peeling off of PDMS sheet containing fluidic channels and oil-filled valve actuation channels. (J) Bonding of PDMS sheet to temperature control chip. (K) Deposition of Parylene C. (L) Packing of streptavidin beads and C_{18} bonded silica microspheres. Dimensions are given in micrometers.

In parallel, a layer of SU-8 photoresist was patterned on another silicon wafer to establish oil-filled channels for microvalve actuation (**Figure 3.3F**). Next, a thin PDMS membrane was spin-coated onto the silicon wafer (**Figure 3.3G**) to which the PDMS sheet with the microchannels was then bonded after treating the bonding interfaces with oxygen plasma for 20 seconds (**Figure 3.3H**). Afterward, the PDMS sheet together with the thin PDMS membrane was peeled off (**Figure 3.3I**), punched to form inlets and then bonded irreversibly onto the temperature-controlled chip after another oxygen plasma treatment (**Figure 3.3J**).

Finally, the surfaces of the SBE microchamber were coated with a thin layer of Parylene C via chemical vapor deposition (**Figure 3.3K**), and streptavidin beads and C_{18} bonded silica microspheres were packed in the SPP chamber and desalting channel (**Figure 3.3L**).

An image of a fabricated device is shown in **Figure 3.4**.

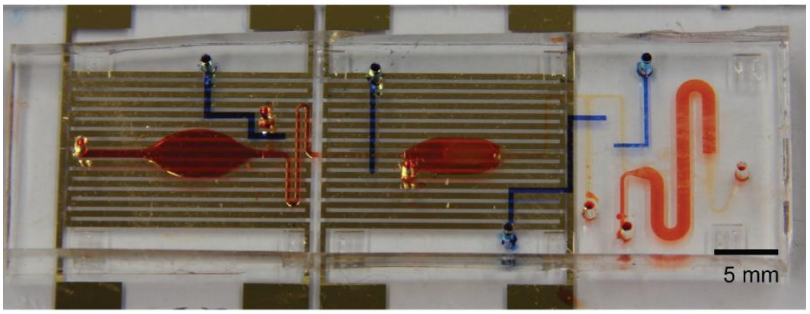

Figure 3.4: Photograph of a fabricated device. Multiple microchambers and microfluidic channels are colored in orange, and oil-filled channels that impinge upon elastomeric valves are shown in blue.

3.3. Experimental

3.3.1. Materials

All chemicals were purchased from Sigma-Aldrich (St. Louis, MO) unless otherwise indicated. Streptavidin beads (Pierce Streptavidin Plus UltraLink Resin) were obtained from Thermo Fisher Scientific (Rockford, IL). Deionized (DI) water was purchased from Life Technologies (Grand Island, NY). Dideoxyribonucleotide triphosphates (ddNTPs) were purchased from Jena Bioscience (Jena, Germany). Primers were synthesized by Integrated DNA Technologies (Coralville, IA). The chemically cleavable biotinylated dideoxyribonucleotide set, ddNTPs-N_3-biotins (ddATP-N_3-biotin, ddGTP-N_3-biotin, ddCTP-N_3-biotin and ddUTP-N_3-biotin), was synthesized in-house as described previously [191], and their molecular weights and chemical structures are shown in Supplementary Information (**Table 3-1** and **Figure 3.5**). Thermo Sequenase™ was purchased from GE Healthcare (Piscataway, NJ). C_{18} modified reversed-phase silica microspheres were obtained from Sorbent Technologies (Norcross, GA).

Table 3-1: Mass of ddNTPs-N_3-biotins (Da)

ddATP-N_3-biotin	ddGTP-N_3-biotin	ddCTP-N_3-biotin	ddUTP-N_3-biotin
1101.89	1231.04	1078.85	1192.99

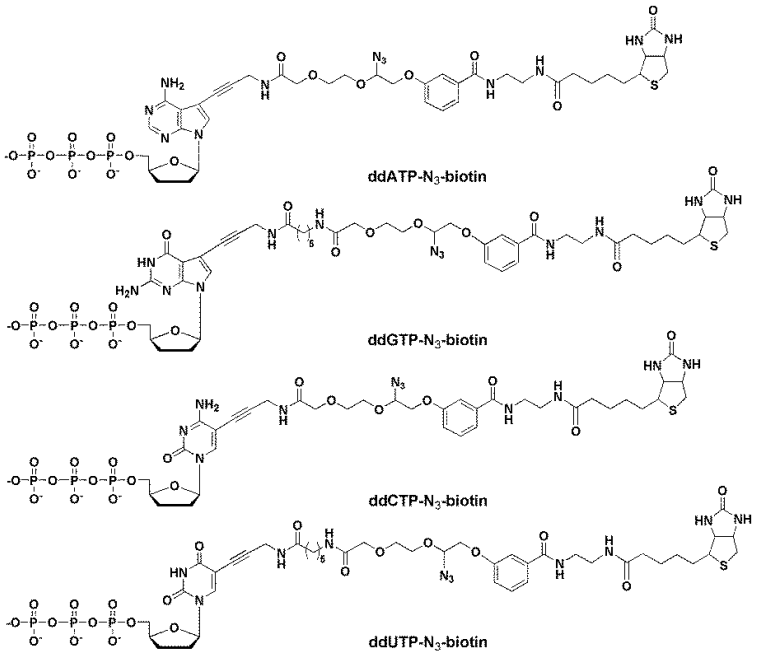

Figure 3.5: Chemical structure of chemically cleavable biotinylated dideoxyribonucleotide set, ddNTPs-N_3-biotins (ddATP-N_3-biotin, ddGTP-N_3-biotin, ddCTP-N_3-biotin and ddUTP-N_3-biotin).

3.3.2. Experimental Setup and Procedure

Closed-loop temperature control of both SBE and SPP microchambers is achieved using two separate temperature control units with a proportional-integral-derivative (PID) algorithm implemented in LabVIEW (National Instruments, TX) and a fan positioned under the temperature control chip. Each temperature control unit contains a serpentine-shaped, gold resistive temperature sensor and heater. The resistance of the two temperature sensors is measured by a digital multimeter (34410A, Agilent Technologies, CA) and a digital micro-ohmmeter (34420A, Agilent Technologies, CA), respectively. The two heaters and the fan are connected to DC power supplies (E3631, Agilent Technologies, CA) respectively (**Figure 3.6**).

Fluid control is achieved using microfabricated pressure-driven valves [192]. Four oil-filled channels, each controlled by an air control valve (6464K16, McMaster-Carr, NJ), are connected to a nitrogen gas tank (Tech Air, NY) via a pressure regulator (CONCOA North America, VA). The microfluidic device inlets are connected to a set of five syringes that contain 50% acetonitrile (ACN), 0.1 M triethylammonium acetate buffer (TEAA), binding and washing (B&W) buffer (5 mM Tris-HCl, 0.5 mM EDTA, 1 M NaCl, and 0.01% Tween 20, pH 7.5), 100 mM TCEP (pH 9.0, adjusted with ammonium hydroxide) and deionized water (DI water) respectively; and the fluidic flow is regulated by syringe pumps (KD210P, KD Scientific, MA, and NE-1000, New Era Pump System, NY). The outlet is connected to a microcentrifuge tube to collect the final genotyping product for MALDI-TOF MS analysis (**Figure 3.6**).

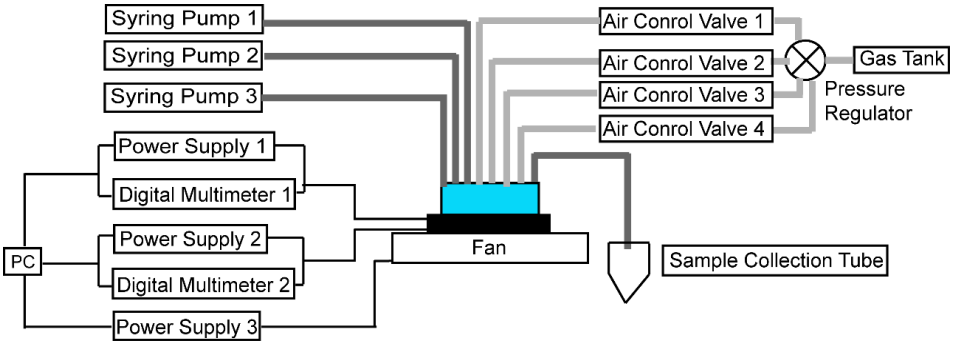

Figure 3.6: Experimental setup for microfluidic SNP genotyping by SBE-SPP.

To conduct the microfluidic SNP genotyping, the C_{18} silica microspheres suspended in methanol were first packed in the desalting channel and dried overnight at 60 °C. Then, the fluidic channels were filled with DI water, and the streptavidin beads were packed in

the SPP chamber (**Figure 3.7A**, **Figure 3.8A**). Pressure-driven microvalves (V1 - V4) were closed by default with 200 kPa pressure.

During an experiment, the C_{18} silica beads were rinsed with 50% ACN (**Figure 3.7B**, **Figure 3.8B**, 20 µL/min for 1 min) followed by 0.1M TEAA (**Figure 3.7C**, **Figure 3.8C**, 20 µL/min for 2 min) for wetting and equilibration. Meanwhile, by opening valve V3, B&W buffer was introduced to rinse the streptavidin beads (**Figure 3.7D**, **Figure 3.8D**, 10 µL/min for 5 min) to provide the optimal binding condition for biotin and streptavidin.

Then, by opening valve V1, a 10 µL reagent composed of 2 µL target template, 75 pmoles of ddATP-N_3-biotin, 50 pmoles of ddUTP-N_3-biotin, 50 pmoles of ddCTP-N_3-biotin, 75 pmoles of ddGTP-N_3-biotin, 40 pmoles of each locus specific primer, 1 × Reaction Buffer and 8 unit Thermo Sequenase™ was introduced into the SBE chamber (**Figure 3.7E**, **Figure 3.8E**) and went through 30 thermal cycles of 94 °C for 15 s, 40 °C for 60 s and 69 °C for 30 s (**Figure 3.7F**).

Next, by opening valves V2 and V3, the SBE product was transferred into the SPP chamber and extracted under continuous flow conditions by the streptavidin beads at a flow rate of 5 µL/min for 2 minutes (**Figure 3.7G**, **Figure 3.8F**), followed by rinsing with 50 µL of B&W buffer at a flow rate of 10 µL/min (**Figure 3.7H**, **Figure 3.8G**). Subsequently, by opening valve V3, 10 µL of 100 mM TCEP (pH 9.0) was introduced into the SPP chamber (**Figure 3.7I**, **Figure 3.8H**), and incubated at 65 °C for 10 minutes to cleave the linker and release the primer extension product from the beads (**Figure 3.7J**).

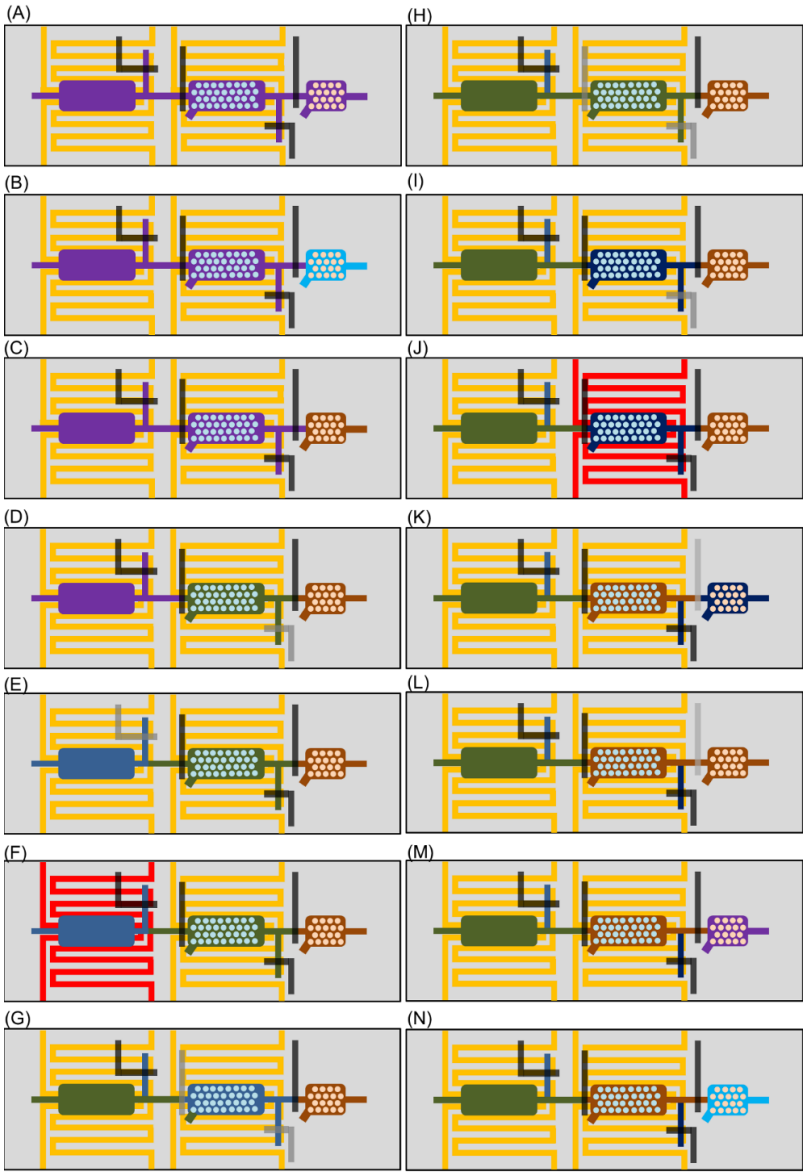

Figure 3.7: (A) Filling of the microfluidic channels with DI water. (B) Rinsing of C_{18} bonded beads with 50% ACN. (C) Rinsing of C_{18} bonded beads with 0.1M TEAA. (D) Rinsing of streptavidin beads with B&W buffer. (E) Introduction of SBE reaction solution. (F) Thermal cycling. (G) Extraction of SBE product by streptavidin beads in SPP chamber. (H) Rinsing of streptavidin beads with B&W buffer to wash off the unextended primer and

other impurities. (I) Introduction of TCEP. (J) Incubation at 65 °C to release the SBE product. (K) Transfer of cleaved SBE fragments to desalting channel. (L) Rinsing of C_{18} bonded beads with 0.1M TEAA. (M) Rinsing of C_{18} bonded beads with DI water. (N) Elution of desalted SBE fragments with 50% ACN. Colored ink is used to represent the actual reagents. Purple: DI water; Dark Orange: TEAA; Light Blue: ACN; Green: B&W buffer; Blue: SBE sample; Dark Blue: TCEP.

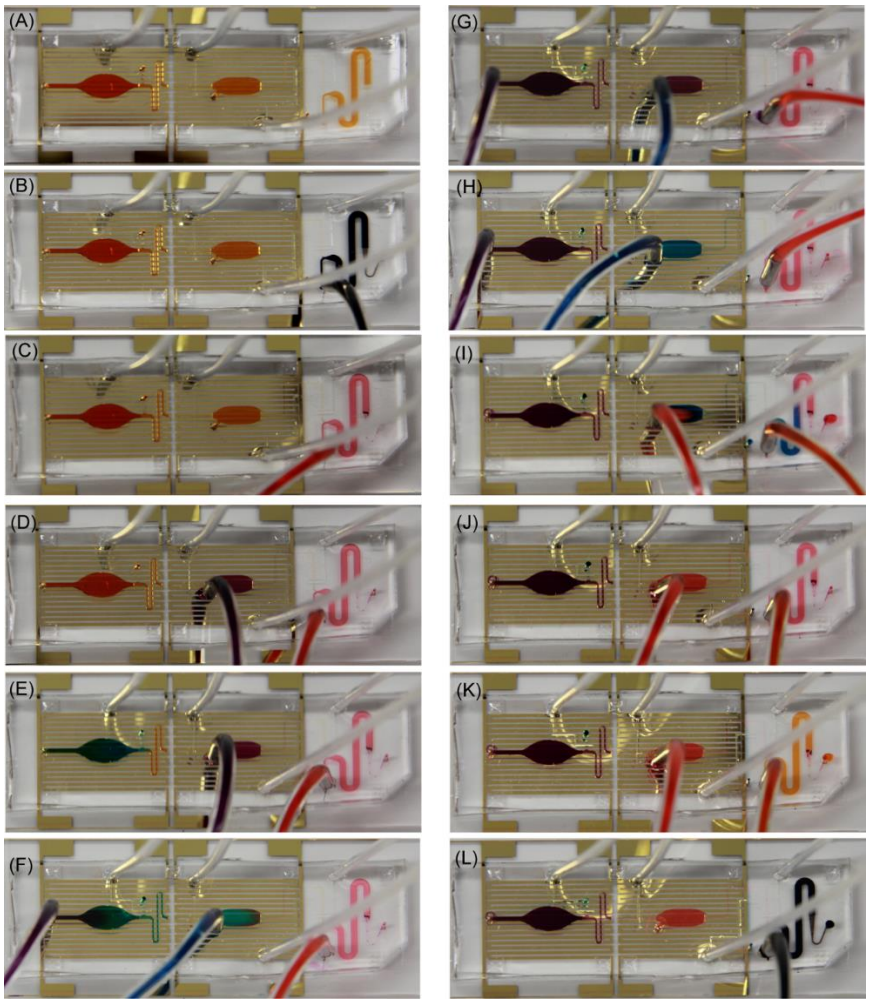

Figure 3.8: (A) Filling of the microfluidic channels with DI water. (B) Rinsing of C_{18} bonded beads with 50% ACN. (C) Rinsing of C_{18} bonded beads with 0.1M TEAA. (D)

Rinsing of streptavidin beads with B&W buffer. (E) Introduction of SBE reaction solution and thermal cycling. (F) Extraction of SBE product by streptavidin beads in SPP chamber. (G) Rinsing of streptavidin beads with B&W buffer to wash off the unextended primer and other impurities. (H) Introduction of TCEP and incubation at 65 °C to release the SBE product. (I) Transfer of cleaved SBE fragments to desalting channel. (J) Rinsing of C_{18} bonded beads with 0.1M TEAA. (K) Rinsing of C_{18} bonded beads with DI water. (L) Elution of desalted SBE fragments with 50% ACN. Colored ink is used to represent the actual reagents. Orange: DI water; Pink: TEAA; Black: ACN; Purple: B&W buffer; Green: SBE sample; Blue: TCEP.

Finally, by opening valve V4, the cleaved SBE products were transferred to the desalting channel at a flow rate of 1 µL/min for 5 min (**Figure 3.7K**, **Figure 3.8I**), followed by rinsing with 100 µL of 0.1 M TEAA (**Figure 3.7L**, **Figure 3.8J**) and 50 µL of DI water (**Figure 3.7M**, **Figure 3.8K**) at a flow rate of 20 µL/min to eliminate any impurities and salts. The desalted product was then eluted with 2 µL of 50% ACN (**Figure 3.7N**, **Figure 3.8L**) and characterized with a Voyager DE™ MALDI-TOF mass spectrometer (Applied Biosystems®, Life Technologies, Grand Island, NY).

3.4. Results and Discussion

This section presents and analyzes experimental results from the microfluidic SNP genotyping device. We first characterize the temperature-controlled chip and evaluate the localized heating and temporal accuracy of the temperature field in the chambers. Then, characterization of SBE, and optimization of SPP, chemical cleavage and desalting are

performed to investigate factors that influence the assay efficiency. Finally, the integrated uniplex and multiplex "SNP" genotyping is carried out to demonstrate the feasibility of the microfluidic device.

3.4.1. Characterization of Temperature Control

The temperature-resistance relationships of the resistive temperature sensors for both the SBE and SPP chambers were calibrated following fabrication to provide accurate temperature control. The resistance of the thin film gold resistor is linearly dependent on temperature, as given by $R = R_0 [1 + \alpha (T - T_0)]$, where R is the sensor resistance at temperature T, R_0 is the sensor resistance at reference temperature T_0, and α is the sensor's temperature coefficient of resistance (TCR). Measurements of SBE sensor resistance at varying temperatures displayed highly linear temperature dependence and the TCR was calculated to be 2.74×10^{-3} °C^{-1}. The temperature-resistance relationship of the SPP sensor also exhibited linear behavior with a TCR value of 2.76×10^{-3} °C^{-1}.

We then characterized the temperature control of the buffer-filled SBE chamber to simulate thermal cycling in the SBE process. The SBE chamber temperature was controlled by an integrated heater and a fan beneath the chip via a closed-feedback loop. In accordance with the experimental fits (**Figure 3.9A**, 10 cycles are shown), the control algorithm was able to ramp rapidly to the specified temperature with approximate closed-loop time constants of 2.13 s from 40 °C to 69 °C, 2.25 s from 69 °C to 94 °C and 10.51 s from 94 °C to 40 °C, respectively. During the thermal cycling for the SBE chamber, the highest temperature reached in the SPP chamber was 33.27 °C (**Figure 3.9A**), which would not affect the streptavidin affinity [193]. **Figure 3.9B** shows a temperature profile in the buffer-

filled SPP chamber during heating, using the closed-loop temperature control. The channel temperature increased from room temperature (25 °C) to 65 °C rapidly in about 13.7 s (with an insignificant overshoot of ~ 0.25 °C) where it remained for approximately 10 min, which was sufficient for the chemical cleavage reaction to release the captured SBE products.

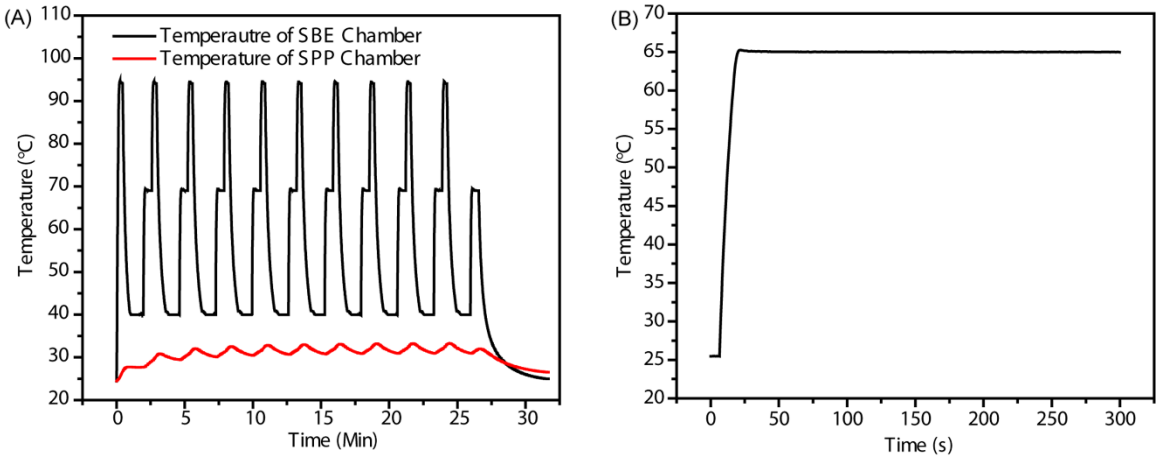

Figure 3.9: Time-resolved tracking of (A) the temperatures inside the buffer-filled SBE chamber and SPP chamber during thermal cycling, and (B) the temperature inside the buffer-filled SPP chamber during the chemical cleavage procedure.

3.4.2. Characterization of Single-Base Extension

To characterize the feasibility and efficiency of on-chip SBE reaction, a synthetic template (5'-GAAGGAGACACGCGGCCAGAGAGGGTCCTGTCCGTGTTTGTGCGTGGAGTTCGACAAGGCAGGGTCATCTAA*TGGTGATGAGTCCTATC*CTTTTCTCTTCGTTCTCCGT-3') was prepared. A primer (5'-GATAGGACTCATCACCA-3', 5163 Da) targeting the template (annealing site underlined and italicized) was extended by a single base (ddUTP-N_3-biotin) in the SBE chamber. The SBE reaction solution contained 10 pmoles (334 ng) of synthetic DNA template, 40 pmoles of primer, 60 pmoles of ddUTP-

N_3-biotin (1192 Da), 1 × Thermo Sequenase™ reaction buffer and 4 units of Thermo Sequenase™ in a total volume of 10 µL. After introduction to the SBE chamber, the solution was subjected to 5 thermal cycles of 94°C for 15 s, 40°C for 60 s and 69°C for 30 s. Theoretically, the mass of extended primer can be calculated according to the equation $m_e = m_r + m_n - m_b$, where m_e is the mass of extended primer, m_r is the mass of unextended primer, m_n is the mass of corresponding ddNTP-N_3-biotin, and m_b is the mass loss upon phosphodiester bond formation (175 Da). Thus, the expected mass of the primer extension product after the SBE extension was calculated to be 6180 Da (5163 + 1192 − 175). As shown in **Figure 3.10**, the appearance of the ddUTP-N_3-biotin extension product peak at 6180 *m/z* and the disappearance of the primer peak at 5163 *m/z* indicated an efficient enzyme incorporation reaction. The use of on-chip thermal cycling also reduces the operation time. For example, 30 on-chip thermal cycles require only 60 min, as compared to 85 min for a traditional thermal cycler (Eppendorf Mastercycler® Personal). With further optimization of the microfluidic device, the number of cycles and the time for each step (denaturation, annealing and extension) can be additionally dramatically reduced. With optimal surface-to-volume ratio design, one can achieve more efficient temperature equilibration in the microchamber to enable rapid thermal response.

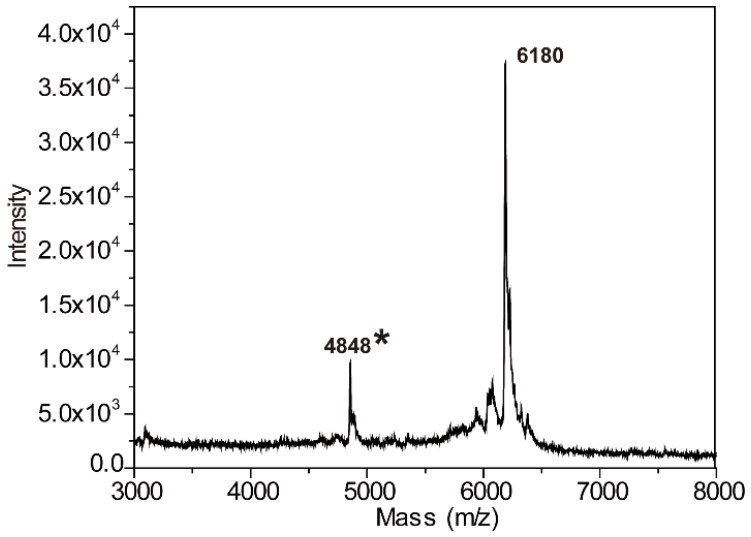

Figure 3.10: MALDI-TOF mass spectrum of SBE product (the peak marked with an asterisk is presumably due to the impurities in the commercial synthetic primer).

3.4.3. Optimization of Solid-Phase Purification and Chemical Cleavage

To optimize the SPP process, various concentrations of biotinylated ssDNA (5163_biotin: 5'-biotin-GATAGGACTCATCACCA-3') in 5 µL of 1 × Thermo Sequenase™ reaction buffer were introduced into a streptavidin bead packed SPP microchamber at different flow rates. After capture, the beads with the biotinylated DNA were washed with DI water at a flow rate of 10 µL/min for 5 min. Waste was collected, vacuum dried and then dissolved in 5 µL of DI water. For both input and output ssDNA solutions, the UV absorbance at 260 nm were measured on a NanoDrop 2000c instrument (Thermo Fisher Scientific, Rockford, IL) using 1 × Thermo Sequenase™ reaction buffer as the reference and the concentration was calculated according to the Beer-Lambert law. Approximately 30 pmoles, 65 pmoles and 170 pmoles of ssDNA 5163_biotin in 5 µL 1 × Thermo Sequenase™ reaction buffer were introduced into the SPP microchamber with

streptavidin beads at 1 μL/min, which were then washed with DI water. After SPP, the total amounts of biotinylated ssDNA not captured by the beads were all below 2 pmoles (**Figure 3.11A**). These results indicate that the binding capacity of the streptavidin beads packed in the SPP microchamber is at least 160 pmoles under a constant flow rate of 1 μL/min.

In another optimization experiment, we evaluated the effect of flow rate on SPP efficiency. Approximately 170 pmoles biotinylated ssDNA in 5 μL 1 × Thermo Sequenase™ reaction buffer was introduced into the SPP microchambers at varying flow rates of 0.2 μL/min, 1 μL/min, 5 μL/min, and 20 μL/min respectively, followed by DI water wash. After SPP, the total amounts of biotinylated ssDNA not captured by the beads for both flow rates of 0.2 μL/min and 1 μL/min were below 2 pmoles (**Figure 3.11B**). However, at flow rates of 5 μL/min and 20 μL/min, the amounts of uncaptured biotinylated ssDNA fragments increased to about 5 pmoles and 13 pmoles (**Figure 3.11B**), respectively. These results imply the binding capacity of streptavidin beads packed in the SPP microchamber decreases as the flow rate increases, since the reaction time between biotin and streptavidin is reduced. Nevertheless, taking into account the operation time, 5 μL/min with 5 pmoles loss in a total of 170 pmoles is still considered an efficient binding condition.

Finally, in order to evaluate the binding specificity of streptavidin to the biotinylated DNA products, approximately 140 pmoles of unbiotinylated ssDNA (5163: 5'-GATAGGACTCATCACCA-3') in 5 μL 1 × Thermo Sequenase™ reaction buffer was flowed into the SPP microchamber packed with streptavidin beads at 1 μL/min, followed by the same DI water wash (**Figure 3.11C**). The amount of ssDNA collected was about 126 pmoles, which indicated a negligible non-specific binding of unbiotinylated ssDNA to

the streptavidin beads. At faster flow rates, the non-specific binding would be even less. Given these results, we conclude that performing SPP at 5 µL/min is both binding- and time-efficient. At this rate, the extraction of 10-µL reaction solution could be simply achieved within 2 min, as compared to in-tube reaction, which requires constant mixing and longer reaction time [194]. The microfluidic SPP device also improves sample recovery, as the physical entrapment of the beads allows extensive washing and provides a more efficient SPP process.

To characterize DNA recovery from the solid phase, the same SBE reactions were performed as described in Section 4.2 using a commercial thermal cycler (Eppendorf Mastercycler® Personal). Similarly to our previous experiments, the SBE extension products (6180 Da) were purified by streptavidin microbeads packed in the SPP microchamber. Then, 10 µL of 100 mM TCEP solution (pH 9.0) was introduced and incubated at 65°C for 10 min. Incubation of the extension products in TCEP solution resulted in the cleavage of the linker tethering the biotin to the dideoxyribonucleotides. Theoretically, the mass of cleaved product can be calculated by the equation $m_p = m_e - m_c$, where m_p is the mass of cleaved product, m_e is the mass of extended primer and m_c is the mass change upon cleavage (476 Da). As shown in **Figure 3.11D**, the mass peak for the extension product completely disappeared, whereas the single peak corresponding to the cleavage product appeared at 5704 *m/z* (6180 − 476) indicating efficient cleavage.

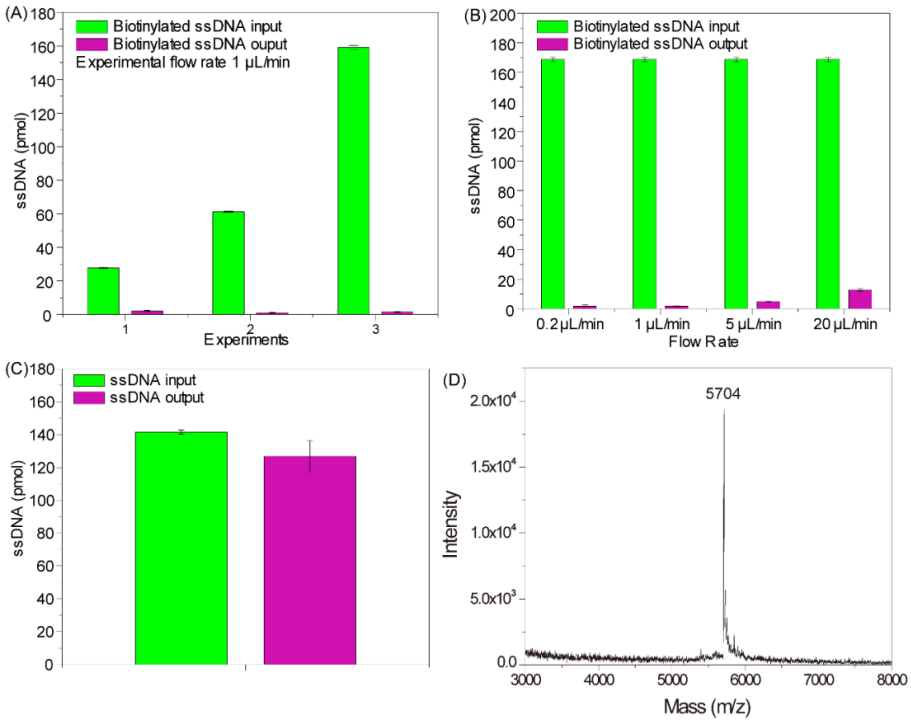

Figure 3.11: (A) Total amounts (pmol) of biotinylated ssDNA (5163_biotin) inflow and outflow from the SPP chamber at a flow rate of 1 µL/min. (B) Total amount (pmol) of biotinylated ssDNA (5163_biotin) introduced into and obtained from the SPP chamber at different flow rates. (C) Total amount (pmol) of ssDNA (5163) inflow and outflow from the SPP channel at a flow rate of 1 µL/min. (D) MALDI-TOF mass spectrum of released extension products from solid phase after TCEP cleavage. The average values were calculated from at least three repeated experiments, with error bars representing the standard deviation.

3.4.4. Optimization of Desalting

It is necessary to remove salts from the cleavage solution while concentrating and purifying enough samples for mass spectrometric analysis [195]. Traditionally, for small

sample amounts, C_{18} bonded resin packed pipette tips are used, and it requires extensive manual pipetting. In contrast, a C_{18} bonded microspheres packed microfluidic desalting channel essentially eliminates the manual procedures and provides great potential to expand this microfluidic method for high-throughput applications using multi-channels.

To optimize the desalting process, various concentrations of ssDNA (4207: 5'-CTCTCTGGCCGCGT-3') in 5 µL of 100 mM TCEP (pH 9.0) were introduced into the desalting channel at different flow rates, followed by a DI water wash at a flow rate of 20 µL/min for 10 min. Waste was collected, vacuum dried and dissolved in 5 µL of DI water. The concentrations of both input and output ssDNA solutions were measured with a NanoDrop instrument based on UV absorption using 100 mM TCEP (pH 9.0) as the reference. Approximately 20 pmoles, 45 pmoles and 100 pmoles of ssDNA were introduced into the desalting channel at 1 µL/min, which was then washed with DI water. After desalting, the total amounts of ssDNA not adsorbed by the C_{18} resin were about 1 pmole, 5 pmoles and 40 pmoles (**Figure 3.12A**). These results indicate that the binding capacity of the C_{18} microspheres packed in the desalting channel is approximately 55 pmoles under a constant flow rate of 1 µL/min. This amount of DNA is far higher than the detection limit of MS [196]. Theoretically, the binding capacity and recovery efficiency increases with a larger binding interface at a constant flow rate, which could be achieved by a larger number of C_{18} particles in the fixed stationary phase [197]. However, this would build up back pressure due to the requirement for a longer microfluidic channel [198]. On the other hand, the size of C_{18} microspheres is inversely proportional to the binding capacity and recovery efficiency [195]. The use of larger particles would result in a lower

surface-to-volume ratio due to the geometrical restriction of the microchannel. But, smaller particles also significantly contribute to the accumulation of back pressure [198]. Therefore, the trade-off between channel length/particle size and binding capacity/recovery efficiency is an important design consideration.

In addition, we evaluated the effect of flow rate on desalting efficiency. Approximately 45 pmoles of ssDNA in 5 µL of 100 mM TCEP (pH 9.0) was flowed into the desalting channel at 0.2 µL/min, 1 µL/min, or 5 µL/min, followed by DI water wash. After desalting, the total amounts of ssDNA not adsorbed by the C_{18} beads were 1 pmole, 5 pmoles and 14 pmoles (**Figure 3.12B**) respectively. These results imply that the binding capacity and recovery efficiency of the C_{18} microspheres packed in the desalting channel decreases as the flow rate increases, since the interaction time between the analyte and stationary phase (microspheres) is reduced [197]. However, lower flow rates result in longer operation time, significantly decreasing the assay efficiency. Therefore, the optimal selection of flow rate is another essential design consideration.

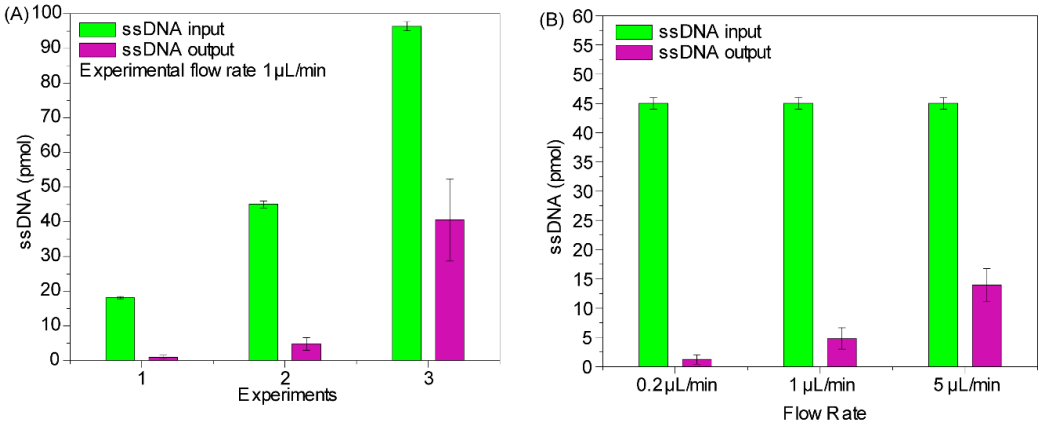

Figure 3.12: (A) Total amount (pmol) of ssDNA (4207) introduced into and obtained from the desalting channel at flow rate of 1 µL/min, followed by DI water wash. (B) Total

amount (pmol) of ssDNA (4207) inflow and outflow from the desalting channel at different flow rates, followed by DI water wash. The average values were calculated from at least three repeated experiments, with error bars representing the standard deviation.

3.4.5. Uniplex and Multiplex Assays

Having demonstrated each functional unit of the microfluidic device, we performed the entire "genotyping" microfluidic operation (SBE, SPP, TCEP cleavage and desalting) within the fully integrated device using the same primer and template as described in Section 3.4.2. The mass of final product can be calculated according to the equation

$$m_p = m_r + m_n - m_b - m_c \quad (1)$$

where m_p is the mass of product, m_r is the mass of unextended primer, m_n is the mass of corresponding ddNTP-N_3-biotin, m_b is the mass loss upon phosphodiester bond formation (175 Da), and m_c is the mass change upon cleavage (476 Da). The nucleotide at the query "SNP" position was identified correctly as the molecular weight of the primer is 5163 Da and therefore the peak at 5704 *m/z* (5163 + 1192 − 175 − 476) corresponds to an extension product with ddUTP-N_3-biotin after cleavage (**Figure 3.13A**). This result demonstrates that the device is able to perform a fully integrated SNP detection as designed.

To validate the multiplex genotyping capability, we used a synthetic template with 4 known positions as the query loci to mimic multiplex SNP genotyping. The SBE reaction contained 40 pmoles each of the 4 SBE primers in a total volume of 10 µL. The final product masses can be calculated according to equation (1). The primer sequences, molecular weights of primer and their potential final genotyping products are listed in **Table 3-2**, while their annealing sites are shown in **Figure 3.13C**. As shown in **Figure**

3.13B, nucleotides at these four sites were unambiguously identified. These results demonstrate the feasibility of using this microfluidic device for integrated and miniaturized SNP multiplex genotyping with high accuracy and sensitivity, with the potential for high-throughput and fully automated nucleotide variant detection. In addition, compared with SBE based genotyping on conventional platforms, the device employs on-chip temperature control, which allows for efficient temperature equilibration in the microchamber, significantly shortening thermal cycling times during amplification. This capability, as well as the ability to accommodate DNA fragments of multiple sizes, also provides the promise for microfluidic mini-MS sequencing, in which the fragments generated from Sanger dideoxyribonucleotide reactions are identified via MS at single nucleotide resolution, rather than by traditional gel electrophoresis and fluorescence detection [191]. With the accuracy and sensitivity of MS, the device has great potential for accurate sequencing of small but highly polymorphic regions [191, 194].

Table 3-2: Masses of SBE primer sequences and corresponding extension products

Query Site ("SNPs")	**Primer Sequence (5'-3')**	**Primer mass (Da)**	**Mass of final genotyping product (Da)**			
			ddATP-N_3-biotin	ddGTP-N_3-biotin	ddCTP-N_3-biotin	ddUTP-N_3-biotin
a	TCTCTGGCCGCGTGTCT	5144	5594	5723	**5571**	5685
b	CTCTCTGGCCGCGT	4207	4657	**4786**	4634	4748
c	TAGATGACCCTGCCTTGTC	6084	**6534**	6663	6511	6625
d	GATAGGACTCATCACCA	5163	5613	5742	5590	**5704**

Note: The masses of genotyping products shown in red bold type refer to the expected extension products using the template shown in **Figure 3.13**.

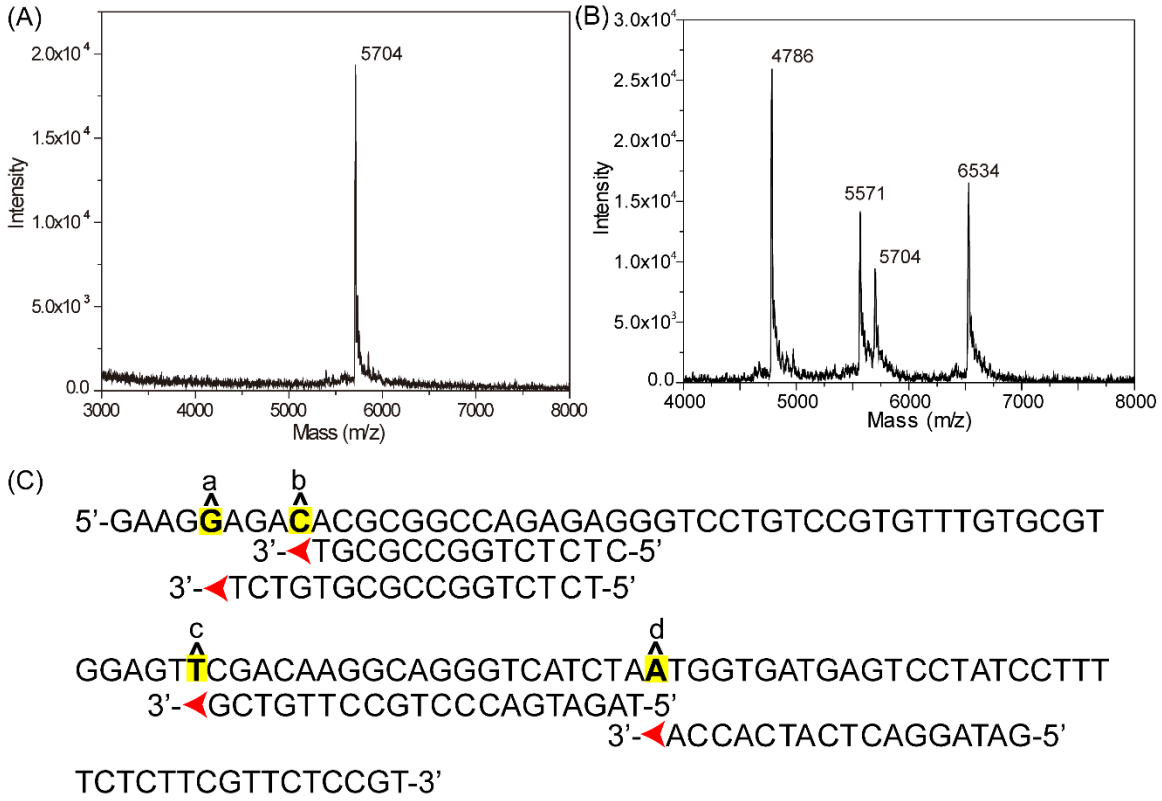

Figure 3.13: MS results for uniplex and multiplex assays: (A) MALDI-TOF mass spectrum of uniplex "SNP" genotyping product with all operations integrated. (B) MALDI-TOF mass spectrum of 4-plex "SNP" genotyping products using the microfluidic device. (C) SBE primer annealing sites and query positions. The letters highlighted in bold and yellow indicate the query positions, mimicking SNPs in a SNP genotyping assay; and the red arrow indicates the direction of primer extension. The template sequence is displayed on three lines.

3.5. Conclusion

The ability to accurately detect SNPs is critical for disease prevention, diagnosis and prognosis, and for prediction of drug response and clinical outcomes of patients. To

demonstrate a critical step towards a potentially high-throughput microfluidic genotyping array, this chapter presents a microfluidic device that automatically performs all the required biochemical steps for multiplex SNP genotyping based on the combined SBE-SPP approach.

The device consists of two microchambers situated on a temperature control chip for respectively carrying out SBE and SPP reactions, as well as a microchannel for desalting. These functional components are connected in series by microchannels with a semi-circular cross section and can be controlled by microfabricated elastomeric valves actuated by the underlying oil-filled channels driven by pressure. Moreover, integrated temperature sensors and heaters beneath the SBE and SPP microchambers allow independent, closed-loop control of chamber temperatures. The surfaces of the SBE microchamber are coated with Parylene C to prevent sample loss during thermal cycling. Streptavidin coated microbeads and C_{18} bonded silica microspheres are fully packed in the SPP chamber and desalting channel respectively to extract SBE products and remove salt in preparation for MS. Due to the serial design, array-based high throughput integration can be simply achieved by parallel control of the above described individual functional units using microvalves. Hence, each of the units can carry out multiplex SNP genotyping of a single sample, and multiple samples can be processed in parallel using the array-based configuration.

The temperature control units were characterized experimentally to ensure localized and efficient heating, as well as temporal accuracy of the temperature field. We demonstrated 100% extension of primer with cleavable mass-tagged ddNTPs and efficient

chemical release of purified SBE products, with shortened temperature cycling time due to higher heat transfer efficiency of on-chip temperature control, leading to improved single-base resolution and ease of product extraction. The device's capability of SPP and desalting was tested at different flow rates. The efficiency of both SPP and desalting were shown to be flow rate dependent. Although lower flow rate leads to higher capture efficiency, it also dramatically increases the total operation time for the microfluidic genotyping. Therefore, the tradeoff between the efficiency of SPP/desalting and that of the full assay is an essential design consideration. Finally, uniplex and 4-plex assays on a mock synthetic template, which mimic the SNP detection process, were carried out within the fully integrated device. The accurate detection of these "SNPs" demonstrates the feasibility of using the microfluidic device for rapid, automated, integrated and miniaturized multiplex SNP genotyping with high accuracy and sensitivity.

Further study will involve high-throughput and fully automated nucleotide variant detection and accurate indel mini-sequencing. Due to the serial design, arrays of this microfluidic device can be simply achieved on single chips by concerted control of the individual functional units arrayed in parallel to allow analysis of samples from many different patients. Such array-based devices can be created essentially by the same process used to fabricate the single device unit.

Chapter 4. Specific Capture and Temperature-Mediated Release of Cells: Demonstration of an Aptameric Microchip

In this chapter, a proof-of-concept microfluidic device for specific capture and temperature-mediated release of cells using nucleic acid aptamers is presented. The device consists of a microchamber situated on a temperature control chip that includes an integrated temperature sensor and heaters. The chamber surface is functionalized with aptamers to capture target cells with high specificity. We demonstrate the device by capturing CCRF-CEM cells, a human acute lymphoblastic leukemia (ALL) T cell line, with a highly selective DNA aptamer sgc8c. Controlled release of CCRF-CEM cells from the aptamer surface is then conducted at an elevated temperature using on-chip temperature control unit. This allows the nondestructive retrieval of target cells, which eliminates the use of potentially harsh chemicals, and enables efficient regeneration of the aptamer surface. The work presented in this chapter has resulted in two peer-reviewed conference proceedings [199, 200] and a journal publication [201].

4.1. Introduction

Isolation of cells from biological samples involves the separation and retrieval of cell subpopulations from a heterogeneous mixture in blood or other body fluids, and is widely used in both fundamental cell biology research and clinical diagnostics. For example, the ability to detect and characterize cancer cells from blood or other body fluids is essential for detecting cancer in early stages and understanding cancer development and progression mechanisms, such as metastasis, would significantly improve survival rates [110]. In

addition, studies of phenotypically pure subpopulations of human lymphocytes can provide valuable information concerning immune responses to injury and disease [202]. To enable these applications, target cells must be selectively captured, and in some instances, such as tissue engineering [203] and cell-based therapeutics [204], retrieved nondestructively without any mechanical or biochemical damage.

Isolation of cells can be based on the size or volume, density, electrical properties, or surface characteristics, using methods such as filtration, centrifugation, dielectrophoresis, or affinity binding [74, 205, 206]. Among these methods, affinity binding, which recognizes cells by binding of ligands to biomarkers on cell membranes, is highly attractive due to its high specificity to target cells. The most commonly employed ligands for affinity cell isolation are antibodies, which are generated *in vivo* against target antigens found on cell membranes. Antibody-based cell isolation techniques have been implemented using methods such as magnetic activated cell sorting (MACS) and fluorescence-activated cell sorting (FACS) [206, 207]. MACS uses a magnetic field to manipulate antibody-coated microbeads specifically bound to the cells and is amenable to high-throughput operation [208]. Relying on a single physical parameter (i.e., the presence or absence of magnetic force) to distinguish between different cell types, MACS is in general a single-parameter cell isolation method. In comparison, FACS usually uses multiple species of fluorescently labeled antibodies and allows sorting of multiple cell types simultaneously [207]. Thus, FACS is a multi-parameter method, although it is relatively low-yield and typically requires more complex and expensive experimental instrumentation.

Microfluidic technology can potentially enable low-cost, automated and portable cell isolation systems with improved sensitivity, resolution and efficiency as well as minimized sample and reagent consumption [209]. Microfluidic cell isolation devices have implemented aforementioned separation principles, for instance exploiting differences in the size [210], acoustic response [91], dielectrophoretic characteristics [211], and the affinity of cells to ligands [110]. In particular, microfluidic affinity assays using ligands with high specificity to cell membrane proteins have shown great promise for cell isolation [110, 212]. For example, by using anti-epithelial cell adhesion molecule (anti-EpCAM) antibodies immobilized on microposts, the isolation of rare circulating tumor cells (CTCs) from samples of whole blood has been demonstrated [110]. Unfortunately, antibodies generally have limited stability, are expensive and time-consuming to develop, and antibody-coated surfaces are susceptible to biofouling due to non-specific interactions between antibodies and other proteins [111]. Moreover, rapid and nondestructive release of antibody-bound cells is generally difficult [213], as the antibody-antigen binding is practically irreversible under normal physiological conditions [214].

Aptamers are oligonucleotides or peptides that bind specifically to target molecules. Isolated from a randomized oligonucleotide or peptide library using a synthetic selection process called systematic evolution of ligands by exponential enrichment (SELEX) [125], aptamers can recognize a large variety of target biomolecules, such as small molecules [112], peptides [114], and proteins [215], via unique three-dimensional conformations formed through interactions with the targets. Recently, aptamers have also been developed for cellular targets, such as ALL precursor T cells [216], liver cancer cells [217], and even

stem cells [218]. Since aptamers are produced using synthetic processes and are stable and amenable to chemical modifications [123], they offer an attractive alternative to antibodies as affinity ligands for isolation of rare cells. Although most aptamers use cell lines as their targets, they are often capable of targeting the more general population of diseased cells from real patient samples. For example, the aptamer sgc8c generated for a type of human ALL T cell line, CCRF-CEM cells, is capable of specifically targeting ALL T cells in patient blood [216, 219, 220]. Thanks to ongoing research efforts to develop improved SELEX methods and instruments, it is expected that aptamers will become readily available to recognize an increasingly broad collection of biological targets [221].

Aptamers have been explored in microfluidic systems as affinity ligands for cell isolation [222-225]. For example, surface-immobilized aptamers targeting prostate-specific membrane antigen (PSMA) and aptamers targeting protein tyrosine kinase 7 (PTK7) have been used to separate LNCaP cells and CCRF-CEM cells, respectively, from heterogeneous cell mixtures [217, 222, 223, 225]. However, there has been very limited work on releasing the captured cells from aptamer-functionalized surfaces. Attempts to rapidly and nondestructively release cells using methods such as tryptic digestion of target proteins [225], exonuclease degradation of aptamers [226], and hydrodynamic shear by infused air bubbles [223] have been hindered by several issues. Trypsin is able to digest only a small portion of biomarkers involved in affinity cell capture [227] and may negatively affect cell viability and phenotypic properties [228, 229], while the use of exonucleases is limited by inefficient diffusive transport of the enzymes, slow enzymatic reaction rates, and the destruction of the cell recognition surfaces. Similarly, air bubbles,

which release cells from aptamer surfaces by shear force, may cause physical damage to cells, while also generating dead volumes in microfluidic devices that lead to low cell release efficiency. There is hence a strong need for methods that allow specific capture and efficient, nondestructive release of subpopulations of cells in microfluidic devices.

Aptamer-target interactions are significantly influenced by environmental conditions; in particular, the affinity binding between aptamers and biomolecules can be strongly temperature dependent [198, 230, 231]. Cell-specific aptamers also target biomolecules, in this case proteins expressed on the cell membrane [217]. Therefore, it is reasonable to expect that interactions between aptamers and cells are also highly temperature sensitive. In this chapter, we investigated the specific capture and subsequent temperature-mediated release of cells in an aptamer-functionalized microfluidic device. Target cells can be captured with high specificity by a surface-immobilized aptamer, enriched by repeated introduction of multiple samples, and purified by washing with buffer. This is followed by a moderate temperature change of the surface, produced on-chip, to reversibly disrupt the cell-aptamer interaction, allowing release and elution of viable target cells for downstream analysis and regeneration of the aptamer-functionalized surface for device reuse. The device is applied to CCRF-CEM cells to demonstrate its potential utility for specific capture and nondestructive release of cells in basic biological research and clinical diagnostics.

4.2. Principle and Design

This section describes the principle and design of our microfluidic device. We first describe the specific cell capture and thermally controlled cell release approach, and then present the device design.

4.2.1. Cell Capture and Release Principle

The principle of aptamer-based specific capture and temperature-mediated release of cells is as follows. Aptamer molecules specific to target cells are immobilized on solid surfaces within a microfluidic device. A cell suspension containing target and non-target cells is introduced into the device and incubated for an appropriate period of time. The target cells are specifically captured by the surface-immobilized aptamer molecules via affinity binding (**Figure 4.1A**)**,** while the non-target cells are removed by washing (**Figure 4.1B**). Next, exploiting the strong temperature-dependence of affinity binding of aptamers and cells, the device temperature is increased to disrupt the binding and release the captured target cells from the surface-immobilized aptamer molecules (**Figure 4.1C**). This temperature-mediated cell release can be accomplished with a temperature increase such that released cells remain viable.

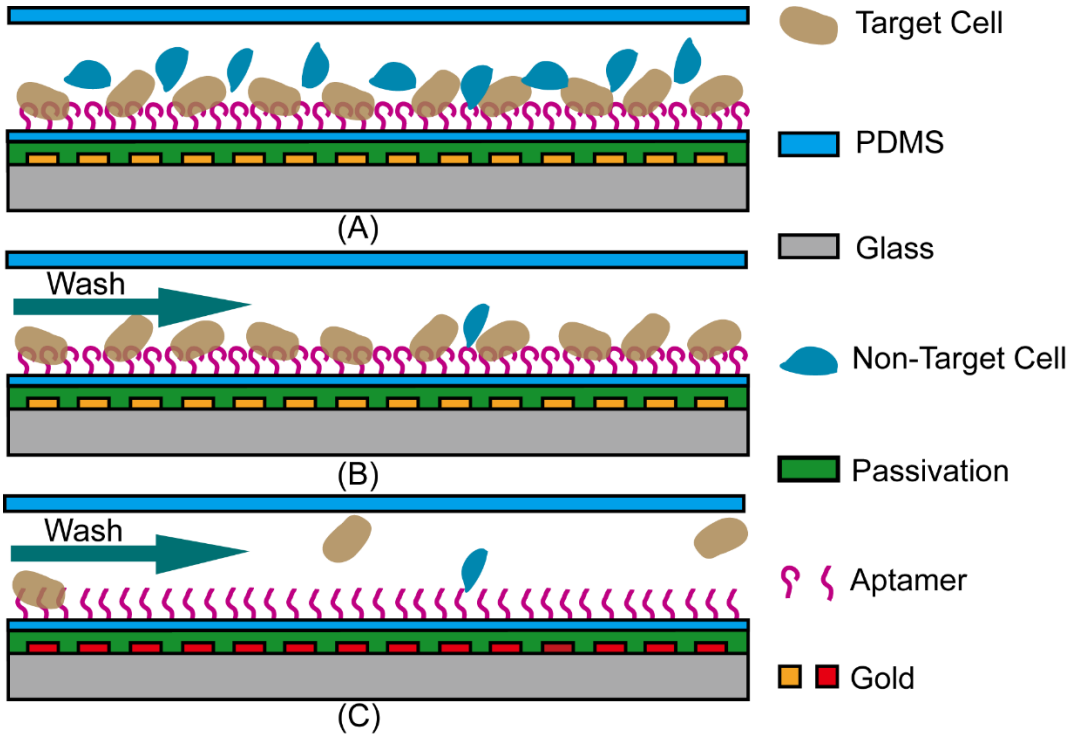

Figure 4.1: Principle of specific cell capture and temperature-mediated release. (A) Cell capture at room temperature. (B) D-PBS wash after capture. (C) Cell release at a moderately higher temperature.

The principle of aptamer-based specific capture and temperature-mediated release of cellular targets will be demonstrated using CCRF-CEM cells, a human-ALL cell line. ALL is the most common cancer for children from 0 to 14 years old, representing one third of all malignancies in that age group [232, 233]. CCRF-CEM cells are recognized by the DNA aptamer sgc8c (**Figure 4.2**) [220, 222, 223], which binds to the extracellular portion of PTK7 [234]. Toledo cells, a human diffuse large-cell lymphoma cell line not recognized by sgc8c, are used as a control target to study nonspecific binding [216, 220].

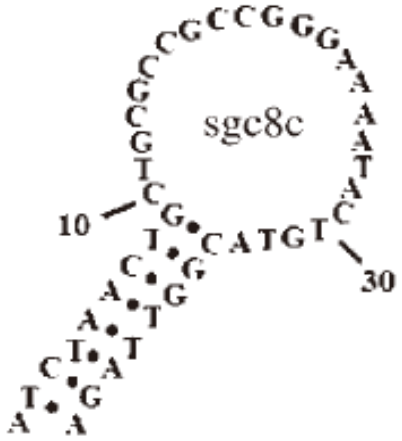

Figure 4.2: Structural formula of sgc8c aptamer [220].

4.2.2. Design

The microfluidic device used for cell capture and temperature-mediated cell release consists of a microchamber situated on a temperature control chip (**Figure 4.3**). The tapered chamber (2 mm in length, 1mm in width and 20 μm in height), whose surfaces are functionalized with aptamers specific to a target cell type, is connected to two inlets (3.5 mm in length, 0.7 mm in width and 600 μm in height) respectively for introduction of sample and washing buffer, and one outlet for collection of released cells or waste fluids. The microfluidic channels connecting these fluidic ports and the chamber are 0.5 mm in width and 20 μm in height. Integrated on the temperature control chip are a serpentine-shaped temperature sensor (linewidth: 25 μm) beneath the center of the chamber, and two serpentine-shaped heaters (linewidth: 300 μm) on each side of the temperature sensor. The chamber temperature can be controlled in closed loop using these integrated temperature sensor and heaters.

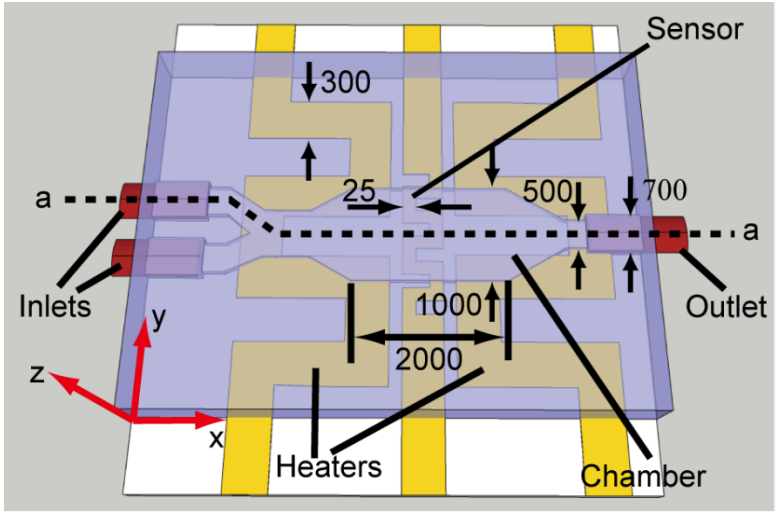

Figure 4.3: Schematic of the microfluidic device for the specific capture and temperature-mediated release of CCRF-CEM cells. Dimensions are given in micrometers.

4.3. Experimental

4.3.1. Materials

Chlorotrimethylsilane, (3-mercaptopropyl) trimethoxysilane (3-MPTS), 4-maleimidobutyric acid N-hydroxysuccinimide ester (GMBS), streptavidin and bovine serum albumin (BSA) were obtained from Sigma-Aldrich (St. Louis, MO). 5,5',6,6'-tetrachloro-1,1',3,3'-tetraethylbenzimidazolylcarbocyanine iodide (JC-1), propidium iodide (PI), RPMI-1640 media, fetal bovine serum (FBS), penicillin-streptomycin (P/S, penicillin 10,000 unit/mL, streptomycin 10,000 µg/mL), Dulbecco's phosphate-buffered saline (D-PBS) and the Vybrant® multicolor cell-labeling kit (DiI, DiO and DiD) were purchased from Invitrogen (Carlsbad, CA). CCRF-CEM and Toledo cell lines were obtained from the American Type Culture Collection (ATCC, Manassas, VA). The biotinylated sgc8c aptamer with a polyT(9) spacer at the 5’ end of the sequence (biotin-5'-

TT TTT TTT TAT CTA ACT GCT GCG CCG CCG GGA AAA TAC TGT ACG GTT AGA-3', K_d = 0.78 nM) was synthesized and purified with high-performance liquid chromatography (HPLC) by Integrated DNA Technologies (Coralville, IA).

4.3.2. Microfluidic Device Fabrication

The temperature control chip was fabricated using standard microfabrication techniques. A glass slide (Fisher HealthCare, Houston, TX) was cleaned by piranha. Chrome (10 nm) and gold (100 nm) thin films were deposited by thermal evaporation and patterned by wet etching to generate the temperature sensor and heaters which were then passivated by 1 µm of silicon dioxide that was deposited using plasma-enhanced chemical vapor deposition (PECVD). Finally, contact regions for electrical connections to the sensor and heaters were opened by etching the oxide layer using hydrofluoric acid (**Figure 4.4A**).

In parallel, the microchamber was fabricated from polydimethylsiloxane (PDMS) (Sylgard 184, Dow Corning Inc. Midland, MI) using soft lithography techniques. Layers of SU-8 photoresist (MicroChem Corp., Newton, MA) were spin-coated on a silicon wafer (Silicon Quest International, Inc., San Jose, CA), exposed to ultraviolet light through photomasks, baked, and developed to form a mold defining the microfluidic features. Next, a PDMS prepolymer solution (base and curing agent mixed in a 10:1 ratio) was cast onto the mold and cured on a hotplate at 72 °C for 1 hour (**Figure 4.4B**). The resulting sheet bearing the microfluidic features was then peeled off the mold (**Figure 4.4C**).

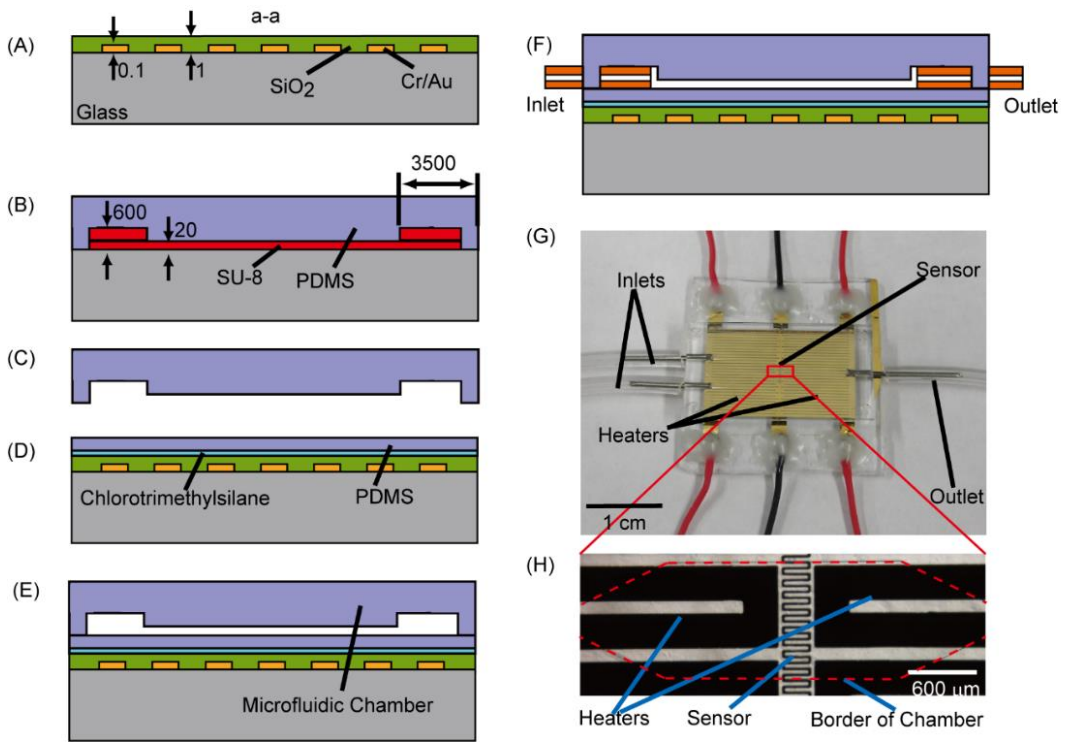

Figure 4.4: Device fabrication: (A) Deposition, patterning and passivation of gold sensor and heaters. (B) Fabrication of SU-8 mold. (C) Demolding of PDMS microchamber. (D) Treatment with chlorotrimethylsilane and PDMS spin-coating. (E) Bonding of PDMS microchamber to PDMS-coated temperature control chip. (F) Insertion of inlet and outlet capillary tubes. (G) Photograph of a fabricated device. (H) Micrograph of the temperature sensor and heaters in the device. Dimensions are given in micrometers.

Subsequently, the surface of the temperature control chip was treated with chlorotrimethylsilane, and a PDMS layer (approximately 100 µm) was spin-coated onto the chip (**Figure 4.4D**). Then, the PDMS sheet was bonded to the PDMS membrane on the chip after treatment of the bonding interfaces with oxygen plasma for 15 seconds (**Figure 4.4E**). Finally, capillary tubes (O.D. = 813 µm and I.D. = 495 µm) were inserted into the

inlet and outlet ports (**Figure 4.4F**), resulting in a packaged device. Following each experiment, the PDMS film and chamber were easily removed from the temperature control chip, allowing the chip to be reused for the next experiment. A fabricated and packaged device is shown in **Figure 4.4 G** and **H**.

4.3.3. Surface Modification

The biotinylated sgc8c aptamer was functionalized in a freshly fabricated device using an established protocol with slight modifications [110]. The microchamber was first treated with 4% (v/v) 3-MTPS in ethanol for 30 min at room temperature, followed by an ethanol wash. Then, 2 mM GMBS in ethanol was introduced and incubated for 20 min at room temperature, followed by an ethanol wash and drying by nitrogen. Next, the chamber was incubated overnight with 100 µg/mL streptavidin in D-PBS at 4 °C, followed by a D-PBS wash. Finally, 10 µM of biotinylated sgc8c aptamer in D-PBS was introduced into the chamber and incubated at room temperature for 20 min. A D-PBS wash was used to remove free aptamer molecules, leaving immobilized aptamer molecules on the surface. Just prior to cell introduction, the chamber was incubated with 1 mg/mL BSA solution in D-PBS at room temperature for at least 30 min to minimize nonspecific adsorption of cells.

4.3.4. Cell Culture and Preparation

Both CCRF-CEM and Toledo cells were incubated with RPMI-1640 media supplemented with 10% FBS and 1% P/S, and were kept at 37 °C in a humidified incubator containing 5% CO_2. Before microfluidic experiments, each cell type was collected through centrifugation, resuspended at 1×10^8 cells/mL in D-PBS supplemented with 1 mg/mL

BSA, and then kept on ice. Cells were mixed or diluted to different concentrations prior to introduction into the microfluidic device.

4.3.5. Experimental Setup

Closed-loop temperature control of the chamber was achieved using the integrated temperature sensor and heaters with a proportional-integral-derivative (PID) algorithm implemented in a LabVIEW (National Instruments Corp., TX) program on a personal computer. The resistance of the sensor was measured by a digital multimeter (34420A, Agilent Technologies Inc., CA), and the two heaters were connected to a DC power supply (E3631, Agilent Technologies Inc., CA). The microfluidic device's two inlets were connected to syringes that respectively contained cell mixture and D-PBS, and was each driven by a syringe pump (KD210P, KD Scientific Inc., MA). The outlet was connected to a microcentrifuge tube for collection of released cells or experimental waste. Unless indicated otherwise, all phase contrast images and fluorescent images of the chamber were taken using an inverted epifluorescence microscope (Diaphot 300, Nikon Instruments Inc., NY) with a CCD camera (Model 190CU, Micrometrics, NH) (**Figure 4.5**).

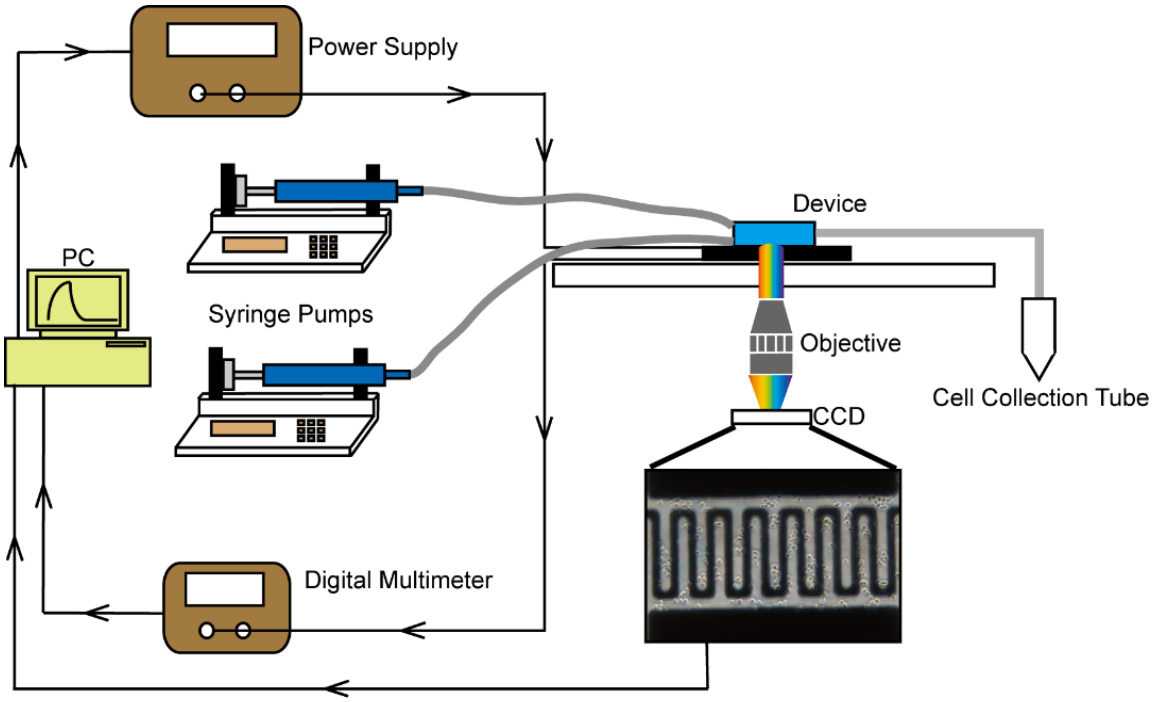

Figure 4.5: Experimental setup for specific capture and temperature-mediated release of cells.

4.3.6. Testing Procedure

During cell capture experiments, a batch of CCRF-CEM cells was introduced into the chamber and incubated without any fluid flow for 1 min. This process was repeated several times, followed by a wash with D-PBS at 5 μL/min for approximately 1 min. An image of the cell-laden chamber was taken and used to manually count the number of captured cells, which was used to compute the captured cell density on the surface. To test the specificity of cell capture, CCRF-CEM and Toledo cells were labeled with the fluorescent dyes DiO and DiI, respectively, and fluorescent images were taken after the first introduction of the cell mixture as well as after D-PBS washing.

In temperature-mediated cell release experiments, the chamber was heated using the integrated heaters via closed loop temperature control to a desired temperature for 2 min, and flows of D-PBS at various rates were used to rinse the chamber. Images of the chamber were taken every 2 seconds, and used to manually count the cells that remained on the aptamer-immobilized surface.

To test cell viability, the retrieved cells were kept in D-PBS with 10% FBS containing PI (2 μM) and JC-1 (10 μg/mL) at 37 °C for 1 hour, and then phase contrast and fluorescent images were taken with an inverted microscope (DMI6000B, Leica Microsystems Inc., IL) equipped with a digital camera (Retiga 2000R, Qimaging, Canada) and commercial image acquisition software (InVitro, Media Cybernetics Inc., MD). Moreover, a batch of cells was treated in a water bath at 48 °C for 2 minutes and then cultured for 4 days. The concentration of cultured cells was determined each day using a hemacytometer (Chang Bioscience Inc., CA).

4.4. Results and Discussion

This section presents and analyzes experimental results from the aptamer-based microfluidic device. We first characterize the temperature control chip and evaluate the uniformity of the temperature field in the chamber. Then, specific capture and temperature-mediated release of cells are performed using CCRF-CEM and Toledo cell lines to investigate factors that influence the efficiency of cell capture and release. Finally, the viability of retrieved cells is evaluated to confirm the nondestructive nature of the cell release mechanism.

4.4.1. Temperature Sensor Characterization

The temperature sensor was first calibrated using an environmental test chamber (9023, Delta Design Inc., CA) maintained at a series of temperatures which are measured with high accuracy temperature reference probes (5628, Fluke Calibration, UT). The measured resistance (R) of the thin-film gold temperature sensor was observed to vary linearly with temperature (T). The dependence could be represented by the relationship $R = R_0 [1 + \alpha (T - T_0)]$, where R_0 is the sensor resistance at a reference temperature T_0, and α is the temperature coefficient of resistance (TCR) of the sensor. Fitting this relationship to the measurement data allowed determination of the parameter values, which were used to determine the chamber temperature from the measured sensor resistance during cell capture and release experiments. The temperature sensor typically had a measured resistance of 209.60 Ω at a reference temperature of 21.9 °C with a TCR of 2.58×10^{-3} 1/°C, as shown in **Figure 4.6A**. We then characterized the temperature control of the chamber through which D-PBS buffer was continuously infused to simulate the cell capture or release process. The chamber temperature, controlled in closed loop by the integrated heaters via feedback from the temperature sensor, was seen to increase from room temperature (~24 °C) to 48 °C rapidly (with an approximate closed loop time constant of 2.7 s based on an exponential fit) while exhibiting a minimal overshoot (~ 0.2 °C) (**Figure 4.6B**). The temperature remained within approximately 0.1 °C of the desired temperature setpoint for the duration of each experiment, as shown in the inset of **Figure 4.6B**.

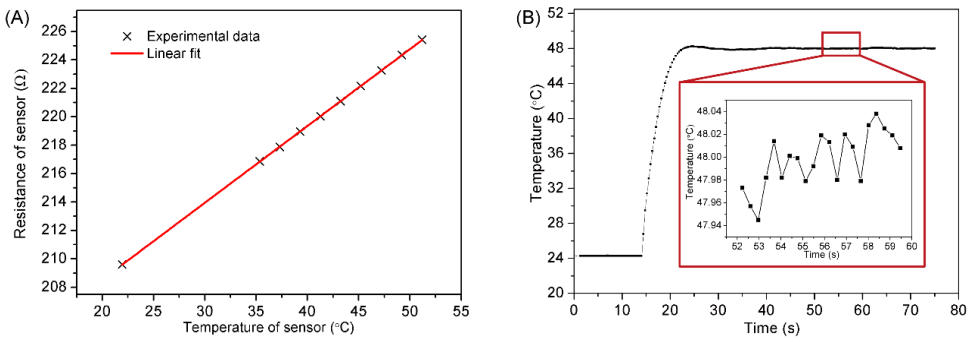

Figure 4.6: (A) Resistance of temperature sensor (R) showing highly linear dependence on temperature (T). The solid line represents a linear fit to the experimental data with a regression equation: $R = 209.6\ [1 + 2.58\times10^{-3}\ (T\text{-}21.9)]$ (coefficient of determination R^2=0.999). (B) Time-resolved tracking of the temperature inside the D-PBS filled chamber, with the inset showing noise that was present during temperature measurements.

4.4.2. Simulation of Temperature Distribution

To evaluate the uniformity of the temperature distribution in the chamber, we present results from numerical simulation using a three-dimensional steady-state heat transfer model [235]. The model considers heat conduction in the solid materials as well as forced convection due to the buffer flow (flow rate: 5 μL/min), with natural convection neglected. Properties at room temperature are used for the solid materials, and the property of the aqueous buffer is evaluated at the average temperature (36 °C) over the range (24 °C to 48 °C) used in the experiments. The model includes the Pyrex glass substrate (thermal conductivity: 1.3 W/m·K), gold heaters (thermal conductivity: 317 W/m·K), a PDMS membrane (thermal conductivity: 0.16 W/m·K) above the SiO_2 electrical passivation layer, liquid buffer in the chamber (thermal conductivity 0.62 W/m·K), and PDMS sheet (thermal conductivity: 0.16 W/m·K), with the SiO_2 passivation layer neglected due to its small

thickness (< 1 μm). The model is solved using the COMSOL Multiphysics software package (COMSOL, Inc., CA).

The temperature distribution in the chamber at a flow rate of 5 μL/min is shown in **Figure 4.7**. It can be seen that the temperature throughout the chamber was quite uniform, thanks to the heater design, which has a relatively large size with respect to that of the chamber. The temperature variation is less than 0.03 °C on the lower chamber surface, to which aptamer molecules are immobilized (**Figure 4.7A**), as well as *xz*-plane of symmetry inside the chamber (**Figure 4.7B**). There is approximately a 0.2 °C difference between the temperatures on the lower chamber surface and on the substrate surface where the temperature sensor is located. This temperature difference is insignificant compared to the magnitude of temperature changes used in thermally activated cell release, and if desired, could be used as a correction value because of the more uniform in-plane temperature distributions. Based on this numerical analysis, it is concluded that the temperature distribution generated by the on-chip heaters is sufficiently uniform in the chamber for the cell capture and release experiments.

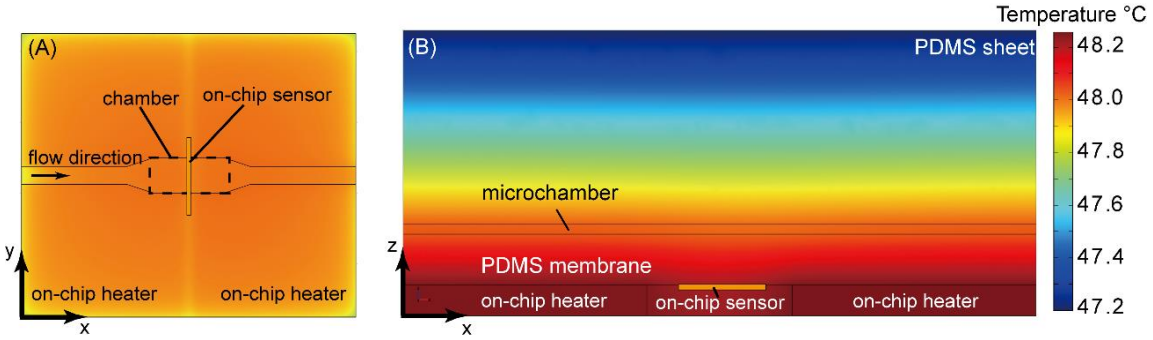

Figure 4.7: Numerically determined temperature distribution in the chamber within (A) *xy*-plane on the lower surface of the chamber and (B) xz-plane of symmetry.

4.4.3. Specific Cell Capture

To verify specific cell capture at room temperature, a mixture of CCRF-CEM cells (target cell type, 3.5×10^6 cells/mL) and Toledo cells (non-target cell type, 5.0×10^6 cells/mL) was introduced into the sgc8c aptamer-modified microchamber and incubated for 1 min. The total number of CCRF-CEM cells observed on the surface, 51 in total, was less than that of Toledo cells, 78 in total (**Figure 4.8A**). However after washing, all non-specifically adsorbed Toledo cells were removed, leaving only specifically captured CCRF-CEM cells on the surface. Moreover, after 10 cell samples were introduced (each followed by rinsing with D-PBS), the target cells dominated the chamber surface, with only 8 non-target Toledo cells visible amongst a few hundred CCRF-CEM cells (**Figure 4.8B**). This demonstrates the specific and effective capture of CCRF-CEM cells using the surface-immobilized aptamers, and the capability of the device to enrich target cells from a heterogeneous mixture.

To test the transient behavior of the cell capture process, CCRF-CEM cell suspensions with concentrations of 5.0×10^6 cells/mL were introduced into the aptamer-functionalized chamber and allowed to incubate for varying lengths of time. After incubation, D-PBS was used to remove unbound cells. The percentage of captured cells in each introduction was calculated by $\eta \approx N_a / N_b$, where N_a is the number of captured cells, i.e., cells that remained on the microfluidic aptamer-functionalized surface after washing, and N_b is the maximum number of cells that can be captured due to geometric limitations. Because of the height of the chamber (20 μm) and the low cell density of the introduced cell suspension, we assumed that only a single monolayer of cells could be arranged on the lower surface of

the chamber. Therefore, N_b is also equal to the number of cells observed in the chamber before washing. As shown in **Figure 4.8C**, increasing incubation time resulted in an increase in cell surface density.

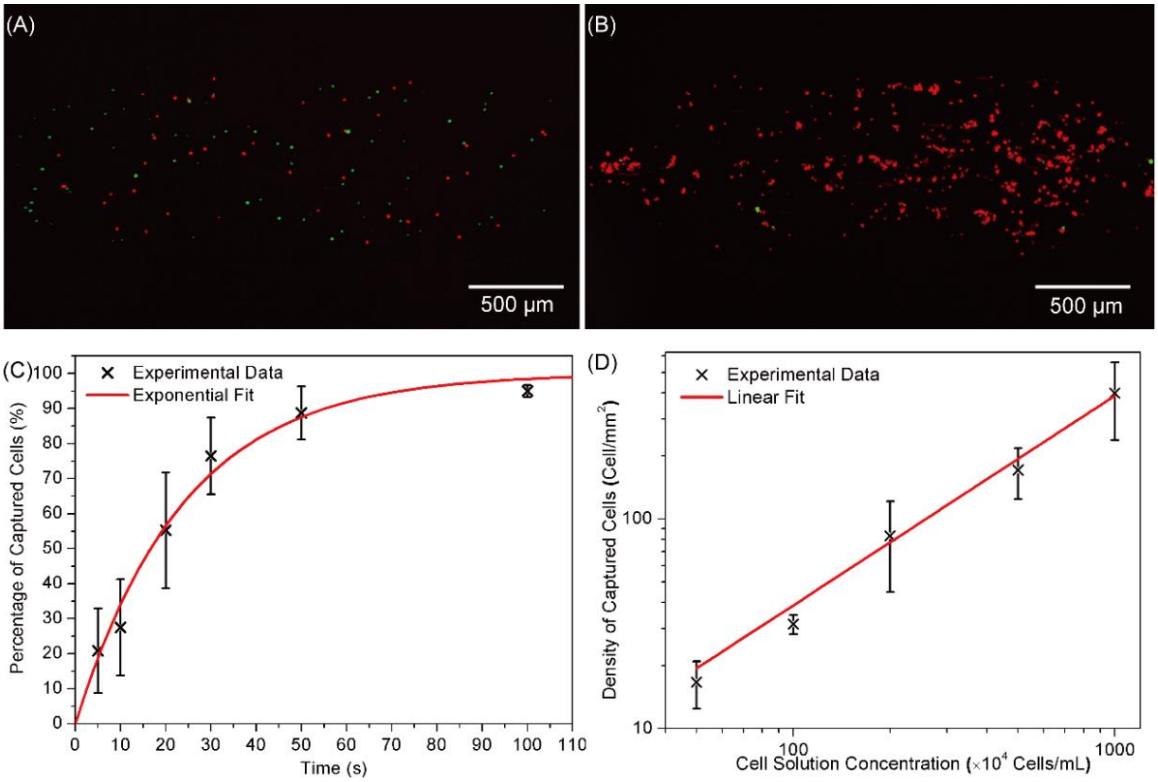

Figure 4.8: (A) Image of the chamber after the introduction of a cell sample. (B) Image of the chamber after the introduction of 10 cell samples and D-PBS washing. (C) Time response of cell capture: percentage of cells captured (η) versus incubation duration (t). The solid line represents an exponential fit to the experimental data with a regression equation: $\eta = 1 - e^{-t/24}$ (R^2=0.982, n=3). (D) Concentration response of cell capture: density of captured cells ($\rho_{capture}$) as a function of the cell suspension concentration (c_{cell}). The solid line represents a linear fit to the experimental data with a regression equation: $\rho_{capture}$ = 0.3874 c_{cell} (R^2=0.995, n=3).

We consider a monovalent model for the equilibrium affinity binding between surface immobilized aptamer sgc8c (of initial surface density γ_0 at $t = 0$) and cell membrane protein PTK7 (approximated as a sheet of protein of initial surface density σ_0 at $t = 0$) to form a complex sgc8c-PTK7 (of surface density y at time t, with $y = 0$ at $t = 0$) [236]: $\text{sgc8c+PTK7} \underset{k_{\text{off}}}{\overset{k_{\text{on}}}{\rightleftharpoons}} \text{sgc8c-PTK7}$, where k_{on} and k_{off} are respectively the association and dissociation rate constants for the binding between sgc8c and PTK7. The binding kinetics is governed by: $\frac{dy}{dt} = k_{\text{on}}(\sigma_0 - y)(\gamma_0 - y) - k_{\text{off}} y$. At equilibrium, $dy/dt = 0$, and therefore $\frac{dy}{dt} = k_{\text{on}}(\sigma_0 - y_{\text{eq}})(\gamma_0 - y_{\text{eq}}) - k_{\text{off}} y_{\text{eq}} = 0$. Assuming a sufficiently high density of surface immobilized aptamer, so $\gamma_0 \gg \sigma_0$. The maximal density of sgc8c-PTK7 (y) is equal to σ_0, $\gamma_0 \gg y$; therefore, $\frac{dy}{dt} \approx k_{\text{on}}(\sigma_0 - y)\gamma_0 - k_{\text{off}} y$, and $k_{\text{on}}(\sigma_0 - y_{\text{eq}})\gamma_0 - k_{\text{off}} y_{\text{eq}} = 0$. In this state, the solution can be represented by $y - y_{\text{eq}} = Ce^{-(k_{\text{on}}\gamma_0 + k_{\text{off}})t}$, and $y_{\text{eq}} = \frac{\sigma_0}{1 + \frac{k_{\text{off}}}{k_{\text{on}}\gamma_0}} = \frac{\sigma_0}{1 + K_d / \gamma_0}$ where $K_{\text{d}} = k_{\text{off}} / k_{\text{on}}$ is the equilibrium dissociation constant (with the unit of surface density). According to the initial condition that $y = 0$ at $t = 0$, this equation can be solved to obtain $y = \sigma_0 \frac{1}{K_{\text{d}} / \gamma_0 + 1}(1 - e^{-(k_{\text{on}}\gamma_0 + k_{\text{off}})t})$. As cell capture happens only when there are sufficient aptamer-protein complexes, the percentage of cells captured (η) is proportional to $y / \sigma_0 = \frac{1}{K_{\text{d}} / \gamma_0 + 1}(1 - e^{-(k_{\text{on}}\gamma_0 + k_{\text{off}})t})$.

This exponential relationship is consistent with our experimental observation (**Figure 4.8C**), and a least square fit suggests that cell capture time constant τ is approximately equal to 24 s (coefficient of determination R^2 = 0.982). Cell loss during washing could be almost completely eliminated via incubation by setting incubation time (t) to a value such that percentage of cells captured (η) approximates to 1. The time constant (τ) indicates the rate at which the surface concentration of captured cells approaches its maximum value, and can be used to calculate the time needed to isolate a number of target cells from the heterogeneous cell suspension. It was estimated that approximately 92% of introduced cells exposed to the aptamer-functionalized surface were captured after incubating for 1 min. These results, which were similarly obtained at other cell concentrations ranging from 0.5×10^6 to 10×10^6 cells/mL, could be further improved by optimizing the channel design [110], surface topography [226], and operation conditions such as flow rates [237].

We next investigated the effects of the cell suspension concentration on the surface density of captured cells. Cell capture experiments were conducted using samples with varying cell concentrations (0.5 to 10×10^6 cells/mL). In each experiment, 5 aliquots of cells were introduced into the chamber, each followed by a 1-min incubation. Each test was performed in triplicate simultaneously on identical devices (n = 3). All of the devices were fabricated at the same time to guarantee chamber surfaces were generated with nominally identical aptamer densities to ensure consistent experimental data. Experiments with the most dilute cell suspension (0.5×10^6 cells/mL) yielded captured cells with a surface density of 17±4 cells/mm^2 (n = 3), while those with the most concentrated cell suspension (10×10^6 cells/mL) resulted in a captured cell density of approximately 399±160 cells/mm^2 (n = 3),

as shown in **Figure 4.8D**. It can be seen that in this range of cell concentrations, the captured cell density was approximately proportional to the cell concentration $\rho_{capture} = A\ c_{cell}$, where c_{cell} is the cell suspension concentration (cells/mL), and A is a proportionality constant that depends on device characteristics such as the surface density of immobilized aptamer molecules and equilibrium cell-aptamer affinity association, and testing parameters such as the number of samples introduced to the chamber. The linear equation fitted the experimental data well ($R^2 > 0.99$), resulting in a value of A equal to 0.3874 mL/mm^2. These results indicate that there is a large dynamic range of cell suspension concentrations over which the device can capture a predictable surface concentration of cells for downstream analysis.

4.4.4. Temperature-Mediated Cell Release

We next tested the thermally induced release of captured cells from the aptamer-functionalized chamber surfaces. Prior to the experiment, CCRF-CEM cells were captured by the surface-immobilized sgc8c aptamer, and unspecific bound cells were removed by D-PBS washing. Then, the cell-laden chamber was rinsed at either room temperature or 48 °C (**Figure 4.9A**). It was seen that approximately 80% of cells were released from the surfaces after rinsing with D-PBS at 5 µL/min and 48 °C for 2 min, whereas negligible cell release was observed when rinsing at room temperature with an identical buffer solution and flow rate. These results suggest that the release of CCRF-CEM cells may have been caused by the conformational changes in the aptamer structure at the elevated temperature.

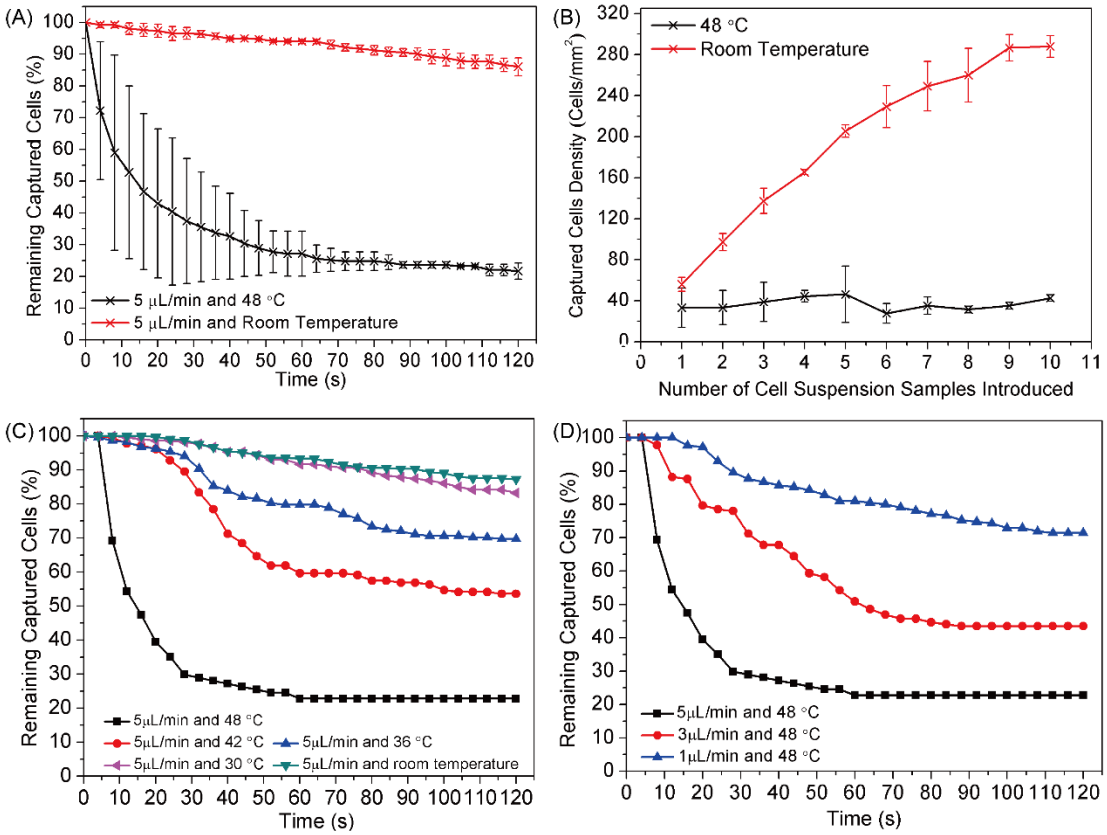

Figure 4.9: (A) Percentage of captured cells remaining on the substrate as a function of time while rinsing at constant temperature (48 °C and room temperature) and flow rate (5 μL/min). (B) Captured cell density versus the number of cell suspension samples introduced while the temperature was maintained at either 48 °C or room temperature. (C) Effect of temperature on cell release efficiency while rinsing at 5 μL/min. (D) Effect of flow rate on cell release efficiency while the chamber temperature was maintained at 48°C.

We then tested this hypothesis of cell release due to heat-induced conformational changes to aptamer structure, seeking to exclude denaturation of cell membrane proteins as the cause of cell release. To do so, we conducted additional tests in which cells were heated prior to capture in the device, and compared the results to those from heating the

device itself during cell capture. The cell suspension, diluted to 5×10^6 cells/mL, was heated at 48 °C for 2 min, followed by introduction to the chamber at room temperature. In parallel, an unheated cell solution of 5×10^6 cells/mL was introduced into a chamber with the chamber temperature set to 48 °C. In both tests, 10 aliquots of cells were introduced into the chamber, followed by 1 min of incubation after each cell introduction. Heat treated cells were captured at room temperature up to a concentration of 288 ± 10 cells/mm^2 (n = 3), as shown in **Figure 4.9B**. Unheated cells in a 48°C chamber achieved a surface density of only 43 ± 3 cells/mm^2 (n = 3), and the presence of these remaining surface-bound cells was attributed to non-specific adsorption. These results suggest that the conformational changes in the aptamer structure, rather than the denaturation of the target cell membrane protein PTK7 [217] at the increased temperature, caused the release of the specifically captured cells.

Having eliminated denaturation of the cell surface protein as the cause of cell release, we then investigated the relative impact on cell release of the chamber temperature compared to the hydrodynamic shear stress applied by the buffer flow. Cell detachment from aptamer-functionalized substrates is governed by the balance between the hydrodynamic shear stress applied on cell surfaces and the temperature-dependent binding strength of aptamers and their target cells. Therefore, changes in either the chamber temperature or the buffer flow rate would result in different cell release efficiencies. We first tested the effects of temperature on cell release by varying the chamber temperature from 30°C to 48°C while rinsing with D-PBS (**Figure 4.9C**). It was clearly seen that with the elevated temperature, an increasing number of cells were detached from the substrate.

Moreover, as the local temperature increased from 30 to 48°C, the viscosity of the aqueous washing buffer would decrease by approximately 35% [238], which would lead to a 35% lower shear stress at the cell membranes. This indicates that at higher temperatures there is a greater loss of binding between the aptamers and the cells, most likely due to temperature-dependent changes in conformational structure of aptamers. Next, we further evaluated the effect of shear stress on cell release, by performing identical experiments while varying the flow rate through the chamber. As shown in **Figure 4.9D**, a higher flow rate caused more cells to detach from the substrate, as a result of increased shear stress disrupting the cell-aptamer binding. As either a higher temperature or a larger shear stress poses a greater risk of cell damage, the tradeoff between them is an important design consideration.

As conformational changes in aptamer structures are reversible, this indicates that we can create a regenerable cell-capture surface, which would reduce the average cost of assays using the microfluidic device. To verify the reusability of the aptamer-functionalized surface, three experimental cycles were performed in the same device, with each cycle consisting of first introducing a dilute cell solution to the microchamber at room temperature, then releasing cells at 48 °C and 5 µL/min for 2 min, and finally regenerating the aptamer-functionalized surface (releasing all remaining cells) via washing with D-PBS at 60 °C and 50 µL/min for 2 min, and then at room temperature and 50 µL/min for 2 min. Following the first cycle, similar densities of captured cells were observed for succeeding cycles, with a maximum difference of captured cell density of only 8% between the first and the second capture (**Figure 4.10**). Given these results, we conclude that the regeneration of cell capture function of the microfluidic device can be both effective and

consistent. Although some residual cells remained on the surfaces after each regeneration, this could be addressed by using a higher temperature and flow rate.

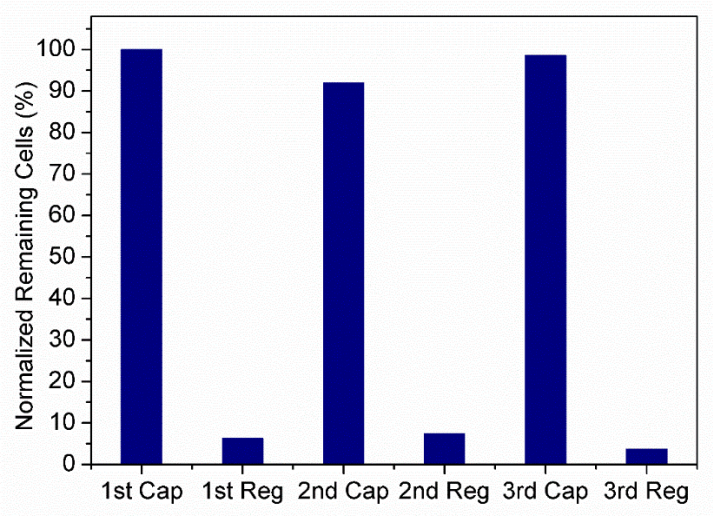

Figure 4.10: Cell capture and re-capture on the regenerated aptamer-functionalized surface: the normalized percentage of remaining cells after the first, second and third capture and regeneration cycle.

4.4.5. Cell Viability Assay

Cell viability is important for downstream applications such as tissue engineering and cell-based therapeutics [203, 204]. To evaluate cell viability, released cells were collected after rinsing at 5 µL/min and 48 °C for 2 min, at which point PI [239] and JC-1 [240, 241] were used to stain cells. PI is a red-fluorescent nuclear stain that is not permeant to live cells. JC-1 accumulates in healthy mitochondria as indicated by red fluorescence, the intensity of which decreases along with mitochondrial depolarization occurring in the early stage of apoptosis. Our experimental results showed that the PI stained cells did not emit

any red fluorescence (**Figure 4.11A**), and the JC-1 stained cells exhibited bright red fluorescence (**Figure 4.11B**), indicating that the collected cells were viable.

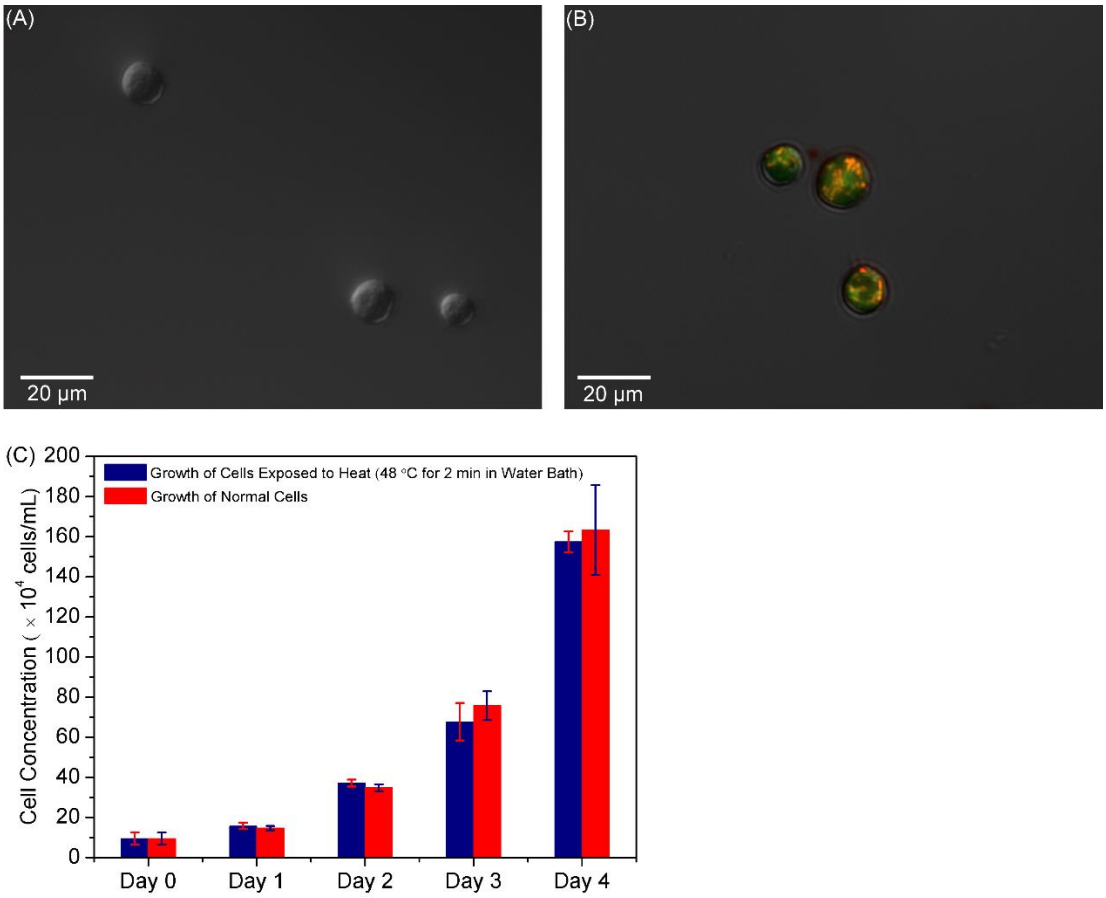

Figure 4.11: Image of PI stained cells (A) and JC-1 stained cells (B) following cell capture and release experiment, generated by a combination of phase contrast and fluorescent micrographs. (C) Concentrations of normal cells and heat-treated cells as a function of culture duration.

To obtain further confirmation of cell viability, we performed cell culture testing. Because of practical difficulties [242] in conducting cell culture using cells directly retrieved from the microfluidic device without an on-chip cell culture component, we

performed off-chip cell proliferation assays, in which cells from a well-mixed suspension were treated in water bath at 48 °C for 2 min and then cultured for several days. Meanwhile, cells from the same suspension were also cultured without any treatment for the same period to serve as a control. The growth curves of normal and heat-treated cells are shown in **Figure 4.11C**, in which heat-treated cells are seen to have a similar proliferation rate as normal cells. This indicates that the brief period of modestly elevated temperature used in the cell release experiment would not induce detectable cell damage, allowing the thermally released cells to remain viable.

4.5. Conclusion

The ability to isolate and retrieve live cells from biological samples is critical in both basic cell biology studies and clinical diagnostics. In this chapter, we have developed an aptamer-based microfluidic device for specific capture and temperature-mediated release of cells. The device consists of a microchamber situated on a temperature control chip that includes an integrated temperature sensor and heaters. The chamber surface is functionalized with aptamers to capture target cells with high specificity. The integrated temperature sensor and heaters allow closed-loop control of the chamber temperature, enabling thermally induced release of the captured cells without causing any physical or chemical damage.

The temperature control chip was first characterized experimentally and numerically to ensure temporal and spatial accuracy of the temperature field, respectively. Further experiments demonstrated highly specific capture and enrichment of CCRF-CEM cells using the sgc8c aptamer, followed by measurements of the sensitivity of cell capture to the

concentration of cell suspension and to the incubation time within the chamber. Subsequently, efficient temperature-mediated release of cells was achieved, and the effects of the chamber temperature and shear stress on the aptamer-cell interaction were investigated. It is found that both higher temperatures and higher shear stresses facilitate cell release, and the tradeoff between these two factors is an important design consideration, due to the greater risk of cell damage when using either a higher temperature or a larger shear stress. Finally, the released cells were shown to be viable, and the aptamer-functionalized surfaces were successfully regenerated and shown to be reuseable. These results demonstrate that our approach can potentially be used in basic biological research and clinical diagnostics for the isolation of viable pure cell subpopulations.

Further studies will involve more stringent cell viability testing, such as using quantitative flow cytometry and gene expression analysis to confirm that thermal release processes induce no variations in cells at both cellular and genetic levels. If necessary, appropriate measures, such as the use of aptamers with lower affinity or stronger temperature dependence to allow cell release at lower temperatures, can be used to minimize such cellular or genetic variations.

Chapter 5. Specific Capture and Temperature-Mediated Release of Cells: Spatial Selectivity via Patterned Aptamer Surfaces

The microfluidic device described in Chapter 4 demonstrated the feasibility of aptamer functionalized surface for highly specific cell isolation. Moreover, it explored, for the first time, the temperature response of binding affinity between aptamers and cells, and therefore allowed thermally activated release and retrieval of captured cells. Although novel, the cell release in Chapter 4 was not spatially selective in that all captured cells were released from the entire microfluidic surfaces.

In this chapter, a proof-of-concept microfluidic device for spatially selective specific capture and temperature-mediated release of cells using nucleic acid aptamers is presented. The device consists of a microchamber situated on a microchip with four groups of micro heaters and temperature sensors. Aptamers are patterned on design-specified regions of the chip surface, and the heat generated by the micro heaters is restricted to each aptamer-functionalized area. We demonstrate the device by performing specific capture of CCRF-CEM cells, a human acute lymphoblastic leukemia (ALL) cell line, with surface patterned DNA aptamer sgc8c. Spatially selective release of CCRF-CEM cells is achieved by utilizing a group of microheater and temperature sensor that restricts temperature changes, and therefore the disruption of cell-aptamer interactions, to a design-specified region. The work presented in this chapter has resulted in a peer-reviewed conference proceeding [243] and a journal publication [244].

5.1. Introduction

Specific cell isolation is important in basic biological research and clinical diagnostics. Antibodies that are specific to cell membrane proteins are most often employed to achieve this goal. For example, magnetic-activated cell sorting (MACS) and fluorescence-activated cell sorting (FACS) are highly attractive due to their high specificity to target cells [206, 207]. The MACS method relies on the presence or absence of magnetic forces to recognize different cell types. Although it is amenable to high-throughput operations, there is generally no difference between the magnetic forces generated by microbeads with different surface-modified antibodies specific to different target cells [208]. Hence, MACS is a single-parameter cell isolation method, and lacks the capability to distinguish and sort multiple types of cells. On the other hand, FACS uses different species of antibodies with different fluorescent labels to recognize target cells. Multiple characteristics of cells can be monitored, and thus different cell types can be separated and collected simultaneously [207]. However, the application of FACS is restricted by its relatively low yield and complex and expensive experimental instrumentation.

Microfluidic technologies have been developing to enable more efficient and effective cell isolation with improved sensitivity and resolution, minimized sample and reagent consumption, lower cost, and the capability of automation and point-of-care (POC) [209]. To achieve specific cell isolation, antibodies have always been employed [110, 212]. For example, the isolation of rare circulating tumor cells (CTCs) from whole blood samples has been achieved in a microfluidic device with micropillars that are functionalized with anti-epithelial cell adhesion molecule (anti-EpCAM) antibodies [110]. Unfortunately,

antibodies are not always stable, and are expensive and time-consuming to develop [111]. In addition, in order to achieve molecular and functional analysis [245] or cell based therapeutics [204], cells must be released with minimal contamination and negligible disruption to their viability. However, the interaction between antibodies and antigens are not reversible under normal physiological conditions [213, 214]. Cells are hence typically released from antibody-functionalized surfaces using trypsin to digest antibody-specific cell membrane proteins [246], or varying the substrate hydrophobicity to detach hydrophobically anchored antibodies [247]. Tryptic digestion is not efficient, only applicable to a small portion of biomarkers involved in affinity cell capture [227], and may influence cell viability and phenotypic properties [228, 229]. Meanwhile, temperature dependent substrate property alteration cannot cause the dissociation of antibodies from the antigens, leaving the antibodies attached to cell membranes [247]. Therefore, there is a strong need for methods that allow rapid and non-destructive release of cells from affinity surfaces.

Aptamers, which are oligonucleotides that bind specifically to target molecules, have the potential to resolve these problems. Aptamers can be selected from a randomized oligonucleotide library using a synthetic process [125]. Compared with antibodies, aptamers are stable, designable and amenable to chemical modifications [123]. Meanwhile, the binding between aptamers and target molecules is reversible due to conformational changes caused by temperature variations [198, 201]. In addition, recent advances in synthetic aptamer development have resulted in aptamers for multiple cellular targets, such as ALL precursor T cells [216], liver cancer cells [217] and stem cells [218]. These

aptamers bind to cell membrane proteins by hydrogen bonds, hydrophobic interactions, van der Waals interactions, aromatic stacking, or their combinations. Such affinity binding allows the aptamers to capture target cells specifically [248, 249]. Therefore, aptamers are attractive alternatives to antibodies as affinity ligands for cell isolation. For example, aptamers targeting prostate-specific membrane antigen (PSMA) have been used in a microfluidic system to separate LNCaP cells from a heterogeneous cell mixture [225]. Release of aptamer-captured cells has been accomplished by methods such as exonuclease degradation of aptamers [226], air bubble dislodging [223], and temperature stimulation [201]. Unfortunately, the use of exonuclease is inefficient due to the slow diffusive transport of enzymes and the low enzymatic reaction rate, while the use of air bubbles may damage cells and generate dead volumes leading to low cell release efficiency.

In the previous chapter, we demonstrated that these issues could be addressed by temperature-mediated cell release, although the release was not spatially selective in that all captured cells were released from the entire microfluidic surfaces. This chapter presents a microfluidic device with a surface selectively functionalized with cell-specific aptamers and integrated micro heaters with temperature sensors to achieve specific cell capture and temperature-mediated release of selected groups of cells. Aptamers are patterned on design-specified regions of the chip surface, and the heat generated by the micro heaters is restricted to each aptamer-functionalized chip area. Target cells can be captured by the surface-patterned aptamers with high specificity. A moderate temperature change is then produced using a group of micro heater and temperature sensor to reversibly break the cell-aptamer binding in the selected chip area, allowing the release and retrieval of viable target

cells from this region for downstream applications. After the temperature change is reversed, the aptamer-functionalized surface recovers its binding affinity to target cells. The device has been applied to CCRF-CEM cells, a human ALL T cell line, and sgc8c, an aptamer specific to these cells [220], to demonstrate its capability for specific capture and non-destructive, spatially selective temperature-mediated release of target cells.

5.2. Experimental

5.2.1. Principle

The principle of aptamer-based specific cell capture and spatially selective temperature-mediated cell release is as follows. Cell specific aptamers are first patterned on design-specified regions of the surface of a temperature-control chip. A cell suspension containing target cells is introduced into the device. Target cells located on the aptamer modified regions are captured specifically by the patterned aptamers (**Figure 5.1A**), while those situated outside the aptamer-functionalized surface are not captured and removed by a Dulbecco's phosphate-buffered saline (D-PBS) wash (**Figure 5.1B**). Next, the temperature of a specific region is increased to change the conformational structure of aptamers, by activating the microheater. Thus, the binding strength between target cells and aptamers is decreased. Cells within this region can then be easily washed away and collected, while cells in other regions are not affected (**Figure 5.1C**). After the temperature is reversed, aptamers recover their ability to capture cells. In addition, this moderate temperature change does not affect the cell viability [201]. For demonstration, the microfluidic device is functionalized with the aptamer sgc8c for specific capture and temperature-mediated release of CCRF-CEM cells, a human-ALL T cell line.

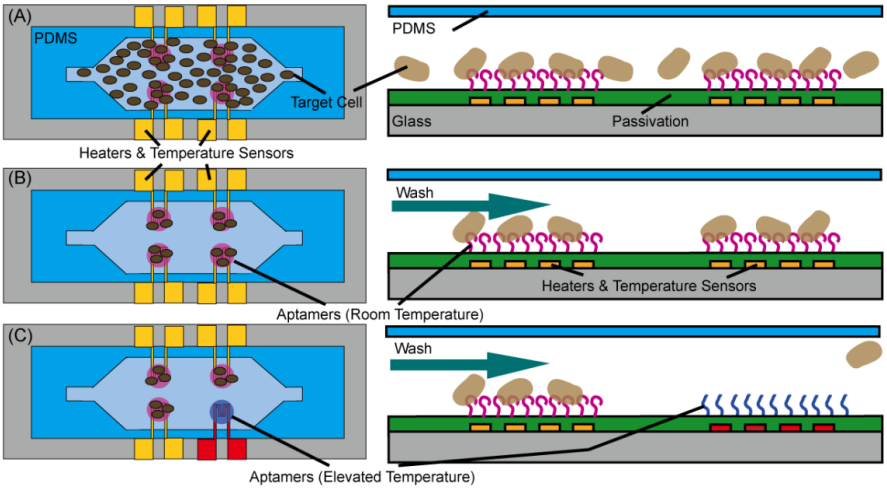

Figure 5.1: Principle of specific cell capture and spatially selective temperature-mediated cell release. (A) Cell capture at room temperature. (B) D-PBS wash to remove non-target cells. (C) Temperature-mediated release of a selected group of cells.

5.2.2. Design and Fabrication

The microfluidic device used for specific cell capture and spatially selective temperature-mediated cell release consisted of a tapered microchamber (2.7 mm in length, 2.2 mm in width, and 20 µm in height) situated on a microchip with four groups of serpentine-shaped heaters (linewidth: 50 µm) and serpentine-shaped temperature sensors (linewidth: 20 µm) (**Figure 5.2**).

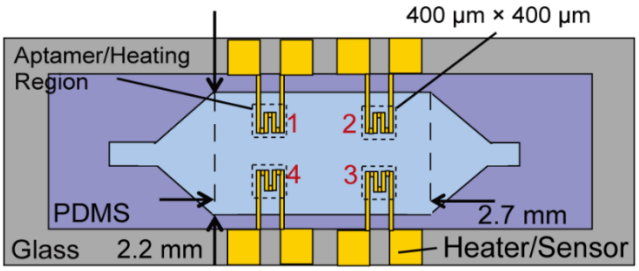

Figure 5.2: Schematic of the microfluidic device for specific cell capture and temperature-mediated selective cell release.

The microchip was fabricated using standard microfabricatation techniques. Briefly, a chrome (~10 nm) / gold (~200 nm) / chrome (~10 nm) thin film was first deposited and patterned to form micro resistive heaters, which were then passivated by approximately 1 μm silicon dioxide using plasma-enhanced chemical vapor deposition (PECVD) (**Figure 5.3A**). The micro heaters generated joule heat when subjected to a DC voltage. Next, an additional chrome (~10 nm) / gold (~200 nm) / chrome (~10 nm) thin film was deposited and patterned to form the temperature sensors, which were also passivated by approximately 1 μm silicon dioxide (**Figure 5.3B**). Subsequently, the microchip was incubated with 4% (v/v) 3-mercaptopropyl trimethoxysilane (3-MPTS) in ethanol for 30 min at room temperature, followed by an ethanol wash. The microchip was then treated with 2 mM 4-maleimidobutyric acid N-hydroxysuccinimide ester (GMBS) in ethanol for 20 min at room temperature, followed by another ethanol wash and drying by nitrogen. Afterward, the microchip was incubated with 100 μg/mL streptavidin in D-PBS at 4 °C overnight, and a polydimethylsiloxane (PDMS) (Sylgard 184, Dow Corning Inc. Midland, MI) membrane with through openings (diameter: 400 μm) was manually attached onto the microchip surface, to which the biotinylated sgc8c aptamers were immobilized through biotin-streptavidin interaction (**Figure 5.3C**). After peeling off the PDMS membrane, only aptamers immobilized on the microchip remained, and those modified on the membrane were removed (**Figure 5.3D**). Finally, the microchamber was fabricated from PDMS using standard soft lithography methods (**Figure 5.3E&F**), and then attached onto the microchip (**Figure 5.3G**). A fabricated and packaged microfluidic device is shown in **Figure 5.3H**.

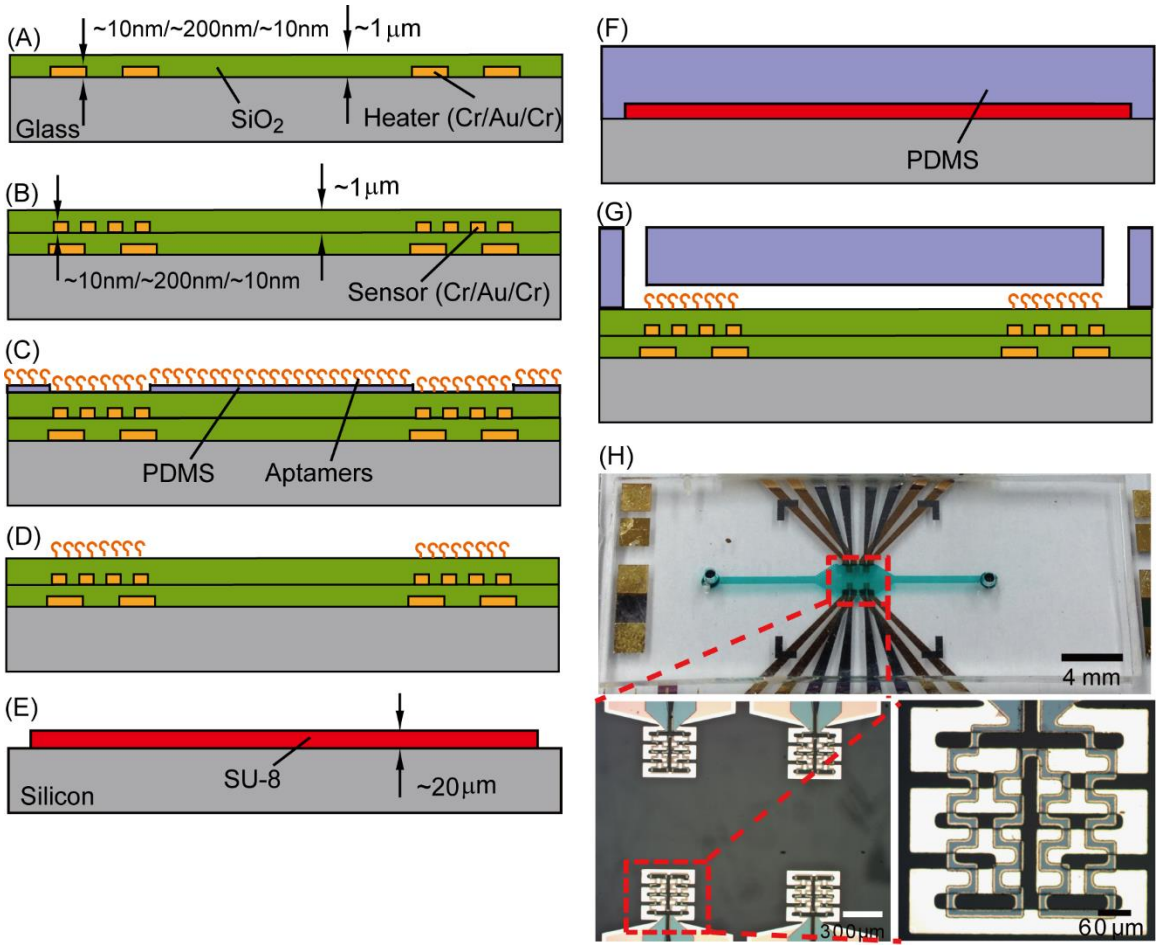

Figure 5.3: Microchip fabrication and aptamer immobilization: (A) Deposition, patterning and passivation of gold heaters. (B) Deposition, patterning and passivation of gold temperature sensors. (C) Attachment of a PDMS membrane with through holes onto the microchip, and functionalization of biotinylated aptamers. (D) Removal of the PDMS membrane. (E) Fabrication of SU-8 mold. (F) Casting of PDMS microchamber. (G) Bonding of the PDMS microchamber onto the microchip. (H) Photograph of a fabricated microfluidic device, and micrograph of the micro heaters and sensors.

5.2.3. Materials

3-MPTS, GMBS, streptavidin and bovine serum albumin (BSA) were obtained from Sigma-Aldrich (St. Louis, MO). 5,5',6,6'-Tetrachloro-1,1',3,3'-tetraethylbenzimidazolylcarbocyanine iodide (JC-1), RPMI-1640 media, fetal bovine serum (FBS), penicillin-streptomycin (P/S, penicillin 10000 units/mL, streptomycin 10000 mg/mL) and D-PBS were purchased from Invitrogen (Carlsbad, CA). CCRF-CEM was obtained from the American Type Culture Collection (ATCC, Manassas, VA). The biotinylated sgc8c aptamer (biotin-5'- (triethylene glycol)$_9$ -AT CTA ACT GCT GCG CCG CCG GGA AAA TAC TGT ACG GTT AGA-3', K_d = 0.78 nM) was synthesized and purified with high-performance liquid chromatography (HPLC) by Integrated DNA Technologies (Coralville, IA).

5.2.4. Experimental Setup

Closed-loop temperature control of each aptamer-modified region was achieved by using the corresponding integrated temperature sensor and heater with a proportional-integral-derivative (PID) algorithm implemented in a LabVIEW (National Instruments Corp., TX) program on a personal computer. The sensor resistances were measured by a digital multimeter (34420A, Agilent Technologies Inc., CA) through a 4-way mechanical switch. The micro heaters were connected to a DC power supply (E3631, Agilent Technologies Inc., CA) through another 4-way mechanical switch. The microfluidic device's inlet was connected to a syringe driven by a syringe pump (KD210P, KD Scientific Inc., MA). The outlet was connected to a microcentrifuge tube in order to collect released cells. Unless indicated otherwise, all phase contrast images of cells captured on

the microchip surface were taken using an inverted epifluorescence microscope (Diaphot 300, Nikon Instruments Inc., NY) with a CCD camera (Model 190CU, Micrometrics, NH) (**Figure 5.4**).

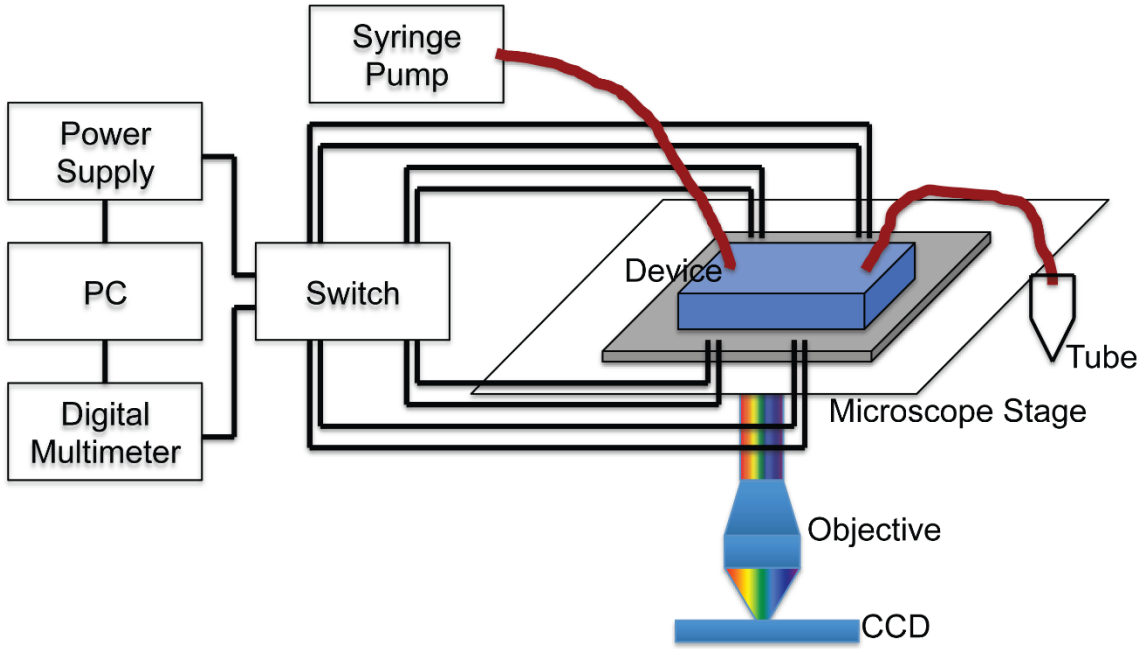

Figure 5.4: Experimental setup for specific cell capture and spatially selective temperature-mediated cell release.

5.2.5. Experimental Procedure

CCRF-CEM cells were incubated with complete culture media that consisted of RPMI-1640 media supplemented with 10% FBS and 1% P/S, and were kept at 37 °C in a humidified incubator containing 5% CO_2. Cells were collected through centrifugation, resuspended at 1×10^8 cells/mL in complete culture media with 1 mg/mL BSA, and kept on ice.

During the cell capture experiments, the microfluidic device was first treated with 1 mg/mL BSA in D-PBS for at least half an hour. Then, a suspension of CCRF-CEM cells was introduced into the microchamber at 1μL/min for 2 min, followed by a D-PBS wash at 5μL/min. An image of the microchip surface was then taken and used to show the specific capture of cells onto the aptamer-modified surface.

In the spatially selective temperature-mediated cell release experiments, the microchamber was rinsed with complete culture media with 10 μg/mL JC-1 at 5 μL/min, and a selected region on the microchip was heated using the integrated heater via closed loop temperature control for 20 s. An image was then taken and used to show the selective release.

To test cell viability, the retrieved cells in complete culture media with 10 μg/mL JC-1 were kept at 37 °C in an incubator with 5% CO_2 for 1 h, and a fluorescent image was taken with an inverted microscope (IX81, Olympus Corp., PA) equipped with a digital camera (C8484, Hamamatsu Corp., NJ).

5.3. Results and Discussion

5.3.1. Temperature Control

To evaluate spatially selective heating through on-chip temperature control, we present results from a numerical simulation using a three-dimensional steady-state heat transfer model in COMSOL Multiphysics® (COMSOL, Inc., Los Angeles, CA) [201]. The model considers heat conduction in the solid materials as well as forced convection due to the buffer flow (flow rate: 5 μL/min), while neglecting natural convection due to relatively small temperature changes and the small length scales of the chamber. The temperature

distribution on the lower surface of the microchamber is shown in **Figure 5.5A**. It can be seen that the temperature increase generated by each micro heater is restricted to the surrounding area as desired, indicating the feasibility of temperature-mediated release of a selected group of cells.

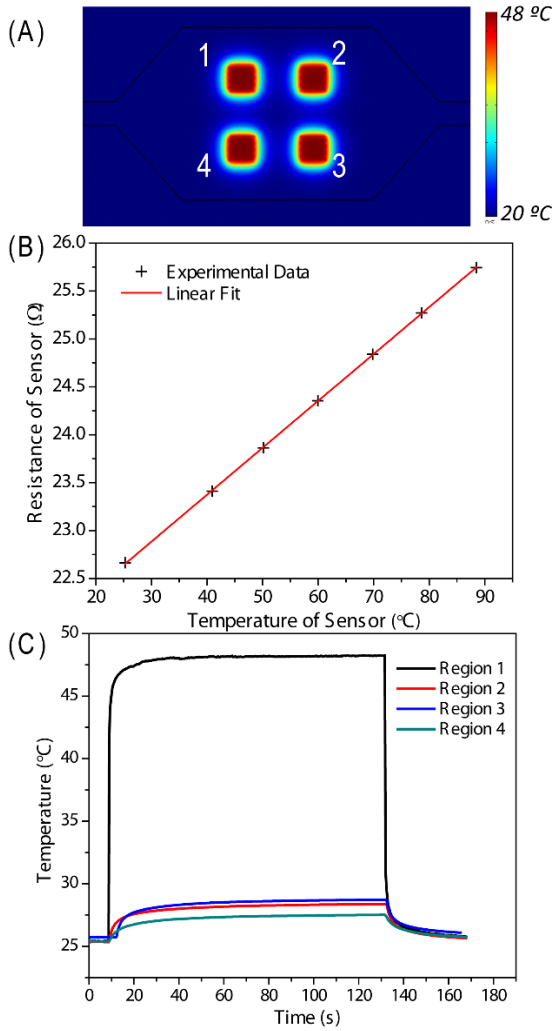

Figure 5.5: On-chip temperature control: (A) Simulated temperature distribution on the lower surface of the microchamber, showing spatially selective heating. (B) Linear temperature dependence of the resistance of the temperature sensor. (C) Time-resolved tracking of the temperature of each heating region inside the buffer filled chamber.

Prior to performing the experiments, we first characterized the temperature sensors using an environmental test chamber (Model 9023, Delta Design Inc., CA) maintained at a series of temperatures which were measured with a high accuracy temperature reference probe (Model 5628, Fluke Calibration, UT) [19]. The resistance (R) of the temperature sensor varied linearly with temperature (T). The dependence was well represented by the relationship $R = R_0 [1 + \alpha (T - T_0)]$, where R_0 is the sensor resistance at a reference temperature T_0, and α is the temperature coefficient of resistance (TCR) of the sensor. Fitting this relationship to the measurement data allowed the determination of TCR, which was used to determine the temperature in the region directly above the sensor from the measured resistance during experiments. A typical micro temperature sensor in this design had a measured resistance of 22.66 Ω at a reference temperature of 25.3 °C with a TCR of 2.16×10^{-3} 1/°C (**Figure 5.5B**).

Further verification of selective heating in the aptamer-patterned regions is provided by on-chip temperature control using the integrated thin-film heaters and temperature sensors. We experimentally monitored the temperature of all four heating regions with continuous D-PBS infusion (flow rate: 5 μL/min) to simulate the cell release process, when the temperature of heating region 1 was controlled in a closed-loop by the integrated heater via feedback from the temperature sensor. The temperature of region 1 increased from room temperature to 48 °C rapidly (approximately 10 seconds) and remained within approximately 0.2 °C of the desired temperature setpoint (48 °C) for the entire heating duration, while those of regions 2-4 all remained below 28 °C during the whole process (**Figure 5.5C**). This implies that the temperature change in one region does not

significantly affect the temperatures in other regions, and thus enables the spatially selective temperature-mediated cell release.

5.3.2. Spatially Selective Specific Capture and Temperature-Mediated Release of Cells

We first tested the patterning of aptamers onto the surface of a microchip. Fluorescently labeled biotinylated ssDNA was used to functionalize the microchip, which was then observed under a fluorescent microscope. As shown in **Figure 5.6**, only the area exposed to reagents, which was in the through opening region, showed bright green fluorescence, indicating the feasibility of immobilizing aptamers onto design-specified regions of a microchip.

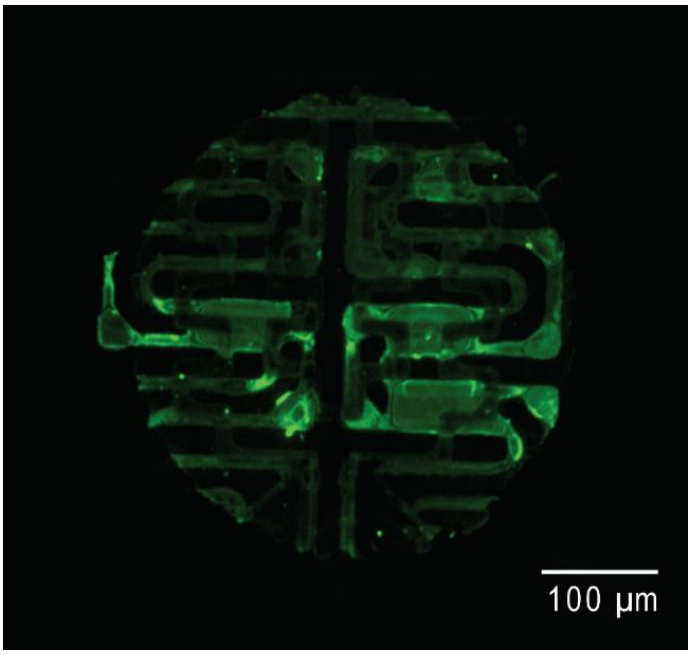

Figure 5.6: Immobilization of aptamers in design-specified regions of the chip surface.

To demonstrate spatially selective cell capture, a CCRF-CEM cell suspension of 5×10^6 cell/mL with 1 mg/mL BSA was introduced into the devices with immobilized

aptamers at 1 µL/min for 2 min, followed by a D-PBS wash at 5 µL/min for 1 min. CCRF-CEM cells only became attached to the aptamer functionalized surfaces (**Figure 5.7A**), and not to the bare surface, confirming spatially selective cell capture. Because of the manually performed surface modification process, aptamers were not precisely immobilized onto the surface above the micro-heaters. Therefore, the shape of aptamer-captured CCRF-CEM cell patterns did not strictly follow the envelope of the micro-heaters.

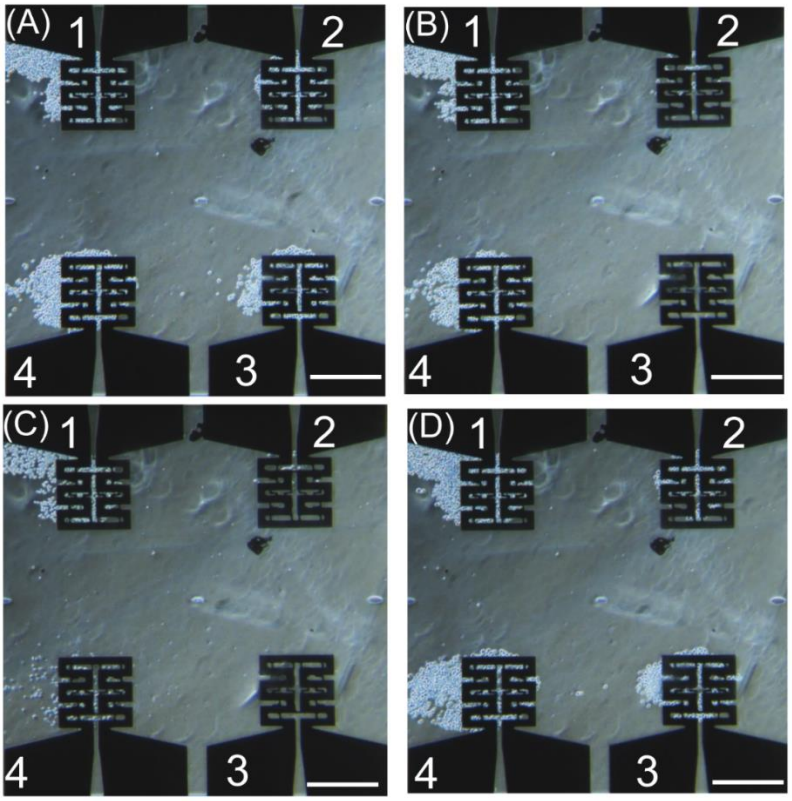

Figure 5.7: Specific cell capture and spatially selective temperature-mediated cell release: (A) CCRF-CEM cells were captured by the aptamer functionalised surface; (B) Temperature-mediated cell release in regions 2 and 3; (C) Temperature-mediated cell release in region 4; (D) Specific cell recapture on the same aptamer functionalised surface. Scale bars: 400 µm.

To test temperature-mediated release of a selected group of cells, the cell laden chamber was then rinsed with complete culture media with 10 μg/mL JC-1 at 5 μL/min, while the temperature in regions 2 and 3 increased to 48 °C in series, by using the integrated heaters. It can be seen that only the cells within regions 2 and 3 became detached from the aptamer-surface, which may have been caused by conformational changes of the aptamer structure [201], whereas negligible cell release was observed in other regions (**Figure 5.7B**). Next, we further increased the temperature in region 4, and observed noticeable cell release in this region, and cells in region 1 were not affected (**Figure 5.7C**). These results indicate the success of temperature-mediated release of selected groups of cells.

To verify the reusability of the aptameric surface, another CCRF-CEM cell suspension with the same concentration was introduced into the same device at 1 μL/min for 2 min. Following a D-PBS wash at 5 μL/min for 1 min, similar densities of captured cells were observed in all the regions (**Figure 5.7A** and **D**), implying that the microfluidic device with aptamers is reusable.

5.3.3. Cell Viability Assay

To enable downstream (e.g., tissue engineering and cell-based therapeutic) applications [203, 204], the released and retrieved cells must be viable. To evaluate cell viability, released cells in complete culture media with 10 μg/mL JC-1 from multiple devices were collected and incubated at 37 °C with 5% CO_2 for 1 h, centrifuged and resuspended in 10 μL of complete culture media. JC-1 exists as a monomer in cytoplasma exhibiting green fluorescence and it accumulates in undepolarized healthy mitochondria showing red fluorescence, the intensity of which decreases along with mitochondrial

depolarization during apoptosis or death of cells [240, 241]. The released cells showed bright red fluorescence (**Figure 5.8**), indicating that they were still viable and the temperature-mediated cell release process did not affect the cell viability. In addition, to further decrease the potential cell damage, releasing cells at lower temperature is possible using appropriately selected aptamers [250].

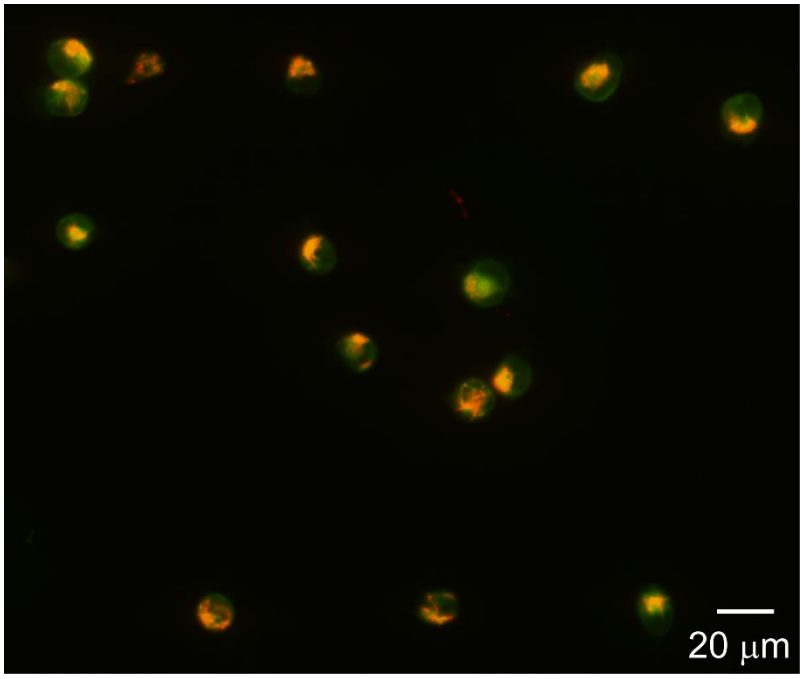

Figure 5.8: Micrograph of JC-1 stained cells following cell capture and temperature-mediated cell release performed on a microfluidic device.

5.4. Conclusion

Spatially selective capture, release and retrieval of cells on affinity surfaces are important in basic biological research and clinic diagnostics. In this chapter, we have developed a microfluidic device for specific cell capture and selective temperature-mediated cell release using cell-specific aptamers and integrated micro heaters and

temperature sensors. The device consists of a microchamber situated on a microchip with four groups of micro heaters and temperature sensors. Aptamers are patterned on design-specified regions of the chip surface, and the heat generated by the micro heaters is restricted to each aptamer-functionalized chip area. A moderate temperature change using a group of micro heater and temperature sensor breaks the cell-aptamer binding in the selected chip area, allowing the release and retrieval of target cells from this region without detectable cell damage. The microchip is first characterized experimentally and numerically to ensure spatially selective temperature control. Further experiments show specific capture of CCRF-CEM cells using the aptamer sgc8c, followed by efficient and spatially selective temperature-mediated release. In addition, the aptamer functionalized surface is shown to be reusable and the retrieved cells are viable. The results demonstrate that our approach can potentially be used for cell purification from biological samples and selective cell retrieval for downstream analysis.

Further studies will involve systems that employ a more controllable surface modification method to precisely control the size of patterned aptamers and use a more delicate temperature control technique to increase the spatial resolution of selective heating.

Chapter 6. Mechanically Tunable Microfluidic Trapping of Cells

The microfluidic devices described in Chapter 4 and Chapter 5 demonstrated the feasibility of using solid surface with patterned aptamer for highly specific cell capture and spatially selective temperature-mediated cell release. However, they lacked flexibility in controlling the number of cells in each spot.

In this chapter, we exploited the large compliance of elastomers to create an array of cell-trapping microstructures, whose dimensions can be mechanically modulated by inducing uniformly distributed strain via application of external force on the chip. The device consists of two elastomer polydimethylsiloxane (PDMS) sheets, one of which bears dam-like, cup-shaped geometries to physically capture cells. The mechanical modulation is used to tune the characteristics of cell trapping to capture a predetermined number of cells, from single cells to multiple cells. Thus, enhanced utility and flexibility for practical applications can be attained, as demonstrated by tunable trapping of MCF-7 cells, a human breast cancer cell line. The work presented in this chapter has resulted in two peer-reviewed conference proceedings [243, 251] and a journal publication [252].

6.1. Introduction

Cell manipulation, such as separation, isolation, positioning, trapping and sorting of cells, has important applications in basic biological research and clinical diagnostics. For example, in order to study the effect of anticancer drugs, cell groups with multiple cells are needed for testing multicellular resistance [253]. However, the analysis of a large

population of cells obscures the heterogeneous information within cell groups, such as the large genetic variation between individual cells [254, 255]. Therefore, in addition to multicellular analysis, investigations on single cell or a small number of cells are necessary. For instance, in order to study the phenotypic heterogeneity driven by cell cycle, cell aging, and epigenetic regulation, single cells must be isolated and identified [256]. Furthermore, in the study of cell-cell contact, such as the communication through junctional proteins [257] and membrane-receptor to membrane-ligand interactions [258], or cell fusion that enables the study of nuclear reprogramming [83], pairing of two cells, either the same type or different types, is required. As a result, target cells have to be trapped in particular positions without any mechanical or biochemical damage, and the number of cells trapped should be able to be adjusted according to the application.

Microfluidic technologies have been developing to allow more effective and efficient cell trapping and cell positioning, offering numerous advantages not possible with conventional platforms [259, 260]. Microfluidic cell trapping that employs either physical barriers, such as microwells [80, 261], microcups [82, 83] and cell-based valves [262, 263], or molecular interactions, such as micropatterning surfaces with polymers [264] or ligands [265], is easy to handle, does not require complicated fabrication procedures, and can realize high-throughput operation. With different dimensions of microwells [80] or microcups [82], or variant diameters of patterned ligand spots [266], cell trapping with different numbers of cells can be achieved. For example, by utilizing weir-like capture cups with different depths, cell trapping with different numbers of cells in each trap have been reported [82]. However, once the design and fabrication of the device have been completed,

it is no longer possible to alter the characteristics of the cell traps. Thus, these methods lack flexibility in precisely controlling the number of trapped cells, while cell arrays of single, two and multiple cells are all needed in cell biology applications [83, 267, 268]. On the other hand, cell trapping methods that use optical [269], acoustic [91], dielectrophoretic [211], hydrodynamic [270], or their combinations [271], employ different kinds of external force during the experiment to separate and restrict cells in particular locations, and thus allow dynamic and precise control over the number of cells trapped. However, the application of these methods is also limited by either sophisticated operation systems or complicated microfabriation processes.

These limitations can potentially be addressed by utilizing physical barrier based cell trapping techniques and employing elastomeric polymers, whose large deformability could provide flexibility and controllability in cell manipulation. In relevant work, large compliance of polymers has been used in micro- and nanofluidic applications. For example, deformable elastomeric microdevices have been used in the gating and regulation of fluids in microflow control, in which a thin compliant flap was used to alter the flow resistance by varying the applied pressure [272]. A nanofluidic system has also been designed and fabricated using oxidized PDMS, in which transport characteristics were dynamically manipulated by the modulation of channel dimensions [273]. In addition, a pneumatically controlled elastomeric microstructure has been reported for patterning and manipulation of a large number of cells at the macro scale [274]. These demonstrate the feasibility of using polymers to achieve flexible and precise control in micro- / nanofluidic applications.

This chapter presents a tunable cell trapping microchip that utilizes the large deformability of elastomeric polymers to precisely control the number of cells captured at the single and individual cell level. The device consists of two thin sheets of the elastomer PDMS, one of which bears microstructures to physically capture cells. The microstructures each feature a dam-like, cup-shaped geometry (called a capture cup) with supporting pillars on both sides. We for the first time exploit the large compliance of elastomers to create an array of cell-trapping microstructures, whose dimensions can be mechanically modulated by inducing uniformly distributed strain via the application of an external force on the chip. The mechanical modulation is used to tune the characteristics of cell trapping to capture a predetermined number of cells, from single cells to multiple cells. The microchip is applied to MCF-7 cells to verify the significant influence of microstructure deformation on the number of cells trapped, and thus demonstrate the effectiveness of using physical modulation to enable nondestructive and flexible cell manipulation, which can potentially be used in cell biology research and clinical diagnostics.

6.2. Experimental

6.2.1. Design and Fabrication

The tunable cell trapping microchip consists of two thin sheets of elastomer PDMS, one of which bears microstructures to physically capture cells. The microstructures each have a dam-like, cup-shaped geometry (approximately 40 μm in height, henceforth called a capture cup) with supporting pillars (approximately 7 μm in height) on both sides (**Figure 6.1**). When a cell approaches a microstructure, the carrier fluid passes over the dam, while the cell is trapped in the capture cup. If one or more cells are trapped in the microstructure,

the flow field upstream will immediately change, attaining a higher velocity component in the transverse direction. Therefore, cells moving into this region will gain more significant transverse kinetic energy and may be more likely to flow around the microstructure, rather than being trapped in the capture cup.

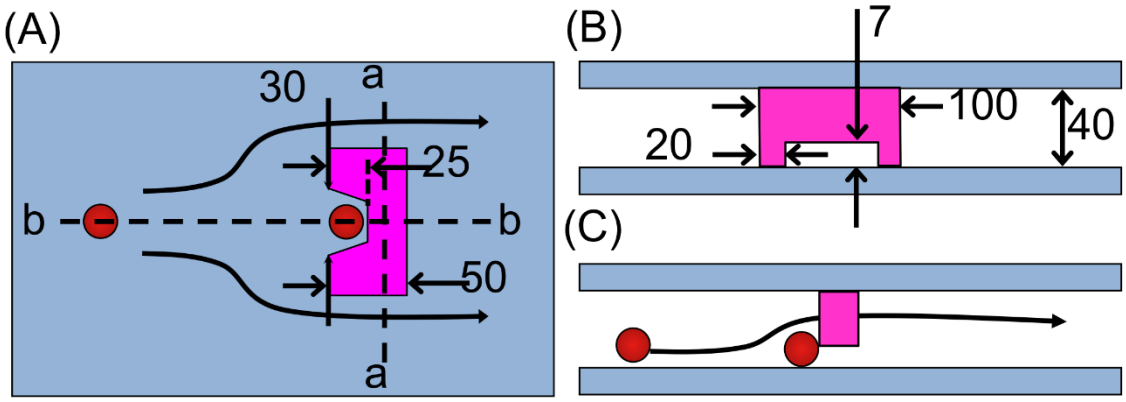

Figure 6.1: The cell trapping principle. (A) Plan view and cross-sectional views along lines (B) a-a and (C) b-b of cell trapping approach. Dimensions are given in micrometers.

The cell trapping characteristics can be tuned through mechanical modulation of microstructures via the application of strain to the chip (**Figure 6.2**). The microchip is stretched by mounting it onto a motherboard. This induces uniform uniaxial tensile strain in the cell trapping region, which is situated in a slender bar-shaped portion of the microchip. Using different microchip mounting pin locations, the strain in the cell trapping region can be varied. This mechanical modulation changes the geometry of the microstructures, and also alters the flow field, thereby allowing the number of cells trapped in each microstructure to be actively tuned according to practical needs.

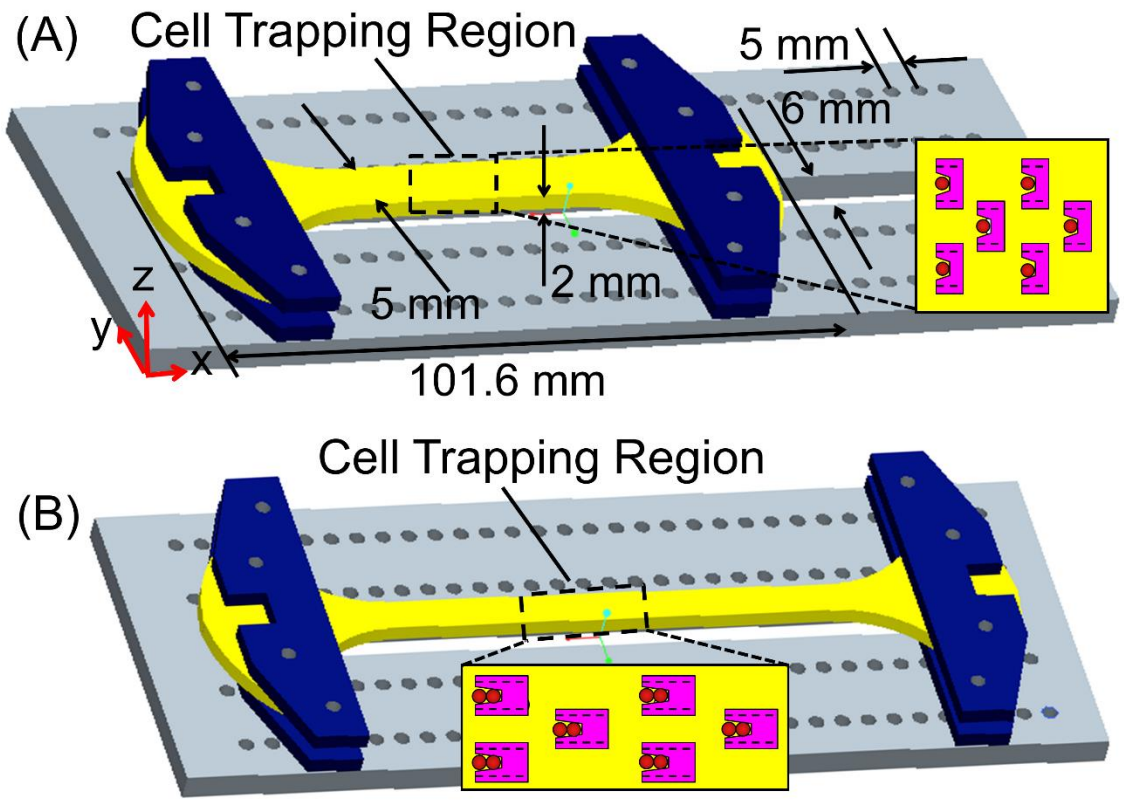

Figure 6.2: Principle of tunable cell trapping via modulation of microstructure dimensions. (A) Single cells are trapped in the microstructures before application of strain. (B) Multiple cells are trapped in the microstructures after application of strain. Inset: detail of microstructure geometries before and after the application of strain.

The tunable cell trapping microchip was fabricated using standard soft lithography techniques. Briefly, the SU-8 (MicroChem Corp., Newton, MA) mold that defines microfluidic features was first fabricated (**Figure 6.3A**). Then two PDMS (Sylgard 184, Dow Corning Inc.,) sheets, one bearing the microfluidic structures and the other used as the substrate, were cast (**Figure 6.3B**) and punched with the inlet and outlet (**Figure 6.3C**). Subsequently, the two PDMS sheets were bonded to each other after oxygen plasma

treatment (**Figure 6.3D**). Finally, an acrylic motherboard, onto which the fabricated microchip was mounted, was fabricated with a laser cutter. The assembled device is shown in **Figure 6.4A**, and the details of cell trapping microstructures are shown in **Figure 6.4 B** and **C**.

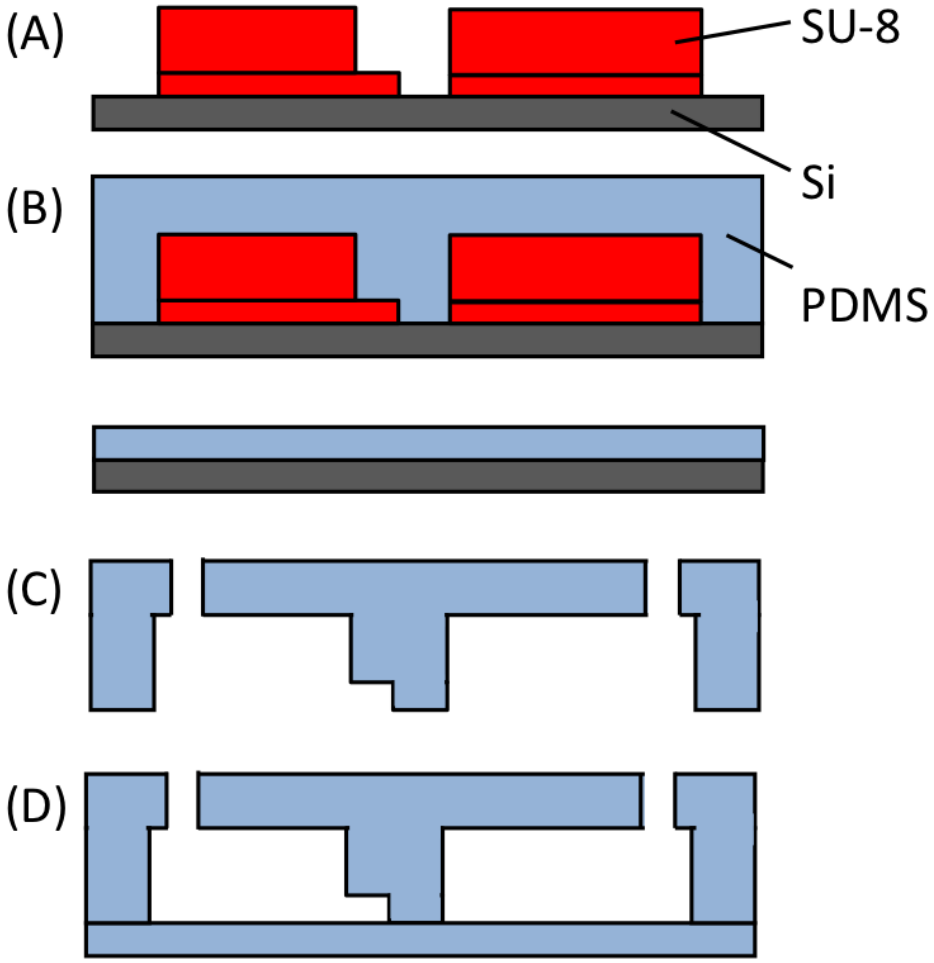

Figure 6.3: The microchip fabrication process. (A) Fabrication of the SU-8 mold. (B) Casting of the PDMS microfluidic sheet and the PDMS substrate. (C) Demolding of PDMS sheet. (D) Bonding of the PDMS microfluidic sheet and PDMS substrate.

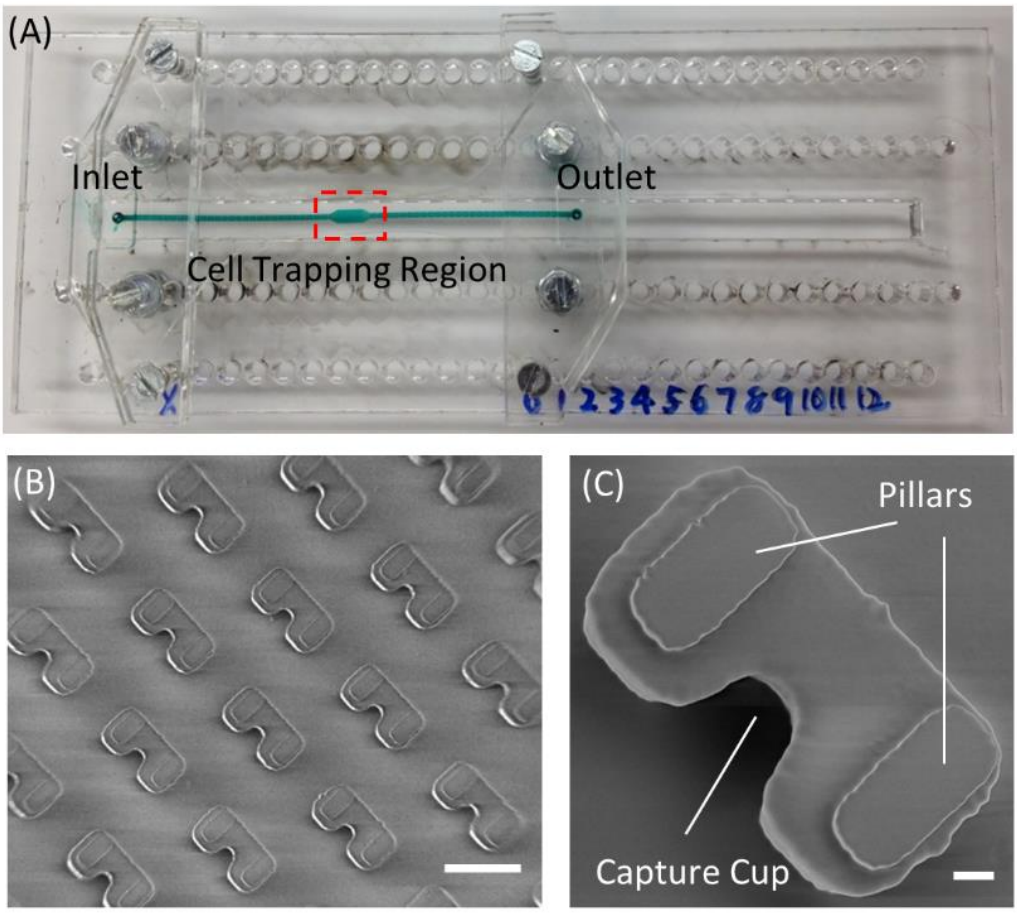

Figure 6.4: (A) A fabricated and assembled tunable cell trapping microchip. (B) Scanning electron micrograph image of the cell-trapping region, showing densely packed cup-shaped microstructures (scale bar: 100 µm). (C) Detail of the trap microstructure, including a dam-like capture cup with supporting pillars on both sides (scale bar: 10 µm).

6.2.2. Materials

Chlorotrimethylsilane, and bovine serum albumin (BSA) were obtained from Sigma-Aldrich (St. Louis, MO). 5,5',6,6'-tetrachloro-1,1',3,3'-tetraethylbenzimidazolylcarbocyanine iodide (JC-1), Minimum Essential Medium (MEM),

fetal bovine serum (FBS), penicillin-streptomycin (P/S, penicillin 10,000 unit/mL, streptomycin 10,000 μg/mL), 0.25% Trypsin-EDTA, Dulbecco's phosphate-buffered saline (D-PBS) and Vybrant® multicolor cell-labeling kit (DiI, DiO and DiD) were purchased from Life Technologies (Grand Island, NY). MCF-7 cell line was obtained from the American Type Culture Collection (ATCC, Manassas, VA).

6.2.3. Experimental Procedure

MCF-7 cells were incubated with the complete culture media, including MEM supplemented with 10% FBS and 1% P/S, and were kept at 37 °C in a humidified incubator containing 5% CO_2. Before microfluidic experiments, cells were labeled by incubating them with 0.5% (v/v) DiO in the complete culture media for 20 min and then treated in the 3mL of trypsin-EDTA for at least 15 min to be detached from substrate and to prevent the nonspecific adsorption. Next, a triple volume of the complete culture media was added to stop trypsinization. Cells were then collected through centrifugation, resuspended at 1×10^8 cells/mL in complete culture media supplemented with 5 mg/mL BSA, and kept on ice.

Prior to experimentation, the microfluidic channel was incubated with 5 mg/mL BSA in D-PBS for at least half an hour to prevent the unspecific adsorption. Then, the cell suspension was diluted to 1×10^6 cells/mL in D-PBS supplemented with 5 mg/mL BSA, and introduced into the microchip with or without extension at 10 μL/min for 1 min. Afterward, D-PBS was used to rinse the channel at 10 μL/min for 1 min. Finally, a fluorescent image of cell-laden chamber was taken and used to manually count the number of cells in each trap.

6.3. Results and Discussion

6.3.1. Microstructure Deformation

The mechanical modulation of microstructures is realized by mounting the microchip onto different locations of a motherboard, initially free of extension (**Figure 6.5A**) to a tensile strain of approximately 79% (**Figure 6.5B**). According to the extension experiments, along with the increased strains, the trapping cup width decreased from 28.8 ± 0.8 µm to 18.0 ± 0.6 µm and the cup depth increased from 25.0 ± 0.4 µm to 36.3 ± 0.7 µm (**Figure 6.5C**). This deformation will significantly alter the number of cells able to be trapped [82].

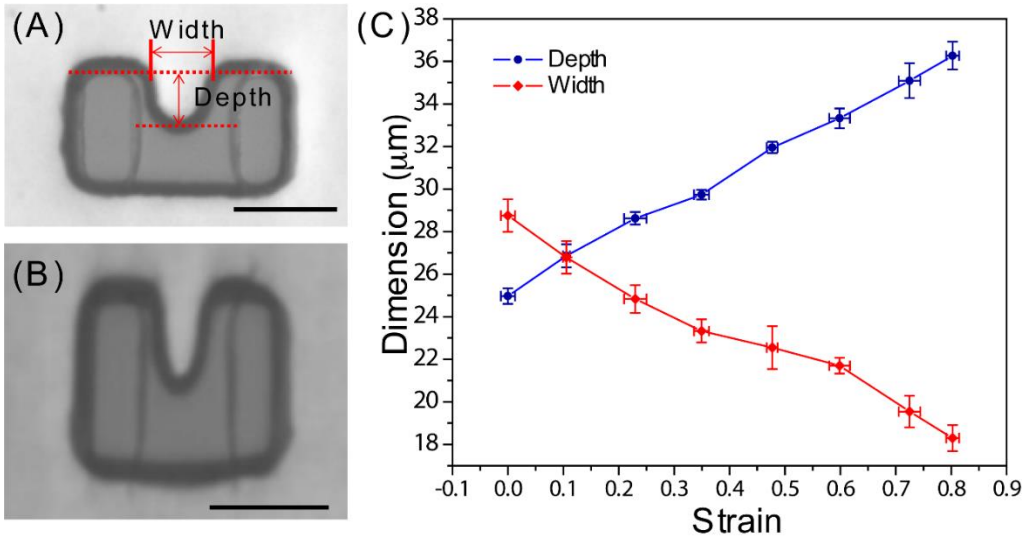

Figure 6.5: Modulation of microstructures for cell trapping: Phase contrast micrographs of cell trapping microstructure before (A) and after (B) after applying 79% relative extension along x direction (scale bars: 50 µm). (C) The depth and width variations of microstructures as the normal strains increased from 0 to 0.8.

To evaluate the uniformity of microstructure deformation, we first tested the strain distribution and present results from a COMSOL Multiphysics® (COMSOL, Inc., Los

Angeles, CA) numerical simulation using a three-dimensional structural model, consisting of the trapping region. The nonlinear elasticity of the structural material (PDMS) and the large strain involved in the microstructure deformation is considered. PDMS is modeled as an isotropic, incompressible hyperelastic material [272], and the Mooney-Rivlin constitutive law is applied [275, 276]. A Young's modulus of 387 kPa is used for PDMS, as determined by the 100:7 base-to-curing agent ratio of the prepolymer solution [277]. Our results show a highly uniform strain distribution in the *xy*-plane throughout the trapping region (**Figure 6.6**), indicating a uniform deformation of the microstructure array.

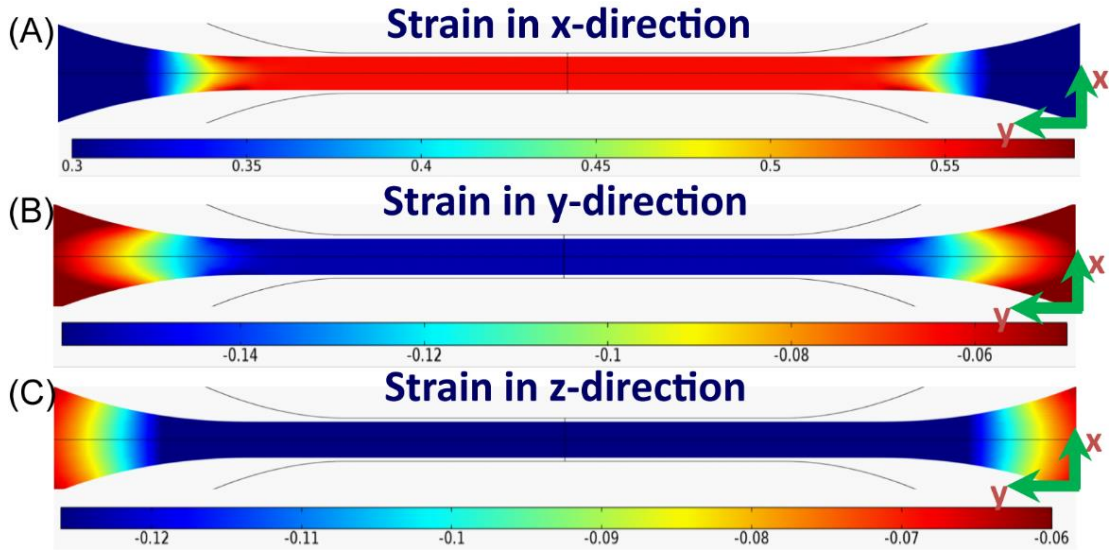

Figure 6.6: Numerically determined distributions of the normal strain components on the lower surface of the microchannel (xy-plane) within cell trapping region: (A) x-component; (B) y-component; and (C) z-component.

A further numerical analysis shows when the gap between each row of microstructures was elongated from 98 µm (**Figure 6.7A**) to 175 µm (**Figure 6.7B**), leading to a 79% relative extension along *x* direction in the trapping region, the cup depth increased from 25

µm (**Figure 6.7A&C**) to 37 µm (**Figure 6.7B&D**), and the cup width decreased from 28 µm (**Figure 6.7A&C**) to 19 µm (**Figure 6.7B&D**). These dimension changes are consistent with the results from the experimental analysis.

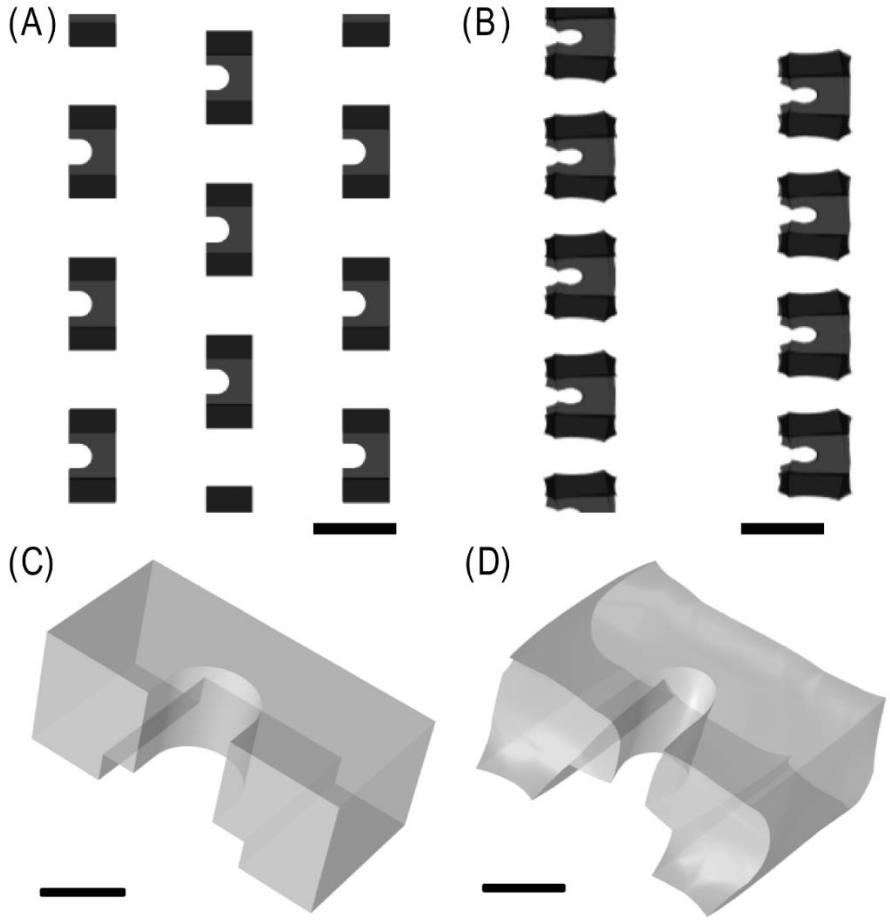

Figure 6.7: Numerically determined microstructure deformation (A) before and (B) after applying 79% relative extension along x direction. 3D models of the microstructure (C) before and (D) after applying 79% extension. Scale bars: (A)(B) 100 µm, (C)(D) 25 µm.

6.3.2. Tunable Cell Trapping

To demonstrate tunable cell trapping, a cell suspension of 1×10^6 cells/mL in D-PBS with 5 mg/mL BSA was introduced into the chip (pretreated with 5 mg/mL BSA in D-PBS)

at 10 μL/min for 1 min, after which D-PBS was used to rinse the channel. The 7 μm height gap between two pillars allows a fraction of fluid carrying cells to enter the capture cup. Based on the dimensions of the cell trapping microstructure, once one cell or multiple cells occupy the capture cup, the fraction of fluid passing through the gap significantly reduces, leading to increased transverse velocity and decreased longitudinal velocity. Thus, more of a cell's longitudinal component of kinetic energy will be converted to the transverse component, increasing the tendency for additional cells to flow around the microstructure and therefore preventing them from being trapped. As shown in **Figure 6.8A**, without extension, single cell trapping was dominant, whereas multiple cells were captured as a result of an approximately 72% strain applied to the chip (**Figure 6.8B**).

Moreover, the results indicate the number of cells trapped strongly depends on the geometrical characteristics of the microstructures (**Figure 6.8C**). Without the application of strain, 41% of microstructure trapped single cells and 31% of them captured two cells. However, when the chip was extended by approximately 72%, the fractions of single-cell trap and two-cell trap decreased to 4% and 24%, respectively, and 39% of microstructures trapped three cells. These results show that the distribution of cell capture per cup shifted up from a mode of 1 without extension to a mode of 3 with the application of 72% uniaxial tensile strain.

To evaluate cell viability after trapping, trapped cells were stained by JC-1 (10 μg/mL) at 37 °C for 30 min, and fluorescent images were taken with an inverted epifluorescence microscope (Diaphot 300, Nikon Instruments Inc., NY) with a CCD camera (Model 190CU, Micrometrics, NH). The intensity of red fluorescence caused by the accumulation of JC-1

in healthy mitochondria will decrease during depolarization occurring in the early stage of apoptosis [240, 241]. The trapped cells from both the unextended and extended (72%) device did not exhibit any degradation of red fluorescence (**Figure 6.8D&E**), indicating the trapped cells were viable.

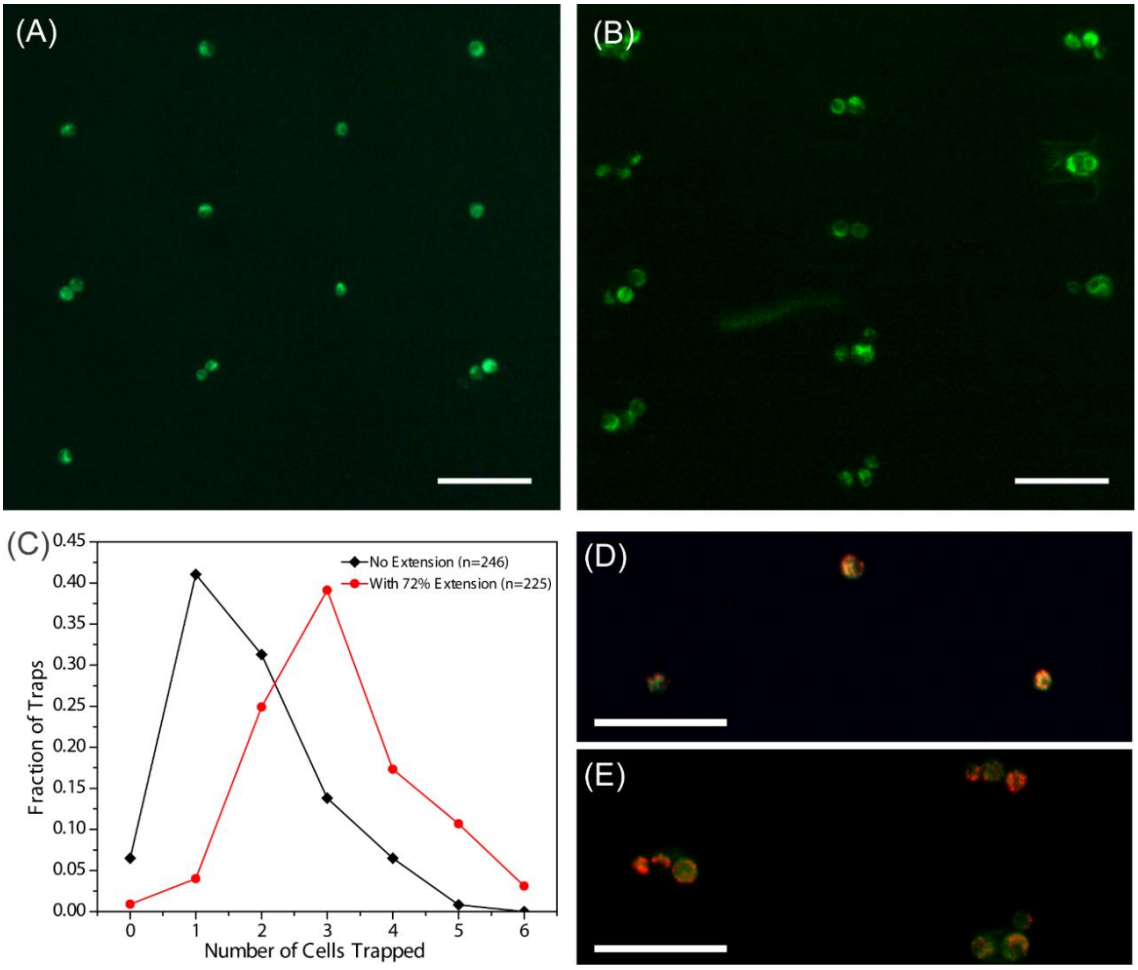

Figure 6.8: Fluorescent micrographs of cell trapping (A) before and (B) after application of strain. (C) The distribution of trapped cells before and after microstructure modulation. Images of JC-1 stained trapped cells (D) before and (E) after application of strain. Scale bars: 100 µm.

These results demonstrate that our approach can potentially allow the formation of a cell array with a predetermined cell number in each cell trap, from single cells to multiple cells.

To explain the observed tunable cell trapping, the flow field before and after extension was analyzed by three-dimensional computational fluidic dynamics (CFD) analysis to explore the characteristic parameters that affect the number of cells trapped using ANSYS Fluent® (ANYSIS, Inc., Canonsburg, PA). 3-D models for the trapping regions were developed considering the cell as a rigid body. Fluid velocity along a reference line, which is denoted a-b (**Figure 6.9A**) and lies slightly above the capture cup centerline, was measured. As a crude approximation, it is assumed the cell travels with same velocity as the carrier flow. The transverse-to-longitudinal kinetic energy ratio can be represented by a dimensionless parameter $R = V_y^2/V_x^2$. As an example, the kinetic energy ratio R for the case without mechanical chip extension and without cells trapped along the line a-b is shown in **Figure 6.9A**, in which a maximum value is denoted by R_{max}. When the cell's transverse kinetic energy is significant compared to its longitudinal kinetic energy, cells are more likely to move around the microstructure instead of becoming trapped in the cup. Therefore, this maximum kinetic energy ratio can be used as an indicator of the microstructure array behavior. That is, a larger value of R_{max} indicates a lower probability of cells to become trapped.

The values of R_{max} were calculated for a microstructure that has captured a varying number of cells when the device is unstretched or extended by 72% (**Figure 6.9B**). The relatively small values of R_{max} when no cell is trapped in a cup on the unstretched device

(0.0114), and when zero (0.0032), one (0.0084) or two (0.0151) cells are trapped in the stretched device, suggest that an additional cell could relatively easily access the cup and become trapped. On the other hand, the relatively large values of R_{max} when a single cell is trapped in a cup on the unstretched device (0.0218) and when three cells are trapped in a cup on the extended device (0.0207) suggest that it is difficult for additional cells to move into the cup. These results are consistent with experimental data.

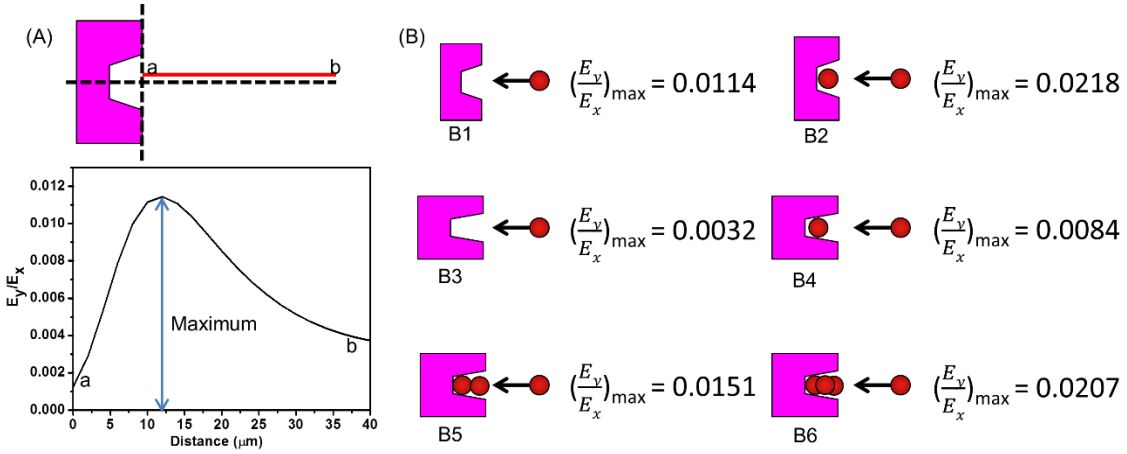

Figure 6.9: (A) Numerically determined transverse-to-longitudinal kinetic energy ratio (R) along the reference line a-b on the middle surface of the microfluidic channel. (B) Dimensionless parameter R_{max} when a varying number of cells are trapped in a cup on an unstretched (B1 and B2) and stretched device (B3-B6).

6.4. Conclusion

Biological research and clinical diagnostics rely on controlled cell manipulation, such as isolation, positioning and trapping. We have developed an elastomeric polymeric microchip for mechanically tunable cell trapping. The device consists of two thin PDMS sheets, one of which bears microstructures to physically capture cells. Each microstructure

consists of a dam-like, cup-shaped geometry with supporting pillars on both sides. The employment of PDMS, which has large deformability, enables the mechanical modulation by inducing uniformly distributed strain via application of external force on the chip. Numerical analysis shows uniform strain distribution in the cell trapping region and effective modulation of cell trapping microstructures. Further analysis of the flow field suggests that the transverse-to-longitudinal kinetic ratio (E_y/E_x) of a cell can be used to reflect the possibility of trapping this cell. The experimental results also demonstrate the application of strain can significantly deform the cell trapping microstructure, thereby allowing for the cell array capable of trapping predetermined quantities of cells. In addition, the trapped cells are shown to be viable. These results demonstrate that our approach can potentially enable effective, efficient and flexible formation of an array of cells on a microchip.

Further studies will involve the system that has a larger dynamic range of the trapped cell quantity while remaining the single-cell-level resolution and the investigation of cell loading efficiency.

Chapter 7. Isolation of Specific Cell-Binding Aptamers: a Hydrodynamically Based Approach and Early Results

In Chapter 4 and Chapter 5, we presented microfluidic devices that utilize surface immobilized aptamers for specific cell capture and temperature mediated cell release. However, the limited availability of currently available cell-specific aptamer hinders its applications.

In this chapter, preliminary results of a proof-of-concept microfluidic device for synthetically isolating cell-targeting aptamers from a randomized single-strand DNA (ssDNA) library is demonstrated. The device consists of two microchambers for selection and amplification respectively, and integrates cell culturing with affinity selection of cell-binding ssDNA, which is then amplified by bead-based polymerase chain reaction (PCR). Coupling of the selection and amplification using pressure-driven flow controlled by microfabricated elastomeric valve realizes multi-round aptamer isolation on a single chip. The work presented in this chapter has resulted in a peer-reviewed conference proceeding [278], and a journal publication is under preparation.

7.1. Introduction

Aptamers are oligonucleotides (typically 12-80 nucleotide long) that recognize biological targets by specific affinity binding [125-127]. Isolated from a randomized oligonucleotide library using an in vitro synthetic selection process called systematic evolution of ligands by exponential enrichment (SELEX), aptamers can recognize a large variety of target molecules, such as metal ions [279, 280], small molecules [112, 113],

peptides [114], amino acids [115, 116], proteins [215], cells [117, 118], viruses [119, 120], and bacteria [44, 122], via unique three-dimensional conformations formed through interactions with target, and shows comparable affinity and selectivity as antibodies [123, 281]. Compared with antibodies, aptamers, which are synthetically produced, can be more stable and more amenable to chemical modifications, have minimal batch-to-batch variability, and exhibit low immunogenicity for in vivo applications [123, 282]. Therefore, aptamers have the potential to be widely used in both fundamental biological researches [283] and clinical diagnostics and therapeutics [284, 285] .

Recognition of cancer cells or cell surface biomarkers from a heterogeneous mixture in blood or other body fluids is critically important in cancer diagnostics [286, 287]. However, the lack of effective molecular ligands targeting cancer biomarkers hinders early cancer detection, and thus the effectiveness of the therapy [216, 288, 289]. Aptamers have been developed for cellular targets, such as acute lymphoblastic leukemia (ALL) precursor T cells [216], liver cancer cells [217] and even stem cells [218], and have been employed to isolate cancer cells from cell mixtures [201, 223] and to identify particular cancer subtypes [122, 216, 290]. However, conventional platforms for developing cell-targeting aptamers are labor-, time- and resource-intensive [124]; it generally takes months or even a year to reliably generate an aptamer [291].

Microfluidic technology has been employed to improve the SELEX efficiency via process integration, but early attempts were limited to molecular targets [139, 142, 143]. More recently, researchers reported several microfluidic systems used for the generation of aptamers targeting cells. For example, Lee and coworkers immobilized cells onto

magnetic bead surfaces for selection, and employed suction-based flow manipulation to transfer samples and reagents [292]. However, chemical modification of cells required by bead-based immobilization may negatively influence their viability, and the generation of single strand DNA (ssDNA) from double strand DNA (dsDNA) in solution by pure heating is inefficient, and could negatively affect the selection efficiency in the next round. In an alternative approach demonstrated in our lab, cells were hydrodynamically trapped in the microchamber, and ssDNA were electrokinetically transferred through an agarose gel filled channel between selection and amplification chambers [293]. However, physical trapping induces stress on cell, potentially compromising the expression of cell membrane proteins [294], to which cell-specific aptamers usually bind. In addition, cells exposed to high electrical fields during the electrophoresis could be irreversibly damaged [295].

To address these issues, this chapter presents a microfluidic device for cell-targeting aptamer development. The device consists of two microchambers, one for selection and one for amplification, with microfabricated resistive heaters and temperature sensors beneath for environmental control and thermal cycling. Cells are cultured on the bottom surface of selection chamber, which not only provides an immobilized layer of cells for cell-binding oligomer selection, but also minimizes changes to cell membrane proteins potentially caused by other immobilization approaches. Meanwhile, primer-coated magnetic beads, retained in the amplification chamber by an external magnet, provide solid support for the oligomer capture and amplification. In addition, the device employs pressure-driven flow controlled by pneumatically actuated microvalves to realize multi-round isolation of cell-targeting aptamers on a single chip. Using MCF-7 cells as a target,

we have demonstrated the capability of our approach to efficiently generate cell-binding oligomers from a random ssDNA library.

7.2. Principle, Device Design and Fabrication

7.2.1. Principle of Microfluidic Cell-Targeting Aptamer Development

Our microfluidic cell-targeting aptamer development approach integrates cell culture, affinity selection of cell-binding ssDNA, and bead-based polymerase chain reaction (PCR) into a single microfluidic device. Cells are first cultured in the selection chamber for a sufficiently long time to ensure cell attachment and surface biomarker regeneration. Selection of ssDNA is then performed by infusing a random ssDNA library into the chamber (**Figure 7.1A**), followed by multiple washes to remove weakly bound ssDNA (**Figure 7.1B**). Next, primer-functionalized magnetic beads are introduced and held in the amplification chamber. The remaining strongly bound ssDNA are thermally eluted (**Figure 7.1C**), hydrodynamically transferred to the amplification chamber (**Figure 7.1D**), captured by the surface immobilized primers (**Figure 7.1E**), and amplified via bead-based PCR (**Figure 7.1F**). Afterward, the ssDNA are released from the bead surfaces (**Figure 7.1G**) and are transported back to the selection chamber (**Figure 7.1H**) as the process is repeated.

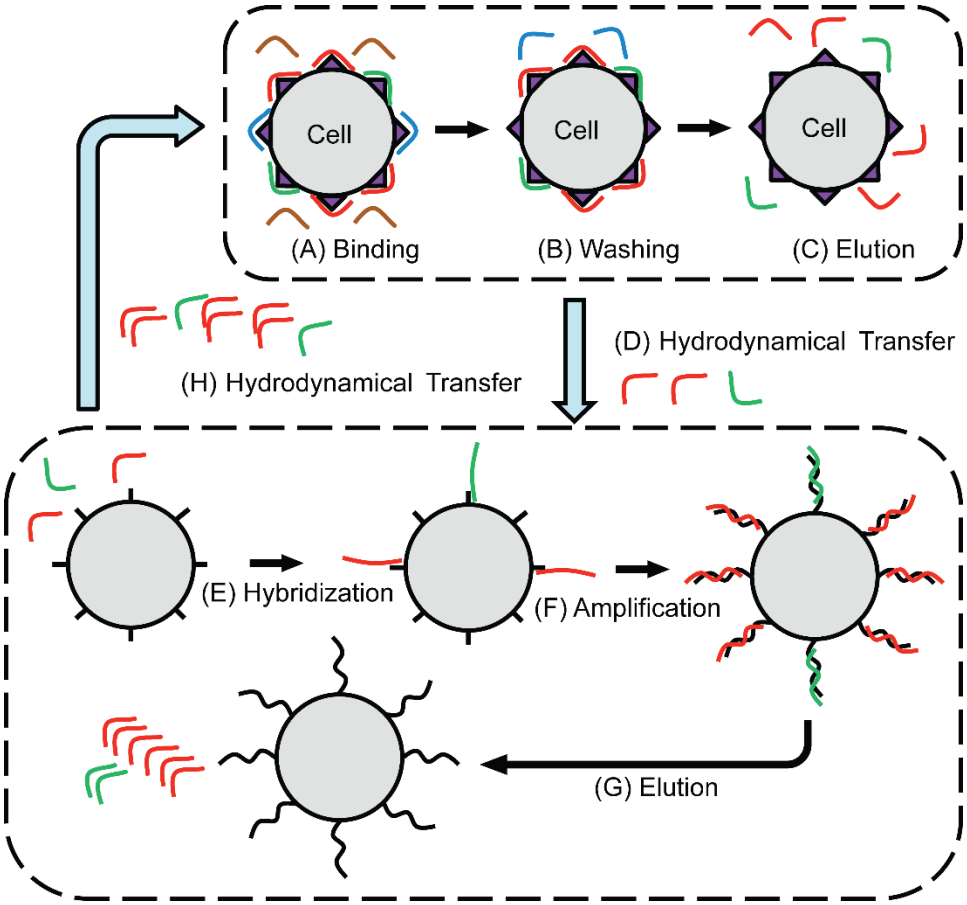

Figure 7.1: Principle of microfluidic aptamer development: (A) ssDNA with random sequence binds to cells in the selection chamber; (B) weak binders are removed by washing; (C) strong binders are eluted and (D) transferred to the amplification chamber; (E) the strands are captured by magnetic beads with surface-immobilized reverse primers and (F) amplified through PCR; (G) the amplified single strands are released from bead surfaces and (H) transported back to the selection chamber for the next round.

7.2.2. Device Design and Fabrication

The microfluidic device consists of two microchambers situated on a temperature control chip for selection and amplification (**Figure 7.2A**). The surfaces of both

microchambers (30 µm in height) with an approximately 1.5 µL volume are coated with Parylene C to prevent evaporative loss of reactants [171]. A permanent magnet is place beneath the amplification chamber to retain the streptavidin-coated magnetic beads (2.8 µm in diameter). The two channels that connect the microchambers are shaped with semi-circular profiles (20 µm in height) that can be completely sealed by elastomeric microvalves actuated by pressure-driven, oil-filled channels (30 µm in height) above (**Figure 7.2B**). Integrated on the temperature control chip are two groups of temperature control units, each containing a serpentine-sharped resistive temperature sensor (linewidth: 25 µm) and serpentine-sharped heater (linewidth: 300 µm) beneath the center of selection or amplification microchamber. The chamber temperatures can be hence controlled in closed loop separately using corresponding integrated temperature sensor and heater.

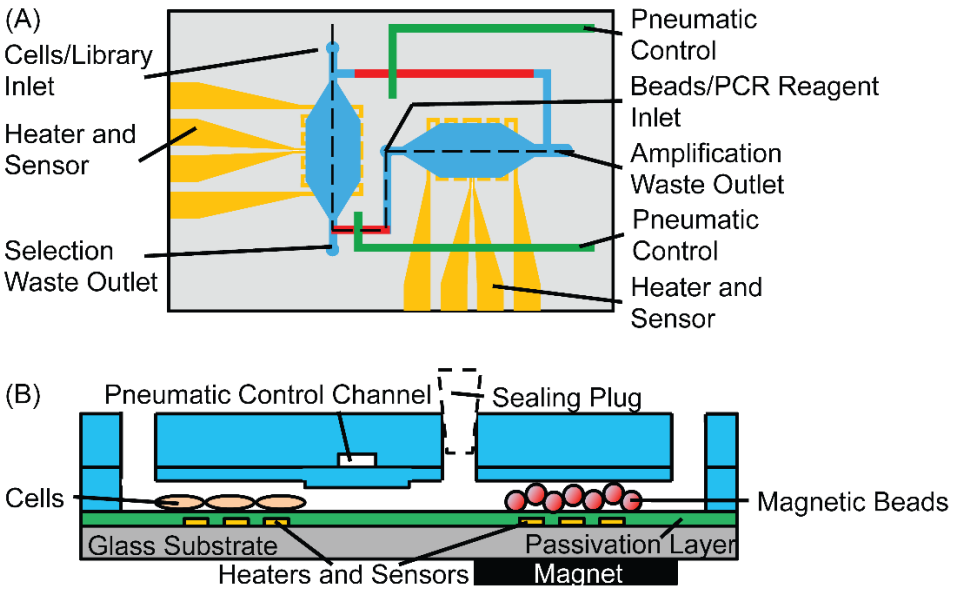

Figure 7.2: (A) Top view and (B) cross-sectional view along line a-a of the aptamer development microfluidic device.

The temperature control chip was fabricated using standard microfabrication techniques. Briefly, gold (100 nm) and chrome (5 nm) thin films were thermally evaporated onto the glass substrate, and patterned by photolithography and wet etching, which resulted in resistive temperature sensors and resistive heaters. Then, 1 μm of silicon dioxide was deposited using plasma-enhanced chemical vapor deposition (PECVD) to passivate sensors and heaters, the contact regions for electrical connections to which were opened by etching the oxide layer using hydrofluoric acid (**Figure 7.3A**).

Subsequently, the microfluidic slab bearing microfluidic and pneumatic features was fabricated from PDMS using soft lithography techniques. A layer of AZ-4620 positive photoresist (20 μm, Clariant Corp. Somerville, NJ) was spin-coated on a silicon wafer (Silicon Quest International, Inc., San Jose, CA), exposed to ultraviolet light through photomasks, developed, and baked to form a round-shaped flow channels that can be sealed completely. Then, a layer of SU-8 photoresist was patterned to finalize the mold defining microfluidic features (**Figure 7.3B**). Next, a PDMS prepolymer solution (base and curing agent mixed in a 10:1 ratio) was spin-coated onto the silicon wafer, and cured on a hotplate at 72 °C for 15 min (**Figure 7.3C**). In parallel, a layer of SU-8 photoresist was patterned on another silicon wafer to establish pneumatic controlled oil-filled valve actuation channels (**Figure 7.3D**). Another PDMS prepolymer solution was cast onto the mold and cured on a hotplate at 72 °C for 1 hour (**Figure 7.3E**). The resulting PDMS slab was peeled off from the mold, punched to form pneumatic inlet, and bonded to the PDMS membrane on the silicon mold bearing the microfluidic features (**Figure 7.3F**). Afterward, the PDMS slab together with the thin PDMS membrane was peeled off, punched to establish fluidic

inlets and outlets, and then bonded onto the temperature control chip irreversibly after another oxygen plasma treatment (**Figure 7.3G**).

Finally, the surface of SBE microchanmber was coated with a thin layer of Parylene C via chemical vapor deposition (**Figure 7.3H**). A fabricated device is shown in **Figure 7.4**.

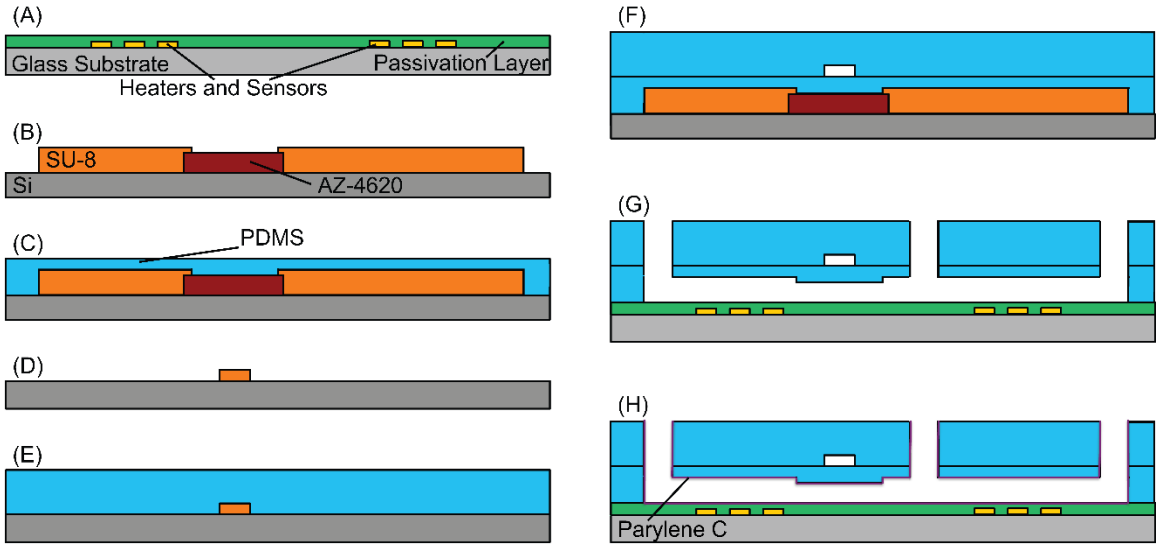

Figure 7.3: (A) Deposition, patterning and passivation of gold sensors and heaters. (B) Fabrication of fluidic channel mold including on-chip valves and microfluidic chambers and channels using positive photoresist AZ-4620 and SU-8. (C) PDMS spin-coating (D) Fabrication of SU-8 mold for pneumatic controlled oil-filled valve actuation channels. (E) Casting of PDMS microfluidic channels. (F) Bonding of PDMS slab for pneumatic controlled oil-filled valve actuation channels to PDMS-coated mold for microfluidic channels. (G) Peeling off and bonding of PDMS sheet containing fluidic channels and pneumatic controlled oil-filled valve actuation channels to temperature control chip. (H) Deposition of Parylene C.

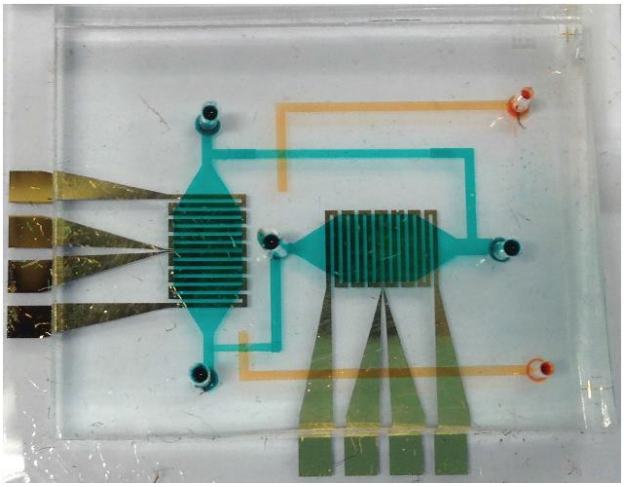

Figure 7.4: Image of a fabricated device.

7.3. Testing Methods

7.3.1. Materials

All chemicals were purchased from Sigma-Aldrich (St. Louis, MO) unless otherwise indicated. ssDNA random library (5’ – GCC TGT TGT GAG CCT CCT GTC GAA – 40N – TTG AGC GTT TAT TCT TGT CTC CC – 3’) and primers (Forward Primer: 5' – FAM – GCC TGT TGT GAG CCT CCT GTC GAA -3', and Reverse Primer: 5' – dual biotin – GG GAG ACA AGA ATA AAC GCT CAA – 3') were synthesized and purified by Integrated DNA Technologies (Coralville, IA). Deoxynucleotide triphosphates (dNTPs) and GoTaq Flexi DNA polymerase were obtained from Promega Corp. (Madison, WI). Minimum Essential Medium (MEM), fetal bovine serum (FBS), penicillin-streptomycin (P/S, penicillin 10,000 unit/mL, streptomycin 10,000 μg/mL), Dulbecco’s phosphate-buffered saline (D-PBS), 0.25% Trypsin-EDTA and streptavidin coupled magnetic beads (Dynabeads® M-270 Streptavidin) were purchased from Invitrogen (Carlsbad, CA). MCF-

7 cell line was obtained from the American Type Culture Collection (ATCC, Manassas, VA).

7.3.2. Testing Setup

Closed-loop temperature control of both selection microchamber and amplification microchamber was achieved using two groups of temperature control units with a proportional-integral-derivative (PID) algorithm implemented in a LabVIEW (National Instruments Corp., TX) program on a personal computer. Each temperature control unit contained a serpentine-shaped resistive temperature sensor and a resistive heater. The resistance of two temperature sensors was measured by a digit multimeter (34410A, Agilent Technologies Inc., CA) and a digit micro-ohm meter (34420A, Agilent Technologies Inc., CA), respectively. Each resistive heater was connected to an independent, dedicated DC power supply (E3631, Agilent Technologies Inc., CA) (**Figure 7.5A**).

Fluid control was achieved using microfabricated pressure-driven valves [192]. Two oil-filled channels, each actuated by an air control valve (6464K16, McMaster-Carr, NJ), are connected to a nitrogen gas tank (Tech Air, NY) via a pressure regulator (CONCOA North America, VA). The microfluidic device inlets are connected to a set of syringes that contain samples, buffers and reagents driven by syringe pumps (KD210P, KD Scientific, MA).

7.3.3. Testing Procedure

Development of aptamers in the microfluidic device starts from culturing MCF-7 cells in the selection chamber for a sufficiently long time (>4 hours) to ensure cell attachment

and surface biomarker regeneration (**Figure 7.5B**). Next, streptavidin magnetic beads with surface immobilized primers (approximately 5 pmol) are introduced and held in the amplification chamber with a magnet (**Figure 7.5C**). Selection of ssDNA is then performed by washing the cells with D-PBS (10 µL/min **Figure 7.5D**), infusing a random ssDNA library (100 pmol) in 20 µL binding buffer (900 mL of D-PBS + 4.5 g of glucose + 5 mL of 1 M $MgCl_2$ + 1 g of bovine serum albumin + 100 mL of FBS) through the chamber (1 µL/min, 37°C), followed by nine washes using washing buffer (900 mL of D-PBS + 4.5 g of glucose + 5 mL of 1 M $MgCl_2$ + 100 mL of FBS) (10 µL/min, 37°C) for 3 min each to remove weakly bound ssDNA (**Figure 7.5E**). Afterward, the remaining strongly bound ssDNA are thermally eluted (60 °C), hydrodynamically transferred to the amplification chamber (1 µL/min, 10 min), and captured by the surface immobilized primers (**Figure 7.5F**). Subsequently, 2 µL of PCR reagent, consisting of 7 pmol of forward primer, 1× GoTaq Flexi buffer, 0.5 U of GoTaq Flexi DNA polymerase, 1 nmol of dNTP and 4 nmol of $MgCl_2$, is introduced and subjected to 30 thermal cycles of 95 °C for 15 s, 59 °C for 30 s, and 72 °C for 45 s (**Figure 7.5G**). Cells in the selection chamber are then detached using 0.25 % trypsin-EDTA, followed by a D-PBS wash (**Figure 7.5H**). Target cells are next cultured (**Figure 7.5I**) and washed (**Figure 7.5J**) again. Afterward, ssDNA are released from the bead surfaces at 95 °C and are transported back to the selection chamber at 37 °C (1 µL/min) for 10 min, followed by nine washes using washing buffer (10 µL/min, 37°C) for 3 min each to remove weakly bound ssDNA (**Figure 7.5K**). Subsequently, streptavidin magnetic beads are removed and the amplification chamber is rinsed using D-PBS (**Figure 7.5L**). Then, the new streptavidin magnetic beads with surface immobilized primers

(approximately 5 pmol) are introduced again (**Figure 7.5M**), and the process can be repeated (**Figure 7.5F**).

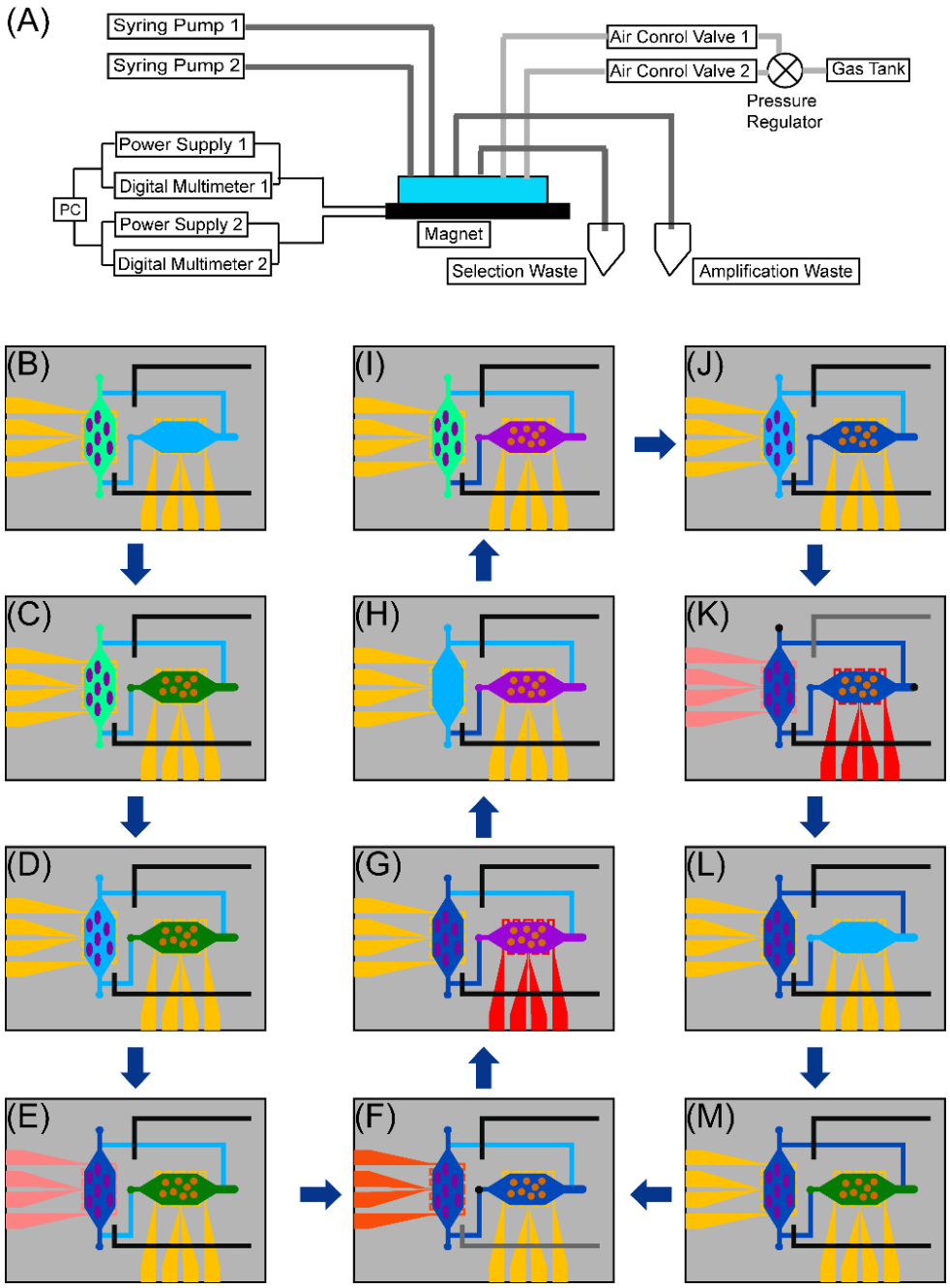

Figure 7.5: (A) Experimental setup for microfluidic cell-targeting aptamer development. (B) Cell culture on chip. (C) Introduction of streptavidin magnetic beads with surface

immobilized reversed primers. (D) Washing of cells using D-PBS. (E) Infusion of random ssDNA library for selection and remove of weakly bound ssDNA by multiple washes. (F) Thermal elution, hydrodynamically transfer and capture of strongly bound ssDNA. (G) Introduction of PCR reagent and thermal cycling. (H) Removal of cells and rinsing of selection chamber. (I) Cell culturing on chip. (J) Washing cells using D-PBS. (K) Thermal release of amplified ssDNA from bead surface, and transfer back to the selection chamber for isolation of strongly bound ssDNA. (L) Removal of used streptavidin beads. (M) Introduction of new streptavidin magnetic beads with surface immobilized reversed primers, and repetition of the entire process (F)-(M).

7.4. Results and Discussion

This section presents and analyzes experimental results from the microfluidic device for cell-targeting aptamer development. We first characterized the temperature-controlled chip and evaluated the temporal accuracy of the temperature field in the amplification chamber. Then, characterization of cell-binding ssDNA selection and cell-binding ssDNA amplification and elution were performed to demonstrate the feasibility of each functional unit. Finally, an integrated and closed-loop three round SELEX process was carried out, with the monitoring of the ssDNA enrichment progress.

7.4.1. Characterization of Temperature Control

The temperature sensor was first calibrated using an environmental test chamber (9023, Delta Design Inc., CA) maintained at a series of temperatures which are measured with high accuracy temperature reference probes (5628, Fluke Calibration, UT). The

measured resistance (R) of the thin-film gold temperature sensor was observed to vary linearly with temperature (T), represented by the relationship $R=R_0[1+\alpha(T-T_0)]$, where R_0 is the sensor resistance at a reference temperature T_0, and α is the temperature coefficient of resistance (TCR) of the sensor.

Fitting this relationship to the measurement data allowed determination of the parameter values, which were used to determine the chamber temperature from the measured sensor resistance during the selection, elution and amplification process. The temperature sensor under the amplification chamber had a measured resistance of 136.42 Ω at a reference temperature of 25.0 °C with a TCR of 3.10×10^{-3} 1/°C. We then characterized the temperature control of the chamber during thermal cycling. Time-resolved tracking of on-chip thermal cycling showed that the amplification chamber temperatures attained specified setpoints via control of the on-chip heater and off-chip fan quickly and precisely (**Figure 7.6**).

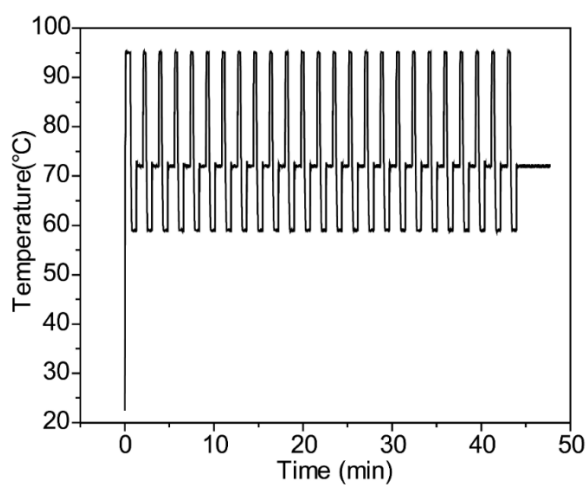

Figure 7.6: Time-resolved tracking of the temperatures inside the buffer-filled amplification during thermal cycling.

7.4.2. Characterization of Cell-Binding ssDNA Selection

We then investigated the on-chip cell culture in the selection chamber. 2 µL of MCF-7 cell suspension at 1×10^7 cells/mL in complete culture media was introduced into the selection chamber, which was then kept at 37 °C in a humidified incubator containing 5% CO_2 for 5 hours. The selection chamber was next rinsed using D-PBS at 10 µL/min for 1 min to remove unattached and dead cells, and a phase contract image was taken with an inverted microscope (IX81, Olympus Corp., PA) equipped with a digital camera (C8484, Hamamatsu Corp., NJ). Cells were attached well on the bottom surface (**Figure 7.7A**), indicating the success of using this method to restrain cells in the chamber and to regenerate cell membrane proteins.

To characterize the isolation of cell-binding ssDNA from a random library, the temperature of selection chamber was kept at 37 °C for the whole procedure by using the temperature control unit located beneath. 100 pmol of ssDNA library in 20 µL binding buffer was infused into the chamber at 1 µL/min for 20 min. Then, cells were washed with 9 aliquots of washing buffer at 10 µL/min, each for 3 min, to remove undesired ssDNA. Waste from each buffer wash were collected, amplified using PCR, and analyzed using polyacrylamide gel electrophoresis (PAGE), as shown in **Figure 7.7B**. As the cells continue to be rinsed, the amount of weakly bound ssDNA in each washing waste (identically amplified) decreases, indicated by the decreased band intensities of lanes W1 to W9 (**Figure 7.7C**). In addition, the comparable band intensity of W9 to negative control (NC, no template in the PCR reagent) suggests that ssDNA did not exist in the waste of final washing. The low intensity of the desired band in lane W1 is caused by an unspecific

amplification when using a high concentration of weakly bound ssDNA from the first wash as the template, indicated by the high fluorescence intensity above the desired band (**Figure 7.7B**). This phenomenon can be potentially avoided by optimizing the PCR conditions when amplifying the ssDNA in the wash waste, which was not the emphasis of this work. The results indicate that the extensive washing step can efficiently remove most of the weakly bound ssDNA from cell surface.

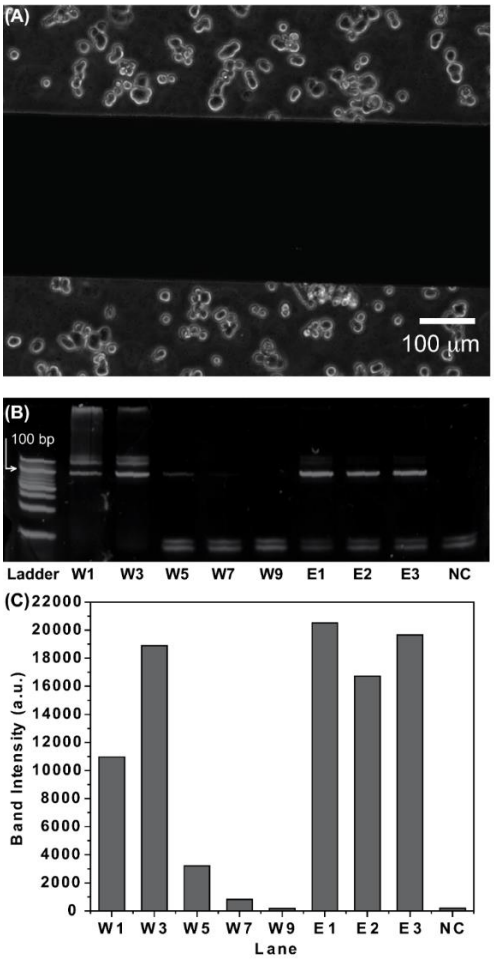

Figure 7.7: (A) A phase contract image of cells cultured in the selection chamber for 5h. (B) Polyacrylamide gel electropherogram of amplified eluents obtained during selection process. (C) Bar graph indicating band intensities for lanes W1-NC. Lane W1: wash 1;

Lane W3: wash 3; Lane W5: wash 5; Lane W7: wash 7; Lane W9: wash 9; Lane E1: thermal elution at 1 µL/min and 60 °C; Lane E2: thermal elution at 5 µL/min and 60 °C; Lane E3: thermal elution at 10 µL/min and 60 °C; Lane NC: negative control, no template.

To demonstrate the thermal elution of strongly bound ssDNA after washing, the microchamber temperature was raised to 60 °C using the same temperature control unit. The cells were then rinsed with 3 aliquots of washing buffer (10 µL) at 1 µL/min, 5 µL/min and 10 µL/min, respectively. The high band intensity of lane E1 (1 µL/min), E2 (5 µL/min) and E3 (10 µL/min) indicates successful enrichment of cell-binding ssDNA (**Figure 7.7B&C**). In addition, although not able to elute all the strongly bound ssDNA, rinsing cells at 1 µL/min for 10 min is sufficient to remove and collect a significant amount of cell-binding ssDNA, as suggested by the highest fluorescence intensity of the desired band at lane E1 (**Figure 7.7B&C**). These results indicate successful enrichment and retrieval of cell-binding ssDNA.

7.4.3. Characterization of Cell-Binding ssDNA Amplification and Elution

To characterize the bead-based amplification of cell-binding ssDNA, 10 µL thermal eluent was driven to the amplification chamber with primer-coated magnetic beads at 1 µL/min and room temperature for 10 min. The magnetic beads were gently stirred by the permanent magnet to achieve a better capture efficiency. Then, 2 µL of PCR reactants were introduced and thermally cycled. After washing, the fluorescent images of beads with and without cycling were taken (**Figure 7.8A&B**), and fluorescence intensities of beads were then measured and compared (**Figure 7.8D**). Following amplification, the fluorescent bead

intensity was 10-fold higher, indicating efficient ssDNA amplification through bead-based PCR.

To collect the amplified cell-binding ssDNA, the magnetic beads were rinsed at 95 °C and 1 µL/min for 10 min. The rinsed beads (**Figure 7.8C**) showed an intensity that was 10% of the pre-elution intensity, and was only 2.6% higher than that of pre-thermal cycling intensity (**Figure 7.8D**), indicating a highly efficient ssDNA dehybridization and separation from surface immobilized complementary strands.

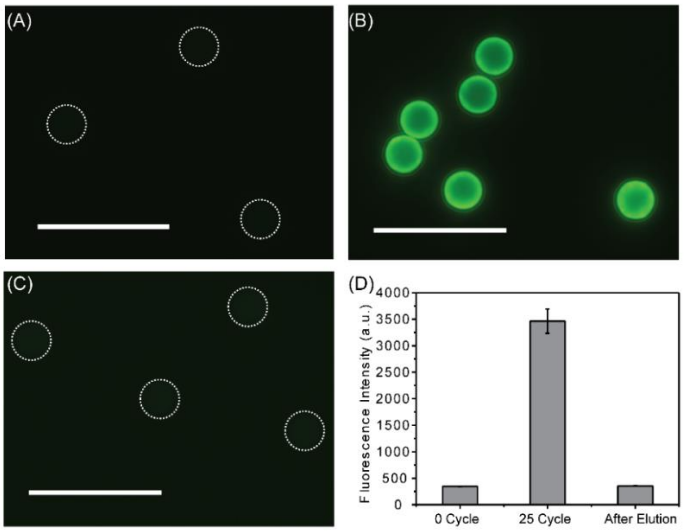

Figure 7.8: Verification of bead-based PCR and ssDNA elution. Fluorescent images of beads (A) before and (B) after 25 cycles of PCR, and (C) after thermally induced ssDNA elution; (D) bar graph depicting the fluorescent intensities of the beads. Scale bar 10 µm.

7.4.4. Demonstration of Closed-Loop Cell-Targeting Aptamer Generation

To demonstrate the feasibility of multiple-round, closed-loop cell specific aptamer generation, a three-round ssDNA selection, enrichment and amplification process was carried out. The weakly bound ssDNA of each wash in all three rounds, and the thermally

eluted strongly bound ssDNA in the third round were collected from the selection chamber (**Figure 7.9A**), amplified and analyzed with PAGE (**Figure 7.9B**). In the first round, there was still some ssDNA in the waste of the 9th wash. However, in the second and third round, there was nearly no ssDNA in the waste of the 9th wash. This indicates that the aptamer generation process was able to successfully increase the binding affinity of ssDNA pool to the target cells after each round. In addition, the high fluorescent intensity of the thermal elution lane in the gel image (**Figure 7.9C**) suggests that ssDNA specific to the target cells were successfully isolated, enriched and amplified.

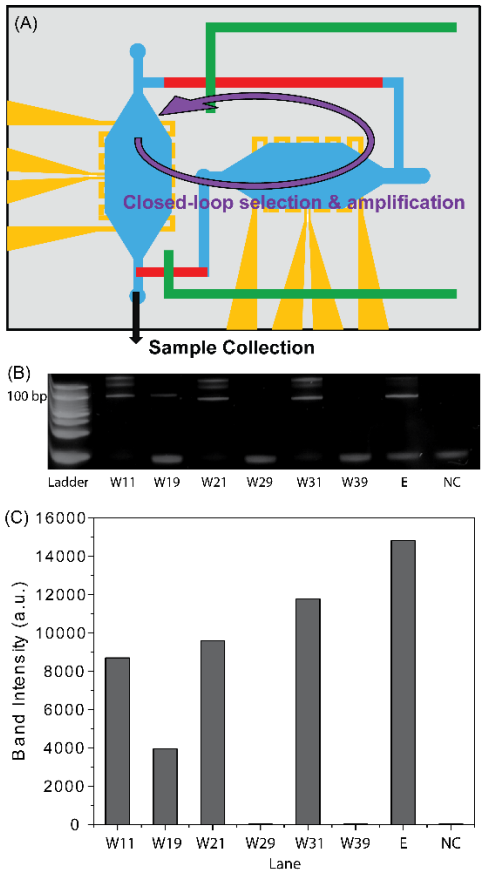

Figure 7.9: (A) Schematic of three-round, closed-loop cell-targeting ssDNA generation. (B) Polyacrylamide gel electropherogram of amplified eluents obtained during the three

selection processes; (B) bar graph indicating band intensities for lanes W11-NC. Lane W11: round 1, wash 1; Lane W19: round 1, wash 9; Lane W21: round 2, wash 1; Lane W29: round 2, wash 9; Lane W31: round 3, wash 1; Lane W39: round 3, wash 9; Lane E: thermal elution; Lane NC: negative control, no template.

7.5. Conclusion

Cell-targeting aptamers are of great importance in a wide variety of field, but their applications have been hindered by the limited choice of aptamers and labor-, time- and resource-intensive development process. We developed a microfluidic device for synthetically isolating and enriching cell-targeting aptamers from a randomized ssDNA library. The device integrates cell culturing with affinity selection of cell-binding ssDNA, which is then amplified by bead-based polymerase chain reaction (PCR). Coupling of the selection and amplification using pressure-driven flow realizes multi-round aptamer isolation on a single chip.

Our experimental results show successful on-chip cell culture in the selection chamber and efficient cell-targeting ssDNA selection from a randomized library. The employment of bead-based PCR allows effective amplification of enriched cell-specific ssDNA, and separation of amplified ssDNA from complementary strands immobilized on the bead surfaces. In addition, the successful three-round cell-targeting ssDNA generation process indicates the feasibility of using this approach for aptamer development. These results demonstrate that our device can be further implemented to achieve fully automated aptamer generation, and thus has the potential to broaden current aptamer applications in fundamental biological researches and clinical diagnostics.

Future study will involve characterization of resulting aptamer candidates, such as cloning and sequencing of isolated cell-binding ssDNA, and dissociation constant (K_d) measurement. Currently cell immobilization approach (cell culture) can only be applied to adherent cells, a refined method may also be investigated to broaden the applicable scope of this device. Moreover, the function of counter selection need to be incorporated into current device, significantly increasing the specificity of isolated aptamer. In addition, besides DNA aptamers, RNA aptamers are another major type of aptamer. Therefore, on-chip transcription and reverse transcription can also be explored, further expanding the application field of microfluidic aptamer development devices.

Chapter 8. Conclusion and Future Work

8.1. Conclusion

Genetic analysis and cell manipulation play an import role in personalized medicine and can greatly benefit from microfluidic technology. In this thesis, several microfluidic devices have been developed for genetic analysis and cell manipulation. With on-chip temperature control, microfluidic handling, and physical modulation, such devices have been demonstrated to be capable of single nucleotide polymorphism (SNP) genotyping, specific cell capture and temperature mediated cell release, tunable cell trapping, and cell-binding aptamer development on microfluidic surfaces.

In Chapter 2, a bead-based SNP genotyping device is presented. This approach utilized solid phase to integrate all the reactions, including polymerase chain reaction (PCR), single base extension (SBE), and purification, into a single chamber. The device consisted of a microchamber situated on a temperature control chip, which was further coupled to matrix-assisted laser desorption/ionization time-of-flight mass spectrometry (MALDI-TOF MS) for product analysis. Closed-loop, accurate temperature control was achieved by a proportional-integral-derivative (PID) algorithm with time constants of 2 s for heating and 9 s for cooling during the thermal cycling process, which was much more efficient than conventional thermal cyclers. The feasibility of our microfluidic device has been demonstrated by applying it to the genotyping of SNP on exon 1 of HBB gene, which causes sickle cell anemia.

As a significant improvement to bead-based SNP genotyping, a multi-step, multiplex SNP genotyping device is presented in Chapter 3. The device consisted of two microchambers situated on a temperature control chip for respectively carrying out SBE and solid-phase purification (SPP) reactions, as well as a microchannel for desalting. These functional components were connected in series by microchannels with a semi-circular cross section and could be controlled by microfabricated elastomeric valves situated beneath. 100% primer extension and efficient chemical release of SBE product have been demonstrated by using house-synthesized cleavable mass-tagged dideoxynucleotide triphosphate (ddNTPs) and on-chip temperature control units. Moreover, the tradeoff between the efficiency of SPP/desalting and that of the full assay has also been investigated. In addition, 4-plex assays on a mock synthetic template, which mimic the SNP detection process, were carried out within the fully integrated device to demonstrate the feasibility of using the microfluidic device for rapid, automated, integrated and miniaturized multiplex SNP genotyping with high accuracy and sensitivity.

Chapter 4 presents the investigation of temperature dependent affinity between aptamers and cells using a microfluidic device integrating on-chip temperature sensing and temperature control. The device consisted of a microchamber, with surface functionalized aptamers to capture target cells with high specificity, situated on a temperature control chip. The specificity of cell isolation has been demonstrated by separating CCRF-CEM cells from a heterogeneous cell solution, followed by measurements of the sensitivity of cell capture to the concentration of cell suspension and to the incubation time within the chamber. To test the temperature-dependent binding between the target cells and surface

coated aptamers, the temperature of the chamber was maintained at different setpoints, while washing buffer was used to continuously rinse the chamber. It was found that both higher temperatures and higher shear stresses facilitated cell release, and the tradeoff between these two factors was an important design consideration, due to the greater risk of cell damage when using either a higher temperature or a larger shear stress. In addition, the released cells were shown to be viable, and the aptamer-functionalized surfaces were successfully regenerated and shown to be reusable.

In Chapter 5, based on the principle demonstrated in Chapter 2, a microfluidic device for spatially selective specific capture and temperature-mediated release of cells is presented. The approach utilized a highly localized heating effect, enabled by a microfabricated resistive heater and temperature sensor, to change the affinity properties of aptamers in a specific region, without affecting those in other regions. The device consisted of a microchamber situated on a microchip with four groups of micro heaters and temperature sensors, and aptamers were patterned on design-specified regions of the chip surface. Both experimental and numerical results have demonstrated spatially selective temperature control. Further experiments showed efficient, spatially selective temperature-mediated and nondestructive release of CCRF-CEM cells, and also indicated a reusable aptamer functionalized surface.

Chapter 6 exploits the large compliance of elastomers (PDMS) to create an array of cell-trapping microstructures, whose dimensions can be mechanically modulated by inducing uniformly distributed strain via the application of external forces on the chip. Both numerical and experimental analysis showed effective deformation of microstructures,

whose width decreased from 28.8 μm to 18.0 μm and depth increased from 25.0 μm to 36.3 μm when a 79% extension was applied. The dependence of the number of cells trapped per trap on the geometrical characteristics of the microstructures was investigated by capturing MCF-7 cells on the device with different applied extensions, and indicated that the mode of the distribution for cells per microstructure shifted from 1 to 3 when applying 72% uniaxial tensile strain. In addition, the trapped cells were shown to be viable.

In Chapter 7, preliminary studies on a microfluidic device for synthetically isolating and enriching cell-targeting aptamers from a randomized single-strand DNA (ssDNA) library are presented. The pure hydrodynamic approach integrated the functions of cell culture, affinity selection of cell-binding ssDNA, and bead-based PCR. The microfluidic device consisted of two microchambers, one for selection and the other for amplification, that were connected through elastomeric microvalves to realize closed-loop, multi-round aptamer development. The success of isolating MCF-7 cell-targeting ssDNA from a randomized library and the efficiency of bead-based ssDNA amplification have been investigated. In addition, the feasibility of using this approach for aptamer development has been demonstrated by a closed-loop, three-round cell specific ssDNA generation process.

8.2. Future Work

The main contributions of the MEMS-based devices detailed in this thesis are demonstrations of proof-of-principle critical functional building blocks that can potentially enable integrated microsystems for personalized cancer medicine, which is a healthcare paradigm that allows physicians to tailor cancer treatment strategies for individual patients,

based on the exclusive patient-specific characteristics of disease revealed by evidence such as genetic variation identification, and cellular and pathological response to pharmaceutical drug candidates. In addition to future work discussed at the end of each individual chapter, the following opportunities can also be pursued in extension of this thesis research.

8.2.1. Integration of Specific Cell Purification and SNP Genotyping

The completion of the human genome and recent advances in whole genome sequencing have contributed to a more detailed understanding of molecular bases of diseases and impacts of genetics to diseases. Analysis of SNPs will contribute to personalized cancer medicine by predicting the risk of genetically related diseases and drug responses. In the research presented in this thesis, we have realized cell isolation from heterogeneous solutions and SNP genotyping from a low concentrated target sequence. To achieve a fully integrated device for genetic variation identification, a functional unit for cell lysis and genome DNA (gDNA) digestion needs to be integrated with cell isolation and SNP genotyping. The strategy of cell lysis, gDNA digestion, and purification of DNA fragments containing target sequences can be investigated in a future study. In addition, the on-chip detection method, such as nanoelectromechanical–mass spectrometry system [296], can also be explored to further increase the integration level, eliminating the requirement for external detection instrumentation.

8.2.2. Integration of Specific Cell Purification and Tunable Cell Array Establishment

High level integration has been a major feature of MEMS device, with significant advantages including reduced consumption of labor and resources, improved efficiency and accuracy, minimized device footprint, and enhanced portability. We have presented

microfluidic devices for specific cell purification and tunable cell array establishment. These two devices can be further integrated to achieve an anti-cancer drug screening device, providing patient-specific information on cellular and/or pathological response to specific pharmaceutical drugs. To do so, circulating-tumor-cells (CTCs) would be separated and enriched from blood samples, followed by nondestructive retrieval, which can be accomplished by the device described in Chapter 2 and 3. The retrieved cells would be introduced into the device presented in Chapter 4 to establish the cell array. Obviously, to achieve the personalized anti-cancer drug screening device, the interface between the two functional units have to be properly defined. Therefore, the development of cell transportation module and the modification of cell trapping geometry that optimizes loading efficiency can be investigated in future studies. In addition, on-chip short-term cell culture with infusion of drugs can be incorporated into the existing device, utilizing a similar reported technique [268].

8.2.3. Gene Expression Analysis for Identification of Substantial Variations among Cells

Gene expression analysis at the single-cell level is critical to understanding the substantial variations among cells in a heterogeneous population [297]. Quantitative reverse transcription polymerase chain reaction (qRT-PCR) allows effective single-cell gene expression analysis with high specificity and sensitivity, and large dynamic ranges. In this thesis, we have described the key techniques and proof-of-principle functional units that are required for a microfluidic qRT-PCR platform, including on-chip temperature control, solid-phase purification, specific cell purification or unspecific cell trapping, bead-

based or solution-based DNA amplification, and on-chip elastomeric micro valves for fluidic regulation. Since conventional qRT-PCR platforms are labor-intensive, have high reagent consumption, and do not offer adequate accuracies in measuring low abundance transcripts [69], it is possible and necessary to investigate and develop a microfluidic device for qRT-PCR of cancer cells, incorporating all required steps on a microbead-based platform, such as trapping and lysis of single or small numbers of cells, capture, purification and reverse transcription (RT) of messenger RNA (mRNA), and quantitative real-time PCR (qPCR) using Taqman® assay. Meanwhile, the efficiency of cell lysis, mRNA capture and RT can be studied, and the feasibility of this fully integrated bead-based approach can be further demonstrated by analyzing cells stimulated with different chemicals, leading to up- and/or down- regulation of some particular genes.

List of Publications Resulting from This Thesis

Refereed Journal Publications

1. Jing Zhu, Timothy Olsen, Renjun Pei, Milan Stojanovic and Qiao Lin, “A microfluidic device for cell specific aptamer development,” in preparation.

2. Hao Sun, Jing Zhu, Brian Ponnaiya, Sally Amundson, David Brenner, Jianguo Tao and Qiao Lin, “A bead-based microfluidic device for gene expression analysis,” in preparation.

3. Jing Zhu, Chunmei Qiu, Mirkó Palla, James Russo, Jingyue Ju and Qiao Lin, "A microfluidic device for multiplex single nucleotide polymorphism genotyping," *RSC Advances*, vol. 4, pp. 4269-4277, 2014.

4. Jing Zhu, Junyi Shang, Timothy Olsen, Kun Liu, David Brenner and Qiao Lin, "A mechanically tunable microfluidic cell-trapping device," *Sensor Actuat A-Phys*, 10.1016/j.sna.2013.10.016.

5. Jing Zhu, Junyi Shang, Yuan Jia, Renjun Pei, Milan Stojanovic and Qiao Lin, "Spatially selective release of aptamer-captured cells by temperature mediation," *IET Nanobiotechnol*, doi: 10.1049/iet-nbt.2013.0028.

6. Jing Zhu, Thaihuu Nguyen, Renjun Pei, Milan Stojanovic and Qiao Lin, "Specific capture and temperature-mediated release of cells in an aptamer-based microfluidic device," *Lab Chip*, 12: 3504-3513, 2012.

7. Jing Zhu, Mirkó Palla, Stefano Ronca, Ronald Warpner, Jingyue Ju and Qiao Lin. "A MEMS-based approach to single nucleotide polymorphism genotyping," *Sensor Actuat A-Phys*, 195: 175-182, 2013.

Refereed Conference Proceedings

1. Jing Zhu, Timothy Olsen, Renjun Pei, Milan Stojanovic and Qiao Lin, “A microfluidic device for isolation of cell-targeting aptamers,” *The 27th IEEE Int. Conf. on Micro Electro Mechanical Systems (MEMS '14)*, San Francisco, CA, pp. 242-245, 2014.

2. Yuan Jia, Bin Wang, Jing Zhu and Qiao Lin, “A polymer-based mems differential scanning calorimeter,” *The 27th IEEE Int. Conf. on Micro Electro Mechanical Systems (MEMS '14)*, San Francisco, CA, pp. 306-309, 2014.

3. Cheng Wang, Jinho Kim, Jing Zhu, Renjun Pei, Guohua Liu, James Hone, Milan

Stojanovic and Qiao Lin, “Graphene nanosensor for detection of small molecules,” *The 27th IEEE Int. Conf. on Micro Electro Mechanical Systems (MEMS '14)*, San Francisco, CA, pp. 1075-1078, 2014.

4. Jing. Zhu, Junyi. Shang, Yuan Jia, Kun Liu, David Brenner and Qiao Lin, "Physical modulation based cell manipulation in microfluidic devices," *The 8th IEEE Int. Conf. on Nano/Micro Engineered and Molecular Systems (NEMS '13)*, Suzhou, China, pp. 1226-1229, 2013. CM Ho Best Paper Award in Micro and Nanofluidics.

5. Jing Zhu, Junyi Shang, David Brenner and Qiao Lin, "An elastomeric polymer microchip for mechanically tunable cell trapping," *The 26th IEEE Int. Conf. on Micro Electro Mechanical Systems (MEMS '13)*, Taipei, Taiwan, pp. 945-948, 2013.

6. Jaeyoung Yang, Jing Zhu and Qiao Lin, "A microfluidic aptasensor integrated with nanodrop generator for MALDI-TOF MS analysis in clinical applications," *The 17th IEEE Int. Conf. on Solid-State Sensors, Actuators and Microsystems (Transducers '13)*, Barcelona, Spain, pp 2544-2547, 2013.

7. Qiao Lin, Jinho Kim, Jing Zhu, Jaeyoung Yang, John Hilton, Thaihuu Nguyen, Renjun Pei, Kyungae. Yang and Milan Stojanovic, "Integrating aptamers and microfluidics for biological manipulation and sensing," *The 8th IEEE Int. Conf. on Nano/Micro Engineered and Molecular Systems (NEMS '13)*, Suzhou, China, pp. 1245-1248, 2013.

8. Jinho Kim, John Hilton, Kyungae Yang, Renjun Pei, Jing Zhu, Milan Stojanovic and Qiao Lin, "Electrokinetically integrated microfluidic isolation and amplification of biomolecule- and cell-binding nucleic acids," *The 26th IEEE Int. Conf. on Micro Electro Mechanical Systems (MEMS '13)*, Taipei, Taiwan, pp. 1007-1010, 2013. Outstanding Poster Paper Finalist.

9. Jing Zhu, Mirkó Palla, Stefano Ronca, Ronald Warpner, Jingyue Ju and Qiao Lin, "A MEMS-based approach to detection of single nucleotide polymorphisms for genetic disorder diagnosis," *The 25th IEEE Int. Conf. on Micro Electro Mechanical Systems (MEMS '12)*, Paris, France, pp. 754-756, 2012.

10. Jing Zhu, Thaihuu Nguyen, Renjun Pei, Milan Stojanovic and Qiao Lin, "Specific capture and temperature mediated release of cells using aptamer-functionalized microfluidic surfaces," *The 16th IEEE Int. Conf. on Solid-State Sensors, Actuators and Microsystems (Transducers '11)*, Beijing, China, pp. 751-754, 2011.

11. Jing Zhu, Chunmei Qiu, Mirkó Palla, Thaihuu Nguyen, Jingyue Ju and Qiao Lin, "A microfluidic device for detection of single nucleotide polymorphisms by allele specific single base extension," *The 15th Int. Conf. on Miniaturized Systems for Chemistry and Life Sciences (MicroTAS '11)*, Seattle, WA, pp. 1442-1444, 2011.

12. Jing Zhu, Thaihuu Nguyen, Renjun Pei, Milan Stojanovic and Qiao Lin, "Reusable microfluidic chip for cell capture and release using surface-immobilized aptamer," *The 14th Int. Conf. on Miniaturized Systems for Chemistry and Life Sciences (MicroTAS '10)*, Groningen, the Netherlands, pp. 920-922, 2010.

Bibliography

[1] G. M. Whitesides, "The Origins and the Future of Microfluidics," *Nature*, vol. 442, pp. 368-73, 2006.

[2] J. W. Hong and S. R. Quake, "Integrated Nanoliter Systems," *Nature Biotechnology*, vol. 21, pp. 1179-1183, 2003.

[3] D. B. Weibel, M. Kruithof, S. Potenta, S. K. Sia, A. Lee, and G. M. Whitesides, "Torque-Actuated Valves for Microfluidics," *Analytical chemistry*, vol. 77, pp. 4726-4733, 2005.

[4] N. T. Nguyen and Z. G. Wu, "Micromixers - a Review," *Journal of Micromechanics and Microengineering*, vol. 15, pp. R1-R16, 2005.

[5] A. Gunther, M. Jhunjhunwala, M. Thalmann, M. A. Schmidt, and K. F. Jensen, "Micromixing of Miscible Liquids in Segmented Gas-Liquid Flow," *Langmuir*, vol. 21, pp. 1547-1555, 2005.

[6] P. Garstecki, M. A. Fischbach, and G. M. Whitesides, "Design for Mixing Using Bubbles in Branched Microfluidic Channels," *Applied Physics Letters*, vol. 86, 2005.

[7] D. J. Laser and J. G. Santiago, "A Review of Micropumps," *Journal of Micromechanics and Microengineering*, vol. 14, pp. R35-R64, 2004.

[8] A. Manz, D. J. Harrison, E. M. J. Verpoorte, J. C. Fettinger, A. Paulus, H. Ludi, and H. M. Widmer, "Planar Chips Technology for Miniaturization and Integration of Separation Techniques into Monitoring Systems - Capillary Electrophoresis on a Chip," *Journal of Chromatography*, vol. 593, pp. 253-258, 1992.

[9] A. Manz, N. Graber, and H. M. Widmer, "Miniaturized Total Chemical-Analysis Systems - a Novel Concept for Chemical Sensing," *Sensors and Actuators B-Chemical*, vol. 1, pp. 244-248, 1990.

[10] E. Livak-Dahl, I. Sinn, and M. Burns, "Microfluidic Chemical Analysis Systems," *Annual Review of Chemical and Biomolecular Engineering, Vol 2*, vol. 2, pp. 325-353, 2011.

[11] D. Janasek, J. Franzke, and A. Manz, "Scaling and the Design of Miniaturized Chemical-Analysis Systems," *Nature*, vol. 442, pp. 374-380, 2006.

[12] E. W. K. Young and D. J. Beebe, "Fundamentals of Microfluidic Cell Culture in Controlled Microenvironments," *Chemical Society Reviews*, vol. 39, pp. 1036-1048, 2010.

[13] S. M. Kim, S. H. Lee, and K. Y. Suh, "Cell Research with Physically Modified Microfluidic Channels: A Review," *Lab on a Chip*, vol. 8, pp. 1015-1023, 2008.

[14] H. Andersson and A. van den Berg, "Microfluidic Devices for Cellomics: A Review," *Sensors and Actuators B-Chemical*, vol. 92, pp. 315-325, 2003.

[15] P. Liu and R. A. Mathies, "Integrated Microfluidic Systems for High-Performance Genetic Analysis," *Trends in Biotechnology*, vol. 27, pp. 572-581, 2009.

[16] K. M. Horsman, J. M. Bienvenue, K. R. Blasier, and J. P. Landers, "Forensic DNA Analysis on Microfluidic Devices: A Review," *Journal of Forensic Sciences*, vol. 52, pp. 784-799, 2007.

[17] G. H. W. Sanders and A. Manz, "Chip-Based Microsystems for Genomic and Proteomic Analysis," *Trac-Trends in Analytical Chemistry*, vol. 19, pp. 364-378, 2000.

[18] Y. H. Zhang and P. Ozdemir, "Microfluidic DNA Amplification-a Review," *Analytica Chimica Acta*, vol. 638, pp. 115-125, 2009.

[19] X. D. Hoa, A. G. Kirk, and M. Tabrizian, "Towards Integrated and Sensitive Surface Plasmon Resonance Biosensors: A Review of Recent Progress," *Biosensors & Bioelectronics*, vol. 23, pp. 151-160, 2007.

[20] J. Mairhofer, K. Roppert, and P. Ertl, "Microfluidic Systems for Pathogen Sensing: A Review," *Sensors*, vol. 9, pp. 4804-4823, 2009.

[21] X. D. Fan, I. M. White, S. I. Shopova, H. Y. Zhu, J. D. Suter, and Y. Z. Sun, "Sensitive Optical Biosensors for Unlabeled Targets: A Review," *Analytica Chimica Acta*, vol. 620, pp. 8-26, 2008.

[22] P. S. Dittrich and A. Manz, "Lab-on-a-Chip: Microfluidics in Drug Discovery," *Nature Reviews Drug Discovery*, vol. 5, pp. 210-218, 2006.

[23] J. Pihl, M. Karlsson, and D. T. Chiu, "Microfluidic Technologies in Drug Discovery," *Drug Discovery Today*, vol. 10, pp. 1377-1383, 2005.

[24] A. W. Chow, "Lab-on-a-Chip: Opportunities for Chemical Engineering," *Aiche Journal*, vol. 48, pp. 1590-1595, 2002.

[25] D. Gonzalez de Castro, P. A. Clarke, B. Al-Lazikani, and P. Workman, "Personalized Cancer Medicine: Molecular Diagnostics, Predictive Biomarkers, and Drug Resistance," *Clin Pharmacol Ther*, vol. 93, pp. 252-9, 2013.

[26] M. A. Hamburg and F. S. Collins, "The Path to Personalized Medicine," *N Engl J Med*, vol. 363, pp. 301-4, 2010.

[27] P. W. Gout and Y. Wang, "Drug Sensitivity Testing for Personalized Lung Cancer Therapy," *J Thorac Dis*, vol. 4, pp. 17-8, 2012.

[28] K. J. Shaw, C. Birch, E. M. Hughes, A. D. Jakes, J. Greenman, and S. J. Haswell, "Microsystems for Personalized Biomolecular Diagnostics," *Engineering in Life Sciences*, vol. 11, pp. 121-132, 2011.

[29] E. S. Lander, I. H. G. S. Consortium, L. M. Linton, B. Birren, C. Nusbaum, M. C. Zody, J. Baldwin, K. Devon, K. Dewar, M. Doyle, W. FitzHugh, R. Funke, D. Gage, K. Harris, A. Heaford, J. Howland, L. Kann, J. Lehoczky, R. LeVine, P. McEwan, K. McKernan, J. Meldrim, J. P. Mesirov, C. Miranda, W. Morris, J. Naylor, C. Raymond, M. Rosetti, R. Santos, A. Sheridan, C. Sougnez, N. Stange-Thomann, N. Stojanovic, A. Subramanian, D. Wyman, J. Rogers, J. Sulston, R. Ainscough, S. Beck, D. Bentley, J. Burton, C. Clee, N. Carter, A. Coulson, R. Deadman, P. Deloukas, A. Dunham, I. Dunham, R. Durbin, L. French, D. Grafham, S. Gregory, T. Hubbard, S. Humphray, A. Hunt, M. Jones, C. Lloyd, A. McMurray, L. Matthews, S. Mercer, S. Milne, J. C. Mullikin, A. Mungall, R. Plumb, M. Ross, R. Shownkeen, S. Sims, R. H. Waterston, R. K. Wilson, L. W. Hillier, J. D. McPherson, M. A. Marra, E. R. Mardis, L. A. Fulton, A. T. Chinwalla, K. H. Pepin, W. R. Gish, S. L. Chissoe, M. C. Wendl, K. D. Delehaunty, T. L. Miner, A. Delehaunty, J. B. Kramer, L. L. Cook, R. S. Fulton, D. L. Johnson, P. J. Minx, S. W. Clifton, T. Hawkins, E. Branscomb, P. Predki, P. Richardson, S. Wenning, T. Slezak, N. Doggett, J. F. Cheng, A. Olsen, S. Lucas, C. Elkin, E. Uberbacher, et al., "Initial Sequencing and Analysis of the Human Genome," *Nature*, vol. 409, pp. 860-921, 2001.

[30] J. Wang, W. Wang, R. Q. Li, Y. R. Li, G. Tian, L. Goodman, W. Fan, J. Q. Zhang, J. Li, J. B. Zhang, Y. R. Guo, B. X. Feng, H. Li, Y. Lu, X. D. Fang, H. Q. Liang, Z. L. Du, D. Li, Y. Q. Zhao, Y. J. Hu, Z. Z. Yang, H. C. Zheng, I. Hellmann, M. Inouye, J. Pool, X. Yi, J. Zhao, J. J. Duan, Y. Zhou, J. J. Qin, L. J. Ma, G. Q. Li, Z. T. Yang, G. J. Zhang, B. Yang, C. Yu, F. Liang, W. J. Li, S. C. Li, D. W. Li, P. X. Ni, J. Ruan, Q. B. Li, H. M. Zhu, D. Y. Liu, Z. K. Lu, N. Li, G. W. Guo, J. G. Zhang, J. Ye, L. Fang, Q. Hao, Q. Chen, Y. Liang, Y. Y. Su, A. San, C. Ping, S. Yang, F. Chen, L. Li, K. Zhou, H. K. Zheng, Y. Y. Ren, L. Yang, Y. Gao, G. H. Yang, Z. Li, X. L. Feng, K. Kristiansen, G. K. S. Wong, R. Nielsen, R. Durbin, L. Bolund, X. Q. Zhang, S. G. Li, H. M. Yang, and J. Wang, "The Diploid Genome Sequence of an Asian Individual," *Nature*, vol. 456, pp. 60-U1, 2008.

[31] D. A. Wheeler, M. Srinivasan, M. Egholm, Y. Shen, L. Chen, A. McGuire, W. He, Y. J. Chen, V. Makhijani, G. T. Roth, X. Gomes, K. Tartaro, F. Niazi, C. L. Turcotte, G. P. Irzyk, J. R. Lupski, C. Chinault, X. Z. Song, Y. Liu, Y. Yuan, L. Nazareth, X. Qin, D. M. Muzny, M. Margulies, G. M. Weinstock, R. A. Gibbs, and J. M. Rothberg, "The Complete Genome of an Individual by Massively Parallel DNA Sequencing," *Nature*, vol. 452, pp. 872-U5, 2008.

[32] E. Check, "Human Genome: Patchwork People," *Nature*, vol. 437, pp. 1084-1086, 2005.

[33] H. Ellegren, "Comparative Genomics and the Study of Evolution by Natural Selection," *Molecular Ecology*, vol. 17, pp. 4586-4596, 2008.

[34] K. E. Herold and A. Rasooly, *Lab on a Chip Technology*. Norfolk, UK: Caister Academic Press, 2009.

[35] D. J. Harrison, K. Fluri, K. Seiler, Z. H. Fan, C. S. Effenhauser, and A. Manz, "Micromachining a Miniaturized Capillary Electrophoresis-Based Chemical-Analysis System on a Chip," *Science*, vol. 261, pp. 895-897, 1993.

[36] J. D. Watson and F. H. C. Crick, "Molecular Structure of Nucleic Acids - a Structure for Deoxyribose Nucleic Acid," *Nature*, vol. 171, pp. 737-738, 1953.

[37] B. Alberts, *Molecular Biology of the Cell*, 4th ed. New York: Garland Science, 2002.

[38] F. Sanger and A. R. Coulson, "A Rapid Method for Determining Sequences in DNA by Primed Synthesis with DNA Polymerase," *Journal of molecular biology*, vol. 94, pp. 441-8, 1975.

[39] F. Sanger, G. M. Air, B. G. Barrell, N. L. Brown, A. R. Coulson, J. C. Fiddes, C. A. Hutchison, P. M. Slocombe, and M. Smith, "Nucleotide-Sequence of Bacteriophage Phichi174 DNA," *Nature*, vol. 265, pp. 687-695, 1977.

[40] S. Brenner, M. Johnson, J. Bridgham, G. Golda, D. H. Lloyd, D. Johnson, S. J. Luo, S. McCurdy, M. Foy, M. Ewan, R. Roth, D. George, S. Eletr, G. Albrecht, E. Vermaas, S. R. Williams, K. Moon, T. Burcham, M. Pallas, R. B. DuBridge, J. Kirchner, K. Fearon, J. Mao, and K. Corcoran, "Gene Expression Analysis by Massively Parallel Signature Sequencing (Mpss) on Microbead Arrays," *Nature Biotechnology*, vol. 18, pp. 630-634, 2000.

[41] J. Shendure, G. J. Porreca, N. B. Reppas, X. X. Lin, J. P. McCutcheon, A. M. Rosenbaum, M. D. Wang, K. Zhang, R. D. Mitra, and G. M. Church, "Accurate Multiplex Polony Sequencing of an Evolved Bacterial Genome," *Science*, vol. 309, pp. 1728-1732, 2005.

[42] G. J. Porreca, "Genome Sequencing on Nanoballs," *Nature Biotechnology*, vol. 28, pp. 43-44, 2010.

[43] M. Kircher and J. Kelso, "High-Throughput DNA Sequencing - Concepts and Limitations," *Bioessays*, vol. 32, pp. 524-536, 2010.

[44] C. P. Fredlake, D. G. Hert, C. W. Kan, T. N. Chiesl, B. E. Root, R. E. Forster, and A. E. Barron, "Ultrafast DNA Sequencing on a Microchip by a Hybrid Separation Mechanism That Gives 600 Bases in 6.5 Minutes," *Proceedings of the National Academy of Sciences of the United States of America*, vol. 105, pp. 476-481, 2008.

[45] J. H. Aborn, S. A. El-Difrawy, M. Novotny, E. A. Gismondi, R. Lam, P. Matsudaira, B. K. Mckenna, T. O'Neil, P. Streechon, and D. J. Ehrlich, "A 768-Lane Microfabricated System for High-Throughput DNA Sequencing," *Lab on a Chip*, vol. 5, pp. 669-674, 2005.

[46] R. G. Blazej, P. Kumaresan, and R. A. Mathies, "Microfabricated Bioprocessor for Integrated Nanoliter-Scale Sanger DNA Sequencing," *Proceedings of the National Academy of Sciences of the United States of America*, vol. 103, pp. 7240-7245, 2006.

[47] A. J. Brookes, "The Essence of Snps," *Gene*, vol. 234, pp. 177-186, 1999.

[48] R. Sachidanandam, D. Weissman, S. C. Schmidt, J. M. Kakol, L. D. Stein, G. Marth, S. Sherry, J. C. Mullikin, B. J. Mortimore, D. L. Willey, S. E. Hunt, C. G. Cole, P. C. Coggill, C. M. Rice, Z. Ning, J. Rogers, D. R. Bentley, P. Y. Kwok, E. R. Mardis, R. T. Yeh, B. Schultz, L. Cook, R. Davenport, M. Dante, L. Fulton, L. Hillier, R. H. Waterston, J. D. McPherson, B. Gilman, S. Schaffner, W. J. Van Etten, D. Reich, J. Higgins, M. J. Daly, B. Blumenstiel, J. Baldwin, N. Stange-Thomann, M. C. Zody, L. Linton, E. S. Lander, and D. Altshuler, "A Map of Human Genome Sequence Variation Containing 1.42 Million Single Nucleotide Polymorphisms," *Nature*, vol. 409, pp. 928-33, 2001.

[49] P. Y. Kwok, "Methods for Genotyping Single Nucleotide Polymorphisms," *Annual review of genomics and human genetics*, vol. 2, pp. 235-58, 2001.

[50] J. Ragoussis, "Genotyping Technologies for Genetic Research," *Annual review of genomics and human genetics*, vol. 10, pp. 117-133, 2009.

[51] M. Ota, H. Fukushima, J. K. Kulski, and H. Inoko, "Single Nucleotide Polymorphism Detection by Polymerase Chain Reaction-Restriction Fragment Length Polymorphism," *Nature protocols*, vol. 2, pp. 2857-64, 2007.

[52] D. Botstein, R. L. White, M. Skolnick, and R. W. Davis, "Construction of a Genetic-Linkage Map in Man Using Restriction Fragment Length Polymorphisms," *American Journal of Human Genetics*, vol. 32, pp. 314-331, 1980.

[53] V. Lyamichev, A. L. Mast, J. G. Hall, J. R. Prudent, M. W. Kaiser, T. Takova, R. W. Kwiatkowski, T. J. Sander, M. de Arruda, D. A. Arco, B. P. Neri, and M. A. Brow, "Polymorphism Identification and Quantitative Detection of Genomic DNA

by Invasive Cleavage of Oligonucleotide Probes," *Nature Biotechnology*, vol. 17, pp. 292-6, 1999.

[54] M. Olivier, "The Invader Assay for Snp Genotyping," *Mutation research*, vol. 573, pp. 103-10, 2005.

[55] G. H. McGall and F. C. Christians, "High-Density Genechip Oligonucleotide Probe Arrays," *Advances in biochemical engineering/biotechnology*, vol. 77, pp. 21-42, 2002.

[56] H. Matsuzaki, H. Loi, S. Dong, Y. Y. Tsai, J. Fang, J. Law, X. Di, W. M. Liu, G. Yang, G. Liu, J. Huang, G. C. Kennedy, T. B. Ryder, G. A. Marcus, P. S. Walsh, M. D. Shriver, J. M. Puck, K. W. Jones, and R. Mei, "Parallel Genotyping of over 10,000 Snps Using a One-Primer Assay on a High-Density Oligonucleotide Array," *Genome research*, vol. 14, pp. 414-25, 2004.

[57] U. Landegren, R. Kaiser, J. Sanders, and L. Hood, "A Ligase-Mediated Gene Detection Technique," *Science*, vol. 241, pp. 1077-1080, 1988.

[58] F. A. De La Vega, K. D. Lazaruk, M. D. Rhodes, and M. H. Wenz, "Assessment of Two Flexible and Compatible Snp Genotyping Platforms: Taqman (R) Snp Genotyping Assays and the Snplex (Tm) Genotyping System," *Mutation Research-Fundamental and Molecular Mechanisms of Mutagenesis*, vol. 573, pp. 111-135, 2005.

[59] F. J. Steemers and K. L. Gunderson, "Whole Genome Genotyping Technologies on the Beadarray Platform," *Biotechnology journal*, vol. 2, pp. 41-9, 2007.

[60] C. Jurinke, P. Oeth, and D. van den Boom, "Maldi-Tof Mass Spectrometry: A Versatile Tool for High-Performance DNA Analysis," *Molecular biotechnology*, vol. 26, pp. 147-64, 2004.

[61] E. Paux, P. Sourdille, I. Mackay, and C. Feuillet, "Sequence-Based Marker Development in Wheat: Advances and Applications to Breeding," *Biotechnology advances*, vol. 30, pp. 1071-88, 2012.

[62] K. Y. Lien and G. B. Lee, "Miniaturization of Molecular Biological Techniques for Gene Assay," *The Analyst*, vol. 135, pp. 1499-518, 2010.

[63] D. Schmalzing, A. Belenky, M. A. Novotny, L. Koutny, O. Salas-Solano, S. El-Difrawy, A. Adourian, P. Matsudaira, and D. Ehrlich, "Microchip Electrophoresis: A Method for High-Speed Snp Detection," *Nucleic acids research*, vol. 28, pp. E43, 2000.

[64] K. Hatakeyama, T. Tanaka, M. Sawaguchi, A. Iwadate, Y. Mizutani, K. Sasaki, N. Tateishi, and T. Matsunaga, "Microfluidic Device Using Chemiluminescence and a DNA-Arrayed Thin Film Transistor Photosensor for Single Nucleotide Polymorphism Genotyping of Pcr Amplicons from Whole Blood," *Lab on a Chip*, vol. 9, pp. 1052-1058, 2009.

[65] P. J. Choi, L. Cai, K. Frieda, and S. Xie, "A Stochastic Single-Molecule Event Triggers Phenotype Switching of a Bacterial Cell," *Science*, vol. 322, pp. 442-446, 2008.

[66] L. Cai, N. Friedman, and X. S. Xie, "Stochastic Protein Expression in Individual Cells at the Single Molecule Level," *Nature*, vol. 440, pp. 358-362, 2006.

[67] I. Dunham, A. Kundaje, S. F. Aldred, P. J. Collins, C. A. Davis, F. Doyle, C. B. Epstein, S. Frietze, J. Harrow, R. Kaul, J. Khatun, B. R. Lajoie, S. G. Landt, B. K. Lee, F. Pauli, K. R. Rosenbloom, P. Sabo, A. Safi, A. Sanyal, N. Shoresh, J. M. Simon, L. Song, N. D. Trinklein, R. C. Altshuler, E. Birney, J. B. Brown, C. Cheng, S. Djebali, X. Dong, J. Ernst, T. S. Furey, M. Gerstein, B. Giardine, M. Greven, R. C. Hardison, R. S. Harris, J. Herrero, M. M. Hoffman, S. Iyer, M. Kelllis, P. Kheradpour, T. Lassmann, Q. Li, X. Lin, G. K. Marinov, A. Merkel, A. Mortazavi, S. C. Parker, T. E. Reddy, J. Rozowsky, F. Schlesinger, R. E. Thurman, J. Wang, L. D. Ward, T. W. Whitfield, S. P. Wilder, W. Wu, H. S. Xi, K. Y. Yip, J. Zhuang, B. E. Bernstein, E. D. Green, C. Gunter, M. Snyder, M. J. Pazin, R. F. Lowdon, L. A. Dillon, L. B. Adams, C. J. Kelly, J. Zhang, J. R. Wexler, P. J. Good, E. A. Feingold, G. E. Crawford, J. Dekker, L. Elinitski, P. J. Farnham, M. C. Giddings, T. R. Gingeras, R. Guigo, T. J. Hubbard, M. Kellis, W. J. Kent, J. D. Lieb, E. H. Margulies, R. M. Myers, J. A. Starnatoyannopoulos, S. A. Tennebaum, Z. Weng, K. P. White, B. Wold, Y. Yu, J. Wrobel, B. A. Risk, H. P. Gunawardena, H. C. Kuiper, C. W. Maier, L. Xie, X. Chen, T. S. Mikkelsen, et al., "An Integrated Encyclopedia of DNA Elements in the Human Genome," *Nature*, vol. 489, pp. 57-74, 2012.

[68] J. S. Marcus, W. F. Anderson, and S. R. Quake, "Microfluidic Single-Cell Mrna Isolation and Analysis," *Analytical chemistry*, vol. 78, pp. 3084-9, 2006.

[69] A. K. White, M. VanInsberghe, O. I. Petriv, M. Hamidi, D. Sikorski, M. A. Marra, J. Piret, S. Aparicio, and C. L. Hansen, "High-Throughput Microfluidic Single-Cell Rt-Qpcr," *Proceedings of the National Academy of Sciences of the United States of America*, vol. 108, pp. 13999-4004, 2011.

[70] N. M. Toriello, E. S. Douglas, N. Thaitrong, S. C. Hsiao, M. B. Francis, C. R. Bertozzi, and R. A. Mathies, "Integrated Microfluidic Bioprocessor for Single-Cell Gene Expression Analysis," *Proceedings of the National Academy of Sciences of the United States of America*, vol. 105, pp. 20173-20178, 2008.

[71] J. D. Adams and H. T. Soh, "Perspectives on Utilizing Unique Features of Microfluidics Technology for Particle and Cell Sorting," *Jala*, vol. 14, pp. 331-340, 2009.

[72] H. Tsutsui and C. M. Ho, "Cell Separation by Non-Inertial Force Fields in Microfluidic Systems," *Mechanics Research Communications*, vol. 36, pp. 92-103, 2009.

[73] P. Chen, X. J. Feng, W. Du, and B. F. Liu, "Microfluidic Chips for Cell Sorting," *Frontiers in Bioscience-Landmark*, vol. 13, pp. 2464-2483, 2008.

[74] D. Recktenwald and A. Radbruch, *Cell Separation Methods and Applications*. New York: M. Dekker, 1998.

[75] X. Chen, D. Cui, C. Liu, H. Li, and J. Chen, "Continuous Flow Microfluidic Device for Cell Separation, Cell Lysis and DNA Purification," *Analytica Chimica Acta*, vol. 584, pp. 237-43, 2007.

[76] S. K. Murthy, P. Sethu, G. Vunjak-Novakovic, M. Toner, and M. Radisic, "Size-Based Microfluidic Enrichment of Neonatal Rat Cardiac Cell Populations," *Biomedical microdevices*, vol. 8, pp. 231-7, 2006.

[77] L. R. Huang, E. C. Cox, R. H. Austin, and J. C. Sturm, "Continuous Particle Separation through Deterministic Lateral Displacement," *Science*, vol. 304, pp. 987-990, 2004.

[78] A. Jain and J. D. Posner, "Particle Dispersion and Separation Resolution of Pinched Flow Fractionation," *Analytical chemistry*, vol. 80, pp. 1641-8, 2008.

[79] S. S. Kuntaegowdanahalli, A. A. S. Bhagat, G. Kumar, and I. Papautsky, "Inertial Microfluidics for Continuous Particle Separation in Spiral Microchannels," *Lab on a Chip*, vol. 9, pp. 2973-2980, 2009.

[80] J. R. Rettig and A. Folch, "Large-Scale Single-Cell Trapping and Imaging Using Microwell Arrays," *Analytical chemistry*, vol. 77, pp. 5628-5634, 2005.

[81] X. Wang, X. Gou, S. Chen, X. Yan, and D. Sun, "Cell Manipulation Tool with Combined Microwell Array and Optical Tweezers for Cell Isolation and Deposition," *Journal of Micromechanics and Microengineering*, vol. 23, pp. 075006, 2013.

[82] D. Di Carlo, N. Aghdam, and L. P. Lee, "Single-Cell Enzyme Concentrations, Kinetics, and Inhibition Analysis Using High-Density Hydrodynamic Cell Isolation Arrays," *Analytical chemistry*, vol. 78, pp. 4925-4930, 2006.

[83] A. M. Skelley, O. Kirak, H. Suh, R. Jaenisch, and J. Voldman, "Microfluidic Control of Cell Pairing and Fusion," *Nature Methods*, vol. 6, pp. 147-152, 2009.

[84] T. B. Jones, *Electromechanics of Particles*. Cambridge ; New York: Cambridge University Press, 1995.

[85] B. Kirby, "Micro- and Nanoscale Fluid Mechanics Transport in Microfluidic Devices." New York: Cambridge University Press, 2010.

[86] H. A. Pohl, "The Motion and Precipitation of Suspensoids in Divergent Electric Fields," *Journal of Applied Physics*, vol. 22, pp. 869-871, 1951.

[87] M. S. Pommer, Y. Zhang, N. Keerthi, D. Chen, J. A. Thomson, C. D. Meinhart, and H. T. Soh, "Dielectrophoretic Separation of Platelets from Diluted Whole Blood in Microfluidic Channels," *Electrophoresis*, vol. 29, pp. 1213-8, 2008.

[88] X. Y. Hu, P. H. Bessette, J. R. Qian, C. D. Meinhart, P. S. Daugherty, and H. T. Soh, "Marker-Specific Sorting of Rare Cells Using Dielectrophoresis," *Proceedings of the National Academy of Sciences of the United States of America*, vol. 102, pp. 15757-15761, 2005.

[89] F. Petersson, A. Nilsson, C. Holm, H. Jonsson, and T. Laurell, "Separation of Lipids from Blood Utilizing Ultrasonic Standing Waves in Microfluidic Channels," *The Analyst*, vol. 129, pp. 938-943, 2004.

[90] F. Petersson, L. Aberg, A. M. Sward-Nilsson, and T. Laurell, "Free Flow Acoustophoresis: Microfluidic-Based Mode of Particle and Cell Separation," *Analytical chemistry*, vol. 79, pp. 5117-5123, 2007.

[91] F. Petersson, A. Nilsson, C. Holm, H. Jonsson, and T. Laurell, "Continuous Separation of Lipid Particles from Erythrocytes by Means of Laminar Flow and Acoustic Standing Wave Forces," *Lab on a Chip*, vol. 5, pp. 20-22, 2005.

[92] A. Ashkin, "Acceleration and Trapping of Particles by Radiation Pressure," *Physical Review Letters*, vol. 24, pp. 156-&, 1970.

[93] S. Chu, J. E. Bjorkholm, A. Ashkin, and A. Cable, "Experimental-Observation of Optically Trapped Atoms," *Physical Review Letters*, vol. 57, pp. 314-317, 1986.

[94] A. Ashkin, J. M. Dziedzic, and T. Yamane, "Optical Trapping and Manipulation of Single Cells Using Infrared-Laser Beams," *Nature*, vol. 330, pp. 769-771, 1987.

[95] A. Ashkin and J. M. Dziedzic, "Optical Trapping and Manipulation of Viruses and Bacteria," *Science*, vol. 235, pp. 1517-1520, 1987.

[96] K. C. Neuman and S. M. Block, "Optical Trapping," *Review of Scientific Instruments*, vol. 75, pp. 2787-2809, 2004.

[97] M. Werner, F. Merenda, J. Piguet, R. P. Salathe, and H. Vogel, "Microfluidic Array Cytometer Based on Refractive Optical Tweezers for Parallel Trapping, Imaging and Sorting of Individual Cells," *Lab on a Chip*, vol. 11, pp. 2432-2439, 2011.

[98] C. Liberale, G. Cojoc, F. Bragheri, P. Minzioni, G. Perozziello, R. La Rocca, L. Ferrara, V. Rajamanickam, E. Di Fabrizio, and I. Cristiani, "Integrated Microfluidic Device for Single-Cell Trapping and Spectroscopy," *Scientific Reports*, vol. 3, 2013.

[99] B. Landenberger, H. Hofemann, S. Wadle, and A. Rohrbach, "Microfluidic Sorting of Arbitrary Cells with Dynamic Optical Tweezers," *Lab on a Chip*, vol. 12, pp. 3177-3183, 2012.

[100] X. L. Wang, S. X. Chen, M. Kong, Z. K. Wang, K. D. Costa, R. A. Li, and D. Sun, "Enhanced Cell Sorting and Manipulation with Combined Optical Tweezer and Microfluidic Chip Technologies," *Lab on a Chip*, vol. 11, pp. 3656-3662, 2011.

[101] M. M. Wang, E. Tu, D. E. Raymond, J. M. Yang, H. C. Zhang, N. Hagen, B. Dees, E. M. Mercer, A. H. Forster, I. Kariv, P. J. Marchand, and W. F. Butler, "Microfluidic Sorting of Mammalian Cells by Optical Force Switching," *Nature Biotechnology*, vol. 23, pp. 83-87, 2005.

[102] C. Janeway, *Immunobiology : The Immune System in Health and Disease*, 5th ed. New York: Garland Publishing., 2001.

[103] S. I. Fox, *Human Physiology*, 7th ed. Boston: McGraw-Hill, 2002.

[104] D. E. Koshland, "Application of a Theory of Enzyme Specificity to Protein Synthesis," *Proceedings of the National Academy of Sciences of the United States of America*, vol. 44, pp. 98-104, 1958.

[105] E. Pavlovic, A. P. Quist, U. Gelius, and S. Oscarsson, "Surface Functionalization of Silicon Oxide at Room Temperature and Atmospheric Pressure," *Journal of Colloid and Interface Science*, vol. 254, pp. 200-203, 2002.

[106] G. D. Sui, J. Y. Wang, C. C. Lee, W. X. Lu, S. P. Lee, J. V. Leyton, A. M. Wu, and H. R. Tseng, "Solution-Phase Surface Modification in Intact Poly(Dimethylsiloxane) Microfluidic Channels," *Analytical chemistry*, vol. 78, pp. 5543-5551, 2006.

[107] W. J. Han, B. A. Allio, D. G. Foster, and M. R. King, "Nanoparticle Coatings for Enhanced Capture of Flowing Cells in Microtubes," *Acs Nano*, vol. 4, pp. 174-180, 2010.

[108] A. Sin, S. K. Murthy, A. Revzin, R. G. Tompkins, and M. Toner, "Enrichment Using Antibody-Coated Microfluidic Chambers in Shear Flow: Model Mixtures of Human Lymphocytes," *Biotechnology and Bioengineering*, vol. 91, pp. 816-826, 2005.

[109] S. Usami, H. H. Chen, Y. H. Zhao, S. Chien, and R. Skalak, "Design and Construction of a Linear Shear-Stress Flow Chamber," *Annals of Biomedical Engineering*, vol. 21, pp. 77-83, 1993.

[110] S. Nagrath, L. V. Sequist, S. Maheswaran, D. W. Bell, D. Irimia, L. Ulkus, M. R. Smith, E. L. Kwak, S. Digumarthy, A. Muzikansky, P. Ryan, U. J. Balis, R. G. Tompkins, D. A. Haber, and M. Toner, "Isolation of Rare Circulating Tumour Cells in Cancer Patients by Microchip Technology," *Nature*, vol. 450, pp. 1235-9, 2007.

[111] T. H. Nguyen, R. Pei, M. Stojanovic, and Q. Lin, "Demonstration and Characterization of Biomolecular Enrichment on Microfluidic Aptamer-Functionalized Surfaces," *Sensors and actuators. B, Chemical*, vol. 155, pp. 58-66, 2011.

[112] C. Mannironi, A. Di Nardo, P. Fruscoloni, and G. P. Tocchini-Valentini, "In Vitro Selection of Dopamine Rna Ligands," *Biochemistry*, vol. 36, pp. 9726-34, 1997.

[113] T. W. Wiegand, P. B. Williams, S. C. Dreskin, M. H. Jouvin, J. P. Kinet, and D. Tasset, "High-Affinity Oligonucleotide Ligands to Human Ige Inhibit Binding to Fc Epsilon Receptor I," *Journal of Immunology*, vol. 157, pp. 221-230, 1996.

[114] D. Nieuwlandt, M. Wecker, and L. Gold, "In Vitro Selection of Rna Ligands to Substance P," *Biochemistry*, vol. 34, pp. 5651-9, 1995.

[115] A. Geiger, P. Burgstaller, H. vonderEltz, A. Roeder, and M. Famulok, "Rna Aptamers That Bind L-Arginine with Sub-Micromolar Dissociation Constants and High Enantioselectivity," *Nucleic acids research*, vol. 24, pp. 1029-1036, 1996.

[116] K. Harada and A. D. Frankel, "Identification of Two Novel Arginine Binding Dnas," *The EMBO journal*, vol. 14, pp. 5798-811, 1995.

[117] J. K. Herr, J. E. Smith, C. D. Medley, D. H. Shangguan, and W. H. Tan, "Aptamer-Conjugated Nanoparticles for Selective Collection and Detection of Cancer Cells," *Analytical chemistry*, vol. 78, pp. 2918-2924, 2006.

[118] A. Wochner, B. Cech, M. Menger, V. A. Erdmann, and J. Glokler, "Semi-Automated Selection of DNA Aptamers Using Magnetic Particle Handling," *Biotechniques*, vol. 43, pp. 344-+, 2007.

[119] W. James, "Aptamers in the Virologists' Toolkit," *Journal of General Virology*, vol. 88, pp. 351-364, 2007.

[120] S. C. B. Gopinath, "Methods Developed for Selex," *Analytical and Bioanalytical Chemistry*, vol. 387, pp. 171-182, 2007.

[121] H. M. So, D. W. Park, E. K. Jeon, Y. H. Kim, B. S. Kim, C. K. Lee, S. Y. Choi, S. C. Kim, H. Chang, and J. O. Lee, "Detection and Titer Estimation of Escherichia Coli Using Aptamer-Functionalized Single-Walled Carbon-Nanotube Field-Effect Transistors," *Small*, vol. 4, pp. 197-201, 2008.

[122] Z. Tang, D. Shangguan, K. Wang, H. Shi, K. Sefah, P. Mallikratchy, H. W. Chen, Y. Li, and W. Tan, "Selection of Aptamers for Molecular Recognition and Characterization of Cancer Cells," *Analytical chemistry*, vol. 79, pp. 4900-7, 2007.

[123] S. D. Jayasena, "Aptamers: An Emerging Class of Molecules That Rival Antibodies in Diagnostics," *Clinical Chemistry*, vol. 45, pp. 1628-1650, 1999.

[124] M. Cho, Y. Xiao, J. Nie, R. Stewart, A. T. Csordas, S. S. Oh, J. A. Thomson, and H. T. Soh, "Quantitative Selection of DNA Aptamers through Microfluidic Selection and High-Throughput Sequencing," *Proceedings of the National Academy of Sciences of the United States of America*, vol. 107, pp. 15373-15378, 2010.

[125] A. D. Ellington and J. W. Szostak, "In Vitro Selection of Rna Molecules That Bind Specific Ligands," *Nature*, vol. 346, pp. 818-22, 1990.

[126] D. L. Robertson and G. F. Joyce, "Selection in Vitro of an Rna Enzyme That Specifically Cleaves Single-Stranded DNA," *Nature*, vol. 344, pp. 467-8, 1990.

[127] C. Tuerk and L. Gold, "Systematic Evolution of Ligands by Exponential Enrichment: Rna Ligands to Bacteriophage T4 DNA Polymerase," *Science*, vol. 249, pp. 505-10, 1990.

[128] A. E. G. Cass and Y. Y. Zhang, "Nucleic Acid Aptamers: Ideal Reagents for Point-of-Care Diagnostics?," *Faraday Discussions*, vol. 149, pp. 49-61, 2011.

[129] S. D. Mendonsa and M. T. Bowser, "In Vitro Evolution of Functional DNA Using Capillary Electrophoresis," *Journal of the American Chemical Society*, vol. 126, pp. 20-21, 2004.

[130] W. S. Yao, K. Adelman, and J. A. Bruenn, "In Vitro Selection of Packaging Sites in a Double-Stranded Rna Virus," *Journal of Virology*, vol. 71, pp. 2157-2162, 1997.

[131] F. Zhang and D. Anderson, "In Vitro Selection of Bacteriophage Phi 29 Prohead Rna Aptamers for Prohead Binding," *Journal of Biological Chemistry*, vol. 273, pp. 2947-2953, 1998.

[132] R. Y. L. Tsai and R. R. Reed, "Identification of DNA Recognition Sequences and Protein Interaction Domains of the Multiple-Zn-Finger Protein Roaz," *Molecular and Cellular Biology*, vol. 18, pp. 6447-6456, 1998.

[133] R. Stoltenburg, C. Reinemann, and B. Strehlitz, "Selex-a (R)Evolutionary Method to Generate High-Affinity Nucleic Acid Ligands," *Biomolecular Engineering*, vol. 24, pp. 381-403, 2007.

[134] R. K. Mosing and M. T. Bowser, "Microfluidic Selection and Applications of Aptamers," *Journal of Separation Science*, vol. 30, pp. 1420-1426, 2007.

[135] J. C. Cox, P. Rudolph, and A. D. Ellington, "Automated Rna Selection," *Biotechnology Progress*, vol. 14, pp. 845-850, 1998.

[136] J. C. Cox and A. D. Ellington, "Automated Selection of Anti-Protein Aptamers," *Bioorganic & Medicinal Chemistry*, vol. 9, pp. 2525-2531, 2001.

[137] G. Hybarger, J. Bynum, R. F. Williams, J. J. Valdes, and J. P. Chambers, "A Microfluidic Selex Prototype," *Analytical and Bioanalytical Chemistry*, vol. 384, pp. 191-198, 2006.

[138] P. Wilding, M. A. Shoffner, and L. J. Kricka, "Pcr in a Silicon Microstructure," *Clinical Chemistry*, vol. 40, pp. 1815-1818, 1994.

[139] X. H. Lou, J. R. Qian, Y. Xiao, L. Viel, A. E. Gerdon, E. T. Lagally, P. Atzberger, T. M. Tarasow, A. J. Heeger, and H. T. Soh, "Micromagnetic Selection of Aptamers in Microfluidic Channels," *Proceedings of the National Academy of Sciences of the United States of America*, vol. 106, pp. 2989-2994, 2009.

[140] K. M. Ahmad, S. S. Oh, S. Kim, F. M. McClellen, Y. Xiao, and H. T. Soh, "Probing the Limits of Aptamer Affinity with a Microfluidic Selex Platform," *Plos One*, vol. 6, 2011.

[141] S. S. Oh, K. M. Ahmad, M. Cho, S. Kim, Y. Xiao, and H. T. Soh, "Improving Aptamer Selection Efficiency through Volume Dilution, Magnetic Concentration, and Continuous Washing in Microfluidic Channels," *Analytical chemistry*, vol. 83, pp. 6883-6889, 2011.

[142] C. J. Huang, H. I. Lin, S. C. Shiesh, and G. B. Lee, "Integrated Microfluidic System for Rapid Screening of Crp Aptamers Utilizing Systematic Evolution of Ligands by Exponential Enrichment (Selex)," *Biosensors & Bioelectronics*, vol. 25, pp. 1761-1766, 2010.

[143] C. J. Huang, H. I. Lin, S. C. Shiesh, and G. B. Lee, "An Integrated Microfluidic System for Rapid Screening of Alpha-Fetoprotein-Specific Aptamers," *Biosensors & Bioelectronics*, vol. 35, pp. 50-55, 2012.

[144] C. J. Easley, J. M. Karlinsey, J. M. Bienvenue, L. A. Legendre, M. G. Roper, S. H. Feldman, M. A. Hughes, E. L. Hewlett, T. J. Merkel, J. P. Ferrance, and J. P. Landers, "A Fully Integrated Microfluidic Genetic Analysis System with Sample-in-Answer-out Capability," *Proceedings of the National Academy of Sciences of the United States of America*, vol. 103, pp. 19272-19277, 2006.

[145] B. S. Ferguson, S. F. Buchsbaum, J. S. Swensen, K. Hsieh, X. H. Lou, and H. T. Soh, "Integrated Microfluidic Electrochemical DNA Sensor," *Analytical chemistry*, vol. 81, pp. 6503-6508, 2009.

[146] R. H. Liu, J. N. Yang, R. Lenigk, J. Bonanno, and P. Grodzinski, "Self-Contained, Fully Integrated Biochip for Sample Preparation, Polymerase Chain Reaction Amplification, and DNA Microarray Detection," *Analytical chemistry*, vol. 76, pp. 1824-1831, 2004.

[147] J. Zhu, M. Palla, S. Ronca, R. Warpner, J. Ju, and Q. Lin, "A Mems-Based Approach to Detection of Single Nucleotide Polymorphisms for Genetic Disorder Diagnosis," *25th IEEE Int. Conf. Micro Electro Mechanical Systems*, pp. 754-756, Paris, France, 2012.

[148] J. Zhu, M. Palla, S. Ronca, R. Wapner, J. Y. Ju, and Q. Lin, "A Mems-Based Approach to Single Nucleotide Polymorphism Genotyping," *Sensors and Actuators a-Physical*, vol. 195, pp. 175-182, 2013.

[149] R. Redon, S. Ishikawa, K. R. Fitch, L. Feuk, G. H. Perry, T. D. Andrews, H. Fiegler, M. H. Shapero, A. R. Carson, W. Chen, E. K. Cho, S. Dallaire, J. L. Freeman, J. R. Gonzalez, M. Gratacos, J. Huang, D. Kalaitzopoulos, D. Komura, J. R. MacDonald, C. R. Marshall, R. Mei, L. Montgomery, K. Nishimura, K. Okamura, F. Shen, M. J. Somerville, J. Tchinda, A. Valsesia, C. Woodwark, F. Yang, J. Zhang, T. Zerjal, L. Armengol, D. F. Conrad, X. Estivill, C. Tyler-Smith, N. P. Carter, H. Aburatani, C. Lee, K. W. Jones, S. W. Scherer, and M. E. Hurles, "Global Variation in Copy Number in the Human Genome," *Nature*, vol. 444, pp. 444-54, 2006.

[150] J. Perkel, "Snp Genotyping: Six Technologies That Keyed a Revolution," *Nature Methods*, vol. 5, pp. 447-453, 2008.

[151] A. M. Glazier, J. H. Nadeau, and T. J. Aitman, "Finding Genes That Underlie Complex Traits," *Science*, vol. 298, pp. 2345-2349, 2002.

[152] K. G. Becker, K. C. Barnes, T. J. Bright, and S. A. Wang, "The Genetic Association Database," *Nature Genetics*, vol. 36, pp. 431-432, 2004.

[153] F. S. Collins, E. D. Green, A. E. Guttmacher, and M. S. Guyer, "A Vision for the Future of Genomics Research," *Nature*, vol. 422, pp. 835-47, 2003.

[154] K. Offit, "Personalized Medicine: New Genomics, Old Lessons," *Human genetics*, vol. 130, pp. 3-14, 2011.

[155] A. J. F. Griffiths, *An Introduction to Genetic Analysis*, 7th ed. New York: W.H. Freeman, 2000.

[156] G. C. Kennedy, H. Matsuzaki, S. Dong, W. M. Liu, J. Huang, G. Liu, X. Su, M. Cao, W. Chen, J. Zhang, W. Liu, G. Yang, X. Di, T. Ryder, Z. He, U. Surti, M. S. Phillips, M. T. Boyce-Jacino, S. P. Fodor, and K. W. Jones, "Large-Scale Genotyping of Complex DNA," *Nature biotechnology*, vol. 21, pp. 1233-7, 2003.

[157] F. M. De la Vega, K. D. Lazaruk, M. D. Rhodes, and M. H. Wenz, "Assessment of Two Flexible and Compatible Snp Genotyping Platforms: Taqman Snp Genotyping Assays and the Snplex Genotyping System," *Mutation research*, vol. 573, pp. 111-35, 2005.

[158] F. J. Steemers, W. Chang, G. Lee, D. L. Barker, R. Shen, and K. L. Gunderson, "Whole-Genome Genotyping with the Single-Base Extension Assay," *Nature Methods*, vol. 3, pp. 31-3, 2006.

[159] J. Staaf, J. Vallon-Christersson, D. Lindgren, G. Juliusson, R. Rosenquist, M. Hoglund, A. Borg, and M. Ringner, "Normalization of Illumina Infinium Whole-Genome Snp Data Improves Copy Number Estimates and Allelic Intensity Ratios," *Bmc Bioinformatics*, vol. 9, 2008.

[160] J. B. Rampal, *DNA Arrays : Methods and Protocols*. Totowa, NJ: Human Press, 2001.

[161] E. Szantai and A. Guttman, "Genotyping with Microfluidic Devices," *Electrophoresis*, vol. 27, pp. 4896-4903, 2006.

[162] Y. Wang, B. Vaidya, H. D. Farquar, W. Stryjewski, R. P. Hammer, R. L. McCarley, S. A. Soper, Y. W. Cheng, and F. Barany, "Microarrays Assembled in Microfluidic Chips Fabricated from Poly(Methyl Methacrylate) for the Detection of Low-Abundant DNA Mutations," *Analytical Chemistry*, vol. 75, pp. 1130-1140, 2003.

[163] M. Noerholm, H. Bruus, M. H. Jakobsen, P. Telleman, and N. B. Ramsing, "Polymer Microfluidic Chip for Online Monitoring of Microarray Hybridizations," *Lab on a Chip*, vol. 4, pp. 28-37, 2004.

[164] M. Bowden, L. N. Song, and D. R. Walt, "Development of a Microfluidic Platform with an Optical Imaging Microarray Capable of Attomolar Target DNA Detection," *Analytical Chemistry*, vol. 77, pp. 5583-5588, 2005.

[165] Y. C. Chung, Y. C. Lin, C. D. Chueh, C. Y. Ye, L. W. Lai, and Q. Zhao, "Microfluidic Chip of Fast DNA Hybridization Using Denaturing and Motion of Nucleic Acids," *Electrophoresis*, vol. 29, pp. 1859-1865, 2008.

[166] A. Russom, N. Tooke, H. Andersson, and G. Stemme, "Single Nucleotide Polymorphism Analysis by Allele-Specific Primer Extension with Real-Time Bioluminescence Detection in a Microfluidic Device," *Journal of Chromatography A*, vol. 1014, pp. 37-45, 2003.

[167] W. Pusch, J. H. Wurmbach, H. Thiele, and M. Kostrzewa, "Maldi-Tof Mass Spectrometry-Based Snp Genotyping," *Pharmacogenomics*, vol. 3, pp. 537-548, 2002.

[168] S. Kim, H. D. Ruparel, T. C. Gilliam, and J. Y. Ju, "Digital Genotyping Using Molecular Affinity and Mass Spectrometry," *Nature Reviews Genetics*, vol. 4, pp. 1001-1008, 2003.

[169] S. Kim, J. R. Edwards, L. Y. Deng, W. Chung, and J. Y. Ju, "Solid Phase Capturable Dideoxynucleotides for Multiplex Genotyping Using Mass Spectrometry," *Nucleic acids research*, vol. 30, 2002.

[170] L. P. Scheunemann and K. I. Ataga, "Delayed Hemolytic Transfusion Reaction in Sickle Cell Disease," *American Journal of the Medical Sciences*, vol. 339, pp. 266-269, 2010.

[171] Y. S. Shin, K. Cho, S. H. Lim, S. Chung, S. J. Park, C. Chung, D. C. Han, and J. K. Chang, "Pdms-Based Micro Pcr Chip with Parylene Coating," *Journal of Micromechanics and Microengineering*, vol. 13, pp. 768-774, 2003.

[172] J. P. Hilton, T. H. Nguyen, M. Barbu, R. Pei, M. Stojanovic, and Q. Lin, "Pathogen Detection Using Microfluidic Bead-Based Polymerase Chain Reaction," *16th International Conference on Solid-State Sensors, Actuators and Microsystems*, pp. 190-193, Beijing, China, 2011.

[173] J. Zhu, C. Qiu, M. Palla, T. Nguyen, J. Ju, and Q. Lin, "A Microfluidic Device for Detection of Single Nucleotide Polymorphisms by Allele Specific Single Base

Extension," *Int. Conf. on Miniaturized Systems for Chemistry and Life Sciences (MicroTAS '11)*, pp. 1442-1444, Seattle, WA, 2011.

[174] J. Zhu, C. Qiu, M. Palla, T. Nguyen, J. Russo, J. Ju, and Q. Lin, "A Microfluidic Device for Multiplex Single-Nucleotide Polymorphism Genotyping," *RSC Advances*, vol. 4, pp. 4269-4277, 2014.

[175] G. Bollag, P. Hirth, J. Tsai, J. Zhang, P. N. Ibrahim, H. Cho, W. Spevak, C. Zhang, Y. Zhang, G. Habets, E. A. Burton, B. Wong, G. Tsang, B. L. West, B. Powell, R. Shellooe, A. Marimuthu, H. Nguyen, K. Y. Zhang, D. R. Artis, J. Schlessinger, F. Su, B. Higgins, R. Iyer, K. D'Andrea, A. Koehler, M. Stumm, P. S. Lin, R. J. Lee, J. Grippo, I. Puzanov, K. B. Kim, A. Ribas, G. A. McArthur, J. A. Sosman, P. B. Chapman, K. T. Flaherty, X. Xu, K. L. Nathanson, and K. Nolop, "Clinical Efficacy of a Raf Inhibitor Needs Broad Target Blockade in Braf-Mutant Melanoma," *Nature*, vol. 467, pp. 596-9, 2010.

[176] P. T. C. Wan, M. J. Garnett, S. M. Roe, S. Lee, D. Niculescu-Duvaz, V. M. Good, C. G. Project, C. M. Jones, C. J. Marshall, C. J. Springer, D. Barford, and R. Marais, "Mechanism of Activation of the Raf-Erk Signaling Pathway by Oncogenic Mutations of B-Raf," *Cell*, vol. 116, pp. 855-867, 2004.

[177] R. Kudchadkar, K. H. Paraiso, and K. S. Smalley, "Targeting Mutant Braf in Melanoma: Current Status and Future Development of Combination Therapy Strategies," *Cancer journal*, vol. 18, pp. 124-31, 2012.

[178] D. Schleinitz, J. K. Distefano, and P. Kovacs, "Targeted Snp Genotyping Using the Taqman(R) Assay," *Methods in molecular biology*, vol. 700, pp. 77-87, 2011.

[179] R. Palacios, D. Comas, J. Elorza, and P. Villoslada, "Genomic Regulation of Ctla4 and Multiple Sclerosis," *Journal of neuroimmunology*, vol. 203, pp. 108-15, 2008.

[180] Y. Zhang and P. Ozdemir, "Microfluidic DNA Amplification--a Review," *Analytica chimica acta*, vol. 638, pp. 115-25, 2009.

[181] N. Beyor, L. Yi, T. S. Seo, and R. A. Mathies, "Integrated Capture, Concentration, Polymerase Chain Reaction, and Capillary Electrophoretic Analysis of Pathogens on a Chip," *Analytical chemistry*, vol. 81, pp. 3523-8, 2009.

[182] R. H. Liu, M. J. Lodes, T. Nguyen, T. Siuda, M. Slota, H. S. Fuji, and A. McShea, "Validation of a Fully Integrated Microfluidic Array Device for Influenza a Subtype Identification and Sequencing," *Analytical chemistry*, vol. 78, pp. 4184-93, 2006.

[183] J. K. K. Ng, H. H. Feng, and W. T. Liu, "Rapid Discrimination of Single-Nucleotide Mismatches Using a Microfluidic Device with Monolayered Beads," *Analytica chimica acta*, vol. 582, pp. 295-303, 2007.

[184] R. D. Sochol, B. P. Casavant, M. E. Dueck, L. P. Lee, and L. Lin, "A Dynamic Bead-Based Microarray for Parallel DNA Detection," *Journal of Micromechanics and Microengineering*, vol. 21, 2011.

[185] J. Chowdhury, G. V. Kagiala, S. Pushpakom, J. Lauzon, A. Makin, A. Atrazhev, A. Stickel, W. G. Newman, C. J. Backhouse, and L. M. Pilarski, "Microfluidic Platform for Single Nucleotide Polymorphism Genotyping of the Thiopurine S-Methyltransferase Gene to Evaluate Risk for Adverse Drug Events," *The Journal of molecular diagnostics : JMD*, vol. 9, pp. 521-9, 2007.

[186] J. Wang, M. Lin, A. Crenshaw, A. Hutchinson, B. Hicks, M. Yeager, S. Berndt, W. Y. Huang, R. B. Hayes, S. J. Chanock, R. C. Jones, and R. Ramakrishnan, "High-Throughput Single Nucleotide Polymorphism Genotyping Using Nanofluidic Dynamic Arrays," *BMC genomics*, vol. 10, pp. 561, 2009.

[187] M. Chan, M. W. Chan, T. W. Loh, H. Y. Law, C. S. Yoon, S. S. Than, J. M. Chua, C. Y. Wong, W. S. Yong, Y. S. Yap, G. H. Ho, P. Ang, and A. S. Lee, "Evaluation of Nanofluidics Technology for High-Throughput Snp Genotyping in a Clinical Setting," *The Journal of molecular diagnostics : JMD*, vol. 13, pp. 305-12, 2011.

[188] Y. He, J. Wu, D. C. Dressman, C. Iacobuzio-Donahue, S. D. Markowitz, V. E. Velculescu, L. A. Diaz, Jr., K. W. Kinzler, B. Vogelstein, and N. Papadopoulos, "Heteroplasmic Mitochondrial DNA Mutations in Normal and Tumour Cells," *Nature*, vol. 464, pp. 610-4, 2010.

[189] M. Gundry and J. Vijg, "Direct Mutation Analysis by High-Throughput Sequencing: From Germline to Low-Abundant, Somatic Variants," *Mutation Research-Fundamental and Molecular Mechanisms of Mutagenesis*, vol. 729, pp. 1-15, 2012.

[190] S. Gabriel, L. Ziaugra, and D. Tabbaa, "Snp Genotyping Using the Sequenom Massarray Iplex Platform," *Current protocols in human genetics / editorial board, Jonathan L. Haines ... [et al.]*, vol. Chapter 2, pp. Unit 2 12, 2009.

[191] C. Qiu, S. Kumar, J. Guo, L. Yu, W. Guo, S. Shi, J. J. Russo, and J. Ju, "Design and Synthesis of Cleavable Biotinylated Dideoxynucleotides for DNA Sequencing by Matrix-Assisted Laser Desorption/Ionization Time-of-Flight Mass Spectrometry," *Analytical biochemistry*, vol. 427, pp. 193-201, 2012.

[192] M. A. Unger, H. P. Chou, T. Thorsen, A. Scherer, and S. R. Quake, "Monolithic Microfabricated Valves and Pumps by Multilayer Soft Lithography," *Science*, vol. 288, pp. 113-116, 2000.

[193] M. Gonzalez, L. A. Bagatolli, I. Echabe, J. L. Arrondo, C. E. Argarana, C. R. Cantor, and G. D. Fidelio, "Interaction of Biotin with Streptavidin. Thermostability and Conformational Changes Upon Binding," *J Biol Chem*, vol. 272, pp. 11288-94, 1997.

[194] C. Qiu, S. Kumar, J. Guo, J. Lu, S. Shi, S. M. Kalachikov, J. J. Russo, A. B. Naini, E. A. Schon, and J. Ju, "Mitochondrial Single Nucleotide Polymorphism Genotyping by Matrix-Assisted Laser Desorption/Ionization Time-of-Flight Mass Spectrometry Using Cleavable Biotinylated Dideoxynucleotides," *Analytical biochemistry*, vol. 427, pp. 202-10, 2012.

[195] M. G. Pluskal, "Microscale Sample Preparation," *Nature biotechnology*, vol. 18, pp. 104-5, 2000.

[196] C. E. C. A. Hop and R. Bakhtiar, "An Introduction to Electrospray Ionization and Matrix-Assisted Laser Desorption/Ionization Mass Spectrometry: Essential Tools in a Modern Biotechnology Environment," *Biospectroscopy*, vol. 3, pp. 259-280, 1997.

[197] J. White, "A Cfd Simulation on How the Different Sizes of Silica Gel Will Affect the Adsorption Performance of Silica Gel," *Model. Simulat. Eng.*, vol. 2012, pp. Article ID 651434, 2012.

[198] T. Nguyen, R. Pei, M. Stojanovic, and Q. Lin, "An Aptamer-Based Microfluidic Device for Thermally Controlled Affinity Extraction," *Microfluidics and Nanofluidics*, vol. 6, pp. 479-487, 2009.

[199] J. Zhu, T. Nguyen, R. Pei, M. Stojanovic, and Q. Lin, "Specific Capture and Temperature Mediated Release of Cells Using Aptamer-Functionalized Microfluidic Surfaces," in *IEEE Int. Conf. Solid-State Sensors, Actuators and Microsystems (Transducers '11)*. Beijing, China, 2011, pp. 751-754.

[200] J. Zhu, T. Nguyen, R. Pei, M. Stojanovic, and Q. Lin, "Reusable Microfluidic Chip for Cell Capture and Release Using Surface-Immobilized Aptamer," in *Int. Conf. on Miniaturized Chemical and Biochemical Analysis Systems (MicroTAS '10)*. Groningen, the Netherlands, 2010, pp. 920-922.

[201] J. Zhu, T. Nguyen, R. Pei, M. Stojanovic, and Q. Lin, "Specific Capture and Temperature-Mediated Release of Cells in an Aptamer-Based Microfluidic Device," *Lab on a chip*, vol. 12, pp. 3504-13, 2012.

[202] S. K. Murthy, A. Sin, R. G. Tompkins, and M. Toner, "Effect of Flow and Surface Conditions on Human Lymphocyte Isolation Using Microfluidic Chambers," *Langmuir*, vol. 20, pp. 11649-11655, 2004.

[203] P. Bianco and P. G. Robey, "Stem Cells in Tissue Engineering," *Nature*, vol. 414, pp. 118-21, 2001.

[204] E. Gomez-Barrena, P. Rosset, I. Muller, R. Giordano, C. Bunu, P. Layrolle, Y. T. Konttinen, and F. P. Luyten, "Bone Regeneration: Stem Cell Therapies and Clinical Studies in Orthopaedics and Traumatology," *Journal of cellular and molecular medicine*, 2011.

[205] D. S. Kompala and P. Todd, *Cell Separation Science and Technology*. Washington, DC: American Chemical Society, 1991.

[206] A. Kumar and A. Bhardwaj, "Methods in Cell Separation for Biomedical Application: Cryogels as a New Tool," *Biomedical Materials*, vol. 3, pp. 034008, 2008.

[207] S. V. Hunt, *Cell Separation Techniques Used in Immunology*: John Wiley & Sons, Ltd, 2001.

[208] J. D. Adams, U. Kim, and H. T. Soh, "Multitarget Magnetic Activated Cell Sorter," *Proceedings of the National Academy of Sciences of the United States of America*, vol. 105, pp. 18165-70, 2008.

[209] A. A. S. Bhagat, H. Bow, H. W. Hou, S. J. Tan, J. Han, and C. T. Lim, "Microfluidics for Cell Separation," *Medical & Biological Engineering & Computing*, vol. 48, pp. 999-1014, 2010.

[210] E. Chmela, R. Tijssen, M. T. Blom, H. J. Gardeniers, and A. van den Berg, "A Chip System for Size Separation of Macromolecules and Particles by Hydrodynamic Chromatography," *Analytical chemistry*, vol. 74, pp. 3470-5, 2002.

[211] Y. Huang, S. Joo, M. Duhon, M. Heller, B. Wallace, and X. Xu, "Dielectrophoretic Cell Separation and Gene Expression Profiling on Microelectronic Chip Arrays," *Analytical Chemistry*, vol. 74, pp. 3362-71, 2002.

[212] Z. Du, K. H. Cheng, M. W. Vaughn, N. L. Collie, and L. S. Gollahon, "Recognition and Capture of Breast Cancer Cells Using an Antibody-Based Platform in a Microelectromechanical Systems Device," *Biomedical Microdevices*, vol. 9, pp. 35-42, 2007.

[213] A. Hatch, G. Hansmann, and S. K. Murthy, "Engineered Alginate Hydrogels for Effective Microfluidic Capture and Release of Endothelial Progenitor Cells from

Whole Blood," *Langmuir : the ACS journal of surfaces and colloids*, vol. 27, pp. 4257-64, 2011.

[214] M. Stenberg and H. Nygren, "Kinetics of Antigen-Antibody Reactions at Solid-Liquid Interfaces," *Journal of Immunological Methods*, vol. 113, pp. 3-15, 1988.

[215] S. E. Lupold, B. J. Hicke, Y. Lin, and D. S. Coffey, "Identification and Characterization of Nuclease-Stabilized Rna Molecules That Bind Human Prostate Cancer Cells Via the Prostate-Specific Membrane Antigen," *Cancer Res*, vol. 62, pp. 4029-33, 2002.

[216] D. Shangguan, Y. Li, Z. Tang, Z. C. Cao, H. W. Chen, P. Mallikaratchy, K. Sefah, C. J. Yang, and W. Tan, "Aptamers Evolved from Live Cells as Effective Molecular Probes for Cancer Study," *Proc Natl Acad Sci U S A*, vol. 103, pp. 11838-43, 2006.

[217] D. Shangguan, L. Meng, Z. C. Cao, Z. Xiao, X. Fang, Y. Li, D. Cardona, R. P. Witek, C. Liu, and W. Tan, "Identification of Liver Cancer-Specific Aptamers Using Whole Live Cells," *Anal Chem*, vol. 80, pp. 721-8, 2008.

[218] K. T. Guo, R. Schafer, A. Paul, G. Ziemer, and H. P. Wendel, "Aptamer-Based Strategies for Stem Cell Research," *Mini Rev Med Chem*, vol. 7, pp. 701-5, 2007.

[219] D. Shangguan, Z. C. Cao, Y. Li, and W. Tan, "Aptamers Evolved from Cultured Cancer Cells Reveal Molecular Differences of Cancer Cells in Patient Samples," *Clin Chem*, vol. 53, pp. 1153-5, 2007.

[220] D. Shangguan, Z. Tang, P. Mallikaratchy, Z. Xiao, and W. Tan, "Optimization and Modifications of Aptamers Selected from Live Cancer Cell Lines," *Chembiochem : a European journal of chemical biology*, vol. 8, pp. 603-6, 2007.

[221] P. R. Bouchard, R. M. Hutabarat, and K. M. Thompson, "Discovery and Development of Therapeutic Aptamers," *Annual review of pharmacology and toxicology*, vol. 50, pp. 237-57, 2010.

[222] J. A. Phillips, Y. Xu, Z. Xia, Z. H. Fan, and W. H. Tan, "Enrichment of Cancer Cells Using Aptamers Immobilized on a Microfluidic Channel," *Analytical Chemistry*, vol. 81, pp. 1033-1039, 2009.

[223] Y. Xu, J. A. Phillips, J. Yan, Q. Li, Z. H. Fan, and W. Tan, "Aptamer-Based Microfluidic Device for Enrichment, Sorting, and Detection of Multiple Cancer Cells," *Anal Chem*, vol. 81, pp. 7436-42, 2009.

[224] O. C. Farokhzad, A. Khademhosseini, S. Jon, A. Hermmann, J. Cheng, C. Chin, A. Kiselyuk, B. Teply, G. Eng, and R. Langer, "Microfluidic System for Studying the

Interaction of Nanoparticles and Microparticles with Cells," *Anal Chem*, vol. 77, pp. 5453-9, 2005.

[225] U. Dharmasiri, S. Balamurugan, A. A. Adams, P. I. Okagbare, A. Obubuafo, and S. A. Soper, "Highly Efficient Capture and Enumeration of Low Abundance Prostate Cancer Cells Using Prostate-Specific Membrane Antigen Aptamers Immobilized to a Polymeric Microfluidic Device," *Electrophoresis*, vol. 30, pp. 3289-300, 2009.

[226] L. Chen, X. Liu, B. Su, J. Li, L. Jiang, D. Han, and S. Wang, "Aptamer-Mediated Efficient Capture and Release of T Lymphocytes on Nanostructured Surfaces," *Advanced materials*, vol. 23, pp. 4376-80, 2011.

[227] H. Baumann and D. Doyle, "Effect of Trypsin on the Cell Surface Proteins of Hepatoma Tissue Culture Cells. Characterization of a Carbohydrate-Rich Glycopeptide Released from a Calcium Binding Membrane Glycoprotein," *J Biol Chem*, vol. 254, pp. 3935-46, 1979.

[228] K. Jung, G. Hampel, M. Scholz, and W. Henke, "Culture of Human Kidney Proximal Tubular Cells - the Effect of Various Detachment Procedures on Viability and Degree of Cell Detachment," *Cellular Physiology and Biochemistry*, vol. 5, pp. 353-360, 1995.

[229] N. Fujioka, Y. Morimoto, K. Takeuchi, M. Yoshioka, and M. Kikuchi, "Difference in Infrared Spectra from Cultured Cells Dependent on Cell-Harvesting Method," *Applied Spectroscopy*, vol. 57, pp. 241-243, 2003.

[230] T. Nguyen, R. J. Pei, D. W. Landry, M. N. Stojanovic, and Q. Lin, "Microfluidic Aptameric Affinity Sensing of Vasopressin for Clinical Diagnostic and Therapeutic Applications," *Sensors and Actuators B-Chemical*, vol. 154, pp. 59-66, 2011.

[231] J. P. Hilton, T. H. Nguyen, R. J. Pei, M. Stojanovic, and Q. Lin, "A Microfluidic Affinity Sensor for the Detection of Cocaine," *Sensors and Actuators a-Physical*, vol. 166, pp. 241-246, 2011.

[232] A. Shah and M. P. Coleman, "Increasing Incidence of Childhood Leukaemia: A Controversy Re-Examined," *British journal of cancer*, vol. 97, pp. 1009-12, 2007.

[233] D. Parkin, E. Kramárová, G. Draper, E. Masuyer, J. Michaelis, J. Neglia, S. Qureshi, and S. CA., Eds., *International Incidence of Childhood Cancer, Vol. Ii (Iarc Scientific Publication, No 144)*. Lyon, International Agency for Research on Cancer, 1998.

[234] Y. Chen, M. B. O'Donoghue, Y. F. Huang, H. Kang, J. A. Phillips, X. Chen, M. C. Estevez, C. J. Yang, and W. Tan, "A Surface Energy Transfer Nanoruler for

Measuring Binding Site Distances on Live Cell Surfaces," *J Am Chem Soc*, vol. 132, pp. 16559-70, 2010.

[235] Q. Lin, F. K. Jiang, X. Q. Wang, Y. Xu, Z. G. Han, Y. C. Tai, J. Lew, and C. M. Ho, "Experiments and Simulations of Mems Thermal Sensors for Wall Shear-Stress Measurements in Aerodynamic Control Applications," *Journal of Micromechanics and Microengineering*, vol. 14, pp. 1640-1649, 2004.

[236] G. Crescenzo, C. Boucher, Y. Durocher, and M. Jolicoeur, "Kinetic Characterization by Surface Plasmon Resonance-Based Biosensors: Principle and Emerging Trends," in *Cellular and molecular bioengineering*, vol. 1. New York: Springer, 2008, pp. 204-215.

[237] M. N. Dickson, P. Tsinberg, Z. L. Tang, F. Z. Bischoff, T. Wilson, and E. F. Leonard, "Efficient Capture of Circulating Tumor Cells with a Novel Immunocytochemical Microfluidic Device," *Biomicrofluidics*, vol. 5, 2011.

[238] R. H. Perry, D. W. Green, and Knovel (Firm), "Perry's Chemical Engineers' Handbook," 8th ed. New York: McGraw-Hill, 2008.

[239] R. F. Hoernlein, T. Orlikowsky, C. Zehrer, D. Niethammer, E. R. Sailer, T. Simmet, G. E. Dannecker, and H. P. Ammon, "Acetyl-11-Keto-Beta-Boswellic Acid Induces Apoptosis in Hl-60 and Ccrf-Cem Cells and Inhibits Topoisomerase I," *J Pharmacol Exp Ther*, vol. 288, pp. 613-9, 1999.

[240] C. B. Avci, C. Gunduz, Y. Baran, F. Sahin, S. Yilmaz, Z. O. Dogan, and G. Saydam, "Caffeic Acid Phenethyl Ester Triggers Apoptosis through Induction of Loss of Mitochondrial Membrane Potential in Ccrf-Cem Cells," *Journal of Cancer Research and Clinical Oncology*, vol. 137, pp. 41-47, 2011.

[241] L. Lossi, S. Alasia, C. Salio, and A. Merighi, "Cell Death and Proliferation in Acute Slices and Organotypic Cultures of Mammalian Cns," *Prog Neurobiol*, vol. 88, pp. 221-45, 2009.

[242] J. P. Mather and P. E. Roberts, *Introduction to Cell and Tissue Culture : Theory and Technique*. New York: Plenum Press, 1998.

[243] J. Zhu, J. Shang, Y. Jia, K. Liu, D. Brenner, and Q. Lin, "Physical Modulation Based Cell Manipulation in Microfluidic Devices," in *IEEE Int. Conf. on Nano/Micro Engineered and Molecular Systems (NEMS '13)*. Suzhou, China, 2013, pp. 1226-1229.

[244] J. Zhu, J. Shang, Y. Jia, R. Pei, M. Stojanovic, and Q. Lin, "Spatially Selective Release of Aptamer-Captured Cells by Temperature Mediation," *IET Nanobiotechnology*, doi: 10.1049/iet-nbt.2013.0028.

[245] S. Hou, H. C. Zhao, L. B. Zhao, Q. L. Shen, K. S. Wei, D. Y. Suh, A. Nakao, M. A. Garcia, M. Song, T. Lee, B. Xiong, S. C. Luo, H. R. Tseng, and H. H. Yu, "Capture and Stimulated Release of Circulating Tumor Cells on Polymer-Grafted Silicon Nanostructures," *Advanced Materials*, vol. 25, pp. 1547-1551, 2013.

[246] A. A. Adams, P. I. Okagbare, J. Feng, M. L. Hupert, D. Patterson, J. Gottert, R. L. McCarley, D. Nikitopoulos, M. C. Murphy, and S. A. Soper, "Highly Efficient Circulating Tumor Cell Isolation from Whole Blood and Label-Free Enumeration Using Polymer-Based Microfluidics with an Integrated Conductivity Sensor," *Journal of the American Chemical Society*, vol. 130, pp. 8633-41, 2008.

[247] H. L. Liu, X. L. Liu, J. X. Meng, P. C. Zhang, G. Yang, B. Su, K. Sun, L. Chen, D. Han, S. T. Wang, and L. Jiang, "Hydrophobic Interaction-Mediated Capture and Release of Cancer Cells on Thermoresponsive Nanostructured Surfaces," *Advanced Materials*, vol. 25, pp. 922-927, 2013.

[248] P. Parekh, J. Martin, Y. Chen, D. Colon, H. Wang, and W. Tan, "Using Aptamers to Study Protein-Protein Interactions," *Advances in biochemical engineering/biotechnology*, vol. 110, pp. 177-94, 2008.

[249] V. J. Ruigrok, M. Levisson, J. Hekelaar, H. Smidt, B. W. Dijkstra, and J. van der Oost, "Characterization of Aptamer-Protein Complexes by X-Ray Crystallography and Alternative Approaches," *International journal of molecular sciences*, vol. 13, pp. 10537-52, 2012.

[250] J. P. Hilton, J. Kim, T. Nguyen, M. Barbu, R. Pei, M. Stojanovic, and Q. Lin, "Isolation of Thermally Sensitive Aptamers on a Microchip," *IEEE Int. Conf. Micro Electro Mechanical Systems (MEMS '12)* pp. 100-103, Paris, France, 2012.

[251] J. Zhu, J. Shang, D. Brenner, and Q. Lin, "An Elastomeric Polymer Microchip for Mechanically Tunable Cell Trapping," *The 26th IEEE International Conference on Micro Electro Mechanical Systems (MEMS '13)*, pp. 945-948, Taipei, Taiwan, 2013.

[252] J. Zhu, J. Shang, T. Olsen, K. Liu, D. Brenner, and Q. Lin, "A Mechanically Tunable Microfluidic Cell-Trapping Device," *Sensor Actuat A-Phys*, doi: 10.1016/j.sna.2013.10.016.

[253] B. Desoize and J. Jardillier, "Multicellular Resistance: A Paradigm for Clinical Resistance?," *Critical reviews in oncology/hematology*, vol. 36, pp. 193-207, 2000.

[254] C. V. Rao, D. M. Wolf, and A. P. Arkin, "Control, Exploitation and Tolerance of Intracellular Noise," *Nature*, vol. 420, pp. 231-7, 2002.

[255] D. G. Spiller, C. D. Wood, D. A. Rand, and M. R. White, "Measurement of Single-Cell Dynamics," *Nature*, vol. 465, pp. 736-45, 2010.

[256] S. V. Avery, "Microbial Cell Individuality and the Underlying Sources of Heterogeneity," *Nature reviews. Microbiology*, vol. 4, pp. 577-87, 2006.

[257] C. J. Wei, X. Xu, and C. W. Lo, "Connexins and Cell Signaling in Development and Disease," *Annual review of cell and developmental biology*, vol. 20, pp. 811-38, 2004.

[258] J. P. Himanen and D. B. Nikolov, "Eph Signaling: A Structural View," *Trends in neurosciences*, vol. 26, pp. 46-51, 2003.

[259] S. Lindstrom and H. Andersson-Svahn, "Overview of Single-Cell Analyses: Microdevices and Applications," *Lab on a chip*, vol. 10, pp. 3363-72, 2010.

[260] J. Nilsson, M. Evander, B. Hammarstrom, and T. Laurell, "Review of Cell and Particle Trapping in Microfluidic Systems," *Analytica chimica acta*, vol. 649, pp. 141-57, 2009.

[261] L. C. Taylor and D. R. Walt, "Application of High-Density Optical Microwell Arrays in a Live-Cell Biosensing System," *Analytical biochemistry*, vol. 278, pp. 132-42, 2000.

[262] J. P. Frimat, M. Becker, Y. Y. Chiang, U. Marggraf, D. Janasek, J. G. Hengstler, J. Franzke, and J. West, "A Microfluidic Array with Cellular Valving for Single Cell Co-Culture," *Lab on a chip*, vol. 11, pp. 231-237, 2011.

[263] R. D. Sochol, M. E. Dueck, S. Li, L. P. Lee, and L. W. Lin, "Hydrodynamic Resettability for a Microfluidic Particulate-Based Arraying System," *Lab on a chip*, vol. 12, pp. 5051-5056, 2012.

[264] A. Revzin, P. Rajagopalan, A. W. Tilles, F. Berthiaume, M. L. Yarmush, and M. Toner, "Designing a Hepatocellular Microenvironment with Protein Microarraying and Poly(Ethylene Glycol) Photolithography," *Langmuir : the ACS journal of surfaces and colloids*, vol. 20, pp. 2999-3005, 2004.

[265] N. Li and C. M. Ho, "Photolithographic Patterning of Organosilane Monolayer for Generating Large Area Two-Dimensional B Lymphocyte Arrays," *Lab on a chip*, vol. 8, pp. 2105-12, 2008.

[266] J. Y. Lee, C. Jones, M. A. Zern, and A. Revzin, "Analysis of Local Tissue-Specific Gene Expression in Cellular Micropatterns," *Analytical Chemistry*, vol. 78, pp. 8305-12, 2006.

[267] D. Wlodkowic, S. Faley, M. Zagnoni, J. P. Wikswo, and J. M. Cooper, "Microfluidic Single-Cell Array Cytometry for the Analysis of Tumor Apoptosis," *Analytical Chemistry*, vol. 81, pp. 5517-23, 2009.

[268] L. Y. Wu, D. Di Carlo, and L. P. Lee, "Microfluidic Self-Assembly of Tumor Spheroids for Anticancer Drug Discovery," *Biomedical microdevices*, vol. 10, pp. 197-202, 2008.

[269] J. E. Molloy and M. J. Padgett, "Lights, Action: Optical Tweezers," *Contemporary Physics*, vol. 43, pp. 241-258, 2002.

[270] T. Tonooka, T. Teshima, and S. Takeuchi, "Clustering Triple Microbeads in a Dynamic Microarray for Timing-Controllable Bead-Based Reactions," *Microfluidics and Nanofluidics*, vol. 14, pp. 1039-1048, 2013.

[271] W. H. Tan and S. Takeuchi, "A Trap-and-Release Integrated Microfluidic System for Dynamic Microarray Applications," *Proceedings of the National Academy of Sciences of the United States of America*, vol. 104, pp. 1146-1151, 2007.

[272] B. Z. Yang and Q. Lin, "A Planar Compliance-Based Self-Adaptive Microfluid Variable Resistor," *Journal of Microelectromechanical Systems*, vol. 16, pp. 411-419, 2007.

[273] D. Huh, K. L. Mills, X. Y. Zhu, M. A. Burns, M. D. Thouless, and S. Takayama, "Tuneable Elastomeric Nanochannels for Nanofluidic Manipulation," *Nature Materials*, vol. 6, pp. 424-428, 2007.

[274] W. Liu, L. Li, J. C. Wang, Q. Tu, L. Ren, Y. Wang, and J. Wang, "Dynamic Trapping and High-Throughput Patterning of Cells Using Pneumatic Microstructures in an Integrated Microfluidic Device," *Lab on a chip*, vol. 12, pp. 1702-9, 2012.

[275] E. M. Arruda and M. C. Boyce, "A 3-Dimensional Constitutive Model for the Large Stretch Behavior of Rubber Elastic-Materials," *Journal of the Mechanics and Physics of Solids*, vol. 41, pp. 389-412, 1993.

[276] T. K. Kim, J. K. Kim, and O. C. Jeong, "Measurement of Nonlinear Mechanical Properties of Pdms Elastomer," *Microelectronic Engineering*, vol. 88, pp. 1982-1985, 2011.

[277] M. Liu and Q. F. Chen, "Characterization Study of Bonded and Unbonded Polydimethylsiloxane Aimed for Bio-Micro-Electromechanical Systems-Related Applications," *Journal of Micro-Nanolithography MEMS and Moems*, vol. 6, 2007.

[278] J. Zhu, T. Olsen, R. Pei, M. Stojanovic, and Q. Lin, "A Microfluidic Device for Isolation of Cell-Targeting Aptamers," *The 27th IEEE International Conference on Micro Electro Mechanical Systems (MEMS '14)*, pp. 242-245, San Francisco, CA, 2014.

[279] M. Rajendran and A. D. Ellington, "Selection of Fluorescent Aptamer Beacons That Light up in the Presence of Zinc," *Analytical and bioanalytical chemistry*, vol. 390, pp. 1067-75, 2008.

[280] H. P. Hofmann, S. Limmer, V. Hornung, and M. Sprinzl, "Ni2+-Binding Rna Motifs with an Asymmetric Purine-Rich Internal Loop and a G-a Base Pair," *RNA*, vol. 3, pp. 1289-300, 1997.

[281] E. N. Brody and L. Gold, "Aptamers as Therapeutic and Diagnostic Agents," *Journal of biotechnology*, vol. 74, pp. 5-13, 2000.

[282] E. Gilboa, J. McNamara, 2nd, and F. Pastor, "Use of Oligonucleotide Aptamer Ligands to Modulate the Function of Immune Receptors," *Clinical cancer research : an official journal of the American Association for Cancer Research*, vol. 19, pp. 1054-62, 2013.

[283] C. Ravelet, C. Grosset, and E. Peyrin, "Liquid Chromatography, Electrochromatography and Capillary Electrophoresis Applications of DNA and Rna Aptamers," *Journal of chromatography. A*, vol. 1117, pp. 1-10, 2006.

[284] E. N. Brody, M. C. Willis, J. D. Smith, S. Jayasena, D. Zichi, and L. Gold, "The Use of Aptamers in Large Arrays for Molecular Diagnostics," *Molecular diagnosis : a journal devoted to the understanding of human disease through the clinical application of molecular biology*, vol. 4, pp. 381-8, 1999.

[285] S. M. Nimjee, C. P. Rusconi, and B. A. Sullenger, "Aptamers: An Emerging Class of Therapeutics," *Annual Review of Medicine*, vol. 56, pp. 555-583, 2005.

[286] H. J. Lee, A. W. Wark, and R. M. Corn, "Microarray Methods for Protein Biomarker Detection," *The Analyst*, vol. 133, pp. 975-83, 2008.

[287] S. Fredriksson, J. Horecka, O. T. Brustugun, J. Schlingemann, A. C. Koong, R. Tibshirani, and R. W. Davis, "Multiplexed Proximity Ligation Assays to Profile Putative Plasma Biomarkers Relevant to Pancreatic and Ovarian Cancer," *Clinical chemistry*, vol. 54, pp. 582-9, 2008.

[288] R. Chen, S. Pan, E. C. Yi, S. Donohoe, M. P. Bronner, J. D. Potter, D. R. Goodlett, R. Aebersold, and T. A. Brentnall, "Quantitative Proteomic Profiling of Pancreatic Cancer Juice," *Proteomics*, vol. 6, pp. 3871-9, 2006.

[289] S. Nishizuka, "Profiling Cancer Stem Cells Using Protein Array Technology," *European journal of cancer*, vol. 42, pp. 1273-82, 2006.

[290] K. Sefah, Z. W. Tang, D. H. Shangguan, H. Chen, D. Lopez-Colon, Y. Li, P. Parekh, J. Martin, L. Meng, J. A. Phillips, Y. M. Kim, and W. H. Tan, "Molecular Recognition of Acute Myeloid Leukemia Using Aptamers," *Leukemia*, vol. 23, pp. 235-44, 2009.

[291] K. Sefah, D. Shangguan, X. Xiong, M. B. O'Donoghue, and W. Tan, "Development of DNA Aptamers Using Cell-Selex," *Nature protocols*, vol. 5, pp. 1169-85, 2010.

[292] C. H. Weng, I. S. Hsieh, L. Y. Hung, H. I. Lin, S. C. Shiesh, Y. L. Chen, and G. B. Lee, "An Automatic Microfluidic System for Rapid Screening of Cancer Stem-Like Cell-Specific Aptamers," *Microfluidics and Nanofluidics*, vol. 14, pp. 753-765, 2013.

[293] J. Kim, J. Hiltion, K. Yang, R. Pei, J. Zhu, M. Stojanovic, and Q. Lin, "Electrokinetically Integrated Microfluidic Isolation and Amplification of Biomolecule- and Cell-Binding Nucleic Acids," *IEEE Int. Conf. on Micro Electro Mechanical Systems (MEMS '13)*, pp. 1007-1010, Taipei, Taiwan, 2013.

[294] T. Nagel, N. Resnick, W. J. Atkinson, C. F. Dewey, Jr., and M. A. Gimbrone, Jr., "Shear Stress Selectively Upregulates Intercellular Adhesion Molecule-1 Expression in Cultured Human Vascular Endothelial Cells," *J Clin Invest*, vol. 94, pp. 885-91, 1994.

[295] V. F. Veiga, L. Nimrichter, C. A. Teixeira, M. M. Morales, C. S. Alviano, M. L. Rodrigues, and C. Holandino, "Exposure of Human Leukemic Cells to Direct Electric Current: Generation of Toxic Compounds Inducing Cell Death by Different Mechanisms," *Cell Biochem Biophys*, vol. 42, pp. 61-74, 2005.

[296] A. K. Naik, M. S. Hanay, W. K. Hiebert, X. L. Feng, and M. L. Roukes, "Towards Single-Molecule Nanomechanical Mass Spectrometry," *Nat Nanotechnol*, vol. 4, pp. 445-50, 2009.

[297] M. B. Elowitz, A. J. Levine, E. D. Siggia, and P. S. Swain, "Stochastic Gene Expression in a Single Cell," *Science*, vol. 297, pp. 1183-6, 2002.